IAEA TECDOC SERIES

IAEA-TECDOC-2001

IAEA-TECDOC-2001

Assessment of Radioactive Contamination and Effectiveness of Remedial Measures in Urban Environments

Report of Working Group 2

Modelling and Data for Radiological Impact Assessments (MODARIA) Programme

IAEA
International Atomic Energy Agency

IAEA SAFETY STANDARDS AND RELATED PUBLICATIONS

IAEA SAFETY STANDARDS

Under the terms of Article III of its Statute, the IAEA is authorized to establish or adopt standards of safety for protection of health and minimization of danger to life and property, and to provide for the application of these standards.

The publications by means of which the IAEA establishes standards are issued in the **IAEA Safety Standards Series**. This series covers nuclear safety, radiation safety, transport safety and waste safety. The publication categories in the series are **Safety Fundamentals**, **Safety Requirements** and **Safety Guides**.

Information on the IAEA's safety standards programme is available at the IAEA Internet site

www.iaea.org/resources/safety-standards

The site provides the texts in English of published and draft safety standards. The texts of safety standards issued in Arabic, Chinese, French, Russian and Spanish, the IAEA Safety Glossary and a status report for safety standards under development are also available. For further information, please contact the IAEA at: Vienna International Centre, PO Box 100, 1400 Vienna, Austria.

All users of IAEA safety standards are invited to inform the IAEA of experience in their use (e.g. as a basis for national regulations, for safety reviews and for training courses) for the purpose of ensuring that they continue to meet users' needs. Information may be provided via the IAEA Internet site or by post, as above, or by email to Official.Mail@iaea.org.

RELATED PUBLICATIONS

The IAEA provides for the application of the standards and, under the terms of Articles III and VIII.C of its Statute, makes available and fosters the exchange of information relating to peaceful nuclear activities and serves as an intermediary among its Member States for this purpose.

Reports on safety in nuclear activities are issued as **Safety Reports**, which provide practical examples and detailed methods that can be used in support of the safety standards.

Other safety related IAEA publications are issued as **Emergency Preparedness and Response** publications, **Radiological Assessment Reports**, the International Nuclear Safety Group's **INSAG Reports**, **Technical Reports** and **TECDOCs**. The IAEA also issues reports on radiological accidents, training manuals and practical manuals, and other special safety related publications.

Security related publications are issued in the **IAEA Nuclear Security Series**.

The **IAEA Nuclear Energy Series** comprises informational publications to encourage and assist research on, and the development and practical application of, nuclear energy for peaceful purposes. It includes reports and guides on the status of and advances in technology, and on experience, good practices and practical examples in the areas of nuclear power, the nuclear fuel cycle, radioactive waste management and decommissioning.

ASSESSMENT OF RADIOACTIVE CONTAMINATION AND EFFECTIVENESS OF REMEDIAL MEASURES IN URBAN ENVIRONMENTS

The following States are Members of the International Atomic Energy Agency:

AFGHANISTAN
ALBANIA
ALGERIA
ANGOLA
ANTIGUA AND BARBUDA
ARGENTINA
ARMENIA
AUSTRALIA
AUSTRIA
AZERBAIJAN
BAHAMAS
BAHRAIN
BANGLADESH
BARBADOS
BELARUS
BELGIUM
BELIZE
BENIN
BOLIVIA, PLURINATIONAL STATE OF
BOSNIA AND HERZEGOVINA
BOTSWANA
BRAZIL
BRUNEI DARUSSALAM
BULGARIA
BURKINA FASO
BURUNDI
CAMBODIA
CAMEROON
CANADA
CENTRAL AFRICAN REPUBLIC
CHAD
CHILE
CHINA
COLOMBIA
COMOROS
CONGO
COSTA RICA
CÔTE D'IVOIRE
CROATIA
CUBA
CYPRUS
CZECH REPUBLIC
DEMOCRATIC REPUBLIC OF THE CONGO
DENMARK
DJIBOUTI
DOMINICA
DOMINICAN REPUBLIC
ECUADOR
EGYPT
EL SALVADOR
ERITREA
ESTONIA
ESWATINI
ETHIOPIA
FIJI
FINLAND
FRANCE
GABON
GEORGIA
GERMANY
GHANA
GREECE
GRENADA
GUATEMALA
GUYANA
HAITI
HOLY SEE
HONDURAS
HUNGARY
ICELAND
INDIA
INDONESIA
IRAN, ISLAMIC REPUBLIC OF
IRAQ
IRELAND
ISRAEL
ITALY
JAMAICA
JAPAN
JORDAN
KAZAKHSTAN
KENYA
KOREA, REPUBLIC OF
KUWAIT
KYRGYZSTAN
LAO PEOPLE'S DEMOCRATIC REPUBLIC
LATVIA
LEBANON
LESOTHO
LIBERIA
LIBYA
LIECHTENSTEIN
LITHUANIA
LUXEMBOURG
MADAGASCAR
MALAWI
MALAYSIA
MALI
MALTA
MARSHALL ISLANDS
MAURITANIA
MAURITIUS
MEXICO
MONACO
MONGOLIA
MONTENEGRO
MOROCCO
MOZAMBIQUE
MYANMAR
NAMIBIA
NEPAL
NETHERLANDS
NEW ZEALAND
NICARAGUA
NIGER
NIGERIA
NORTH MACEDONIA
NORWAY
OMAN
PAKISTAN
PALAU
PANAMA
PAPUA NEW GUINEA
PARAGUAY
PERU
PHILIPPINES
POLAND
PORTUGAL
QATAR
REPUBLIC OF MOLDOVA
ROMANIA
RUSSIAN FEDERATION
RWANDA
SAINT KITTS AND NEVIS
SAINT LUCIA
SAINT VINCENT AND THE GRENADINES
SAMOA
SAN MARINO
SAUDI ARABIA
SENEGAL
SERBIA
SEYCHELLES
SIERRA LEONE
SINGAPORE
SLOVAKIA
SLOVENIA
SOUTH AFRICA
SPAIN
SRI LANKA
SUDAN
SWEDEN
SWITZERLAND
SYRIAN ARAB REPUBLIC
TAJIKISTAN
THAILAND
TOGO
TONGA
TRINIDAD AND TOBAGO
TUNISIA
TURKEY
TURKMENISTAN
UGANDA
UKRAINE
UNITED ARAB EMIRATES
UNITED KINGDOM OF GREAT BRITAIN AND NORTHERN IRELAND
UNITED REPUBLIC OF TANZANIA
UNITED STATES OF AMERICA
URUGUAY
UZBEKISTAN
VANUATU
VENEZUELA, BOLIVARIAN REPUBLIC OF
VIET NAM
YEMEN
ZAMBIA
ZIMBABWE

The Agency's Statute was approved on 23 October 1956 by the Conference on the Statute of the IAEA held at United Nations Headquarters, New York; it entered into force on 29 July 1957. The Headquarters of the Agency are situated in Vienna. Its principal objective is "to accelerate and enlarge the contribution of atomic energy to peace, health and prosperity throughout the world".

IAEA-TECDOC-2001

ASSESSMENT OF RADIOACTIVE CONTAMINATION AND EFFECTIVENESS OF REMEDIAL MEASURES IN URBAN ENVIRONMENTS

REPORT OF WORKING GROUP 2

MODELLING AND DATA FOR RADIOLOGICAL IMPACT ASSESSMENTS (MODARIA) PROGRAMME

INTERNATIONAL ATOMIC ENERGY AGENCY
VIENNA, 2022

For further information on this publication, please contact:

Waste and Environmental Safety Section
International Atomic Energy Agency
Vienna International Centre
PO Box 100
1400 Vienna, Austria
Email: Official.Mail@iaea.org

Printed by the IAEA in Austria
June 2022

IAEA Library Cataloguing in Publication Data

Names: International Atomic Energy Agency.
Title: Assessment of radioactive contamination and effectiveness of remedial measures in urban environments / International Atomic Energy Agency.
Description: Vienna : International Atomic Energy Agency, 2022. | Series: IAEA TECDOC series, ISSN 1011–4289 ; no. 2001 | Includes bibliographical references.
Identifiers: IAEAL 22-01512 | ISBN 978–92–0–124322–5 (paperback : alk. paper) | ISBN 978–92–0–124222–8 (pdf)
Subjects: LCSH: Metropolitan areas — Radioactive contamination. | Dispersion. | Radiation — Safety measures. | Radiation — Measurement.

FOREWORD

The IAEA has been organizing programmes of international model testing since the 1980s. These programmes have contributed to a general improvement in models, in the transfer of data and in the capabilities of modellers in Member States. IAEA publications on this subject over the past three decades demonstrate the comprehensive nature of these programmes and record the associated advances made.

The IAEA organized a programme from 2012 to 2015 entitled Modelling and Data for Radiological Impact Assessments (MODARIA), which aimed to improve capabilities in the field of environmental radiation dose assessment by acquiring improved data, model testing and comparison of model inputs, assumptions and outputs, reaching a consensus on modelling philosophies, aligning approaches and parameter values, developing improved methods and exchanging information.

Different aspects were addressed by ten working groups covering four themes: remediation of contaminated areas; uncertainties and variability; exposures and effects on biota; and marine modelling. This publication describes the activities of Working Group 2, Exposures in Contaminated Urban Environments and Effect of Remedial Measures.

The IAEA wishes to express its gratitude to all those who participated in the work of the MODARIA programme and gratefully acknowledges the valuable contribution of the Working Group Leader, K. Thiessen (United States of America). The IAEA officer responsible for this publication was T. Yankovich of the Division of Radiation, Transport and Waste Safety.

CONTENTS

SUMMARY

This publication describes the work undertaken by Working Group 2 (WG2) on Exposures in Contaminated Urban Environments and Effect of Remedial Measures (Urban Environments WG) of the IAEA's Modelling and Data for Radiological Impact Assessments (MODARIA) Programme.

The Urban Environments WG was organized within the MODARIA Programme, as part of a theme entitled 'Remediation of Contaminated Areas'. The Working Group has built on the work done by the Urban Remediation Working Group of the first phase of the IAEA's Environmental Modelling for Radiation Safety (EMRAS) Programme [1–5] and the Urban Areas Working Group of the EMRAS II Programme [6–8]. The goal of the Urban Environments WG was to test and improve the applicabilities of models used in assessment of radioactive contamination in urban settings, including dispersion and deposition events, short and long term contaminant redistribution following deposition events, and potential countermeasures or remedial actions for reduction of public exposures and doses following deposition events.

The Urban Environments WG was involved in four major areas of activity during the MODARIA Programme, including four modelling exercises. These WG2 activities include:

(1) Two modelling exercises applicable to contaminant transport inside an urban area (short range);
(2) A modelling exercise applicable to contaminant transport to urban areas from an external location (mid-range);
(3) A modelling exercise applicable to redistribution and remediation of urban contamination;
(4) A review of models for assessment of public exposures from short term releases.

The four modelling exercises were designed to enable intercomparison of model predictions and, when possible, comparison of model predictions with measurements for selected endpoints. Reasons for similarities and discrepancies among model predictions are discussed in terms of the modelling approaches, models, and parameter values used by different assessors. An important objective is the identification of areas in which models or selection of parameter values could be improved. The fourth area of activity was a review of existing models relevant to assessment of short term releases of radioactive materials.

The first modelling exercise was a continuation of a short range atmospheric dispersion exercise from the EMRAS II Programme [6]. The exercise was based on data from several field tests performed by the Czech National Radiation Protection Institute on a test area belonging to the National Institute for Nuclear, Chemical and Biological Protection in Kamenná, near Prague, Czech Republic [9]. The exercise was designed to enable comparison of model predictions with measurements of surface contamination, time integrated air concentrations, and dose rates, up to 50 m downwind. Intercomparisons of model predictions were made for distances up to 2000 m downwind and for additional modelling endpoints.

In these field tests, a short lived radionuclide (^{99m}Tc) in liquid form was spread by detonation of a small amount of explosive in an open field (flat terrain) or in an open field with some simulated structures. Measurements included external dose rates, surface contamination, radionuclide concentrations in air, particle size distributions, time distributions of dust particles in air, and thermo-camera snapshots. The test area was selected for a stable wind direction under usual meteorological conditions.

Two individual field tests were used in the exercise. Participants in the modelling exercise were asked to submit predictions for surface contamination as a function of distance. Participants were provided with all available measurements for the four tests used in the EMRAS II Programme [6] providing an opportunity for calibration of their models if desired. For the fifth and sixth tests, the new ones considered during MODARIA, participants were asked to submit model predictions before having access to measurements of the modelling endpoints.

Three participants submitted calculations for the short range exercise. The models represented two main types of approaches to modelling atmospheric dispersion and had been developed for several different purposes. Model predictions varied considerably in the predicted angles of the plume and the amounts of deposited activity. Explanations include differences in the computational types, the intended domain size, and values selected for important parameters, including wind speeds and directions, dry deposition velocity, and atmospheric stability class. Participants also differed in use of mean vs. time dependent meteorological data and use of meteorological data from one or several measurement locations. Comparison of model results was facilitated by use of contour plots of predicted and measured deposition with the same coordinate system and color scale. Comparison of predictions with measurements indicated that the models could not fully reproduce apparent instabilities in the actual plume.

An additional short range exercise was undertaken by two participants to compare their respective decision support models. The exercise was based on a hypothetical release situation located in a dense urban area in Paris, France and was designed to provide useful information about the importance of buildings and street canyons. Two scenarios were employed, one involving a 10 minute continuous release from a 5 m stack, and one involving a release due to 1 kg of an explosive. The modelling results were generally in good agreement between the two models, with greater differences observed for the explosion scenario, as expected, given the difficulty in accounting for building effects (obstacles) in the vicinity of the explosion.

The third modelling exercise was a mid-range atmospheric dispersion exercise, intended to be applicable to situations such as nuclear power plant accidents (e.g. in the context of emergency preparedness), in which contamination from an accident site could be transported to urban areas. The exercise was based on the Šoštanj Thermal Power Plant (TPPŠ) in Slovenia, a challenging situation with complex terrain and meteorology. Tracer data (concentrations in air) from a three week measuring campaign in 1991 were available for use in validation of model predictions for selected locations. For other endpoints (e.g. additional locations, deposition at any location), it was a model intercomparison exercise.

Two test cases were prepared from the existing information. The first test case consisted of a 24 hour period in March 1991 when only one release point was active and wind conditions were stable in a single primary direction. The second test case was a 2 day period in April 1991 when the meteorological situation as well as the release situation (two release points) were much more complex. Requested results for the first case (March) included a time series of ground level tracer concentration at a single sampling location and nearby locations, the predicted plume rise, and the predicted wind field at the effective release height. For the second case (April) prediction of tracer concentrations (as time series) for several sampling locations and of plume rise and wind fields for two release points were requested.

Five participants submitted calculations for this exercise, with one participant submitting calculations from two models. Both test cases, particularly the second one, proved to be very challenging for the participants. The exercise demonstrated the greater utility of numerical Lagrangian particle models over Gaussian models for modelling atmospheric dispersion over complex terrain, as well as the importance of including vertical profiles of meteorological conditions in addition to data from ground based meteorological stations.

The fourth modelling validation exercise focused specifically on urban contamination and remediation. The exercise was prepared by the Japan Atomic Energy Agency (JAEA), based on monitoring data in an area of Japan evacuated following the Fukushima accident and on information about experimental decontamination efforts and human behavioural patterns. Initial modelling was kept simple, with the aim of expanding the scenario during the second phase of the IAEA's MODARIA Programme (MODARIA II). The requested results for this first phase of modelling included the ambient effective external dose rates for each land use definition and the annual effective external dose for designated categories of persons. Calculations were made for a 10 year period and assumed that no decontamination was implemented. Plans for later stages of this exercise to be carried out under MODARIA II include assessment of the effects of various decontamination or remediation measures on external doses.

The final area of WG2 activities was a review of models for assessment of public exposures from acute releases. This activity was identified during the initial meeting of MODARIA as an area of great interest to many WG2 participants. The goal was to provide a review and comparison of models (computer codes) for predicting transport of radioactive contaminants to urban environments, especially atmospheric dispersion, deposition and environmental transport for situations such as an accident at a nuclear power plant. Although the review is not exhaustive, it includes key models in use at the time of the review (or still named in national regulations), their applicabilities and needs (computational and in terms of necessary input data), intended uses and other important features. The intent was not to provide an evaluation of which model is 'best', but to provide information that could help a participant to select the most appropriate model for his or her own situation.

The format of the review is an Excel workbook with a separate page (worksheet) for each model and a table comparing major features or attributes of all of the included models. The latest version of the workbook (information collected through 2017) contains information on 31 models and is available as a complementary Electronic Appendix. Selected material from the review is summarized in the main text of this publication.

1. INTRODUCTION

1.1. BACKGROUND OF THE MODARIA PROGRAMME

The IAEA organized a programme from 2012 to 2015, entitled Modelling and Data for Radiological Impact Assessments (MODARIA), which had the general aim of improving capabilities in the field of environmental radiation dose assessment by means of acquisition of improved data for model testing; model testing and comparison; reaching consensus on modelling philosophies, approaches and parameter values; development of improved methods; and exchange of information.

The following topics were addressed in ten working groups:

Remediation of Contaminated Areas

- Working Group 1: Remediation strategies and decision aiding techniques
- Working Group 2: Exposures in contaminated urban environments and effect of remedial measures
- Working Group 3: Application of models for assessing radiological impacts arising from NORM and radioactively contaminated legacy sites to support the management of remediation

Uncertainties and Variability

- Working Group 4: Analysis of radioecological data in IAEA Technical Reports Series publications to identify key radionuclides and associated parameter values for human and wildlife exposure assessment
- Working Group 5: Uncertainty and variability analysis for assessments of radiological impacts arising from routine discharges of radionuclides
- Working Group 6: Common framework for addressing environmental change in long term safety assessments of radioactive waste disposal facilities
- Working Group 7: Harmonization and intercomparison of models for accidental tritium releases

Exposures and Effects on Biota

- Working Group 8: Biota modelling: Further development of transfer and exposure models and application to scenarios
- Working Group 9: Models for assessing radiation effects on populations of wildlife species

Marine Modelling

- Working Group 10: Modelling of marine dispersion and transfer of radionuclides accidentally released from land based facilities

The activities and results achieved by the Working Groups are described in individual IAEA Technical Documents (IAEA-TECDOCs). This publication describes the activities of WG2, the Urban Environments Working Group (Working Group 2).

1.2. BACKGROUND FOR MODARIA WORKING GROUP 2: EXPOSURES IN CONTAMINATED URBAN ENVIRONMENTS AND EFFECT OF REMEDIAL MEASURES

The MODARIA Theme entitled 'Remediation of Contaminated Areas' included three areas of interest: remediation strategies and decision aiding techniques, assessment of urban contamination and remediation effectiveness, and assessment of radiological impacts of naturally occurring radioactive materials (NORM) and contaminated legacy sites. The Urban Environments Working Group (WG2) has built on the work done by the Urban Remediation Working Group of the EMRAS Programme and the Urban Areas Working Group of the EMRAS II Programme. In particular, an objective of WG2 has been to test and improve the applicabilities of models used in assessment of radioactive contamination in urban settings, including dispersion and deposition events, short and long term contaminant redistribution following deposition events, and potential countermeasures or remediation efforts for reducing human exposures and doses.

1.3. OBJECTIVES

The primary objective of the Urban Environments WG was to test and improve the prediction of (1) contamination densities and radioactivity concentrations in air following an atmospheric dispersion and deposition event, (2) changes in radionuclide concentrations or external dose rates as a function of location and time, (3) the most important contributors (e.g. surfaces or exposure pathways) to human doses in an urban location following a deposition event, and (4) expected reductions in radionuclide concentrations, external dose rates, or doses due to various countermeasures or remediation efforts. Specific objectives included the development and carrying out of four modelling exercises for different types of situations, plus a review of existing models for assessment of public exposures from acute releases. Analysis of the modelling exercises included comparison of approaches, models, and modelling results for each type of contamination situation. This WG2 publication describes each of the modelling exercises, the models used in the exercises, the approaches and parameter selection used by individual participants, and the results of each exercise. Section 6 of this publication includes a summary of the model review. This publication is intended to provide information about the performance of various models in specified contexts, both for assessing the radiological impact of a situation and (where appropriate) for evaluating proposed countermeasures or remediation measures for a situation.

1.4. SCOPE

The Working Group developed and carried out four modelling exercises, including three atmospheric dispersion exercises (two short range and one mid-range) and a fourth exercise dealing with urban contamination and remediation. In addition to these modelling exercises, the Working Group prepared a review of a number of existing models for assessment of atmospheric dispersion and/or public exposure from acute releases.

The first short range atmospheric dispersion exercise was based on field tests involving dispersion of a radionuclide by a small amount of explosive. This exercise, which continued an exercise from the EMRAS II Programme, involved comparison of model predictions with measurements, as well as intercomparison of predictions. An additional hypothetical short range modelling exercise was also conducted. The mid-range atmospheric dispersion exercise was based on a set of measurements (atmospheric concentrations of a tracer) of releases from a power plant and the necessary prediction of the subsequent transport and deposition of the contamination. For each of these exercises, modellers were asked to predict the downwind surface contamination densities and radionuclide concentrations in air. The fourth modelling exercise focused specifically on urban contamination and remediation, based on monitoring data in an area of Japan evacuated following the Fukushima accident and on information about experimental decontamination efforts and human behavioural patterns. Initial modelling included prediction of the ambient effective external dose rates for several land use definitions and the annual effective external dose for designated categories of persons, over a 10 year period assuming no decontamination. This publication describes each modelling exercise, the models used by participants in each exercise, and conclusions and applications based on the exercises.

1.5. STRUCTURE OF THE PUBLICATION

Section 1 provides a brief description of the background of the MODARIA Programme and the Urban Environments WG, the objectives of WG2 and the scope of its activities. Sections 2–5 describe the modelling exercises, including the scenario description, the models used in the exercise, the modelling results, and explanations for agreement or discrepancies among modellers. Section 2 covers the short range atmospheric dispersion exercise based on field tests, and Section 3 the comparison of decision support systems based on a hypothetical release situation. Section 4 describes the mid-range atmospheric dispersion exercise. Section 5 describes the contaminant transport and countermeasures exercise. Section 6 summarizes the review of models for assessing acute releases of radioactive contamination. Section 7 provides some general conclusions and applications based on the modelling exercises. Appendix I provides the scenario description and documentation for the first modelling exercise, and Appendix II provides supplemental information for the contaminant transport and countermeasures exercise. Appendix III provides detailed descriptions of several of the models used in the exercises.

Tables comparing major features or attributes of atmospheric dispersion models are provided in a complementary Electronic Appendix to this publication. The format of this model review is an Excel workbook with a separate page (worksheet) for each model and a table comparing models. The latest version of the workbook (information collected through 2017) contains information on 31 models.

2. SHORT RANGE ATMOSPHERIC DISPERSION EXERCISE

2.1. OVERVIEW AND RATIONALE

The short range atmospheric dispersion scenario is based on experimental data obtained from a series of field tests performed by the Czech National Radiation Protection Institute (SÚRO), involving the dispersal of a short lived radionuclide with a small amount of explosive [6, 9]. The scenario is intended to provide an opportunity to test model predictions for a short range dispersion event, including the deposition resulting from the event. The present exercise includes two field tests; four earlier tests were previously considered during the EMRAS II Programme [6]. The experimental conditions for the two events are summarized in Section 2.2, and full details are provided in Appendix I. Input information for each event included the amount of radioactive material involved, the arrangement of the various detectors in the vicinity of the explosion, and meteorological information.

The radioactive material, a short lived radionuclide (^{99m}Tc) in liquid form, was spread by detonation of a small amount of explosive in an open field with a simulated structure to provide obstacles to the dispersion. The measurements performed included monitoring of dose rate, surface contamination of ground and structures, activity concentrations in air, particle size distribution, time distribution of dust particles in air, and thermo-camera snapshots. The test area was selected for a stable wind direction under usual meteorological conditions.

All available data for the four earlier tests [6] were provided to the participants to be used for model calibration if desired. These data included measurements of surface contamination, dose rates, and time integrated activity concentrations in air. The two tests in the current exercise (Tests 5 and 6 in the larger set of field tests[1]) were conducted as fully blind model tests, and only the input information was provided to participants during the exercise. Comparisons were made with measurements only after the modelling results were submitted.

Endpoints to be modelled for Tests 5 and 6 included: (1) surface contamination (Bq/m^2) as a function of distance; (2) time integrated activity concentrations in air ($Bq{\cdot}min{\cdot}m^{-3}$) as a function of height and distance along the center line; and (3) estimated percentile contamination zones (50%, 75%, 95%) for each explosion event. As described in an earlier publication [6], the scenario can also be used for validation of location factors, data assimilation to improve initial modelling results, and estimation of the source term from measurements. Full details about the scenario are provided in Appendix I and the earlier publication [6]. The analysis discussed in the following sections is limited to the predicted and measured surface contamination.

2.2. SUMMARY OF INITIAL CONDITIONS FOR TESTS 5 AND 6

Table 1 summarizes the initial conditions for the two events considered as blind model tests in this exercise, Test 5 (4 May 2010) and Test 6 (22 June 2010). Table 2 provides a summary of the meteorological data for Tests 5 and 6; more detailed meteorological data were provided in electronic form (see Appendix I). Meteorological data were provided at heights of 2 m, 4 m, and 10 m for one location, and at 2 m for four additional locations. A height of 10 m is generally considered the standard for meteorological measurements.

---

[1] Different numbering schemes have been used in some of the documentation of these field tests. This publication refers to Tests 5 and 6 in the text or to Tests 5/3P and 6/4P in Tables 25–30 of Appendix I. Dates of the field tests are provided in these tables to facilitate identification of individual field tests.

TABLE 1. SUMMARY INFORMATION FOR TESTS 5 AND 6

Test No. **Date**	**Test 5/3P** **4 May 2010**	**Test 6/4P** **22 June 2010**
Explosion time[a]	14:15	12:06
Time of measurement of ^{99m}Tc activity[a]	11:00	12:00
Activity of ^{99m}Tc (MBq)	2119	2045
Amount of liquid containing the activity	6 mL	6 mL
Amount and type of explosive used[b]	Permon 10T 350 g	Permon 10T 350 g

[a] Twenty four hour system (12:00 = noon).
[b] Descriptions of the explosives were provided separately.

TABLE 2. SUMMARY OF WEATHER CONDITIONS DURING TESTS 5 AND 6[a]

Test No. **Date**	**Test 5/3P** **4 May 2010**	**Test 6/4P** **22 June 2010**
Temperature (°C)	10.1–10.2	18.5–18.9
Relative air humidity (%)	77–79	41–46
Condensation point (°C)	6.3–6.7	5.2–6.8
Wind speed (km/h)	3.2–13	4.7–11.2
Gust wind speed (km/h)	7.9–20.9	6.5–17.6
Wind direction (degrees)	90–270	0–270
Air pressure (hPa)	1013.6–1013.7	1013–1013.4

[a] More detailed meteorological data were provided in electronic form (see Appendix I). Measurements are at 10 m height. The indicated wind direction is the direction wind is blowing from.

For both field tests, a simulated structure was erected in the test area (see Fig. 84 given in Appendix I below). The obstacle had dimensions of 11 m × 2.5 m × 3 m (length, width, height) and was located on the centerline of the grid.

2.3. MODELS USED IN THE EXERCISE

Table 3 summarizes the models and parameter values used by participants in the short range atmospheric dispersion exercise. The models represented two main types of computational approaches to modelling atmospheric dispersion (Gaussian and Lagrangian) and were developed for various purposes. Three participants provided predictions for this exercise. Descriptions of the individual models as used in this exercise are provided in [6] and Appendix III of the present publication.

2.4. METEOROLOGICAL SITUATION DURING TESTS 5 AND 6

For the simulation of the atmospheric dispersion for Tests 5 (4 May 2010) and 6 (22 June 2010), two Gaussian type models and one Lagrangian type model were used (see Table 3). The meteorological input data are handled differently depending on the design of the model. Specifically, some models make use of averaged data, whereas other models can use time dependent data sets with a time resolution of down to 1 minute (transient wind conditions).

Wind speed and direction are essential for good results when measurements and model predictions are compared. For Tests 5 and 6, the meteorological situations were not as homogeneous as expected. Figures 1 and 2 show the 1 minute averaged wind speed and the wind direction at 10 m height for Tests 5 and 6, respectively, at a location 20 m behind the dispersion point (grid coordinates: 0, –20). The time of the explosion is indicated by a triangle.

TABLE 3. COMPARISON OF MODELS AND SELECTED PARAMETERS USED IN THE SHORT RANGE ATMOSPHERIC DISPERSION EXERCISE

Model name	ADDAM/CSA-ERM	LASAIR	URD
Participant and country	S.L. Chouhan Canada	H. Walter Germany	B.K. Tay Singapore
Type of model	Gaussian	Lagrangian	Gaussian puff
Purpose of model	ADDAM: safety assessment for accidents; CSA-ERM, research tool	Decision support	Decision support[a]
Domain size	ADDAM: centerline from 100 m; CSA-ERM, fine grid	40 × 40 km² 5 m grid, increasing to the outside	2 km × 2 km at 10 m resolution; 40 m × 60 m at 1 m resolution
Calibration	Tests 1 and 2 [6]	None	None
Stability classes	Test 5: Class A Test 6: Class A	Test 5: Class D Test 6: Class D	Not applicable
Wind speed (m/s)	Test 5: 1.44 Test 6: 1.46	Test 5: 0.5–3.6 Test 6: 0.5–3.6	Time dependent measurements at 10 m height
Wind conditions (transient or steady state)	4–10 minutes average (all heights and locations)	Transient; time dependent measurements at 10 m height	Transient; time dependent measurements at 10 m height
Dry deposition velocity (m/s)	1×10^{-1}	< 2.5 µm, 1×10^{-3} 2.5–10 µm, 1×10^{-2} 10–50 µm, 5×10^{-2} > 50 µm, 2×10^{-1}	Calculated within a deposition model in URD
Source term partitioning	_[b]	Uniformly distributed within initial cloud	Uniformly distributed within cloud
Column dimensions (x,y,z)	Height = 12.9 m Width = 11 m Effective release height = 6.45 m	Height = 7 m Base = 3 m × 3 m (box shaped)	Height = 11 m 5 initial puffs of same size
Surface roughness	Grass terrain; roughness length, 0.4 m	Test ground, 0.1 m close vicinity (trees), 1.0 m obstacles regarded with actual heights	Grassland (roughness = 0.05 m)
Particle size distribution (% of activity per particle size intervals)	_[b]	0–2.5 µm, 40% 2.5–10 µm, 40% 10–50 µm, 10% ≥ 50 µm, 10%	< 0.39 µm, 40% 0.39–1.3 µm, 12% 1.2–0.2 µm, 38% > 10.2 µm, 10%
Time to set up and run	< 30 min	< 5 min	< 15 min
Time to process results	< 30 min	< 10 min	< 15 min
Number of Lagrangian particles	Not applicable	500 000	Not applicable

[a] The URD (Urban Release and Dispersion) model, developed by the Technical University of Denmark (DTU), was used as part of the ARGOS decision support system (developed by PDC-ARGOS) under test and evaluation by the participant's organization at the time of the exercise.
[b] Not provided.

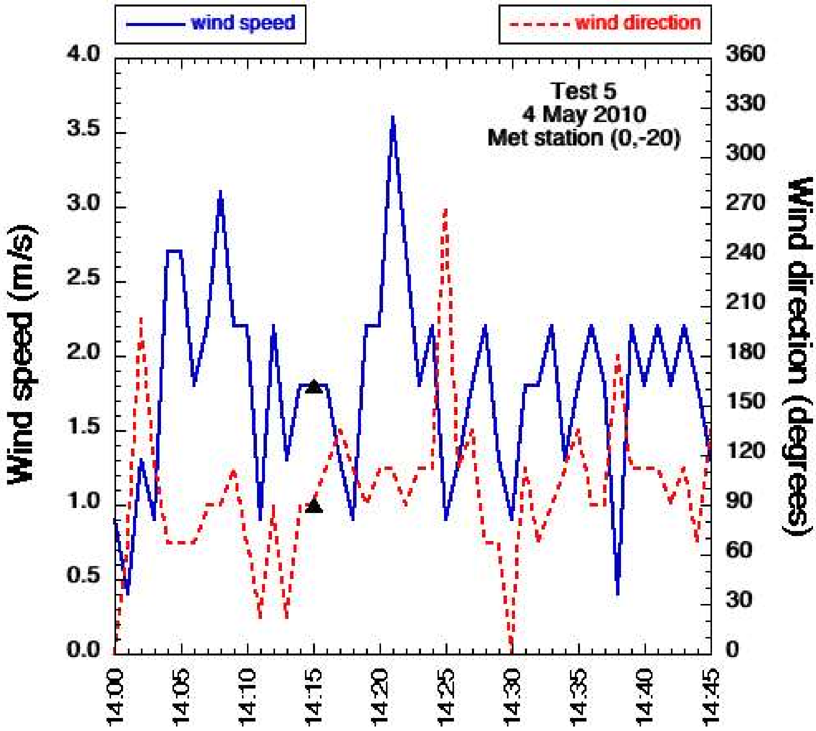

FIG. 1. Wind speed and wind direction (1 minute averages) at 10 m height for Test 5 (4 May 2010). The triangles indicate the time of the explosion.

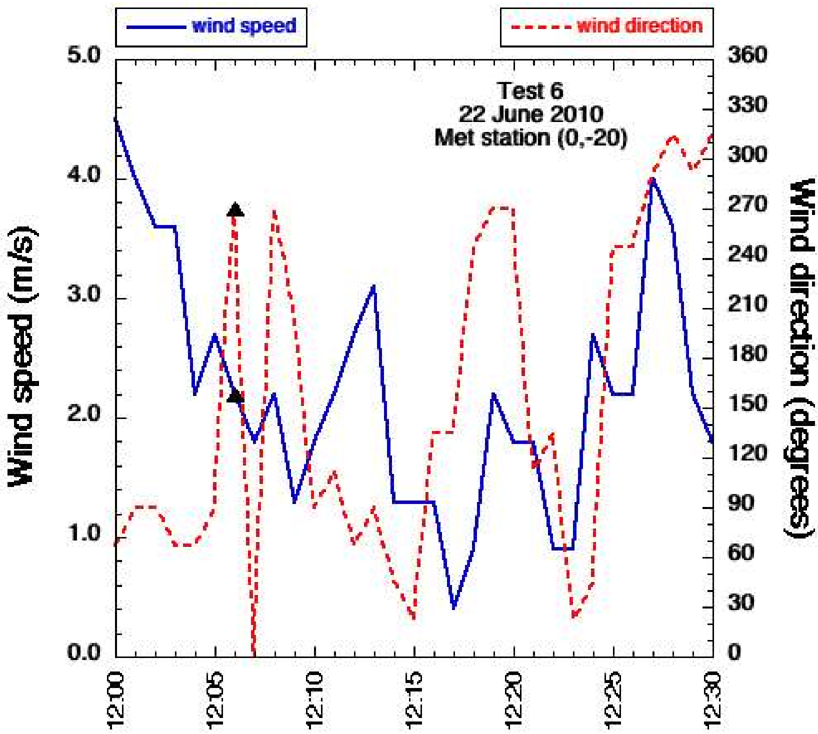

FIG. 2. Wind speed and wind direction (1 minute averages) at 10 m height for Test 6 (22 June 2010). The triangles indicate the time of the explosion.

In Test 5, the wind speed varied from 1.8 m/s, dropping down to below 1 m/s roughly 2 minutes after the explosion, increasing significantly to 3.6 m/s for another two minutes, and then falling back to an average of 1.5 m/s. Wind direction data indicate a steady wind current for roughly 8 minutes after the explosion, then showed two peaks (270° and 0°). As most of the material after the explosion is dispersed or moved within a few minutes, it was expected that the models were likely to be able to reproduce this meteorological situation.

In Test 6, the wind speed fell back from roughly 2.2 m/s to 1.4 m/s after the explosion and then varied from 0.4 to 3.1 m/s within the next 12 minutes. Wind direction data show similar but more significant changes. Within 2 minutes there was a change of 90° and back to the previous wind direction, and during the next 8 minutes the wind direction changed counterclockwise from 270° to 20°, coming back to the former direction (270°) after another 4 minutes. This is a typical convective and unstable situation where air masses were lifted (e.g. due to insolation) and therefore create a change to the main wind direction; after a while, when the updraft has finished, it switches back to the main wind direction again. Atmospheric dispersion models can handle such a situation only if the input data for wind speed and wind direction correspond to the meteorological situation. Rapid change in wind direction, in particular, can cause errors within the simulation when only averaged input data are used. This is the case especially for Gaussian type models.

2.5. ANALYSIS OF MODELLING RESULTS

2.5.1. General approach

This analysis concentrates on the predicted and measured deposition (surface contamination), using an approach developed during the EMRAS II Programme [6]. Deposition profiles were defined by the dispersion point (0,0) and the coordinates of points with predicted or measured deposition (Bq/m^2). Comparisons were made of the measurements and the model outputs (predictions) from the participants. Only the area of the test site (the area with measurements, or the grid area) was considered. Although some model predictions extended to greater distances, there are no measured values at those distances for comparisons. Measurement points used during the tests are shown in Appendix I. The selected area for comparisons is slightly larger than the actual measurement area in order to contain all the points, both measurement points and points with model predictions.

Values of activity concentrations were calculated from measurements using a Multilevel B-Spline interpolation [10] method with System for Automated Geoscientific Analyses Geographic Information System (SAGA GIS)[2] software, and the interpolated values were used instead of the measured values [6]. Both the model predictions and the measurements were interpolated, using the same method and settings, so that the results could be easily compared for the same set of point locations. Negative values obtained from the calculations were replaced with zeros. Thus, interpolated grids were created for each set of model predictions and for the measurements, and these grids were used as data input for the profiles discussed later in this section. For the comparisons, it was necessary to put all model outputs into the same coordinate system, which was a custom Cartesian system with the planned dispersion direction to the North. The development of the grids was described in detail in Ref. [6].

[2] http://www.saga-gis.org/saga_module_doc/2.1.3/grid_spline_4.html

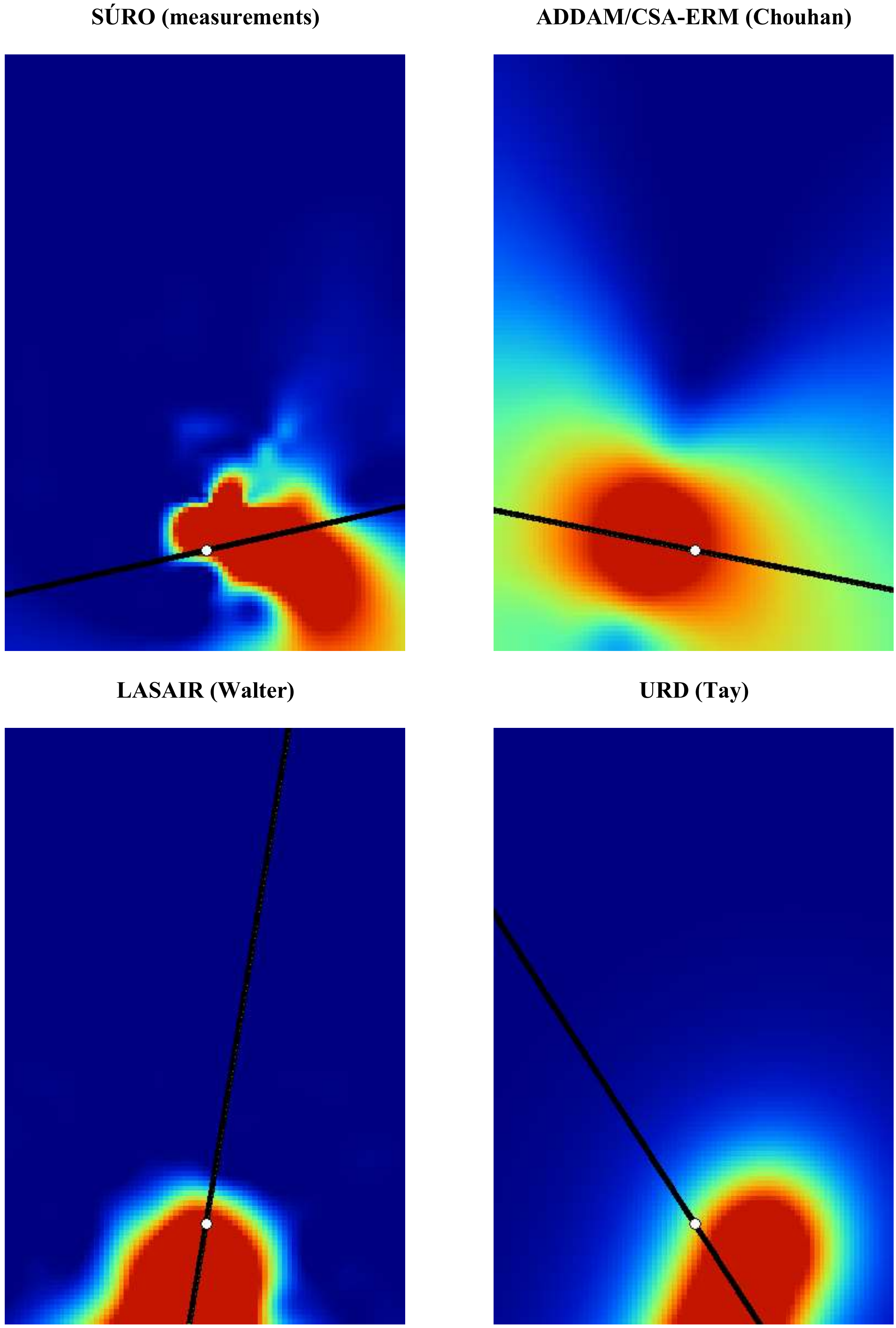

FIG. 3. Cloud axis profiles of the predicted deposition from models (ADDAM/CSA-ERM, LASAIR, URD) in comparison with the measurements (SÚRO) for Test 5. The white dot indicates the dispersion point, and the black line indicates the cloud axis.

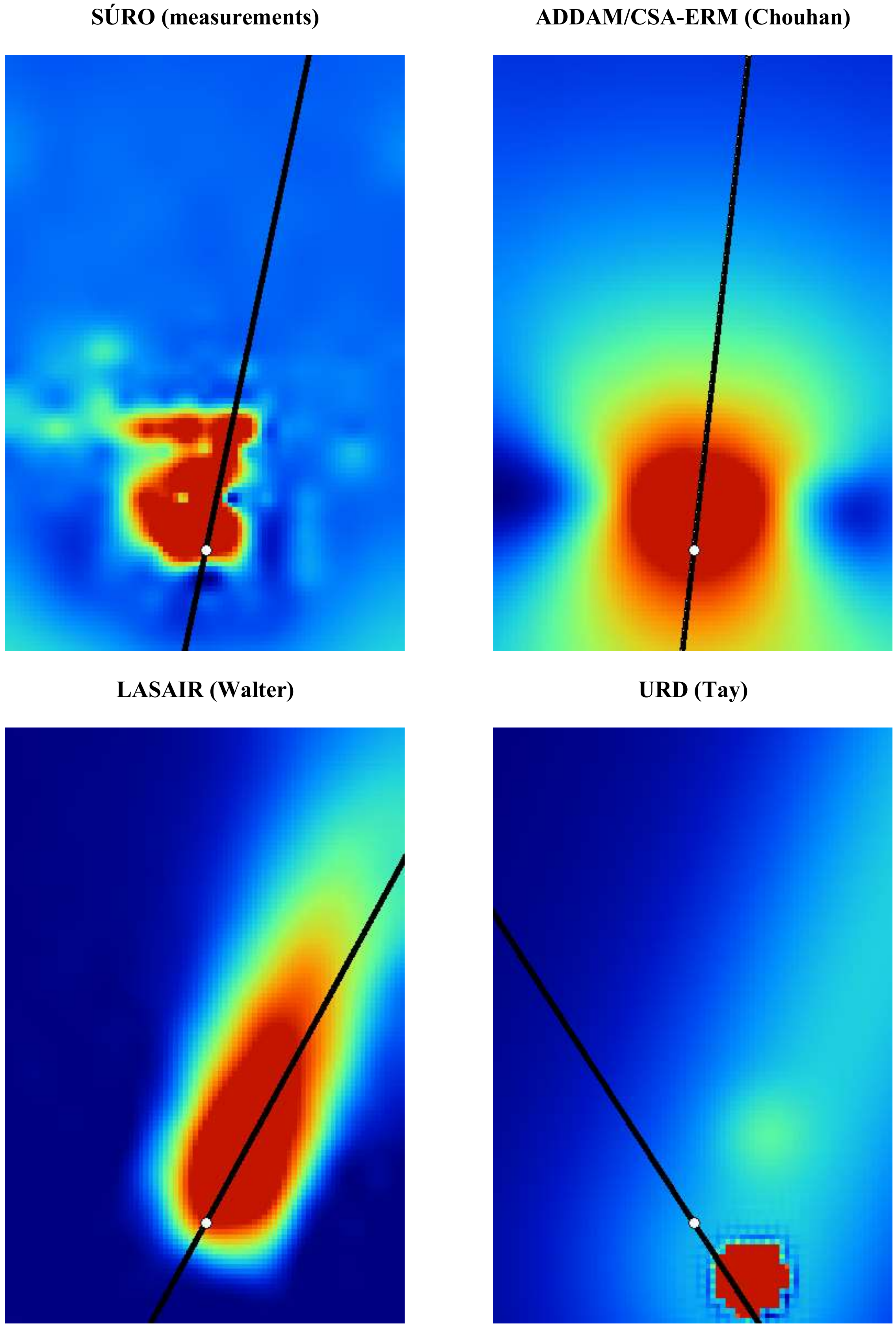

FIG. 4. Cloud axis profiles of the predicted deposition from models (ADDAM/CSA-ERM, LASAIR, URD) in comparison with the measurements (SÚRO) for Test 6. The white dot indicates the dispersion point, and the black line indicates the cloud axis.

The plots of the processed data sets (see Figs 3 and 4 above) show the predictions and measurements in the same coordinate system and with the same color scale. The plots thus provide a visual comparison of the 2-D predicted or measured contamination and the degree of contamination. For Test 5, the measurements show deposition to the grid east, with components to the north and eventually to the south. In contrast, the models predicted the primary deposition to west-northwest, south-southwest, and southeast (the last actually looks like dispersion to the south-southwest but displaced slightly to the east from the dispersion point). For Test 6, the measurements show deposition largely to the grid north, slightly to the northeast. Two models predicted deposition to the north-northeast or the northeast, consistent with the measurements, while the third predicted deposition largely to the southeast. For both tests, the measurements indicate that the plume was not stable in direction during the deposition event, and the models did not fully reproduce this effect.

2.5.2. Maximum activity and total activity in the grid area

Tables 4 and 5 summarize the maximum deposited activity (Bq/m^2, with the coordinates for the location) and the total activity deposited in the grid area (MBq) for the measurements and for each set of model predictions, for Tests 5 and 6, respectively.

For Test 5, predicted maximum deposited activity varied from 5.9×10^5 to 1.4×10^6 Bq/m^2; Two models (ADDAM/CSA-ERM and LASAIR) were very close, and the third (URD) was about a factor of 2 higher. The measured maximum deposited activity was 2.1×10^6 Bq/m^2, which was greater than the predicted values by a factor of 1.5–3.5. The predicted total deposited activity within the grid area ranged from 67 to 330 MBq, a range of about a factor of 5. The measured total deposited activity within the grid area was 202 MBq. One model (URD) was very close, while the other two were a factor of 3 lower (LASAIR) and a factor of 1.6 higher (ADDAM/CSA-ERM). The total activity dispersed by Test 5 was 2119 MBq.

For Test 6, values of the predicted maximum deposited activity from the three models were very close, ranging from 5.3×10^5 to 6.4×10^5 Bq/m^2. The measured maximum deposited activity was 9.6×10^5 Bq/m^2, about a factor of 1.5–1.8 higher. The predicted total deposited activity within the grid area ranged from 123 to 382 MBq, a range of about a factor of 3. The measured total deposited activity within the grid area was 38 MBq; the model predictions were a factor of 3–10 higher than the measured value. The total activity dispersed by Test 6 was 2045 MBq.

2.5.3. Profiles from (0,0) to maximum

Profiles of model predictions from the dispersion point (0,0) to the point with the maximum value of deposited activity (Tables 4 and 5) were developed as previously described [6]. Tables 6 and 7 provide the predicted or measured profile integrals (profiles of deposited activity) along the line from the dispersion point through the maximum deposited activity for each model for Tests 5 and 6, respectively. Results are shown both in units of Bq (total activity under the profile) and as normalized values.

Figures 5 and 6 show the normalized profiles of the predicted deposition in comparison with the measurements, for all participating models. Only the range from the dispersion point (0,0) to the maximum was plotted. The stepped shape of the graphed lines is caused by differences in resolution between the profile and the grid. All profiles were checked to be sure that they crossed the maximum value of the input grid (the maximum value predicted by the model). Differences in the predicted directions of the profiles are not reflected in Figs 5 and 6.

TABLE 4. PREDICTED AND MEASURED MAXIMUM VALUES OF DEPOSITED ACTIVITY AND TOTAL ACTIVITY DEPOSITED WITHIN THE GRID AREA[a] FOR TEST 5

Model	Coordinates[b] X	Coordinates[b] Y	Maximum deposited activity (Bq/m^2)	Total activity deposited within the grid area (MBq)
Measurements (SÚRO)	0	3.0	2.1×10^6	202
Model Predictions				
ADDAM/CSA-ERM (Chouhan)	-5.0	1.0	6.3×10^5	334
LASAIR (Walter)	-1.0	-6.0	5.9×10^5	67.2
URD (Tay)	6.0	-9.0	1.4×10^6	207

[a] The total dispersed activity for Test 5 was 2119 MBq.
[b] Coordinates for the locations of the maximum predicted and measured activities, assuming a dispersion point (origin of the explosion) at (0,0); distances are in m.

TABLE 5. PREDICTED AND MEASURED MAXIMUM VALUES OF DEPOSITED ACTIVITY AND TOTAL ACTIVITY DEPOSITED WITHIN THE GRID AREA[a] FOR TEST 6

Model	Coordinates[b] X	Coordinates[b] Y	Maximum deposited activity (Bq/m^2)	Total activity deposited within the grid area (MBq)
Measurements (SÚRO)	0	3.0	9.6×10^5	38.0
Model Predictions				
ADDAM/CSA-ERM (Chouhan)	0.5	4.5	5.3×10^5	382
LASAIR (Walter)	3.0	5.5	5.3×10^5	189
URD (Tay)	5.5	-8.5	6.4×10^5	123

[a] The total dispersed activity for Test 6 was 2045 MBq.
[b] Coordinates for the locations of the maximum predicted and measured activities, assuming a dispersion point (origin of the explosion) at (0,0); distances are in m.

TABLE 6. PROFILE INTEGRALS OF DEPOSITION FOR TEST 5

Model	Profile through maximum		Profile through cloud axis	
	Normalized values (unitless)	Measured or predicted values (Bq)	Normalized values (unitless)	Measured or predicted values (Bq)
Measurements (SÚRO)	36.85	7.61×10^6	97.64	1.20×10^7
ADDAM/CSA-ERM (Chouhan)	10.20	9.41×10^6	10.20	9.41×10^6
LASAIR (Walter)	9.93	5.88×10^6	9.93	5.88×10^6
URD (Tay)	7.62	1.12×10^7	7.62	1.12×10^7

TABLE 7. PROFILE INTEGRALS OF DEPOSITION FOR TEST 6

Model	Profile through maximum		Profile through cloud axis	
	Normalized values (unitless)	Measured or predicted values (Bq)	Normalized values (unitless)	Measured or predicted values (Bq)
Measurements (SÚRO)	35.08	3.35×10^6	56.12	3.30×10^6
ADDAM/CSA-ERM (Chouhan)	19.94	1.31×10^7	19.94	1.31×10^7
LASAIR (Walter)	24.87	1.31×10^7	24.87	1.31×10^7
URD (Tay)	9.01	4.77×10^5	9.01	4.77×10^5

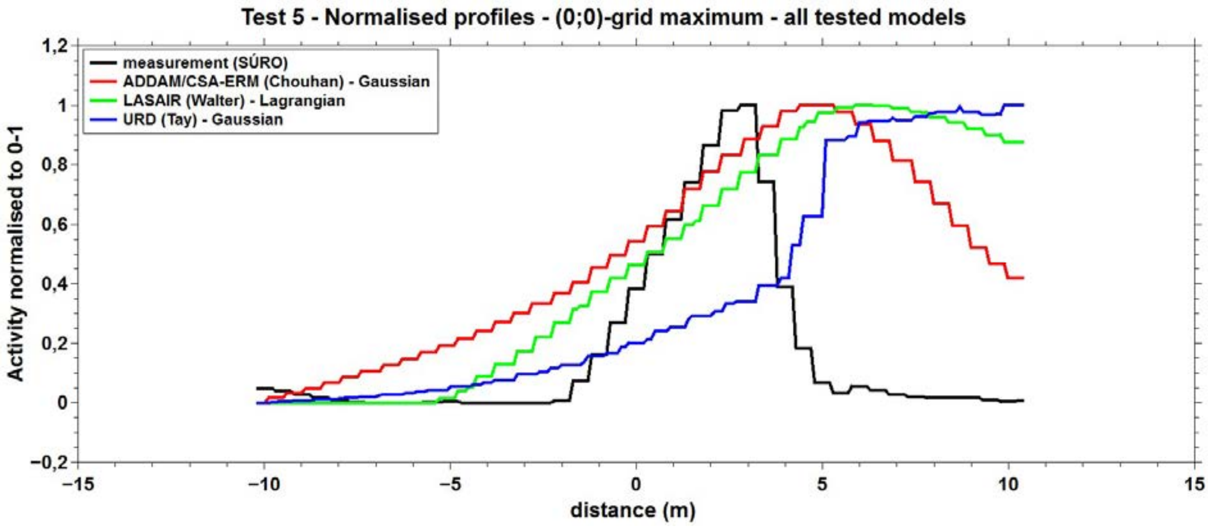

FIG. 5. Normalized profiles of the predicted deposition in comparison with the measurements for Test 5.

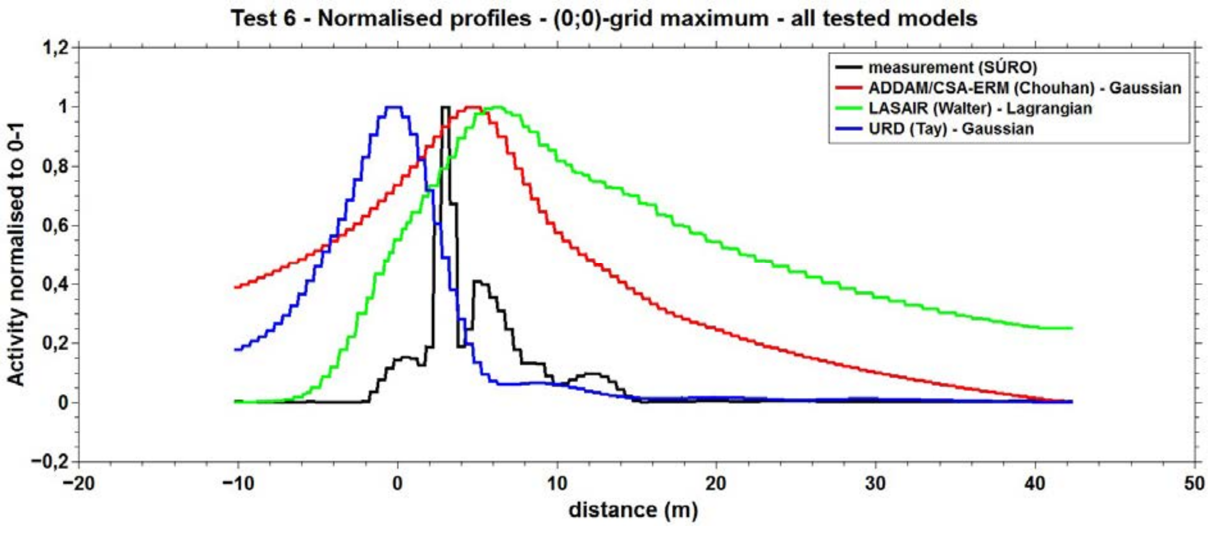

FIG. 6. Normalized profiles of the predicted deposition in comparison with the measurements for Test 6.

For Test 5, predicted profile integrals from the dispersion point through the maximum value ranged from 5.9×10^6 Bq to 1.1×10^7 Bq, a range of almost a factor of two (see Table 6 above). The measured profile integral was 7.6×10^6 Bq, within the range of the predicted values, which were a factor of 0.8–1.5 times the measured value.

For Test 6, predicted profile integrals from the dispersion point through the maximum value ranged from 4.8×10^5 Bq to 1.3×10^7 Bq, a range of about a factor of 27 (see Table 7 above). The measured profile integral was 3.4×10^6 Bq, within the range of the predicted values, which were a factor of 0.14–3.9 times the measured value. While two models (ADDAM/CSA-ERM and LASAIR) gave the same result for the profile integral for Test 6, the overall range of predictions was greater for Test 6 than for Test 5.

2.5.4. Profiles along the cloud axis

Profiles of model predictions from the dispersion point (0,0) along the measured or predicted cloud axis were developed as previously described [6]. The cloud axis was manually defined, and the profile orientation (crossing the 0,0 point) was defined in the same direction.

Figures 3 and 4 (above) show all processed data sets including the cloud axis profiles for Tests 5 and 6, for each participating model. Tables 6 and 7 (above) provide the predicted or measured profile integrals (profiles of deposited activity) along the cloud axis for Tests 5 and 6. Note that for the three models used in this exercise, the profile through the grid maximum was the same as the profile through the cloud axis for a given test. For the measurements, the two profiles were different.

Figures 7 and 8 show the normalized profiles along the cloud axis of the predicted deposition in comparison with the measurements, for all participating models. The stepped shape of the graphed lines is caused by differences in resolution between the profiles and the grid.

For Test 5, predicted profile integrals from the dispersion point along the cloud axis ranged from 5.9×10^6 Bq to 1.1×10^7 Bq, a range of almost a factor of two (see Table 6). The measured profile integral was 1.2×10^7 Bq, slightly above the range of the predicted values, which were a factor of 0.5–0.9 times the measured value. The measured profile integral along the cloud axis was about 1.6 times higher than the measured profile integral through the maximum measured activity.

For Test 6, predicted profile integrals from the dispersion point along the cloud axis ranged from 4.8×10^5 Bq to 1.3×10^7 Bq, a range of about a factor of 27 (see Table 7). The measured profile integral was 3.3×10^6 Bq, within the range of the predicted values, which were a factor of 0.14–4 times the measured value. The measured profile integral along the cloud axis was very slightly less than the measured profile integral through the maximum measured activity. While two models gave the same result for the profile integral for Test 6, the overall range of predictions was greater for Test 6 than for Test 5.

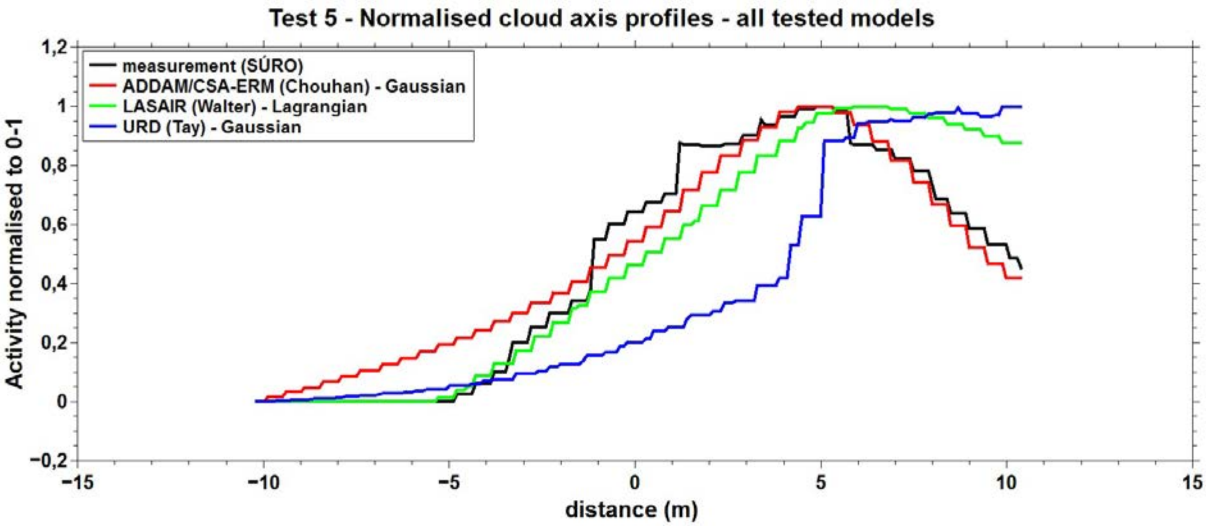

FIG. 7. Normalized profiles of the predicted deposition along the cloud axis in comparison with the measurements for Test 5.

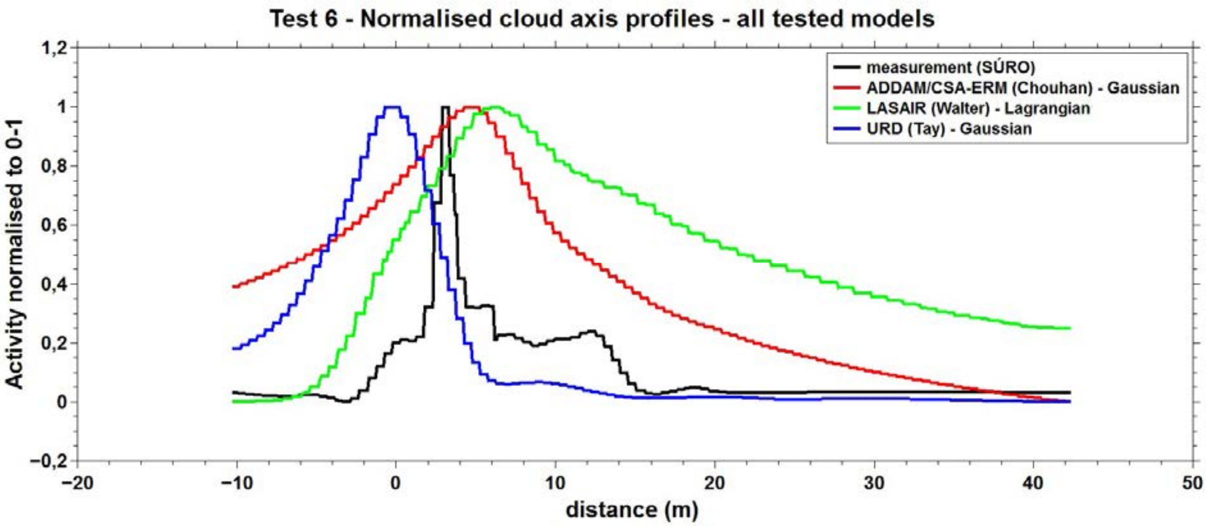

FIG. 8. Normalized profiles of the predicted deposition along the cloud axis in comparison with the measurements for Test 6.

2.6. CONCLUSIONS FROM THE SHORT RANGE ATMOSPHERIC DISPERSION EXERCISE

The short range atmospheric dispersion exercise posed considerable challenges in the modelling of dispersion and deposition from a small explosion. The explosion itself was not modelled directly; participants started with the initial cloud or plume but differed in their characterization of the initial cloud (see Table 3 above) as well as in the computational approach used to predict the dispersion of the initial cloud. Model predictions for Tests 5 and Test 6 varied considerably in the predicted angles of the plume (which direction the plume travelled) and the predicted amounts of deposited activity (the maximum values, the totals in the grid area, and the integrated values along defined profiles), although two models (ADDAM/CSA-ERM and LASAIR) gave nearly identical results for some endpoints for Test 6. Possible explanations include differences among the computational types of models, the scale (domain size) for which a model was intended, and different values selected for important parameters. There were significant differences among models in the wind speeds and wind directions used (both differences in selected values, and whether the model used averages or time dependent information), in the dry deposition velocity, and in the atmospheric stability class (see Table 3 above). Wind measurements and other meteorological data were available for heights of 2 m, 4 m, and 10 m at one location, and at 2 m for several additional locations. Two participants used only the time dependent meteorological data at a height of 10 m, while the third participant (ADDAM/CSA-ERM) used data averaged over several locations and heights. Visual comparison of plots of predicted and measured deposition, using the same coordinate system and color scale, probably provides the most useful way for an overall comparison of model predictions and measurements. For both of these tests, the plot of the measurements indicates that the plume was not stable in direction during the deposition event, and the models did not fully reproduce this effect.

3. COMPARISON OF TWO DECISION SUPPORT SYSTEMS (CERES CBRN-E, LASAIR) FOR AN URBAN AREA DISPERSION SCENARIO

3.1. INTRODUCTION

Within the context of WG2, a comparison of two decision support systems (CERES CBRN-E and LASAIR) was conducted in order to find out more about similarities and differences between these models.

3.2. THE FRENCH DECISION SUPPORT TOOL, CERES CBRN-E

CERES CBRN-E is an operational computational tool devoted to hazmat atmospheric dispersion modelling and impact assessment, gathering several source term models, various dispersion approaches (from Gaussian puff to advanced four dimensional (4-D) flow and dispersion computations) and health consequence modules adapted respectively to R-N, C or B noxious agents. CERES CBRN-E is able to compute atmospheric dispersion in complex environments including buildings (industrial sites or urban areas), assess the health consequences of the toxic releases on the population and first responders, and deliver operational results (e.g. danger zones, intervention zones) in less than 15 minutes to rescue teams and decision makers. Figure 9 shows the graphical user interface of the CERES CBRN-E Geographic Information System as well as its three dimensional (3-D) viewer.

3.2.1. Atmospheric dispersion in CERES CBRN-E

For dispersion in urban environments, CERES CBRN-E uses a Lagrangian Particle Dispersion Model developed by ARIA Technologies and the CEA. The model is called 'PMSS' for Parallel Micro Swift Spray.

PMSS embedded in CERES CBRN-E is a 3-D Lagrangian particle dispersion model which simulates the transport, dispersion, and dry and wet deposition of airborne chemically inert species released in complex meteorological conditions (low wind speed, flow over complex topography), often marked by spatial and temporal inhomogeneities of the meteorological diffusive variables (e.g. vertical wind shear, breeze due to the presence of terrain discontinuities). In addition, it is also possible to reproduce the dispersion of particulate releases, taking into account the gravitational vertical settling phenomenon. The P-SPRAY model can simulate releases from point, area or line, continuous and discontinuous sources, as well as exploit the available wind and turbulence measurements provided by advanced meteorological instruments [11]. P-SPRAY can compute mean and instantaneous concentrations on a 3-D grid defined by the user [11].

The velocity of the particles is mainly characterized by two components: a mean component, or 'transport component', which is defined by the mean velocity of the local wind, and a stochastic component, simulating the dispersion and reproducing the atmospheric turbulence. Mean values for wind speed are computed by another model, which is external to the code, and which is able to build 3-D fields, taking into account the presence of topography.

P-SPRAY is able to take into account the presence of obstacles, represented by filled cells of the meteorological grid, by using the P-SWIFT model as a meteorological preprocessor [12] to perform simulations at microscale with a smallest resolution of 3 meters. In these conditions, particles are also reflected at the obstacle 'facades'.

(a)

(b)

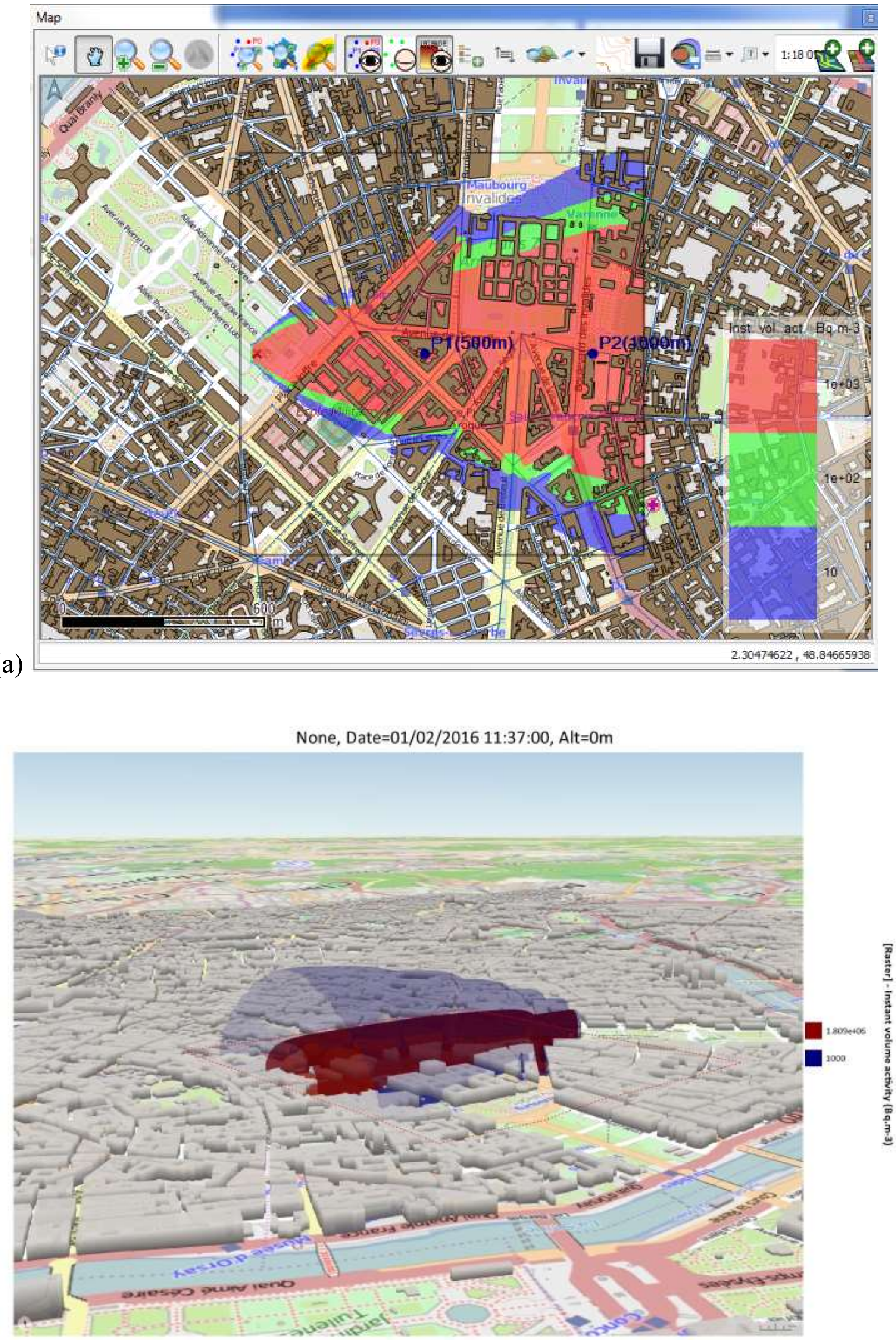

FIG. 9. Geographic Information System (a) and 3-D CERES CBRN-E viewer; (b) show the results of a fictitious radioactive dispersion.

Wind fields are generated by P-SWIFT, which is a 3-D wind field model for complex terrain. It produces a mass-consistent wind field using data from a dispersed meteorological network. Temperature and humidity fields can also be interpolated. Figure 10 shows an example of a wind field calculated by P-SWIFT at two heights (9 m and 24 m) in Paris.

P-SWIFT is designed to rapidly compute wind fields from on-site observations. These comply with the first Navier-Stokes equation [13], the mass conservation, to account for terrain effect on the flow structure. The influence of atmospheric stability on wind flow over terrain is modelled using a weighting factor alpha (ratio of the horizontal wind component to the vertical wind component). If obstacles such as buildings are included in a local scale simulation, their influence is modelled using a first guess prescription of the flow structure, and then mass consistency and impermeability are applied.

3.2.2. Explosion module in CERES CBRN-E

CERES CBRN-E uses a preprocessor to deal with the source term released into the atmosphere from the explosion time to the cloud stabilization time. The explosion effect is to release mechanical and thermal energy causing ejection of materials. As surrounding air is carried along, the cloud reaches a stabilized state. From this moment, cloud development no longer depends on the energy provided by the explosion. Subsequent dispersion of the cloud is simulated by the dispersion code PMSS.

The stabilized cloud is represented by a sphere on top of a cylinder, with dimensions depending on the height reached by the cloud. The stabilization height depends on atmospheric stability, which is determined by the temperature profile (given by a meteorological mast, a rawinsonde or a weather prediction code). This profile sets a vertical grid of the atmosphere.

In order to take into account the wind blowing in the time period between an explosion and stabilization, the cloud is cut out in layers defined by the meteorological vertical grid. In each layer, wind velocity and wind direction are known by observations or 3-D model output. Layers are moved using local wind conditions. The displacement, a component in the logarithmic wind profile shifting the increase of the wind speed to higher levels, takes into account topography and the presence of obstacles as the 3-D wind field integrates these effects.

3.3. THE GERMAN DECISION SUPPORT SYSTEM, LASAIR

An existing system program, LASAT [14, 15], based on Lagrangian Particle Simulation, was adapted to for a dirty bomb scenario. Conducted by the German Federal Office for Radiation Protection (BfS) and under the direction of the German Federal Ministry for Environment, Nature Conservation, and Nuclear Safety (BMU), the program LASAIR (Lagrangian Simulation of the Dispersion and Inhalation of Radionuclides [16–19]) was developed to provide an initial, rapid overview of atmospheric dispersion, deposition, ground activity, and different exposure pathways (inhalation, ground and cloud shine) after an instantaneous release of radioactive material.

The program can be used by radiation emergency authorities that are responsible for emergencies within the different German States or to other users performing tasks within radiation protection. The program was developed in the year 2000 and has been continuously upgraded since then. The model LASAIR in its latest version is able to simulate an explosion of a radiological dispersion device (RDD) with additional radioactive material and computes the dispersion in the planetary boundary layer. In order to assess the dose to the population, the inhalation, ground and cloud shine doses to individuals can be computed. The model has been introduced as a rapid decision support system within the German Federal Office for Radiation Protection (BfS) and authorities in Federal States in Germany.

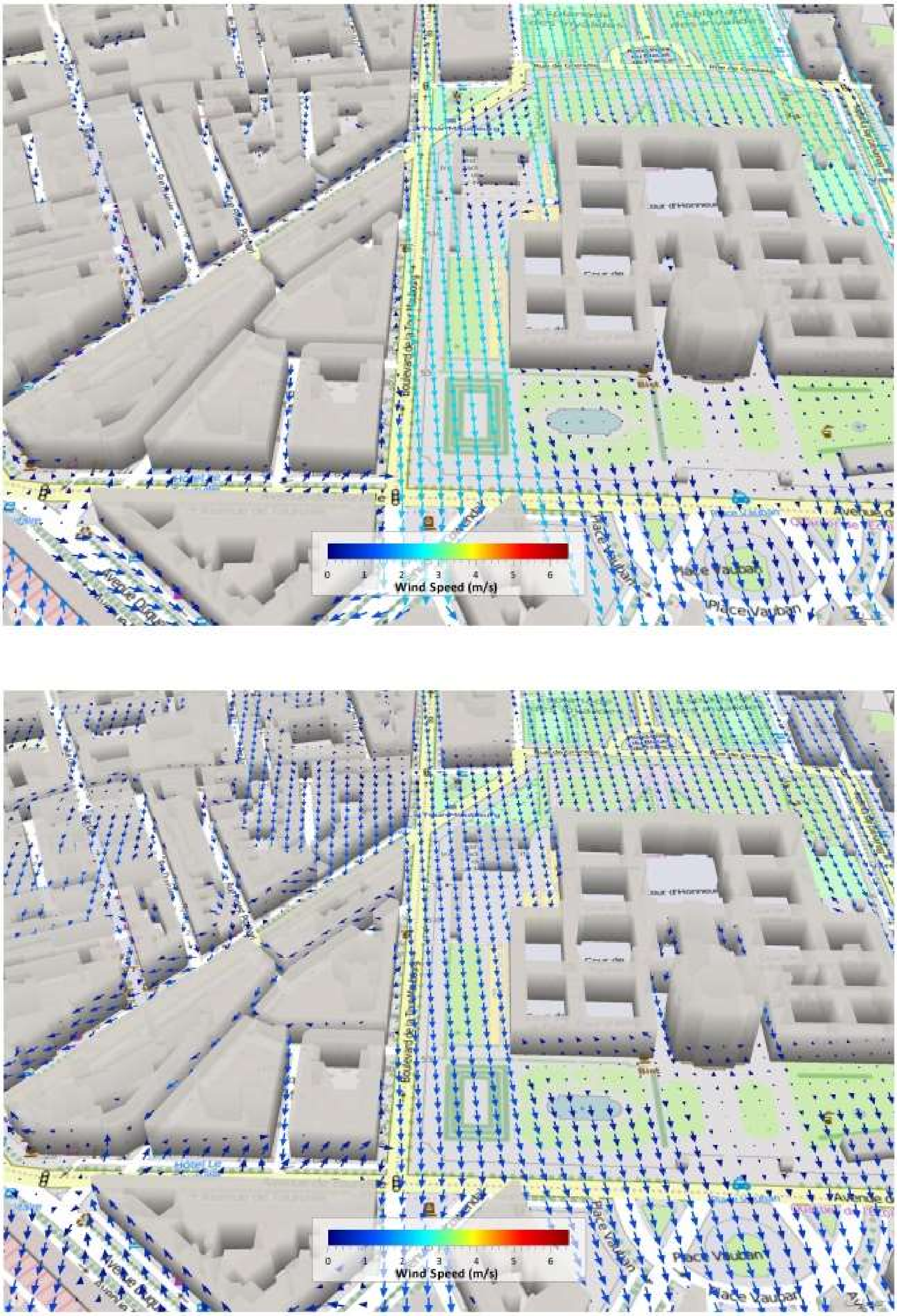

(a)
(b)

FIG. 10. Mass-consistent diagnostic wind field calculated by P-SWIFT for a part of the domain (Paris) and for two heights: (a) 9 m and (b) 24 m.

3.3.1. LASAIR Features

Special attention has been directed to the usage of the program in emergency cases. The program can be run on a (high end) laptop, is extremely easy to handle, and allows the user a strict straightforward step-by-step usage only in order to grant maximum security feeding the program with data input.

The model needs only basic meteorological input, such as:

- Wind speed and wind direction;
- Stability class;
- Roughness length in the vicinity;
- Amount of explosives;
- Radionuclide and activity.

The results of the calculation are activity concentration, deposition, ground shine, cloud shine, inhalation dose and time dependent information (activity, dose) in different scales.

The latest version of LASAIR (Version 5.1.20, April 2020) includes the following additional features:

- Actual mesoscale turbulence parameterization (harmonized in Germany)
- Verification according to radioactive dispersion experiments with ^{99m}Tc;
- Consideration of radioactive half-life;
- More release scenarios (fire, releases with momentum, long lasting releases);
- Worldwide orography and individual topography;
- Rapid online integration of urban structures;
- Use of Open Street Maps for EU or worldwide operation.

3.3.2. Actual Turbulence Parameterization

In Germany, the VDI (Verein Deutscher Ingenieure, Association of German Engineers) strongly supports the idea of harmonization in different aspects. One aspect is to develop state of the art standards for the turbulence parameterization in mesoscale dispersion models. In the course of 2014 the basic work for a new turbulence parameterization based on measurements at a weather mast close to the city of Hamburg (in the northern part of Germany) was completed. This parameterization resulted in a guideline that is applicable for all modellers [20]; the final version of the guideline was published in 2017. This guideline, which has set a standard in Germany as well as in other countries, is used in different dispersion models and thus harmonizes their output. The new turbulence parameterization has been implemented in LASAT and therefore in LASAIR, ensuring that the scientific improvement is available for model users.

3.3.3. Integration of Urban Structures

The application of the decision support system LASAIR is aimed especially for use within urban areas. This area is dominated by buildings of different height and dimensions, which will influence the wind flow as well as the dispersion. In order to consider both effects, a new procedure was implemented in LASAIR. Using OSM (Open Street Map[3]) LASAIR has a special menu that allows loading specific maps from OSM servers in different scales and preparing them for use within the program. After loading of the maps, the user can define different buildings in the centre of the area viewed online (see Fig. 11) within the program through a few mouse clicks. This is quite a simple method, but together with the mass-consistent flow model in LASAIR (lprwnd), it becomes a powerful tool to study effects triggered by the buildings, which can now be studied in more detail. Figures 12 and 13 show examples of wind fields and model output.

The online integration of urban structures into the simulation with LASAIR offers the opportunity to study the effects of buildings on the atmospheric dispersion as well as giving a better picture of the dispersion as influenced by buildings, for example, regarding affected areas or where measures have to be applied in an emergency. The definition of the buildings on the basis of Open Street Maps is completed within a few minutes.

After more than a decade of development, LASAIR has proven to be a simple but sophisticated tool for the assessment of a dirty bomb scenario. Further applications of LASAIR in a scientific context have also been made within the MODARIA project, including study of additional explosion experiments in the Czech Republic (see Section 2 of this publication) and of routine releases from a conventional power plant in Slovenia (see Section 4 of this publication).

3.4. COMPARISON OF CERES CBRN-E AND LASAIR

3.4.1. Scenario description

In order to test and compare the models, a scenario in a dense urban area (Paris, France) was defined. One gram [g] of inert aerosol was assumed to be released in the street 'Rue Jean Nicot' at the center of Paris (see Fig. 14).

An academic meteorological situation was used for the simulation of atmospheric dispersion. The wind was assumed to come from the north with a speed of 1 m/s measured at 10 m height. The atmospheric stability situation, slightly unstable, corresponds to Class C of Pasquill stability classifications. The weather was assumed to be dry (no rain). The temperature was 20°C and humidity was 70%. For LASAIR, the roughness length z_0 was assumed to be z_0 = 2.0 m in general for the Paris area and z_0 = 0.1 m for two defined areas in the vicinity of the release point (Champ de Mars and Parc des Invalides). The source term release was assumed to be composed of aerosols with an aerodynamic diameter less than 10 µm.

Two scenarios were studied:

(1) A continuous release for 10 minutes from a stack of 5 meters height and with a horizontal release area of 0.8 m²;
(2) A release due to 1 kg of explosives.

[3] See https://www.openstreetmap.org

(a) 

(b) 

FIG. 11. Definition of buildings (cubic elements) based on OpenStreetMaps in LASAIR at the site; (a) top view; (b) 3-D view.

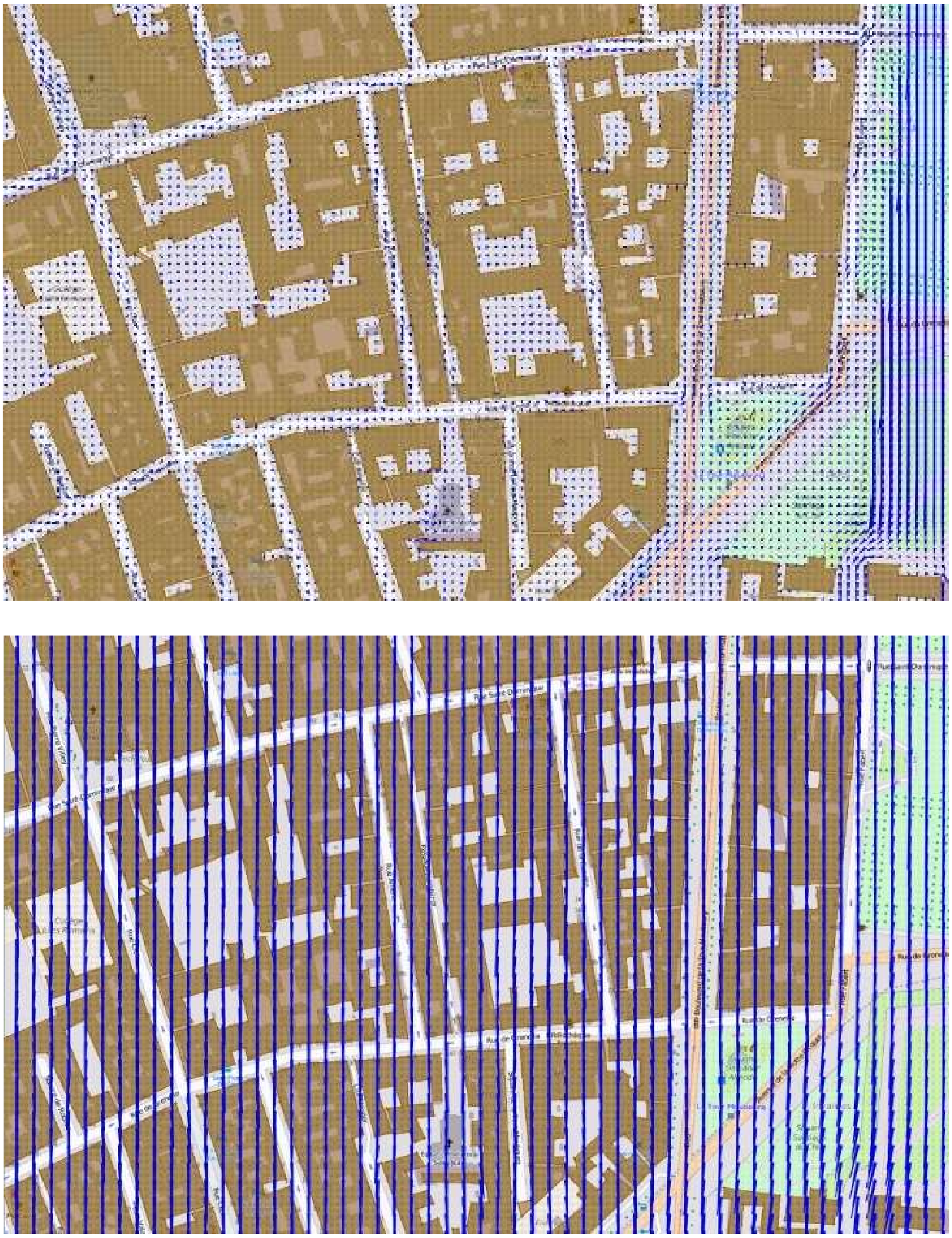

(a)

(b)

FIG. 12. Mass-consistent diagnostic wind field calculated by LASAIR for a part of the domain (Paris) and for two different height intervals: (a) 0–3 m and (b) 16–25 m.

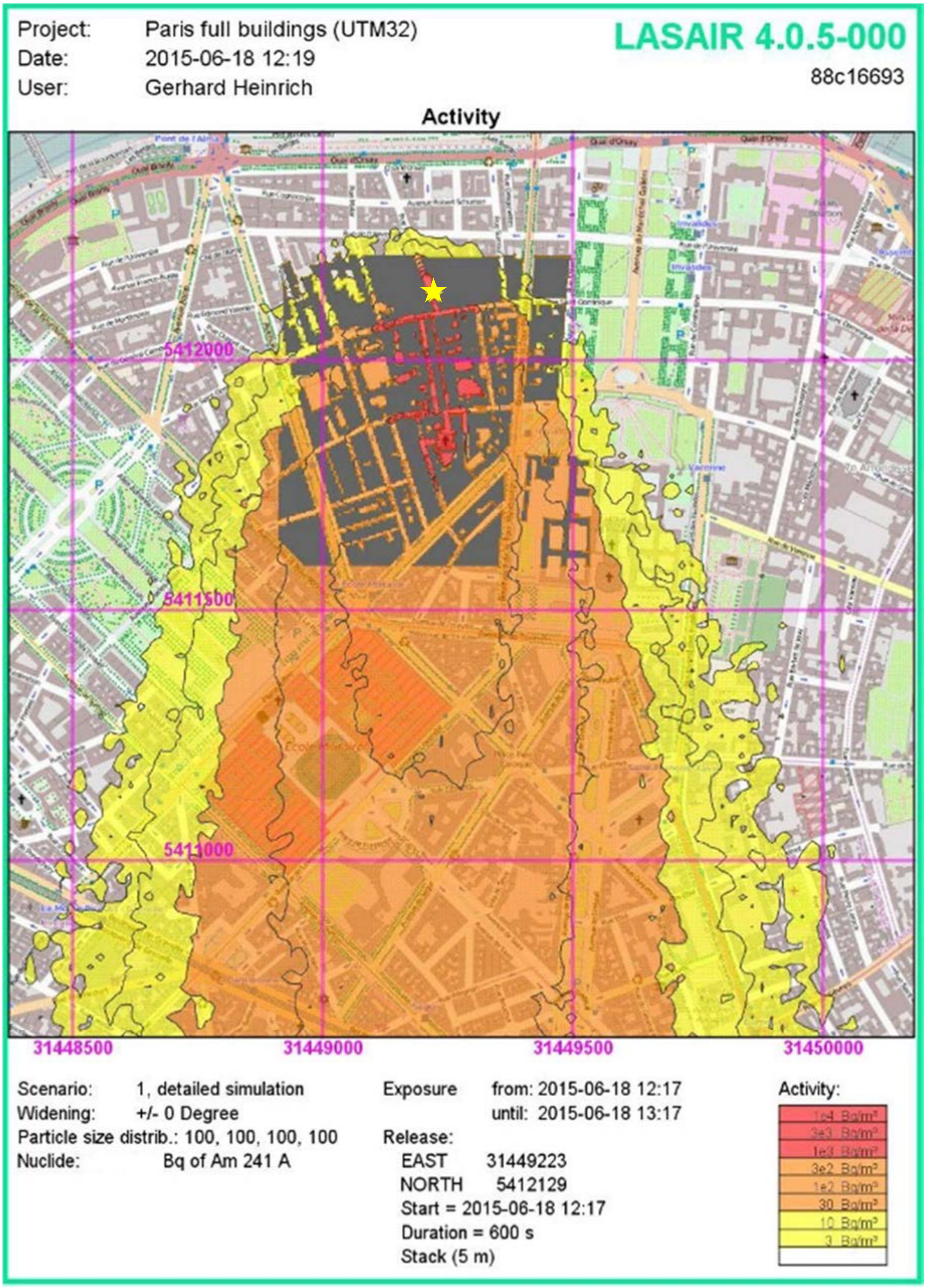

FIG. 13. Graph for decision makers giving essential information on the radiation exposure (here shown in terms of activity) after the simulated release. The release site is marked with yellow star.

FIG. 14. Map of the center of Paris. The release takes place in Rue Jean Nicot. Five receptors are located downwind of the release.

In order to compare the models, five receptor points were selected downwind from the release point in the model domain. The downwind distances from the release point are:

Receptor 1 120 m;
Receptor 2 220 m;
Receptor 3 420 m;
Receptor 4 810 m;
Receptor 5 1430 m.

3.4.2. Scenario model input

The source location is Paris. The coordinates of release in UTM-WGS84 are x = 449 223 m and y = 5 412 118 m (Zone 31).

Name of the road: 'Rue Jean Nicot', 25 m north of crossing with 'Rue San Dominique'. The area is significantly affected by houses in the vicinity.

3.4.3. Source term

The source term is assumed to be 1 g of radionuclide X (a specific radionuclide is not named for classification reasons), released in the form of aerosols or liquid, AED < 10 µm (everything is respirable). Two scenarios were used:

(1) Continuous release for 10 min (stack, height 5 m, horizontal release area 0.8 m^2);
(2) Explosion with 1 kg explosives, dimensions of initial volume to be compared:
   - CERES, a cylinder with dimensions d = 16 m and h = 37 m, resulting in a volume V = 7439 m^3,
   - LASAIR, a cube with dimensions 17 m × 17 m × 28 m, resulting in a volume V = 8092 m^3.

It is important to note that the height of the cylinder in LASAIR is considerably lower (by 9 m) than the height in CERES, which is expected to lead to slightly higher concentrations near the ground for the LASAIR results (see Fig. 16 below).

3.4.4. Meteorological data

The following meteorological data were specified for the exercise:

— Stability: Slightly unstable, Pasquill Class C (slightly unstable);
— Wind direction: 0°N;
— Wind velocity: 1 m/s (at 10 m height);
— Dry weather, no rain;
— Air temperature: 20°C;
— Hygrometry: 70%;
— Roughness length:
  z0 = 2.0 m in general for the Paris area, except for the local model domain with buildings, and
  z0 = 0.1 in two defined areas (Parc de Champ de Mars, Parc des Invalides).

3.4.5. Model domain

The following model domains were used for this exercise:

— CERES: model domain 5 × 5 km^2, with a grid resolution of 3 m;
— LASAIR: model domain of 10 × 10 km^2, with a maximum of 40 × 40 km^2 and a finest grid resolution of 5 m. The release point was specified as the center of the domain. Building heights were assumed to be constant at 15 m.

3.4.6. Number of particles / Time for computation

The following particle numbers were specified for this exercise, along with the corresponding computational time needed:

— CERES: 1 000 000 particles, taking approximately 5 minutes with a 15 core computer.
— LASAIR: 500 000 particles, taking approximately 6 minutes with a 4 core PC (standard office PC).

3.5. RESULTS OF THE COMPARISON

Figures 15 and 16 show the results of the two models, CERES and LASAIR, for the activity at different downwind locations (Receptors 1–5) during selected time intervals. The results for the model CERES are shown in blue, and for LASAIR in red.

Scenario 1, a continuous release (stack with 5 m height) and predicted activities at different receptor sites

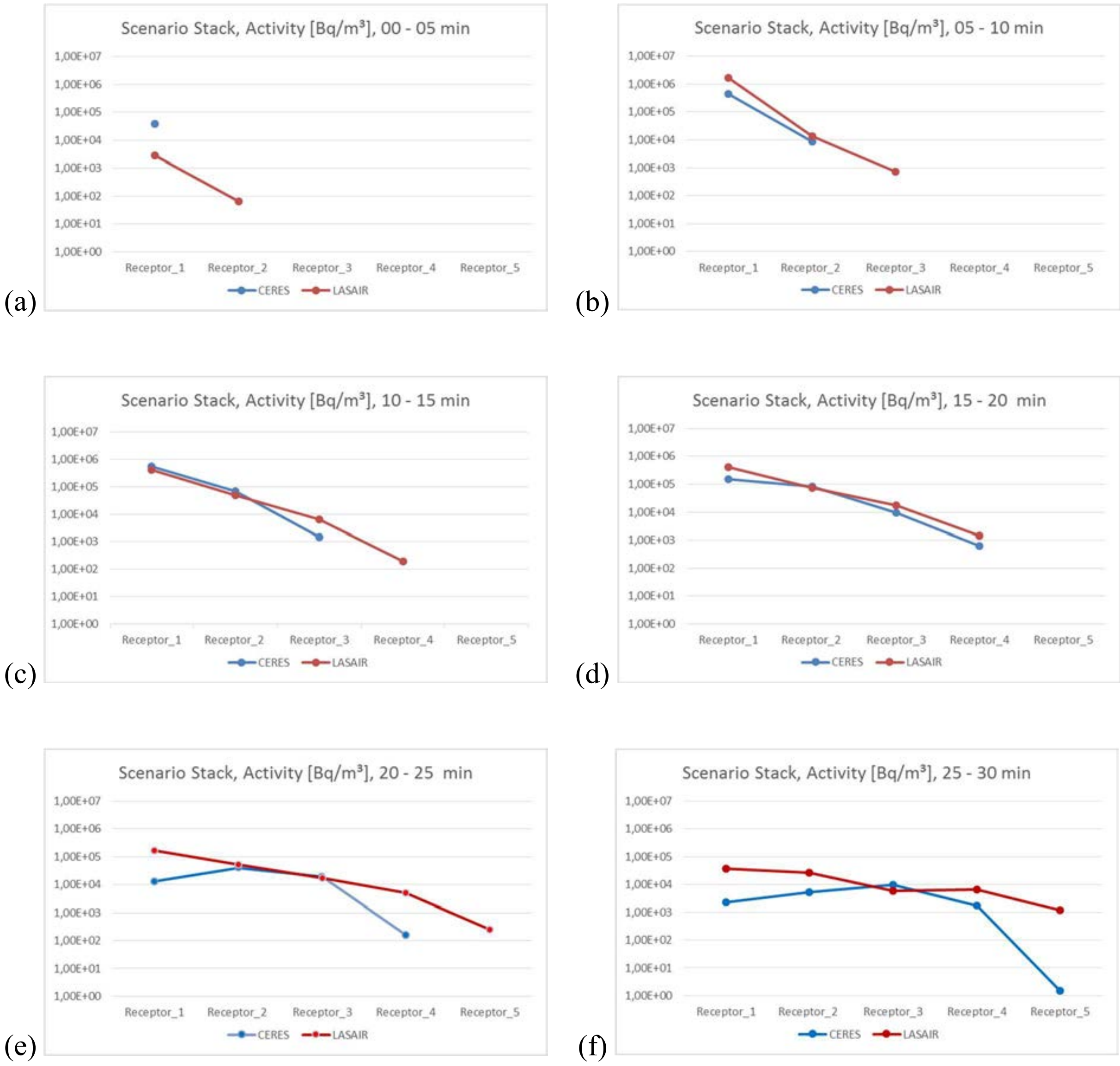

FIG. 15. Results for Scenario 1, a continuous release (stack with 5 m height); activity concentrations (Bq/m³) for different time intervals from 0 to 30 minutes: (a) 0–5 minutes; (b) 5–10 minutes; (c) 10–15 minutes; (d) 15–20 minutes; (e) 20–25 minutes; (f) 25–30 minutes. Predictions for CERES are shown in blue, and for LASAIR in red.

Scenario 2, an explosion and predicted activities at different receptor site

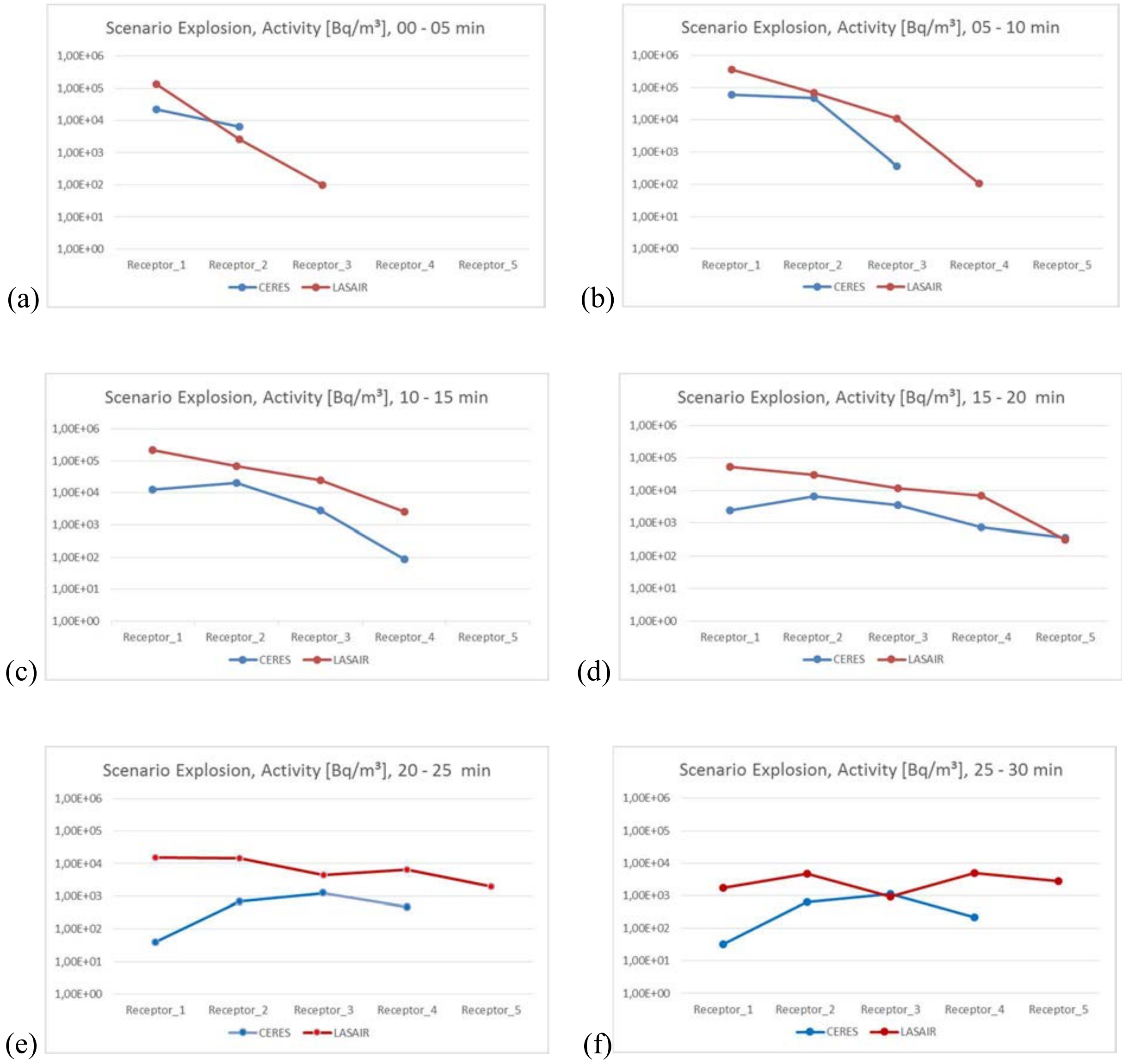

FIG. 16. Results for Scenario 2, an explosive release; activity concentrations (Bq/m³) for different time intervals from 0 to 30 minutes: (a) 0–5 minutes; (b) 5–10 minutes; (c) 10–15 minutes; (d) 15–20 minutes; (e) 20–25 minutes; (f) 25–30 minutes. Predictions for CERES are shown in blue, and for LASAIR in red.

3.6. DISCUSSION

Both models, CERES and LASAIR, can be used to compute the dispersion downwind and take into account the building wake effects. The general downwind dispersion, as well as the additional dispersion due to the mechanical turbulence, are reflected by the results.

The two models differed in the grid resolutions (CERES 3 m and LASAIR 5 m), assumed heights of buildings, and for the second scenario, the height of the initial cloud from the explosion. However, it is assumed that the height of the cloud has only small effects on the results, since the assumed volumes of the initial cloud are similar.

As shown in Fig. 15 (a)–(f), both models have rather similar results for the first (stack) scenario. They differ only in the results for the time interval 0–5 minutes; this can be explained by different building heights assumed within CERES and LASAIR, which causes a different roughness length and corresponding different wind speeds. For CERES, receptors 2–5 are not affected during the first time interval (0–5 minutes), whereas LASAIR already simulates some activity at receptor 2 during that interval, which can be explained by the lower height of the source term in LASAIR. The same applies for time intervals 20–25 and 25–30 minutes, where CERES tends to predict smaller activities at both receptor 1 and receptor 5.

For the stack scenario, when the quotients of the results from the two models (CERES / LASAIR) are compared at different receptor locations, the values range from 1.11 (best agreement) to 0.0303, were LASAIR computes the higher activities (factor of 33). In general the results for the activities are in very good agreement between the two models.

For the explosion scenario (see Fig. 16 (a)–(f)), one expects larger differences between the models because the instantaneous release is much more difficult for the dispersion models to handle. For example, the explosion modules used by the models are based on different assumptions but have been trimmed for this scenario to give almost the same initial volume for the source term (7439 and 8092 m^3 for CERES and LASAIR, respectively). This will lead to smaller changes in the results for both models, especially in the short term phase (0–5 minutes) of the simulation. In addition, the explosion modules do not take into account obstacles (buildings) in the vicinity of the area of the explosion, which causes different effects in the results of the two models, something that has to be investigated in more detail in the future. Within this context the results for the models are in good agreement for time intervals 0–5 to 15–20 minutes, but differ more significantly for the last two intervals (20–25 and 25–30 minutes). For these intervals CERES in general computes considerably lower results than LASAIR, except for one receptor location (receptor 3, 25–30 minutes). This might be explained by the lower height of the initial volume of the source term applied in LASAIR, as this leads to higher activity concentrations close to the ground where the receptors are located.

For the explosion scenario, when the quotients of the results from the two models (CERES / LASAIR) are compared at different receptor locations, the values range from 1.20 (best agreement) to 0.0026, where LASAIR again computes the higher activities (factor of 384).

In general, the results of the activities in this urban scenario are in good agreement between the two models. This comparison indicates the applicability of up-to-date atmospheric dispersion models and the necessity to include the effect of urban buildings for decision support systems. It also shows that urban dispersion modelling provides far more realistic results than Gaussian models, with only slightly increased computation times. This is an essential result for the application of these decision support models in the context of radiation protection for the public.

4. MID-RANGE ATMOSPHERIC DISPERSION EXERCISE

4.1. INTRODUCTION TO THE ŠOŠTANJ SCENARIO

To assess the effect of nuclear facilities on the air and the population in a region, it is of key importance to understand and appropriately model the dispersion of atmospheric releases of radionuclides. This section is focused on the validation of various dispersion models. The validation in this case is understood as a comparison of the model results with the results measured in nature within the relevant experiment (see Fig. 17 below).

To assess potential exposures of a population from nuclear facilities, focus has been placed on cases where the nuclear power plant is situated in a relatively close vicinity to populated areas, which is a common situation. The first direct exposures of the population to radiation would usually occur through releases to the atmosphere. Therefore, a correct understanding of these phenomena is of key importance in identifying appropriate protective actions. Focus is placed on protective actions in the case of a nuclear or radiological emergency, but it is important to note that atmospheric dispersion modelling can also be used to optimize or reduce environmental exposures to routine discharges of radionuclides.

It is of key importance to compare the modelling results with the measured actual state of the relevant event in a natural environment. The objective of this exercise was to search for measurement data from a tracer experiment, which would cover the dispersion of contaminants from a point source (release from the chimney) over complex terrain. An area within a few tens of kilometres from the source of the contamination was considered. The experiment has to include detailed meteorological data, as well as data on releases and subsequent concentrations in the region (the principle of a controlled experiment). It is also essential that the experiment has a minimum of disruptions, such as releases of the same pollutants from uncontrolled sources.

Data sets that use radionuclides as a tracer are difficult to obtain. Not even data recorded at the Chernobyl and Fukushima accidents fulfill what is needed, since they contain too many shortcomings in all three aspects (meteorology, releases, environmental concentrations). However, there are data available from the Šoštanj campaign in 1991, which fulfill most needs and enable a comparative validation of various models.

The Šoštanj measurement campaign is a set of measurement and other data, describing three weeks of detailed monitoring of SO_2 releases from the Šoštanj thermal power plant in Slovenia (TPPŠ). In effect, the data provide a tracer experiment for the dispersion of contamination from point sources — thermal power plant chimneys — to the surrounding area, where small settlements and two towns are scattered over a complex terrain. The meteorological data were measured in half hour intervals at several ground based weather stations which comply with the WMO standards, and additionally with the SODAR (Sonic detection and ranging, vertical wind profiler), which is key for the quality of data. The data on SO_2 releases were measured automatically in half hour intervals directly in the thermal power plant chimneys, while data on SO_2 concentrations in the region were measured automatically in half hour intervals at modern measuring stations, positioned on key spots in the area.

During 1991 the thermal power plant was not yet equipped with wet desulphurization units, so the SO_2 concentrations were very high and subsequently very easily measurable with a minimal error of measurement. All other small sources in the area were a few classes smaller than the power plant and therefore did not disturb the tracer experiment. The meteorological conditions included relatively simple patterns of contaminant dispersion, as well as very complex patterns.

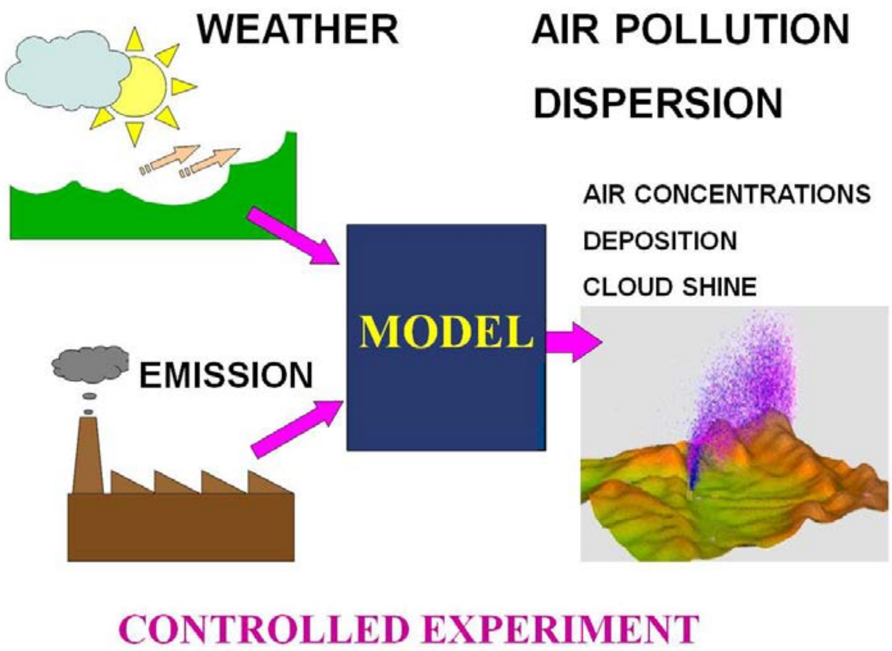

FIG. 17. Diagram of the modelling system summarizing what input and output data are needed for a controlled experiment about dispersion of atmospheric releases of radionuclides.

The model testing exercises within the MODARIA Programme therefore included two meteorological situations:

(1) The first situation was simple, with a strong wind blowing directly from the chimney towards one of the measuring stations on top of a hill in the near surrounding area.
(2) The second situation was a complex situation with night temperature inversion, the deposition of pollutants under the inversion and the convective mixing on the following day, which almost simultaneously polluted the measuring stations in the surroundings of the thermal power plant at very different locations and in different directions.

The primary objective of testing the models with these validation data was to understand the applicabilities of particular models, the conditions for which they can be used, and the approximate spatial and time error of the models in the representation of the dispersion of the cloud of contamination over complex terrain. For this purpose, a special method of evaluation has been used, which enables the assessment of the spatial and time error.

This testing is very valuable, because it deals with real measured situations over complex terrain, which is rarely the case in tracer experiments. Yet many nuclear facilities in the world are located on more or less complex terrain and consequently in complex meteorological conditions, so testing over flat terrain alone would not be sufficient.

In the following sections, a description of the Šoštanj measuring campaign, the available data, the models used in the exercise, the modelling results, and conclusions from the exercise are provided.

4.2. OBJECTIVE OF MODEL VALIDATION

Validation of an atmospheric dispersion model is an important process. It determines the performance and efficiency of the model in well defined conditions [21]. Conditions include the type of terrain orography (flat or complex), the size of the domain (local, regional, continental, or global), the number of grid cells in the domain, the meteorological conditions (strong or weak winds, etc.), and the types of releases (stacks, traffic, domestic heating). Ideally, the results of validation give good guidelines as to how, where and when a model can be successfully applied.

Validations over complex terrain are still very rare. They are very important for the research community and for governmental environment agencies. The research community uses the results for further development and improvement of modelling techniques, and environment agencies use the results for design and implementation of regulatory policies.

A study has been made to improve traditional atmospheric contaminant model validation methodology by upgrading the methodology to estimate inaccuracy in position and time. The new validation methodology has been demonstrated using the Šoštanj validation set.

4.3. METHODOLOGY

4.3.1. Traditional validation methodology

Traditional validation methodology for atmospheric contaminant modelling is based on statistical comparison between measured and reconstructed data about air contaminant concentrations in an environment. In the atmospheric contaminant model, usually an area of interest consists of a grid of cells where each cell describes an average air contamination situation in a certain part of the domain (e.g. in the study case presented in Section 4.4, the domain is split into 100 × 100 cells in the horizontal direction and 20 layers in the vertical direction, which gives 200 000 cells for the domain). For the comparison, the reconstructed average concentration from the ground cell where the measuring station is located is taken. An example is presented in Fig. 18.

Statistical analysis of data is performed for a selected time interval where measured and reconstructed data are available. For this time interval, a set of data patterns needs to be prepared. Each data pattern from this set consists of a pair of measured and reconstructed concentrations obtained at time step *t* as presented in Eq. (1):

$$\{C_{meas}(t), C_{recon}(t)\} \tag{1}$$

Using traditional validation methodology, the most common statistical indexes are determined: the correlation coefficient (r), root mean square error (RMSE), mean fractional bias (MFB), FACTOR2, mean square error (MSE) and the coefficient of determination (R^2).

Definitions of variables and functions for determination of statistical indexes are as follows:

Cmeas(t)	measured concentration at time step *t*;
Crecon(t)	reconstructed concentration at time step *t*;
$\hat{C}meas$	average measured concentration;
$\hat{C}recon$	average reconstructed concentration;
σC	standard deviation of (measured or reconstructed) concentrations;
t	time step index;
T	length of full time interval (number of measured concentrations).

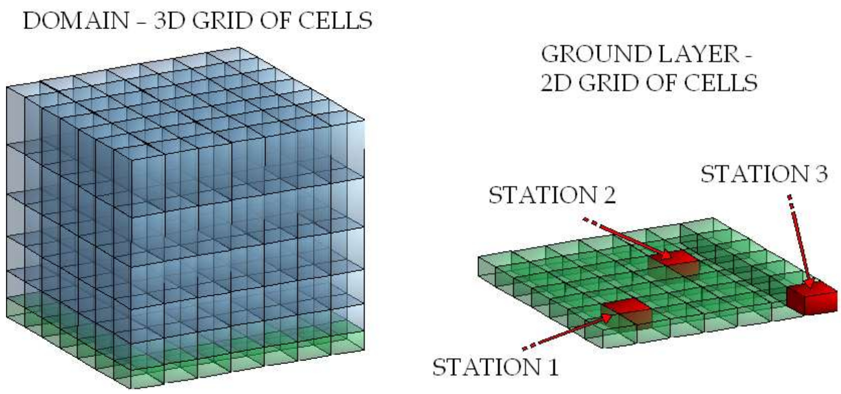

FIG. 18. The domain split in a 3-D grid of cells is presented on the left side, showing the ground layer coloured in green. On the right side only the ground layer is presented; cells where stations are located are highlighted in red.

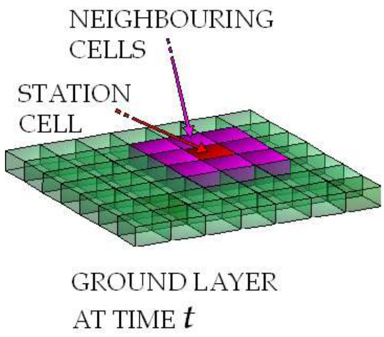

FIG. 19. Example of neighbouring cells in position (ΔH = 1), where the set of neighbourhood concentrations (NC) consists of 9 cells.

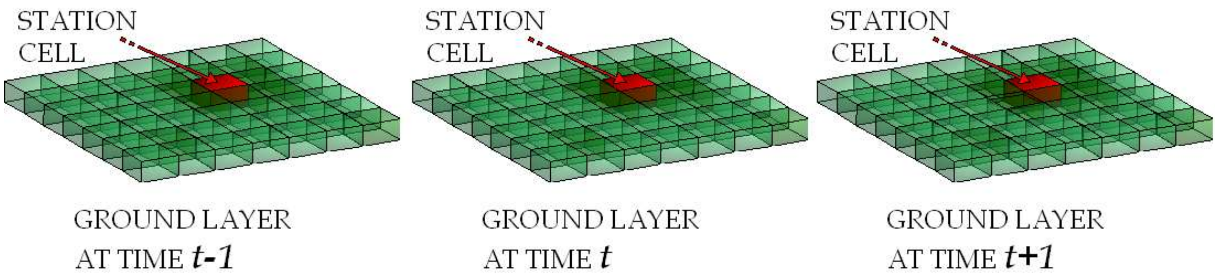

FIG. 20. Example of neighbouring cells in time (ΔT = 1), where the set of neighbourhood concentrations (NC) consists of 3 cells.

4.3.2. Enhanced validation methodology

Differences between measured and reconstructed concentrations are caused by measuring errors, inherent uncertainty, input uncertainty and model formulation error. It was determined that inaccuracy in position and time exists in the model [22]. To estimate these inaccuracies, an enhanced validation methodology is presented which uses additional reconstructed ground level concentrations in neighbouring cells of the cell where a station is located. During enhanced validation, each measured value is compared with one reconstructed concentration selected from a set of reconstructed concentrations. The set of these reconstructed concentrations NC (neighborhood concentrations) as described in Eq. (2) consists of the average concentrations in the cell where the station is located and in neighbouring cells. Neighbourhood is defined in terms of position (space) and time scale. In other words, for the neighbourhood of 1 cell in terms of position, a set of 9 cells has been created, as presented in Fig. 19 and Eq. (3). For the neighborhood in terms of time scale, the neighborhood consists of 3 time intervals (the time interval of interest and the preceding and following time intervals) as presented in Fig. 20 and Eq. (4).

$$NC(t,m,n) = \begin{Bmatrix} C_{recon}(t,m,n); \\ t - \Delta T < t < t + \Delta T; \\ m - \Delta H < m < m + \Delta H; \\ n - \Delta H < n < n + \Delta H \end{Bmatrix} \tag{2}$$

Definitions of variables for determination of the set of neighbourhood concentrations NC:

NC is the set of reconstructed concentrations in the neighbourhood of the station;
t is the time step index;
ΔT is the length of neighbourhood in time scale (number of time steps);
m is the index (number) of cell in east-west direction;
n is the index (number) of cell in north-south direction;
ΔH is the length of neighbourhood in position (space) (number of cells).

$$NC_{position}(t,m,n) = \begin{Bmatrix} C_{recon}(t,m,n); \\ m - \Delta H < m < m + \Delta H; \\ n - \Delta H < n < n + \Delta H \end{Bmatrix} \tag{3}$$

$$NC_{time}(t,m,n) = \begin{Bmatrix} C_{recon}(t,m,n); \\ t - \Delta T < t < t + \Delta T \end{Bmatrix} \tag{4}$$

Finally, in the enhanced validation methodology, each measured value is compared with one reconstructed concentration selected from a set of neighbourhood concentrations NC. From this set of reconstructed concentrations, one concentration $C_{BMrecon}$ is selected using a best matching function according to the measured concentration as described in Eq. (5):

$$C_{BMrecon}(t,m,n) = BM(NC(t,m,n)) \tag{5}$$

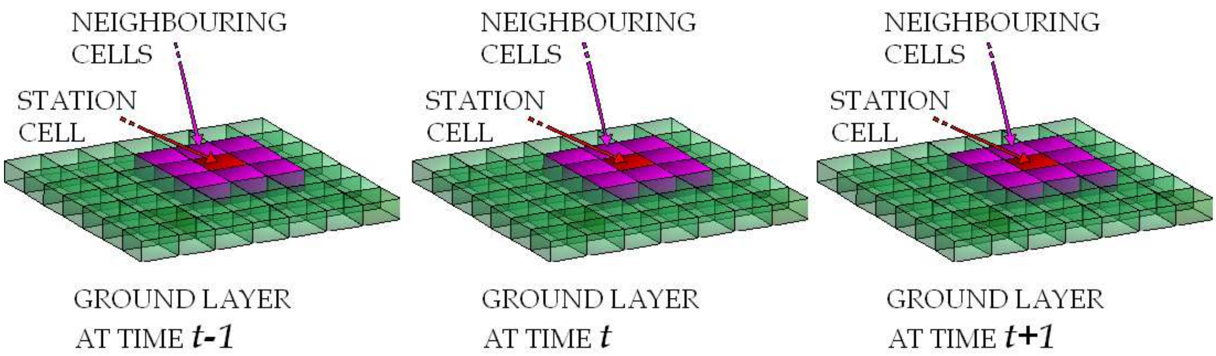

FIG. 21. Example of neighbouring cells in position and time ($\Delta H = 1$ and $\Delta T = 1$), where the set of neighbourhood concentrations (NC) consists of 27 cells.

The best matching function selects one element from the set NC where the difference between this element and the measured concentration is lowest compared to other elements in the set NC. The combination of time and space neighbourhoods is shown in Fig. 21.

4.4. ŠOŠTANJ CASE STUDY

The presented method is demonstrated using a field data set from a complex terrain. The following subsections describe a set of field data from the Šaleška region of Slovenia. This data set has been chosen for several reasons:

(1) The complex terrain of the region, in which all typical complex terrain meteorological conditions occur [22, 23].
(2) High releases from a thermal power plant, which were about 100 000 tons of sulphur dioxide (SO_2) and 12 400 tons of nitrogen oxides (NO_x) per year [24], because no desulphurization plant had yet been installed. These high releases represented the main source of atmospheric SO_2 contamination in the region, where ambient SO_2 concentrations higher than 1 mg/m^3 were measured at surrounding automatic environmental measuring stations. All other local sources of atmospheric SO_2 contamination can be practically neglected for this reason. The experimental campaign had therefore been organized as a tracer experiment.
(3) The availability of all measured data from the automatic environmental measuring stations and the release station for the whole period of the measuring campaign. The database is described in a final report [24], which was made available to MODARIA WG2 participants.

4.4.1. Description of the 'Šoštanj91' field data set

An experimental measuring campaign (Šoštanj91[4]) was performed in the spring of 1991, i.e. from 15 March 1991 to 5 April 1991, in the area surrounding the thermal power plant Šoštanj (TPPŠ). The main purpose of the campaign was determination of the environmental impact of the atmospheric SO_2 contamination from the three stacks of the thermal power plant. The emphasis was on the meteorological conditions that cause severe air contamination episodes.

---

[4] See http://www.meis.si/tes-campaign91/indexe.html

TPPŠ is located in the centre of Šaleška valley, as presented in Fig. 22. In the central part of Šaleška valley there is a plain, located north of the Paka River. The average altitude of the valley is three hundred meters above sea level. The valley is surrounded by hills on the south side and by high mountains (Karavanke Alps) on the west, north and east side. There are two towns and several small villages in the valley and its surrounding area, where approximately 36 000 people lived at the time the campaign was performed [24]. The map shown in Fig. 23 shows the location of Šaleška valley in the north-eastern part of Slovenia.

The experimental campaign was performed by researchers from three research institutions: ENEL-CRAM and CISE, Milano, Italy, and Jozef Stefan Institute, Ljubljana, Slovenia. Data obtained during the campaign were used to validate several available atmospheric contaminant models: standard and advanced Gaussian models, a Gaussian puff model and a Lagrangian particle dispersion model [25–27]. Final results of these studies demonstrated that the Lagrangian particle dispersion model is the most effective tool for atmospheric contamination modelling in very complex terrain. The campaign was described in detail in a final report [24], in which all measured data are available. The database consists of measurements from different measuring systems: automatic measuring stations of the Environmental Information System (EIS) maintained by TPPŠ, an automatic mobile laboratory, one mobile Doppler SODAR (used for wind profiling) and DIAL (Differential absorption lidar). Pictures of some of the equipment are presented in Fig. 24.

The EIS of TPPŠ consisted of six stationary automatic measuring stations and one mobile station. Locations of the stations are presented in Fig. 22 above. The environmental parameters measured at the stations are presented in Table 8.

At the time of the measuring campaign, TPPŠ had three operating stacks (chimneys) of different heights: 100 m, 150 m and 230 m. None of the stacks had an installed wet desulphurization plant during the experimental campaign. Measured releases are presented in Table 9, where both static and dynamic parameters are given. Releases from generators Block 1, Block 2 and Block 3 are emitted from one stack, named Block 1,2,3. Pictures of TPPŠ are presented in Section 4.4.2. Details about the measurements are described in [28].

4.4.2. The complexity of the Šoštanj area

The following pictures show the complexity of the meteorology over the Šoštanj area. Figure 25 presents a classification of wind fields over the domain into 10 classes. The wind fields are simplified and represented by measured ground level wind (at 10 m) at 5 stations. The classification was done by a Kohonen neural net. Data included 26 000 measured intervals (from winter 1991 until winter 1993). Each class is represented by wind roses for all 5 stations.

Figure 25 shows the diversity of classes among the group. In addition, it shows that each class is not purely homogenous, but could be further divided into subclasses for a more detailed wind overview. Details about this classification can be found in [29].

Figure 26 shows the TTPŠ in 1995, a few years after the campaign; the building configuration was the same as in 1991. Figures 27 and 28 show the present situation.

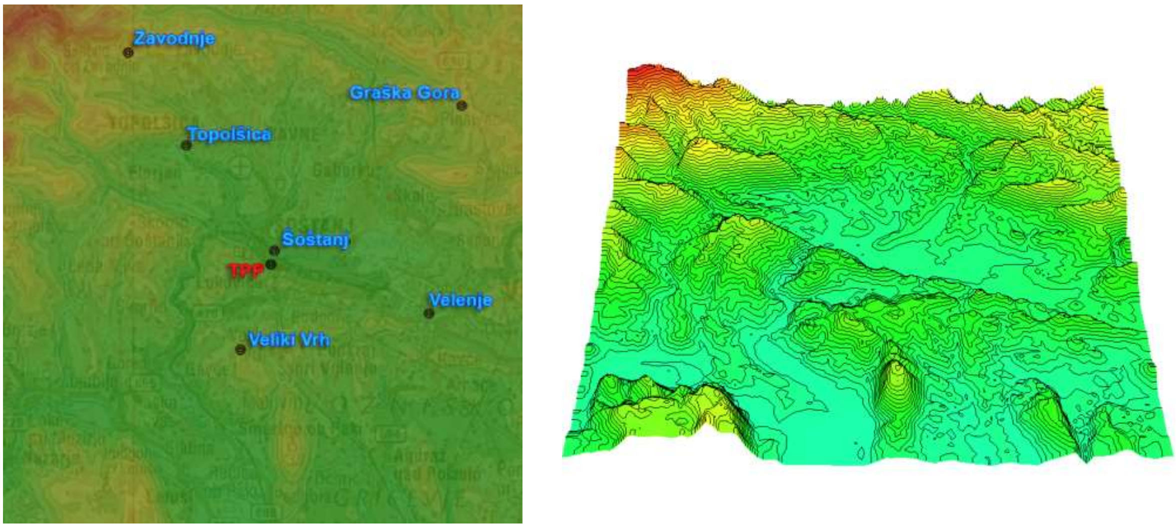

FIG. 22. Map of Šaleška region with locations of automatic environmental stations (from north to south: Zavodnje, Graška Gora, Topolšica, Šoštanj, Velenje, Veliki Vrh) and location of the thermal power plant Šoštanj (TPPŠ) in the centre (left), and the topography of the region (right).

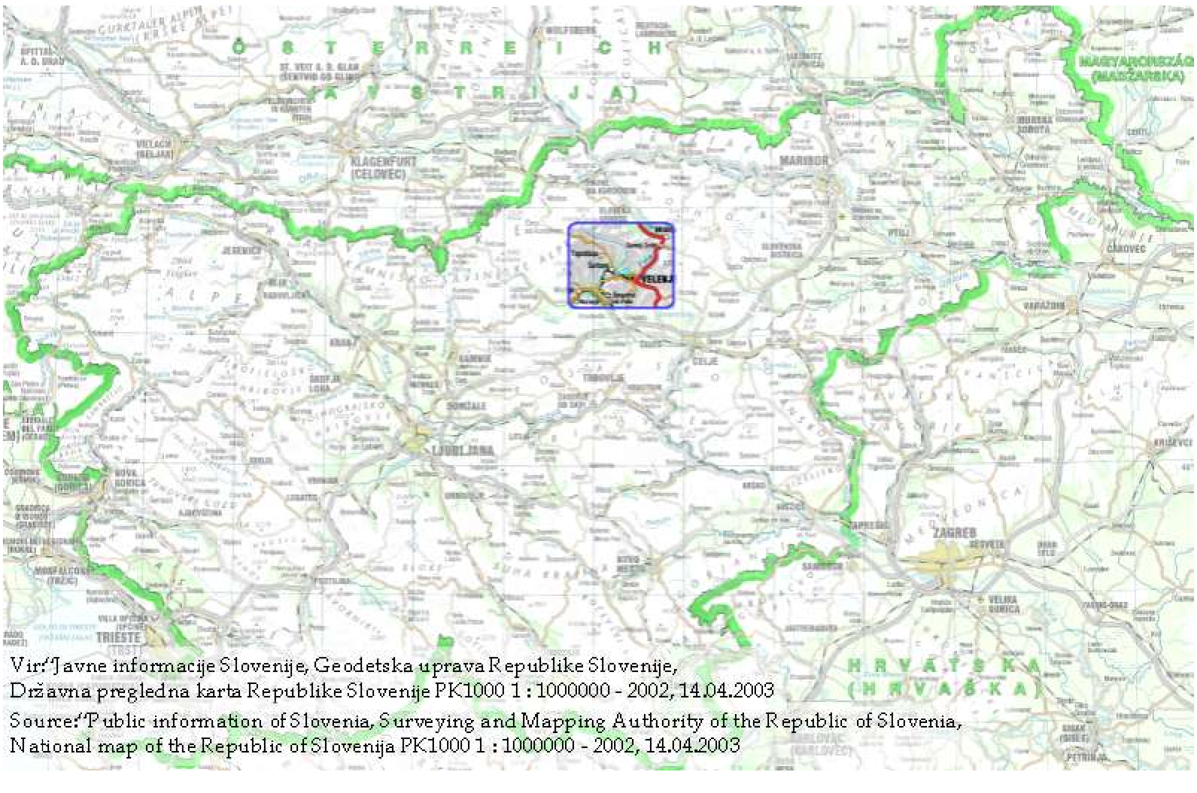

FIG. 23. Location of Saleška region in the north-eastern part of Slovenia.

FIG. 24. Pictures of some of the equipment used in the measuring campaign in the spring of 1991: environmental automatic measuring station (left), mobile SODAR (upper right) and mobile DIAL (lower right).

TABLE 8. LIST OF PARAMETERS MEASURED AT AUTOMATIC ENVIRONMENTAL STATIONS[a]

Parameter name	**Station name**					
	Zavodnje	**Graška Gora**	**Topolšica**	**Veliki Vrh**	**Šoštanj**	**Velenje**
Air temperature (°C)	x	x	x	x	x	X
Relative humidity (%)	x	x	x	x	x	X
Global solar radiation (Watt/m^2)						X
Precipitation (mm)					x	
Air pressure (mbar)					x	
Wind velocity (m/s) and direction (deg)	x	x	x	x	x	X
SO_2 (µg/m^3)	x	x	x	x	x	X
NO (µg/m^3)	x					
NO_x (µg/m^3)	x					
O_3 (µg/m^3)	x					

[a] 'x' denotes that the parameter is measured at the indicated station.

TABLE 9. LIST OF RELEASE PARAMETERS FOR ALL TPPŠ STACKS OPERATING DURING THE EXPERIMENTAL CAMPAIGN IN SPRING 1991

Stack name		Static parameters	
	Height	**Diameter**	**Location**
Block 1,2,3	100 m	6.50 m	46.373N 15.052E
Block 4	150 m	6.34 m	46.372N 15.053E
Block 5	230 m	6.20 m	46.371N 15.055E
		Dynamic parameters	
	Release rate	**Exit temperature**	**Exit velocity**
Block 1,2,3	0.01–0.24 kg/s	155–171°C	0.7–2.9 m/s
Block 4	0.87–2.05 kg/s	155–183°C	8.8–12.3 m/s
Block 5	0.53–2.46 kg/s	172–202°C	8.6–12.7 m/s

FIG. 25. Presentation of wind roses for all clusters for the division into 10 classes.

FIG. 26. Thermal power plant Šoštanj (1995).

FIG. 27. Area photo of the TPPŠ (photo: Uroš Hočevar, 2013).

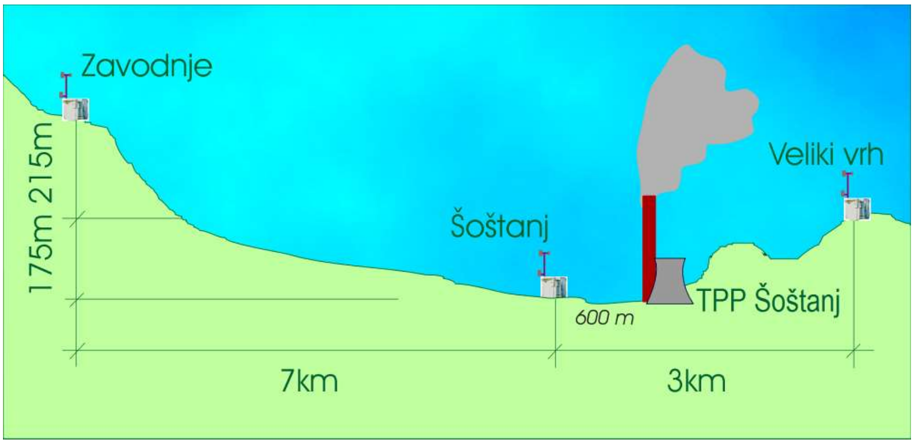

FIG. 28. Schematic vertical cross section of the TPPŠ area.

4.4.3. Modelling exercise

As described below, two time periods were selected for the present modelling exercise. The first of these (Case 1, Section 4.4.3.1) was based on a single day (30 March 1991) with one active source of release and a direct wind to a single monitoring station. The second of these (Case 2, Section 4.4.3.2) was based on a 2 day period (1–2 April 1991) with two active sources release and a complex meteorological situation that led to accumulation of atmospheric contamination.

For both cases, participants in the exercise were provided with details of the monitoring stations and release points (locations, altitudes, types of data recorded), a digital elevation model for the area, data on surface roughness length and CORINE land use cover[5] for the area. For each separate case, participants were provided with SODAR data (18 layers between 50 m and 1000 m height), meteorological data (temperature, relative humidity, air pressure, wind speed and direction, precipitation, global solar radiation), and data on releases (exhaust gas temperature, gas flow, and SO_2 concentration) at half hour intervals for the relevant time period. Participants were asked to predict the time dependent SO_2 concentrations for comparison with measured values at six monitoring stations. All data were provided to participants in electronic format.

4.4.3.1. Case 1, 30 March 1991, Veliki Vrh

On 30 March 1991, the Veliki Vrh station recorded direct atmospheric SO_2 contamination in a predominantly neutral atmosphere when relatively strong winds (5 m/s) blew the air directly from the stacks in the direction of the station. This event was relatively simple in terms of meteorology [28]. Figure 29 shows measured concentrations of atmospheric contamination for the period. Elevated concentrations of atmospheric contamination were measured at the Veliki Vrh station, but low or negligible concentrations at the other stations. Figure 30 shows the SODAR data for the same period. The SODAR equipment was located in the vicinity of the Šoštanj station and near the lake shore.

---

[5] See https://www.syke.fi/en-US/Research__Development/Research_and_development_projects/Projects/Producing_land_cover_and_land_use_data_in_CORINE_Land_Cover_2000_project_in_Finland; also see https://land.copernicus.eu/pan-european/corine-land-cover

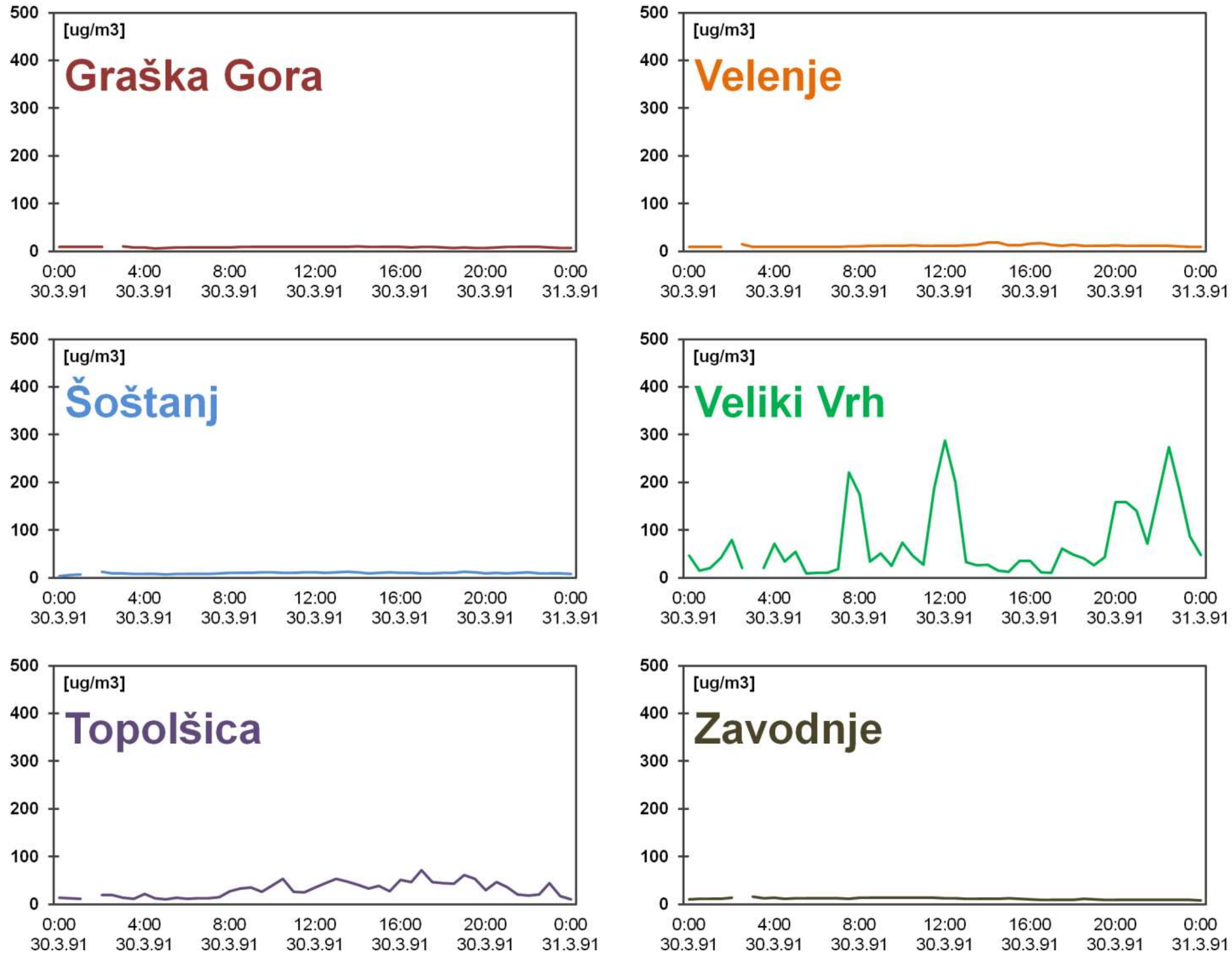

FIG. 29. Measured concentrations of atmospheric SO_2 ($\mu g/m^3$) for 30 March 1991, Veliki Vrh Case.

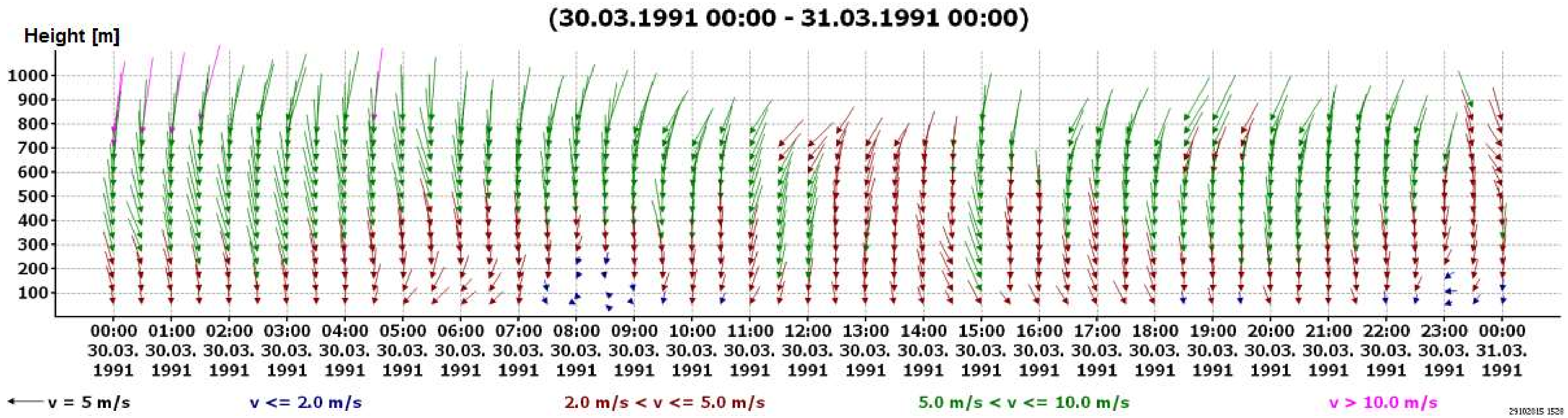

FIG. 30. SODAR data for 30 March 1991, Veliki Vrh Case. The direction of arrows represents the horizontal wind direction at the specified height. The length and colour of the arrow represent the horizontal wind speed at the specified height. Height is presented in meters above the ground (y-axis).

4.4.3.2. *Case 2, 2 April 1991, multiple stations*

On 2 April 1991, there was an SO_2 accumulation under an inversion layer during the night. During the sunny day that followed, convective mixing brought the accumulated pollutant from high in the atmosphere back down to the ground, causing multiple stations to record very high (up to 1 mg/m^3) concentrations almost simultaneously. This event was very difficult to model.

This is a typical complex terrain situation, very difficult for reconstruction, and still represents the greatest challenge to all available atmospheric dispersion models. The situation is described in detail in a published paper (see Ref. [22]). Its most interesting part lasted from 1 April 1991 at 20:00 until 2 April 1991 at 20:00.

The plume spread in all directions over the domain during a relatively short period of time. This is demonstrated by measurements of half hour average SO_2 concentrations at four environmental stations at different directions from TPPŠ, as presented in Fig. 31.

This spread is also seen from the Doppler SODAR measurements presented in Fig. 32. This graph represents measurements from SODAR for each half hour time interval at different heights. Each arrow on the graph represents the direction of the horizontal wind component at a certain height. The length of the arrow represents the magnitude of the horizontal wind speed component.

It was also reported that during this selected period, the phenomenon of accumulation of atmospheric contamination occurred [22]. A very stable meteorological situation was the main cause for a very slow mixing of the plume with air. The contaminant plume was moving very slowly, according to the measured average wind speed and direction. Based on data collected at a measuring station, at the beginning of this event, it was determined that the atmospheric contamination originated from the direction of the source; however, when the main wind changed its direction to the opposite direction, the cloud of atmospheric contamination also changed its direction. From now on, from the point of view of a measuring station, it appeared that the source of the cloud was a virtual source of release located on the other side of the station from the source.

4.5. MODELS USED IN THE EXERCISE

Table 10 provides a summary of the six models used in the Šoštanj exercise. More information about individual models as used in this exercise is provided in Appendix III. The models represent several different purposes (e.g. emergency assessment and research) and two major types of modelling approach (Gaussian and Lagrangian).

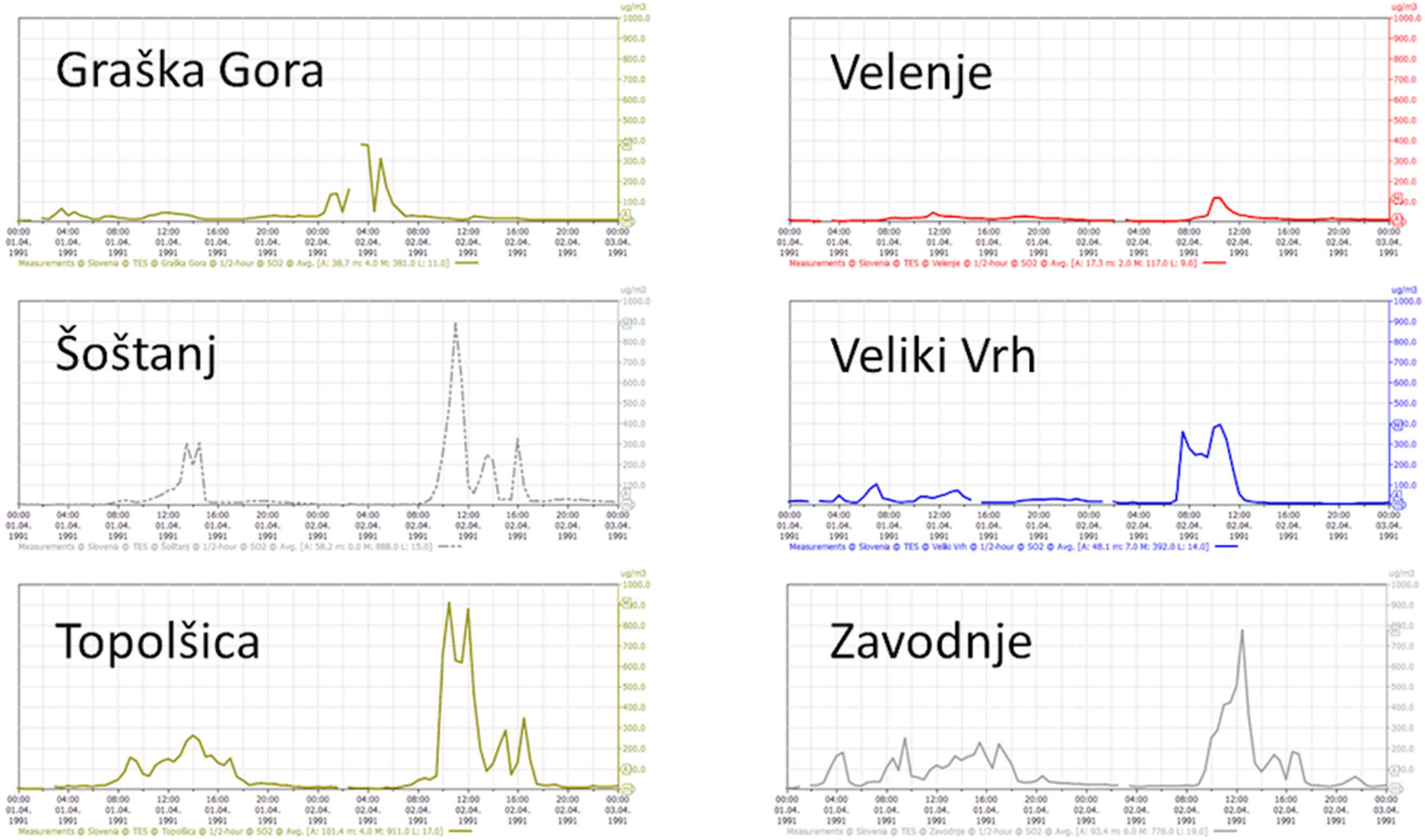

FIG. 31. Measured concentrations of atmospheric SO_2 ($\mu g/m^3$) for 2 April 1991.

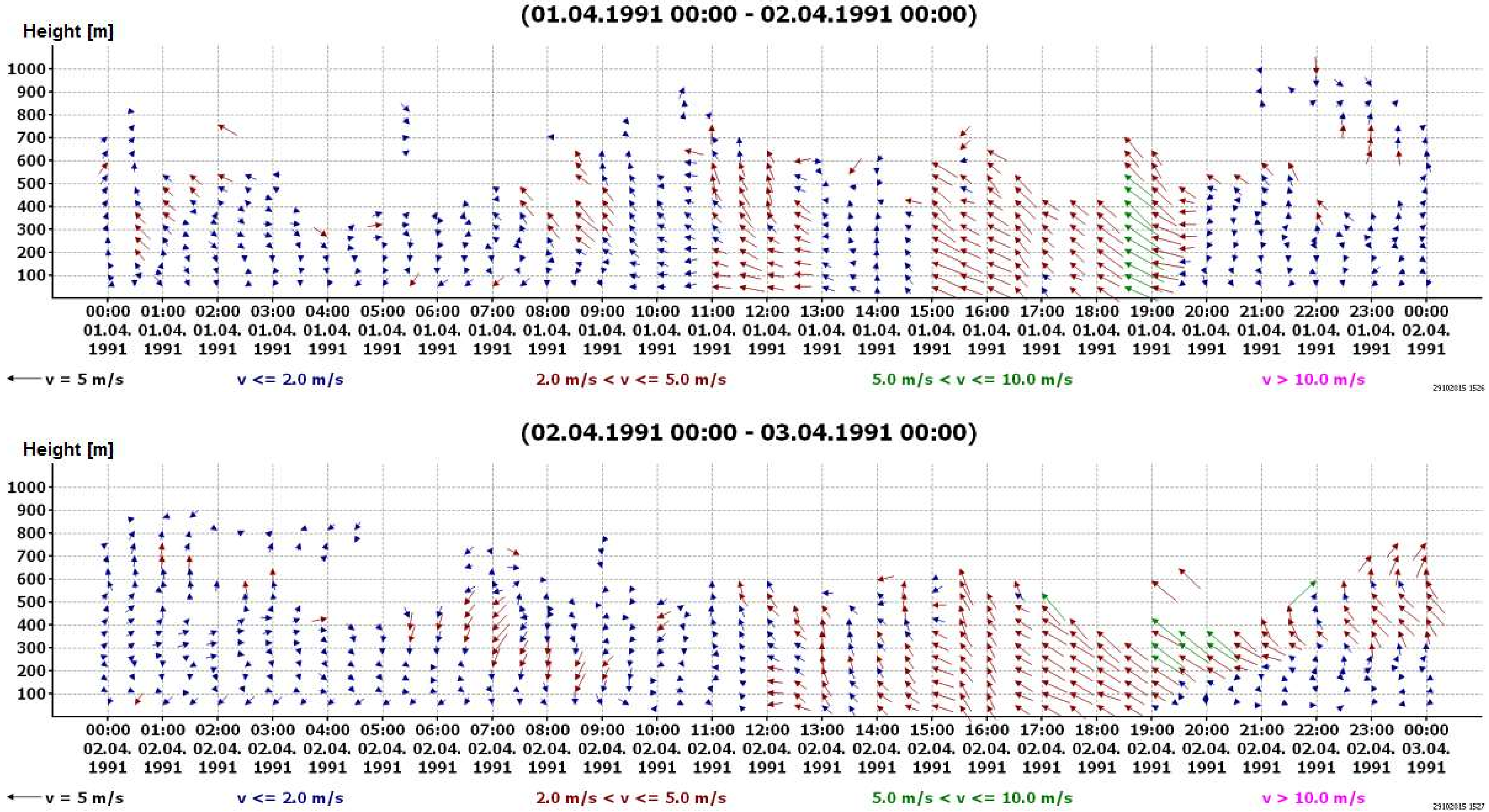

FIG. 32. SODAR measurements during a specific release of atmospheric contamination from 1 April 1991 at 00:00 until 3 April 1991 at 00:00 when accumulation of atmospheric contamination has occurred. The direction of arrows represents the horizontal wind direction at the specified height. The length and colour of the arrow represent the horizontal wind speed at the specified height. The height is presented in meters above the ground (y-axis).

TABLE 10. SUMMARY OF MODELS USED FOR THE ŠOŠTANJ SCENARIO

Model name	**SPRAY**	**CERES CBRN-E**	**RASCAL 3.0.5**	**ARTM**	**LASAIR**	**NFS_Vinca**
Participant and organization	M.Z. Boznar, P. Mlakar, B. Grašič MEIS (Slovenia)	L. Patryl CEA (France)	F. Mancini Sogin (Italy)	S. Hettrich BfS (Germany)	S. Hettrich BfS (Germany)	Z. Grsic NFS (Serbia)
Purpose of model	Atmospheric dispersion modelling	Hazmat atmospheric dispersion modelling and impact assessment	Radiological emergency assessment	Long term dispersion model, annual dose calculations near nuclear facilities	Short term dispersion modelling, sudden releases	Research and operative use in Public Company Nuclear Facilities of Serbia
Type of model	Lagrangian particle dispersion model	Lagrangian particle dispersion model	Gaussian plume (TADPLUME) and Lagrangian puff (TADPUFF)	Lagrangian particle dispersion model	Lagrangian particle dispersion model	Gaussian plume (for continual releases); Gaussian puff model (for instant and continual pollutant releases)
Number of particles (Lagrangian models only)	10–30 per second (capability, 100 000 per hour)	10^7 (60 per second)	Not applicable	1.008×10^9 per hour	1.008×10^6 per hour	Not applicable in Sostanj , Case 1. NFS_Vinca Lagrangian model of Gaussian type, 1 puff per minute
Domain size/calculation range	15 km × 15 km	15 km × 15 km	User defined	User defined	User defined	User defined (Sostanj scenario 15 km ×15 km)
Grid size	150 m × 150 m	100 m × 100 m	User defined	150 m × 150 m	150 m × 150 m	User defined (Sostanj scenario 150 m ×150 m spatial resolution)
Grid height	Model: 20 layers, first 13, top at 6000 m, For elaboration of concentrations: 20 layers, first 10, top at 3000 m	25 grid levels; ground level, 13 m height; last level, 6000 m height	User defined	User defined	User defined	In prognostic mode of the model 800, 850, 900, 925, 950, 975, 1000 m. Not used in Sostanj scenario, Case 1.

TABLE 10. SUMMARY OF MODELS USED FOR THE ŠOŠTANJ SCENARIO (cont.)

Model name	SPRAY	CERES CBRN-E	RASCAL 3.0.5	ARTM	LASAIR	NFS_Vinca
Release height	Actual stack + dynamic plume rise	Effective height, accounting for dynamic and buoyant sources	Effective release heights: Case 1, 100 m; Case 2, Stack 1-2-3, 100 m; Stack 5, 200 m	User defined	Limited to 200 m	Physical stack height 100 m. Effective stack height, time dependent (Briggs, Holland, Concawe)
Receptor height	First cell is 0–10 m above the ground	Ground level, 13 m in height	10 m height	Ground level	Ground level	2 m above surface
Stability class	Dynamic, Monin-Obukhov length [30]	Dynamic, Monin-Obukhov length [30]	Defined by time period, using wind speed and solar radiation	Klug/Manier dispersion classes [31], based on SODAR data; Monin-Obukhov length [30]	Not provided	Case 1, Pasquill stability class by the surface wind speed and quasi vertical temperature gradient (Sostanj-Veliki Vrh). Pasquill stability class C
Wind speed and direction	Mass consistent wind field based on several ground level measurements and SODAR vertical profile	Vertical wind profiles, interpolated as needed	Hourly data from Sostanj location and SODAR location	Not provided	Not provided	Case 1, TPPŠ, SODAR multi levelwind data; Veliki Vrh, wind data at a height of 10 m above the ground. Bivariate interpolation on the calculation domain, on the basis of wind data from TPPŠ and Veliki Vrh.

TABLE 10. SUMMARY OF MODELS USED FOR THE ŠOŠTANJ SCENARIO (cont.)

Model name	**SPRAY**	**CERES CBRN-E**	**RASCAL 3.0.5**	**ARTM**	**LASAIR**	**NFS_Vinca**
Air temperature	Ground level measurements from several stations	Not provided	Hourly data from Sostanj location	Not provided	Not provided	Case 1, air temperature at 2m above ground Sostanj automated meteorological station, TPPŠ, SODAR multi-level air temperature measurement. air temperature at 2m above ground. Veliki Vrh.
Dispersion parameters	Calculated by meteo pre-processor	Wind field model P-SWIFT	NRC parameterization, function of Pasquill-Gifford stability class and distance	Not provided	Not provided	Briggs sigma parameters for rural area
Plume rise	Calculated by meteo pre-processor	Simulated by bulk equations	Not provided	Not provided	Manually calculated	Briggs, Holland, Concawe plume rise theories
Release time step	10–30 s (internally in the model) and half hour for Sostanj initial data	Not provided	Not provided	Half hour	Half hour	30 minutes, linear 1 minute release interpolation of SO_2 for generating puffs
Time step for meteorological data	Half hour	Half hour	Not provided	Hour	Hour	1 minute or 10 minutes
Calculation time step	10 s internally and elaborated each half hour	Half hour	Not provided	Half hour	Half hour	1 minute
Simulation time	1 d (Case 1) or 2 d (Case 2)	1 d (Case 1) or 2 d (Case 2)	1 d (Case 1) or 2 d (Case 2)	Hourly resolution	5 minutes to 1 hour	Case 1, 11:30–12:00
Terrain/topography	Digital model of the heights	Shuttle Radar Topography Mission (SRTM) database	Not considered	Adapted orographic data; with and without buildings	With and without buildings	Egan's theory [32]

TABLE 10. SUMMARY OF MODELS USED FOR THE ŠOŠTANJ SCENARIO (cont.)

Model name	SPRAY	CERES CBRN-E	RASCAL 3.0.5	ARTM	LASAIR	NFS_Vinca
Rugosity	Surface roughness length from CORINE land cover	Not provided	Not provided	Manually determined	Not provided	Taken into account through the Briggs sigma parameters for rural area
Time to set up and run	Calculation time for one case, approximately 2 h for 2 days of real time (one core PC)	Not provided	Not provided	Not provided	Not provided	Significant time of manual preparation input meteorological data and making software to prepare the minute meteorological data by using bivariate interpolation on the calculation domain, on the basis of wind data from Sostanj and Veliki Vrh. Several hours.
Reference(s) for code (URL)	http://www.aria-net.it/	Not provided	Not provided	Not provided	Not provided	Listed below[a]

[a] see Ref. [33] (http://www.doiserbia.nb.rs/img/doi/1451-9372/2015/1451-93721400022G.pdf)
see Ref. [34] (http://www.doiserbia.nb.rs/img/doi/1451-9372/2010/1451-93721000027G.pdf)
see Ref. [35] (http://www.doiserbia.nb.rs/img/doi/1451-9372/2012/1451-93721200115M.pdf)
see Ref. [36] (http://ntrp.vin.bg.ac.rs/2014_5/Nikezic2015_4.htm)
see Ref. [37] (https://www.researchgate.net/publication/334251245_VERIFICATION_MATHEMATICAL_MODELS_FOR_ATMOSPHERIC_DISPERSION_UNDER_IAEA_PROGRAMME_MODARIA/link/5d1f233092851cf4406690ce/download)

4.6. MODEL VALIDATION RESULTS

The following sections describe the results from each model in turn, for both cases. Table 11 summarizes the sets of predictions made with each model.

4.6.1. SPRAY

4.6.1.1. SPRAY results, Case 1, 30 March 1991

Validation of modelling results was performed for the Veliki Vrh station, which was directly downwind of the stacks during a period of relatively simple meteorology with strong winds (30 March 1991; see Fig. 29 above). Modelling was carried out both with the operational version of the SPRAY model and with SPRAY using revised values for the sigma terms ('new sigmas'). The 'new sigmas' were based on a meteorological profile (wind, temperature, turbulence, stability) reconstructed for noon on 30 March 1991 (the center of the period being modelled). Modelling results compared with measurements are shown in Fig. 33. Results from the operational version of the SPRAY model are shown on the left in the figure; results with 'new sigmas' are shown on the left. The upper graphs show the model predictions for the specified location and time; the lower graphs show the model predictions for the specified location and 5 cells in each direction, for the specified time period and the preceding and following time period (Δt), corresponding to the best fit to the measurements within the range of location and time.

4.6.1.2. SPRAY results, Case 2, 1–2 April 1991

Validation of modelling results was performed for stations located in different directions from the point of view of TTPŠ. Locations corresponded to positions of four automatic environmental measuring stations. From all these stations measurements of half hour average SO_2 concentrations are available for a specific release of atmospheric contamination from 1 April 1991 at 20:00 until 2 April 1991 at 20:00.

Measured SO_2 concentrations were increased due to a wind change at the beginning of a specific release of atmospheric contamination. Wind at an approximate height of 250 m changed direction from northwest to southeast. The next wind change was toward the south, which caused an increase of SO_2 concentrations at Šoštanj and Veliki Vrh stations. Figures 34–37 present comparisons of modelled and measured SO_2 concentrations at four of the measuring stations. Results for the Zavodnje station (see Fig. 37 below), which is the most distant station from the TPPŠ, are especially interesting because of the measured SO_2 concentration peak at the end of the atmospheric release. This peak was caused by the accumulation of atmospheric contamination. Because the station is located near the border of the domain (see Fig. 22 above), it is expected that the model results will be an underestimate for this case.

An additional set of modelling results was obtained using prognostic weather information for the relevant dates, obtained from WRF (Weather Forecasting Model[6]). These results are shown in Figs 37–41 for the same four measuring stations. All results in these figures show the best fit to the measurements for 5 cells in each direction from the specified location and $\pm 3\Delta t$. 'Run 2' was based only on measured data from the ground stations, including SODAR. 'Run 4' used the measurements plus prognostic wind and temperature information for heights > 800 m. 'Run 5' used the measurements plus prognostic wind and temperature information for heights > 1100 m. 'Run 7' used the measurements plus prognostic temperature information.

---

[6] https://www.mmm.ucar.edu/weather-research-and-forecasting-model

TABLE 11. SUMMARY OF THE PREDICTIONS MADE WITH EACH PARTICIPATING MODEL

Model	Case 1 30 March 1991	Case 2 1–2 April 1991	Notes
SPRAY	Yes	Yes	Operational version of model; revised meteorological profile (‘new sigmas’); prognostic meteorological information; 3C×3C, 3C×3C×3T, 5×5C×3T versions
CERES CBRN-E	Yes	Yes	5C×5C×1T
RASCAL 3.0.5	Yes	Yes	Specified locations only
ARTM	Yes	Yes	1 h time steps; 4 methods of handling meteorology; with and without building influence; 5C×5C or 3C×3C
LASAIR	Yes	Yes	1 h time steps; 4 methods of handling meteorology; with and without building influence; 5C×5C or 3C×3C
NFS_VINCA	Yes	No	Single half hour time period; time dependent results not provided;1 min or 10 min interpolations of meteorological data used; detailed use of meteorological data

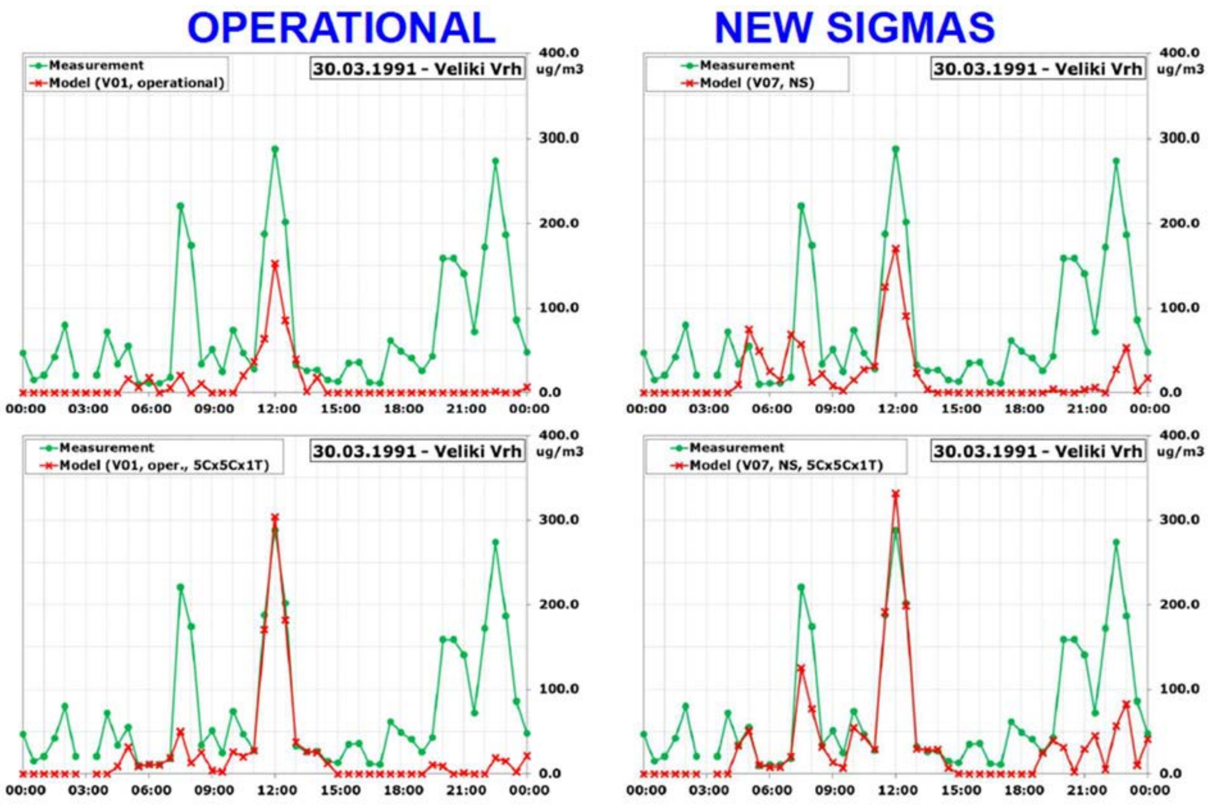

FIG. 33. Comparison of model predictions (red) using SPRAY with the measurements (green) of SO_2 ($\mu g/m^3$) for the period 30 March 1991 at the Veliki Vrh station. Graphs on left show the operational version of the SPRAY model; graphs on right show results with revised values for the sigma terms. Upper graphs show predictions for the specified location and time; lower graphs show the best fit to the measurements for a range of location (5 cells in each direction) and time periods (± Δt).

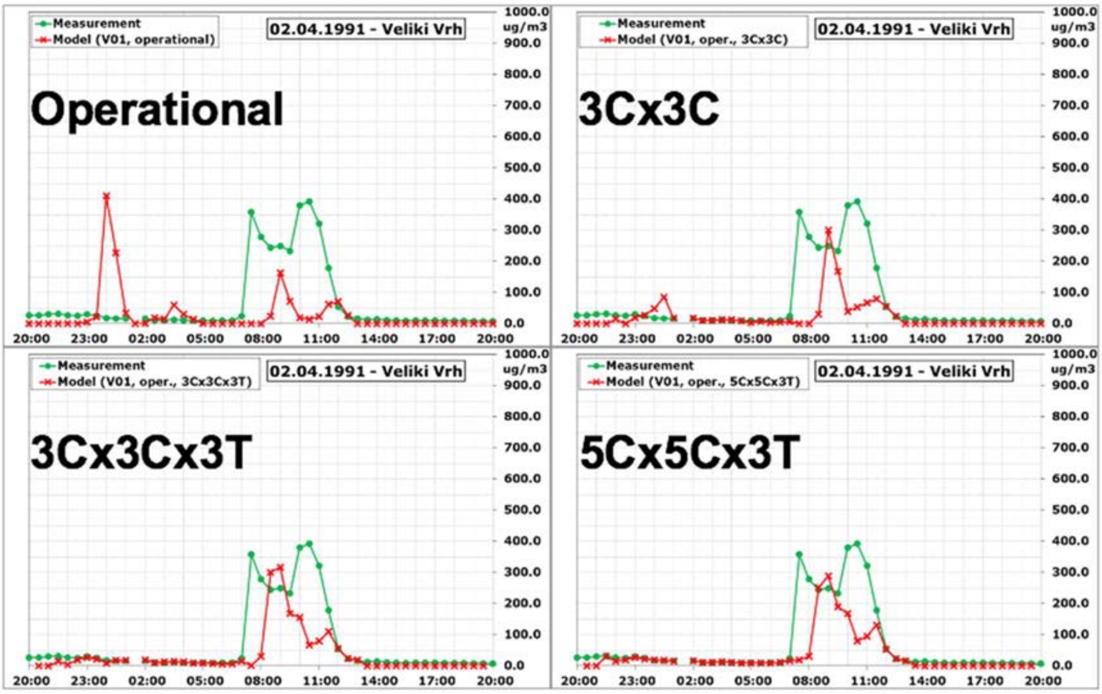

FIG. 34. Comparison of model predictions (red) using SPRAY (operational version) with the measurements (green) of SO_2 ($\mu g/m^3$) for the period 1–2 April 1991 at the Veliki Vrh station. Upper left graph shows results for the specified location and time; remaining graphs show the best fit to the measurements for a range of location (3 or 5 cells in each direction) and time periods ($\pm 3\Delta t$).

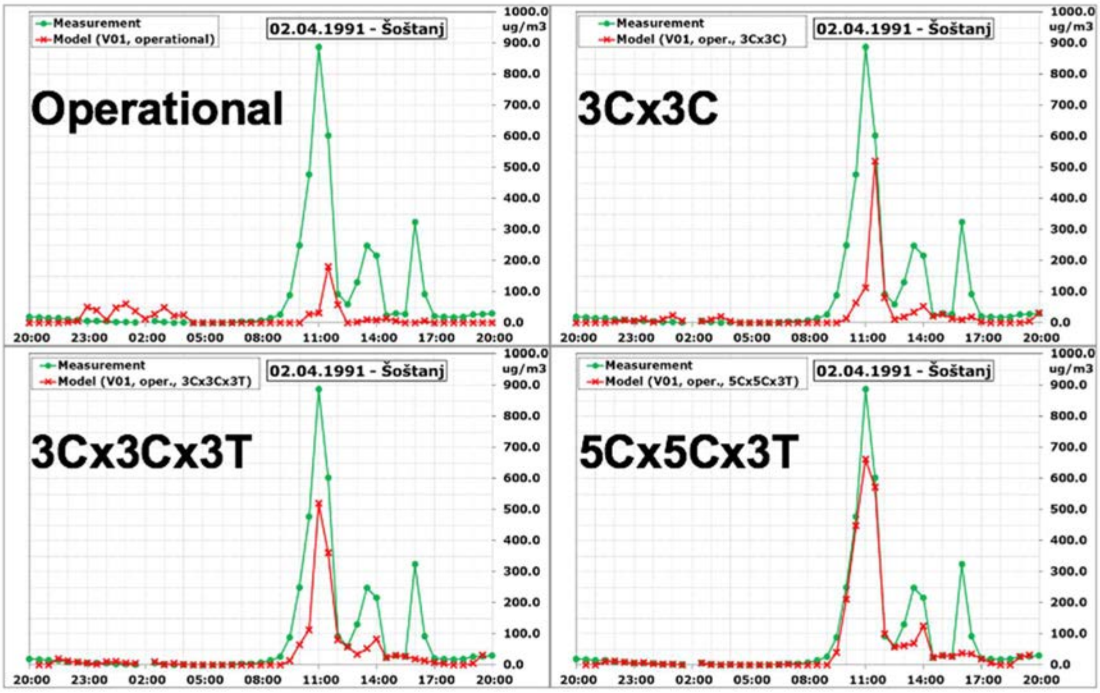

FIG. 35. Comparison of model predictions (red) using SPRAY (operational version) with the measurements (green) of SO_2 ($\mu g/m^3$) for the period 1–2 April 1991 at the Šoštanj station. Upper left graph shows results for the specified location and time; remaining graphs show the best fit to the measurements for a range of location (3 or 5 cells in each direction) and time periods ($\pm 3\Delta t$).

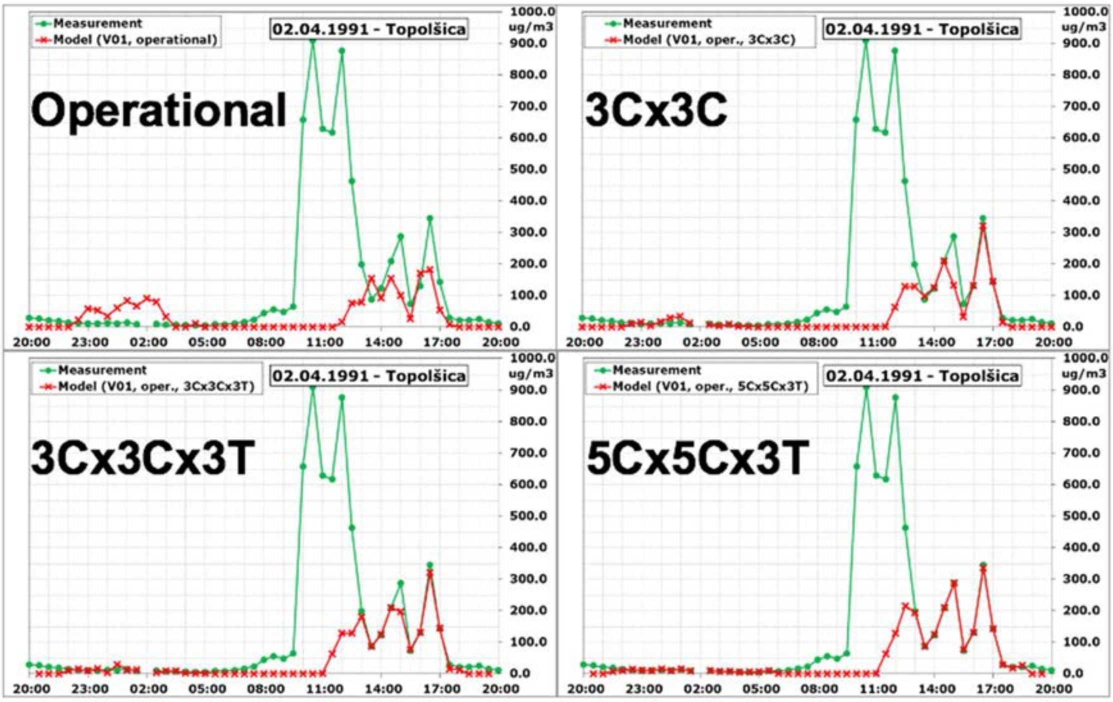

FIG. 36. Comparison of model predictions (red) using SPRAY (operational version) with the measurements (green) of SO_2 ($\mu g/m^3$) for the period 1–2 April 1991 at the Topolšica station. Upper left graph shows results for the specified location and time; remaining graphs show the best fit to the measurements for a range of location (3 or 5 cells in each direction) and time periods ($\pm 3\Delta t$).

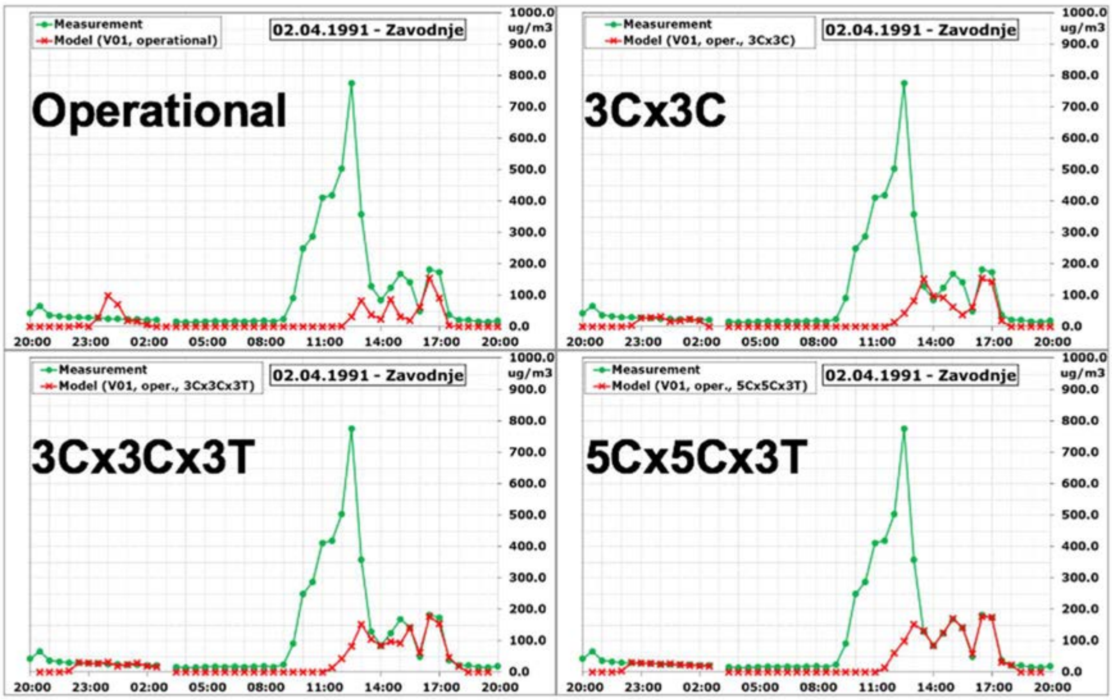

FIG. 37. Comparison of model predictions (red) using SPRAY (operational version) with the measurements (green) of SO_2 ($\mu g/m^3$) for the period 1–2 April 1991 at the Zovodnje station. Upper left graph shows results for the specified location and time; remaining graphs show the best fit to the measurements for a range of location (3 or 5 cells in each direction) and time periods ($\pm 3\Delta t$).

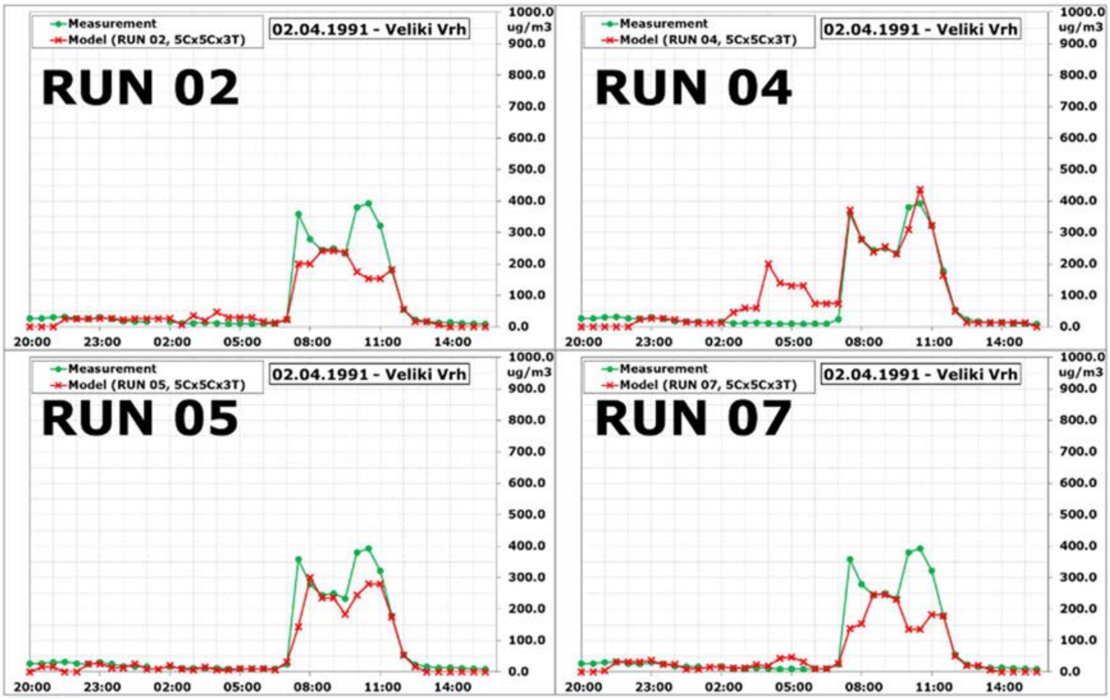

FIG. 38. Comparison of model predictions (red) using SPRAY with the measurements (green) of SO_2 ($\mu g/m^3$) for the period 1–2 April 1991 at the Veliki Vrh station. Graphs show the best fit to the measurements for a range of location (5 cells in each direction) and time periods (± 3Δt). See text for explanation of the different runs.

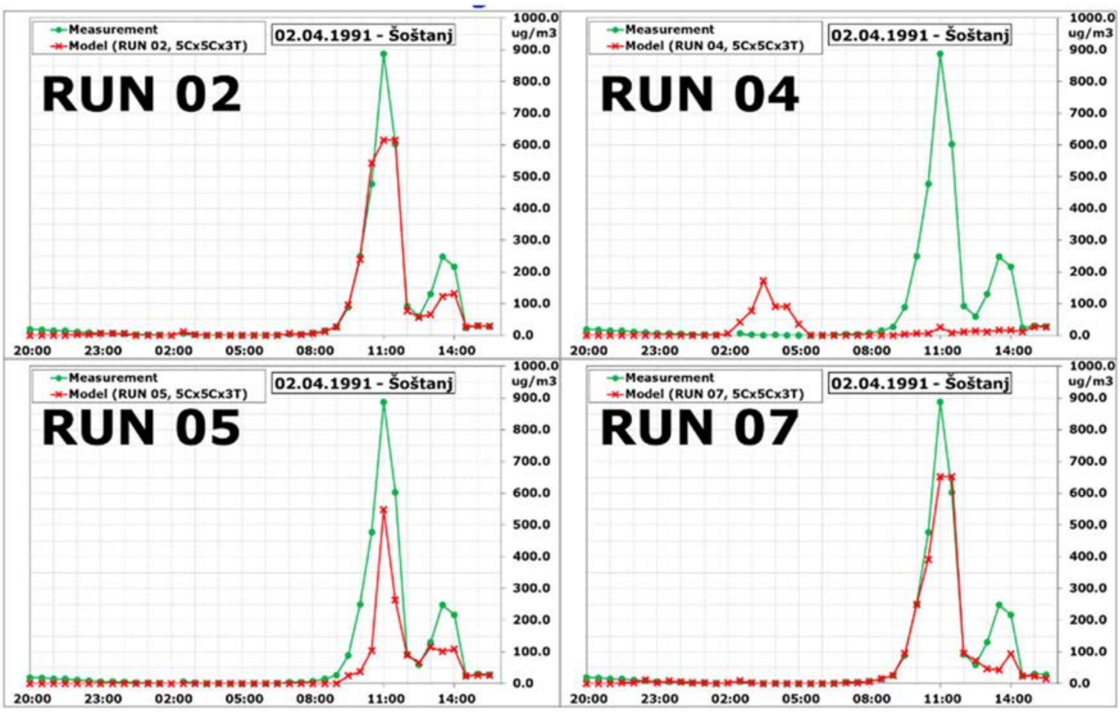

FIG. 39. Comparison of model predictions (red) using SPRAY with the measurements (green) of SO_2 ($\mu g/m^3$) for the period 1–2 April 1991 at the Šoštanj station. Graphs show the best fit to the measurements for a range of location (5 cells in each direction) and time periods (± 3Δt). See text for explanation of the different runs.

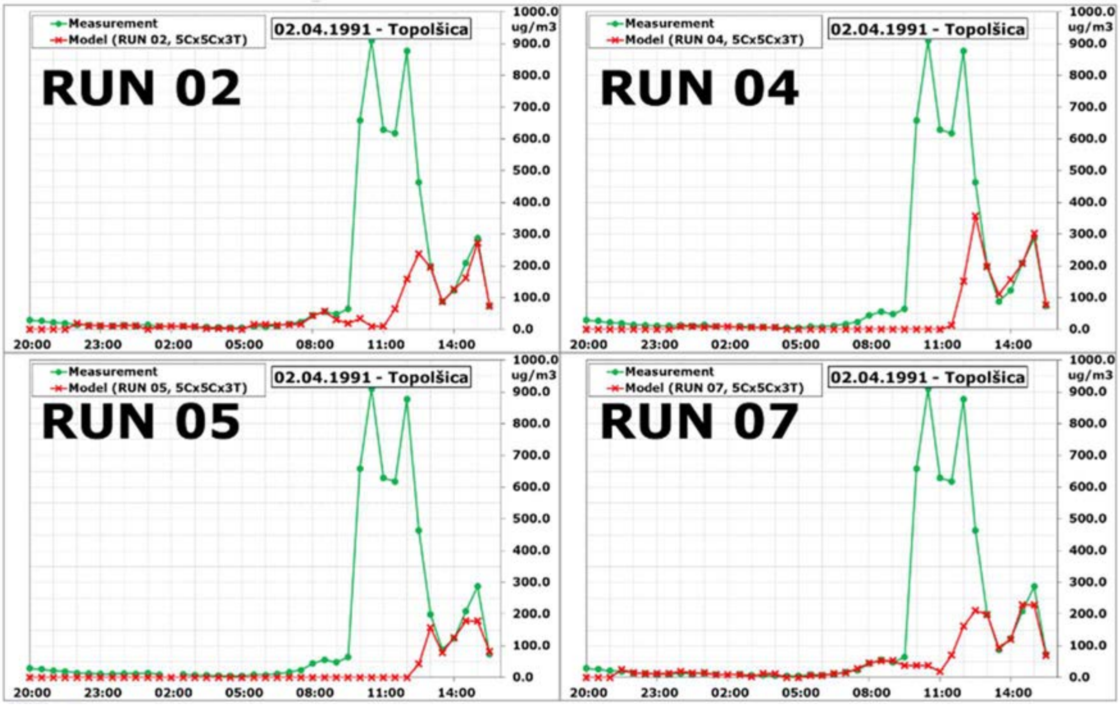

FIG. 40. Comparison of model predictions (red) using SPRAY with the measurements (green) of SO_2 ($\mu g/m^3$) for the period 1–2 April 1991 at the Topolšica station. Graphs show the best fit to the measurements for a range of location (5 cells in each direction) and time periods ($\pm 3\Delta t$). See text for explanation of the different runs.

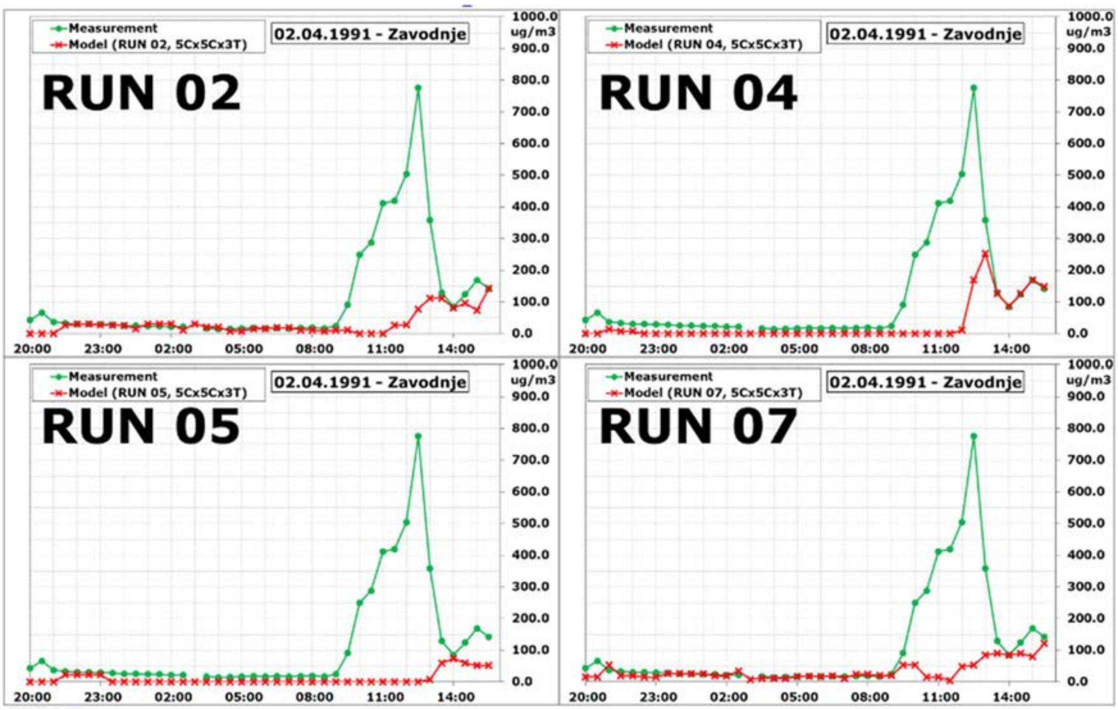

FIG. 41. Comparison of model predictions (red) using SPRAY with the measurements (green) of SO_2 ($\mu g/m^3$) for the period 1–2 April 1991 at the Zavodnje station. Graphs show the best fit to the measurements for a range of location (5 cells in each direction) and time periods ($\pm 3\Delta t$). See text for explanation of the different runs.

4.6.2. CERES CBRN-E

4.6.2.1. CERES CBRN-E results, Case 1, 30 March 1991

Case 1 was modelled with P-SWIFT and P-SPRAY by using, respectively, 16 and 32 cores (DELL T5600 60 MO memory ram). Times of computation were about 1 minute for P-SWIFT and about 30 minutes for P-SPRAY.

Figure 42 shows the wind field simulated at the SODAR coordinates for the 30 March 1991 case. The wind direction and wind horizontal speed calculated by P-SWIFT are very close to the SODAR measurements. Figure 43 shows the comparison between measured and reconstructed concentrations (5 by 5 cells and ±1 time interval) with CERES CBRN-E (PMSS) for the 30 March 1991 case at the Veliki Vrh station. The reconstructed concentrations give good agreement with the measurements, especially for the highest concentrations at 07:30, 12:00 and 22:30.

4.6.2.2. CERES CBRN-E results, Case 2, 1–2 April 1991

Case 2 was modelled with P-SWIFT and P-SPRAY by using, respectively, 16 and 32 cores (DELL T5600 60 MO memory ram). Times of computation were about 2 minutes for P-SWIFT and about 120 minutes for P-SPRAY.

Figure 44 shows the wind field simulated at the SODAR coordinates for the 1–2 April 1991 case. The wind direction and wind horizontal speed calculated by P-SWIFT are very close to the SODAR measurements for the 1–2 April case. Figure 45 shows the comparison between measured and reconstructed concentrations (5 by 5 cells and ±1 time interval) with CERES CBRN-E (PMSS) for the 1–2 April 1991 case and for all stations.

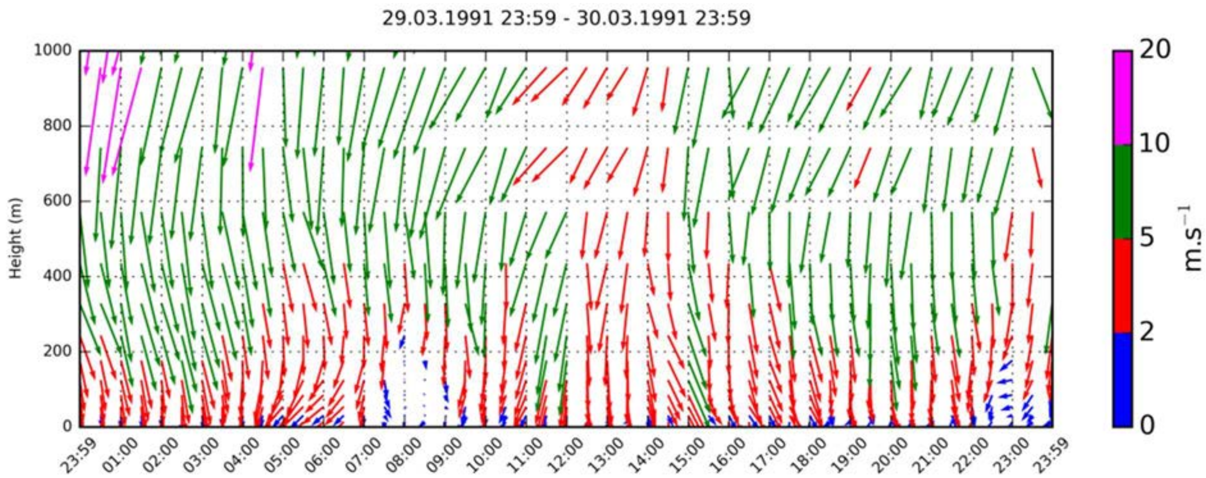

FIG. 42. Wind field simulated at the SODAR coordinates for the 30 March 1991 case. Direction of arrows indicates horizontal wind direction for each vertical layer up to 1000 m height. Length and colour of arrow indicate horizontal wind speed.

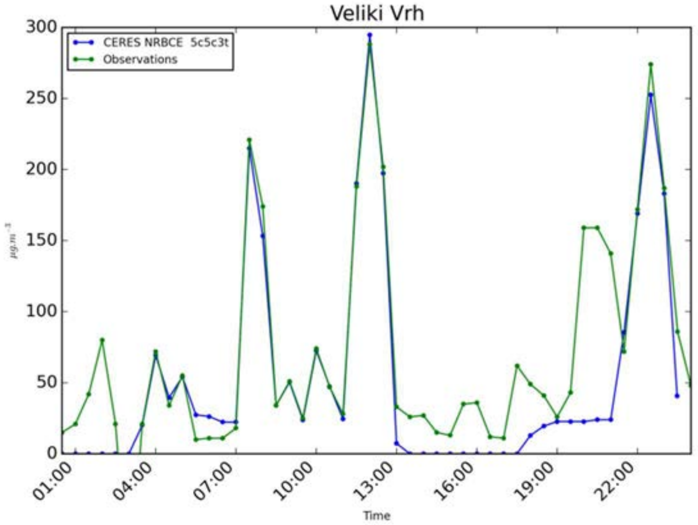

FIG. 43. Comparison between measured (green) and reconstructed (blue) concentrations (5 by 5 cells and ±1 time interval) of SO_2 ($\mu g/m^3$) with CERES CBRN-E (PMSS) for the 30 March 1991 case at the Veliki Vrh station.

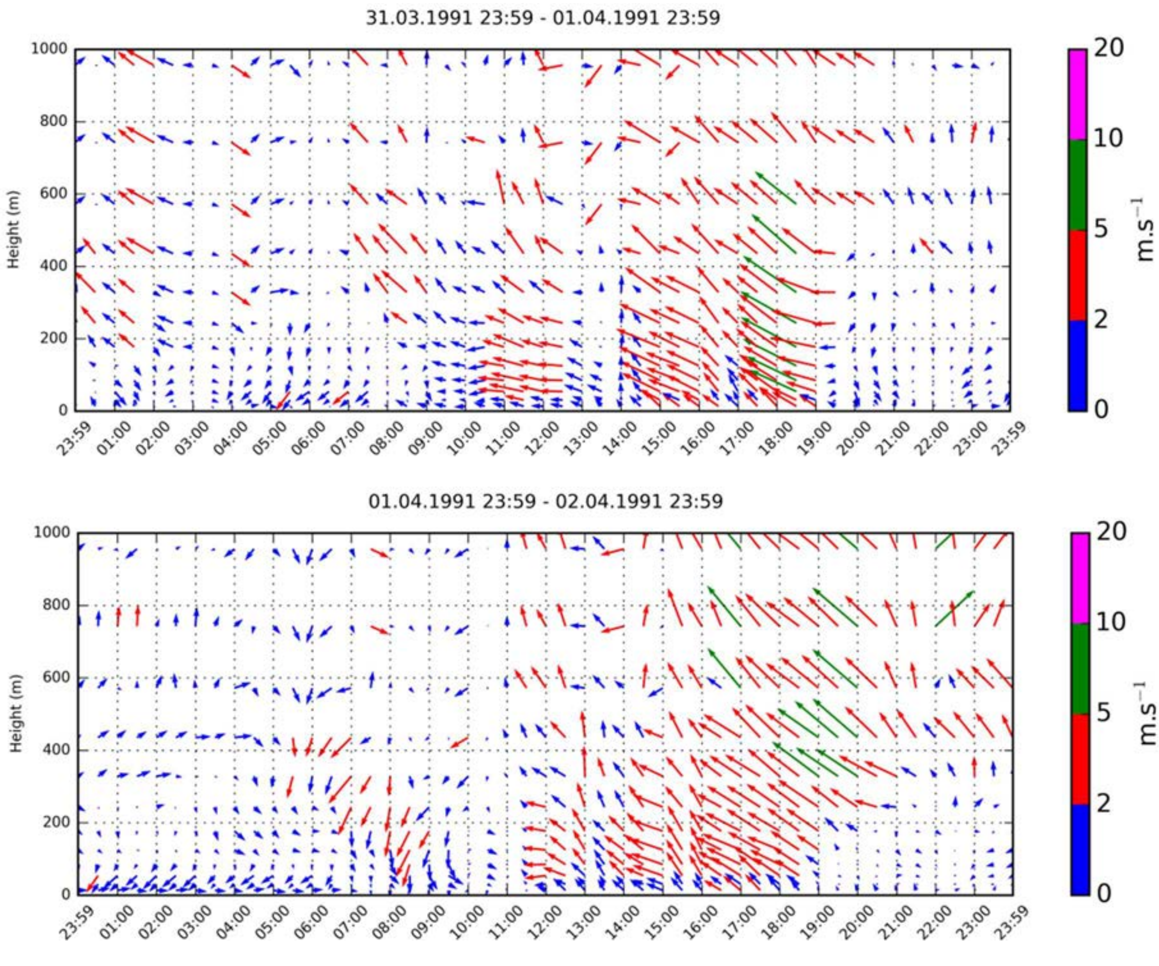

FIG. 44. Wind field simulated at the SODAR coordinates for the 1–2 April 1991 case. Direction of arrows indicates horizontal wind direction for each vertical layer up to 1000 m height. Length and colour of arrow indicate horizontal wind speed.

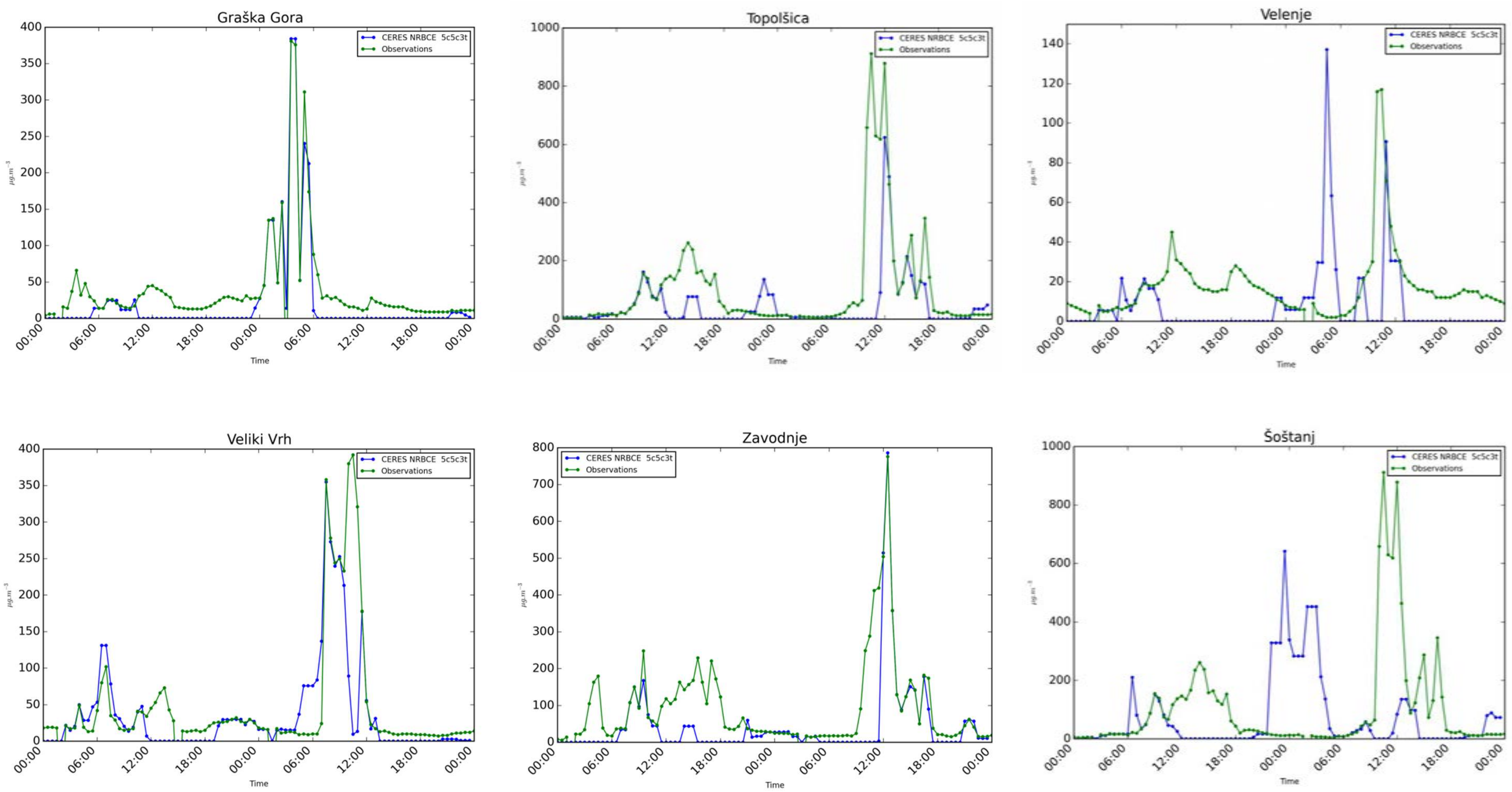

FIG. 45. Comparison between measured (green) and reconstructed (blue) concentrations (5 by 5 cells and ± 1 time interval) of SO_2 ($\mu g/m^3$) with CERES CBRN-E (PMSS) for the 1–2 April 1991 case for all stations.

4.6.3. RASCAL 3.0.5

4.6.3.1. RASCAL 3.0.5 results, Case 1, 30 March 1991

Figure 46 shows the model predictions compared with measurements for 30 March 1991 at the Velikhi Vrh station. Several of the predicted peaks coincide with measured peaks, especially during the middle of the time period, although the largest predicted peak overpredicts the measurements by a factor of about 3. The model predictions underestimate the predictions for the earliest and latest parts of the time period.

4.6.3.2. RASCAL 3.0.5 results, Case 2, 1–2 April 1991

Releases from each of the two stacks were simulated separately, and the results for each specified location were added together. Figures 47 and 48 show the model predictions compared with measurements for 1–2 April 1991 at all six stations, with each figure showing three of the six stations, respectively. The model simulated some peaks reasonably well in terms of either timing or magnitude, but missed some measured peaks entirely.

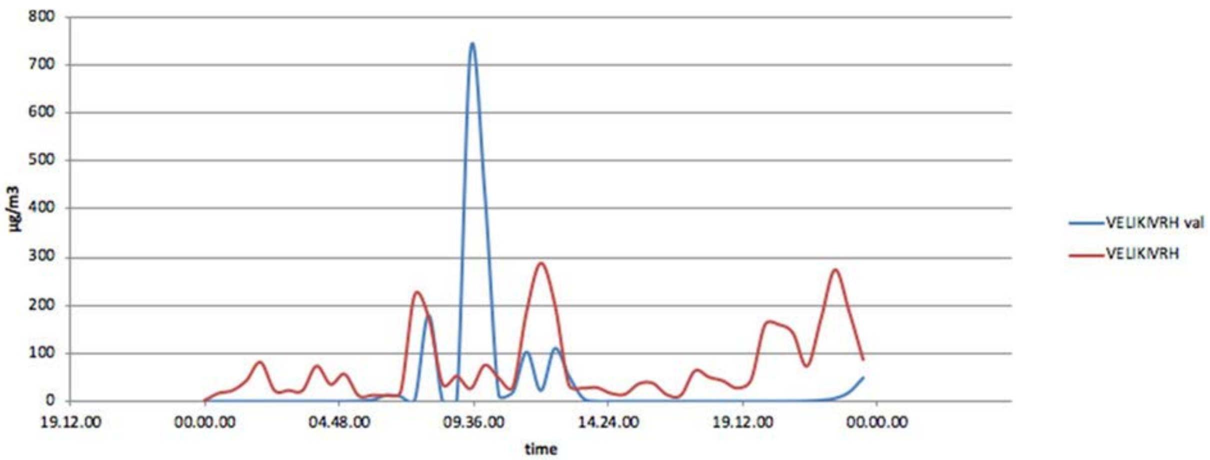

FIG. 46. Comparison between measured (blue) and reconstructed (red) concentrations of SO_2 ($\mu g/m^3$) with RASCAL 3.0.5 for the 30 March 1991 case at the Veliki Vrh station.

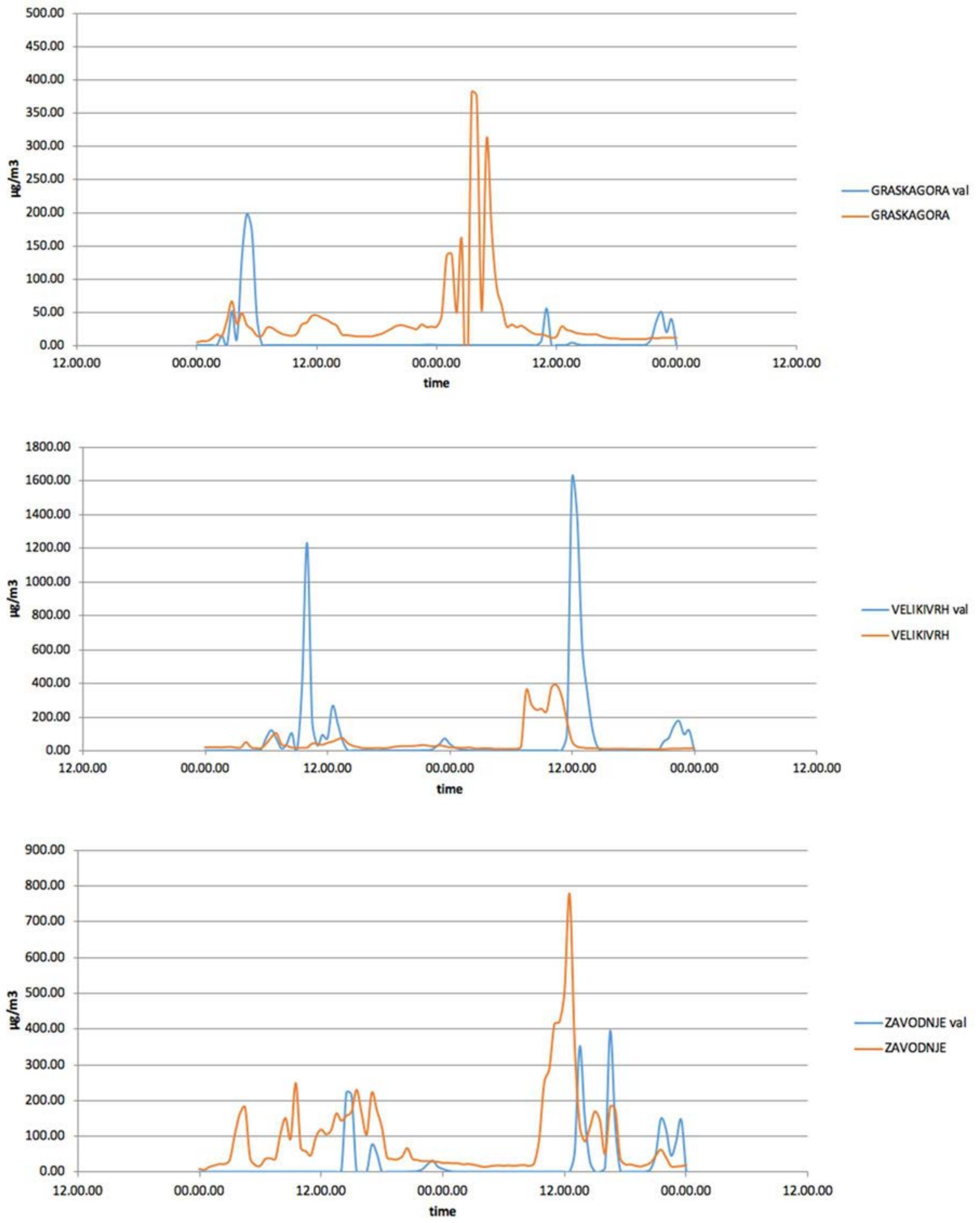

FIG. 47. Comparison between measured (orange) and reconstructed (blue) concentrations of SO_2 ($\mu g/m^3$) with RASCAL 3.0.5 for the 1–2 April 1991 case for 3 of the total 6 stations (for the other 3 stations, please see Fig. 48 below).

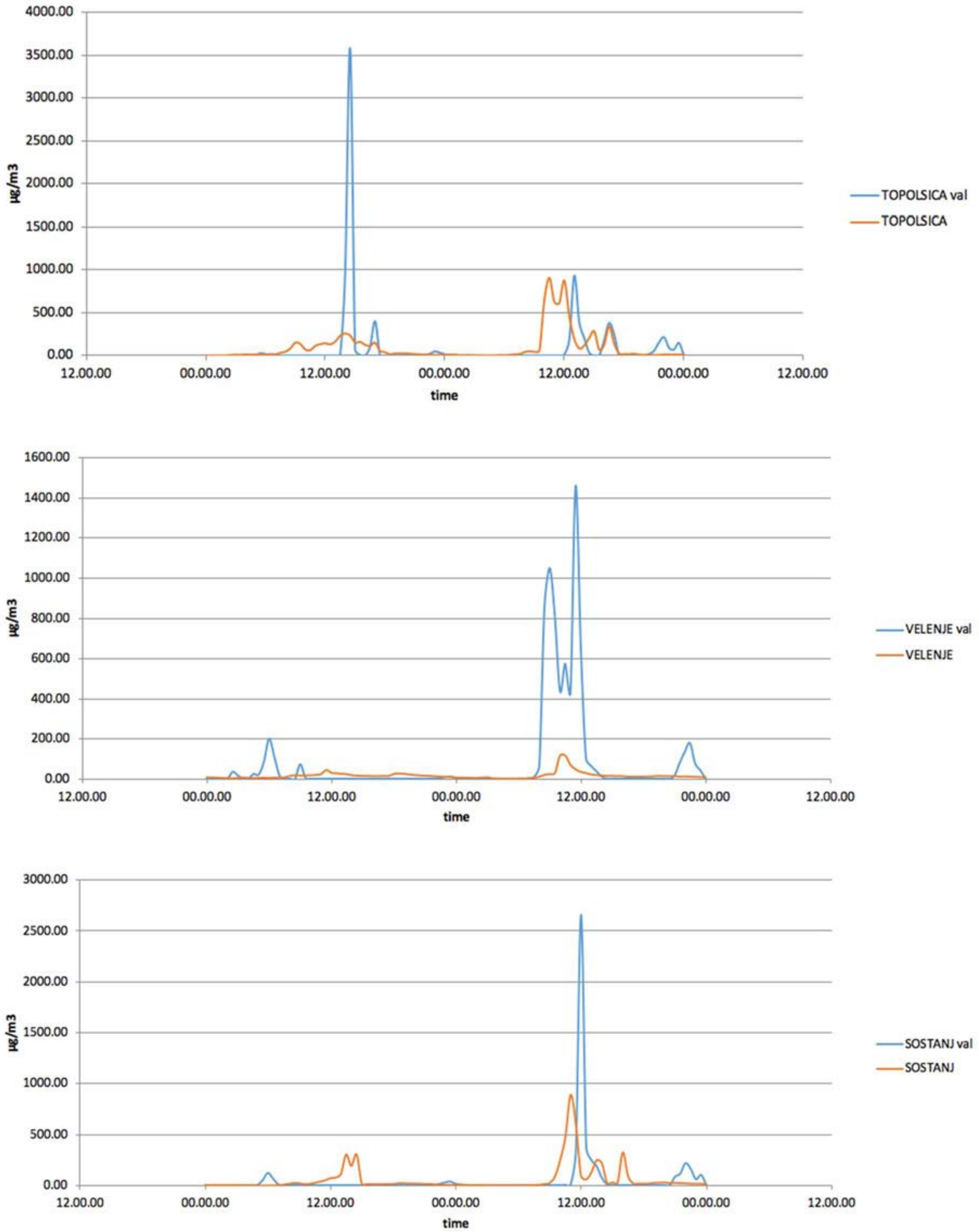

FIG. 48. Comparison between measured (orange) and reconstructed (blue) concentrations of SO_2 ($\mu g/m^3$) with RASCAL 3.0.5 for the 1–2 April 1991 case for the remaining 3 of total six stations (for the other 3 stations, please see Fig. 47 above).

4.6.4. ARTM

The Atmospheric Radionuclide Transport Model (ARTM) is a simulation software to reproduce and predict the atmospheric dispersion of radionuclides from nuclear facilities and to calculate the exposure of the population for long term dispersion during routine operations [38]. Originally developed for the modelling of the annual releases of a nuclear facility, ARTM was used at its lower limitation to model the Šoštanj scenario. Details of the model are described in Appendix III.

In several iterations of ARTM simulations, the Šoštanj scenario, based on its initial data set and certain adaptations (see Appendix III), was modelled, and the results were compared with the measured data. Since the measurement values are available in half hour time steps, in contrast to the simulation intervals of one hour, the measurements were averaged using the arithmetic mean to obtain hourly measurements necessary for the comparison.

The two cases, Case 1 (30 March 1991) and Case 2 (1–2 April 1991), were modelled both considering the buildings of the Šoštanj plant and without considering the influence thereof. Additionally, there are up to four different simulation modes (described in Appendix III): 'old', 'averaged', 'new categories', and 'averaged and new categories', based on different approaches in the preparation of the meteorological data used as input for the ARTM simulations.

Due to the complex terrain and the resulting wind fields, adding a complex building structure to the simulation turned out to be successful only in the cases where not very stable dispersion conditions (dispersion category F according to Klug/Manier [31]) occurred. The different types of simulations performed are summarized in Table 12.

For all of these calculations, a grid size of 150 m by 150 m was chosen. The grid had to be specifically prepared for use in ARTM and is not based on the one provided in the Šoštanj data set; rather, it was based on a Digital Elevation Model obtained from geocomm.com (for details see Appendix III).

The Šoštanj simulations in ARTM were performed with the maximum number of simulation particles (1 008 000 000 released particles per hour), to obtain the highest possible resolution of the results. In order to further improve the simulation results and make them more robust to statistical deviations resulting from the starting distribution of the simulation particles, 16 simulations were always conducted for each of the eight successful calculations indicated in Table 12 ARTM offers the possibility of inserting a starting random number. Depending on the choice of this number, the particle distribution at the start of the simulation varies, which can cause recognizable differences in the results between two simulations with different starting random numbers. The 16 chosen starting random numbers (1, 10, 100, 1000, 10000, 2476, 2475, 2477, 2466, 2486, 2376, 2576, 1476, 3476, 12 476, 22 476) were kept constant throughout all simulated cases. The resulting data files from these 16 simulations were combined and averaged into one file, providing the basis for all data and diagrams of the ARTM simulations that are presented here.

TABLE 12. LIST OF SIMULATIONS PERFORMED WITH ARTM FOR THE ŠOŠTANJ SCENARIO[a]

Type of simulation	Case 1: 30 March 1991		Case 2: 1–2 April 1991	
Influence of Buildings	no	yes	no	yes
'old'	X	X	X	*
'new categories'	X	*	–	–
'averaged'	X	X	X	*
'averaged and new categories'	X	*	–	–

[a] X indicates simulations performed successfully; * indicates simulations abnormally aborted due to the appearance of a very stable dispersion category in the meteorological data and the influence of buildings; – indicates that a simulation was not performed.

The resulting data consist of data files containing the air concentration in different altitude layers for the calculation area with a grid size of 150 m, and a file containing the time series for the measurement points in hourly steps. ARTM unfortunately has a limit of only 50 measurement points, for which a user can print out a time series of the air concentration. For Case 1, only the points 'Šoštanj' and 'Veliki Vrh' were chosen, as pre-studies with ARTM showed that these were the only two measurement locations that would get hit by the cloud, and to provide at least one set of comparable 5 × 5 cell results to compare with other models. To account for deviations, this measurement grid containing 5 × 5 points was chosen for each of these two locations, with the distance between them being the same as the size of the simulation grid, 150 m. For the Case 2 simulations, including all 6 measurement stations, a grid of only 3 × 3 points around the measurement stations (for Graška Gora, only 5 points: the station and the points north, east, south and west) could be chosen, due to the limitation of measurement points given by ARTM.

Even though the simulation was conducted several times with different input parameters for the meteorological data (see Table 12), in all cases only the most optimal simulation results were chosen to be described in detail in the following sections.

4.6.4.1. ARTM results, Case 1, 30 March 1991

In the evaluation of the simulation results compared with the measurement results, it turned out that the worst results were delivered by the simulation runs using the 'new categories' of dispersion based on the Monin-Obukhov length [30]. These results led to concentration peaks only around noon, while none of the other measured peaks appeared at all in these simulations. As for the Šoštanj station, the simulated results appeared to contain only one peak around noon and to be zero for the 'averaged' meteorology; therefore, only the Veliki Vrh station was selected to be evaluated and compared. In Fig. 49, the results for the remaining simulation runs with the hourly meteorology ('old') and the averaged half hours ('averaged'; details described in Appendix III) are shown.

Both diagrams were created considering a 5 by 5 cell grid for the evaluation of the simulation data, to cover the possibilities for spatial deviations of the simulated results. The simulated values shown in the diagrams as red or blue points are those predicted directly at the measurement location. The respective red and blue error bars consist primarily of the values of the maximal value from the 5 × 5 cell field as the upper value and the lowest as the lower value. Additionally added (or subtracted, respectively) are the standard deviations for the maximum (or minimum, respectively) points, as they resulted from the combination of the 16 different

ARTM runs for each of the scenarios. The black line in the graphics depicts the averaged measurement data with an hourly resolution.

While in the top graph shown in Fig. 49, no buildings of the TTPŠ are considered, the simulations in the lower graph in Fig. 49 show the results after introducing the buildings into the scenario. The main difference appearing in the diagrams is that for the building scenario, the value range in the 5 × 5 field seems to be lower than without buildings. Also, some predicted concentrations are lower in the building scenario (e.g. the ones at 05:00), while others are a bit higher when buildings are included (e.g. the ones at 09:00).

Looking at the differences between the two different meteorological approaches, the one where only meteorological data at the full hour were considered ('old') and the one where the half hourly values were averaged to gain an hourly value ('averaged'), the diagrams show that for most of the time intervals, the 'old' meteorology, which physically is more incorrect than the 'averaged' one, in both scenarios produces overall better results in relation to the measured values. Only at 07:00, 12:00, and around 20:00 and 21:00 the red (averaged) lines reach closer to the actual measurement data.

4.6.4.2. ARTM results, Case 2, 1–2 April 1991

For Case 2, the options 'new categories' and the building scenario were not available (shown in Table 12 above). For the first option, the Monin-Obukhov lengths [30] were not available from which to obtain the 'new categories', and for the latter option, ARTM simply could not be used to calculate the scenarios with building influence (see Section 4.6.4). While the data were evaluated for 6 stations, the results for only 4 stations are shown here. For the other two stations, Graška Gora and Velenje, non-zero values were not obtained for the simulated concentrations, and therefore these two stations were discarded from the analysis. The remaining 4 stations are shown in Figs 50 and 51 for the no building scenario, considering both the 'old' and the 'averaged' meteorological data. Just as for Case 1, the respective red and blue error bars show the maximal and minimal values, also considering the standard deviation, for the neighbouring cells. The only difference here is, that instead of 5 × 5 cells, only 3 × 3 cells were taken into consideration. Again, the black line in the graphics depicts the actual measurement data in an hourly resolution.

For the Šoštanj station, the simulation results are quite poor. The measured peak on 1 April 1991 does not appear in either of the two simulations, and for the 2 April 1991, only the simulation with the physically less correct 'old' meteorological data shows some concentration values after the noon peak. While the two simulated values for 12:00 and 13:00 come close to the actual measurement values, the large peaks at 11:00, 14:00 and 16:00 do not show up in the simulation.

At the Topolšica station, for both meteorologies, the simulation shows a small peak on 1 April 1991 where the measurement data suggest a series of peaks around 150–250 $\mu g/m^3$, but the main peak on this day could not be reconstructed by the simulations, either in time or in size. For 2 April 1991, the simulation data suggest that there are some peaks in the afternoon, but again without hitting the major peaks before noon and the two smaller ones at 15:00 and 17:00.

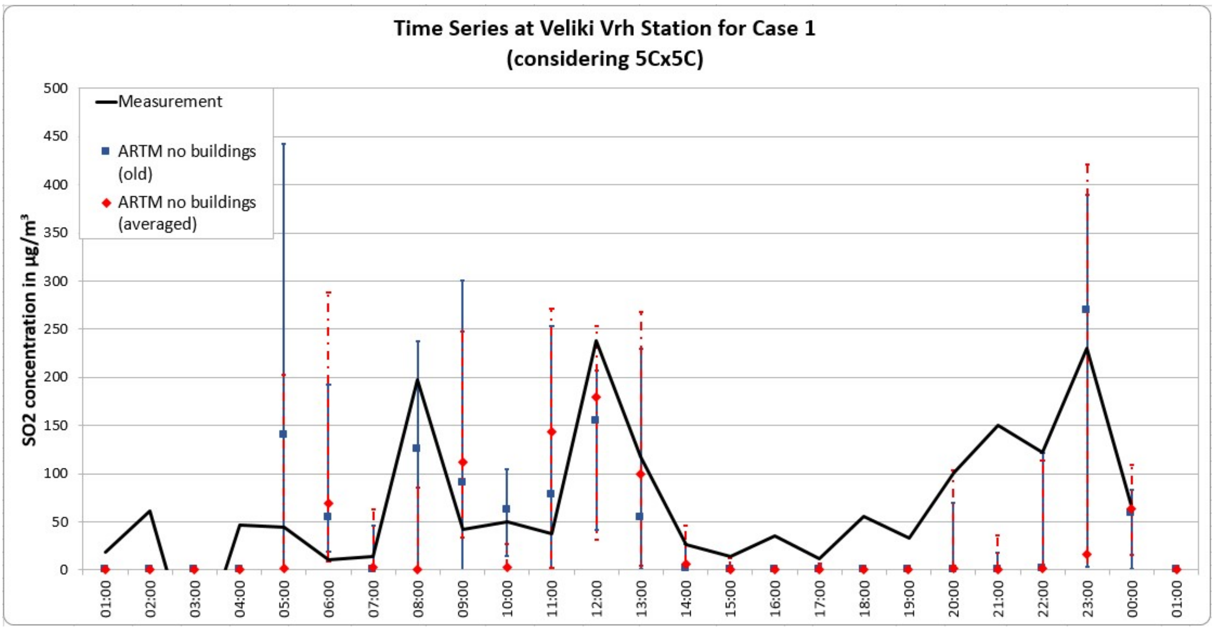

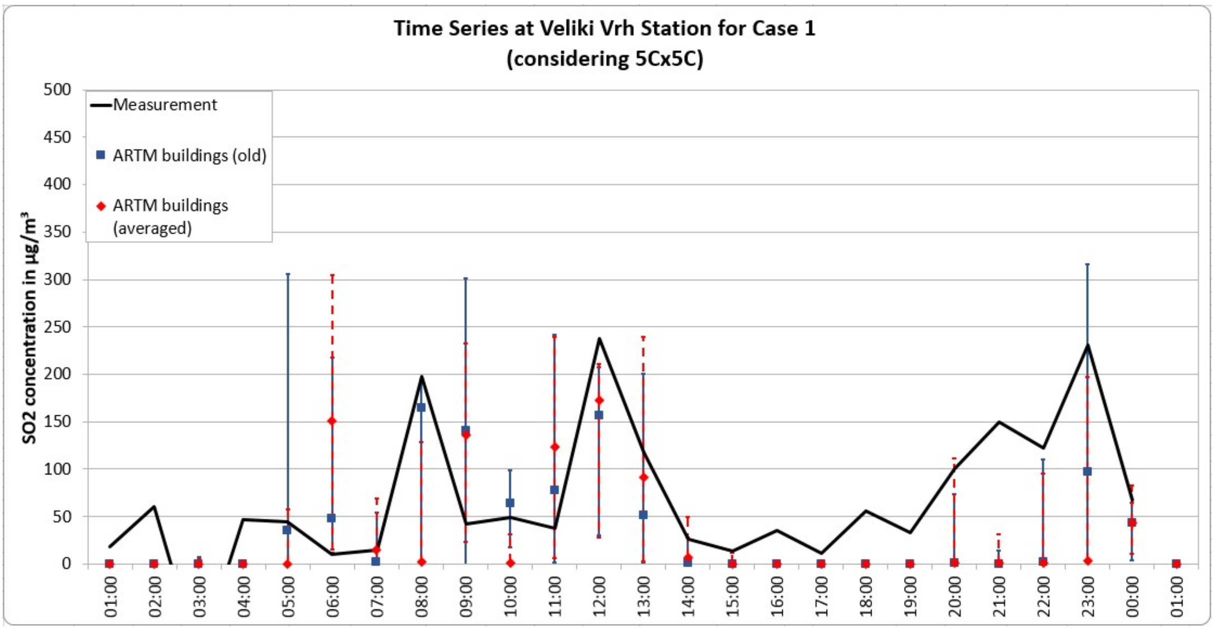

FIG. 49. ARTM results without accounting for buildings (top graph) and with accounting for buildings (bottom graph).

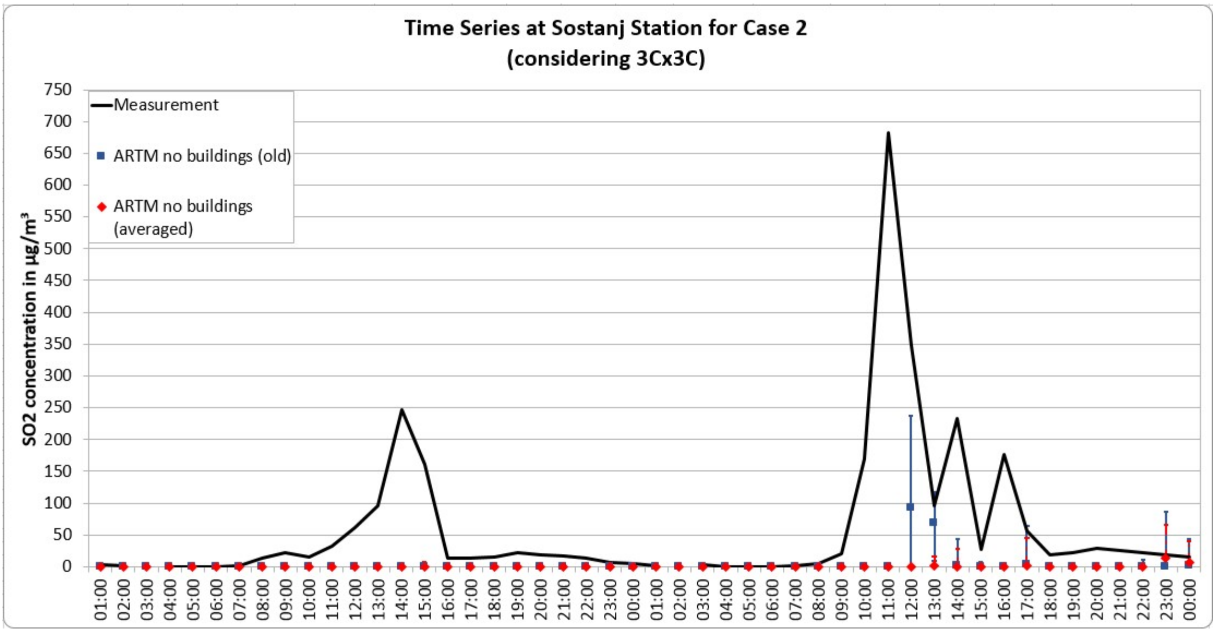

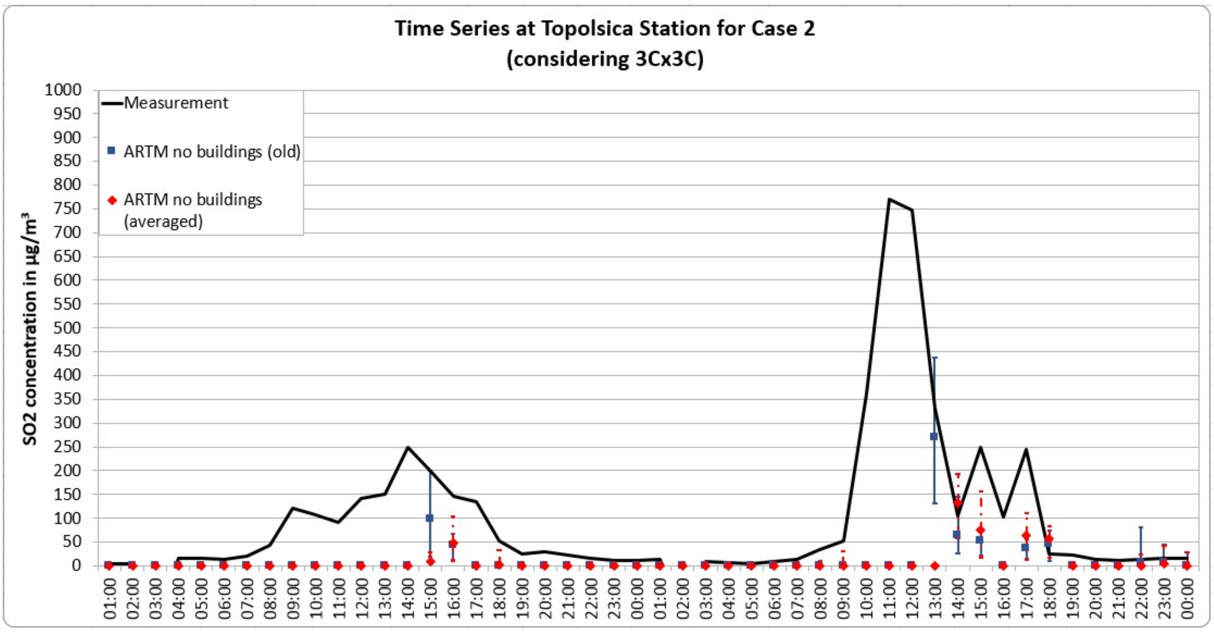

FIG. 50. ARTM results for the Šoštanj and Topolšica stations.

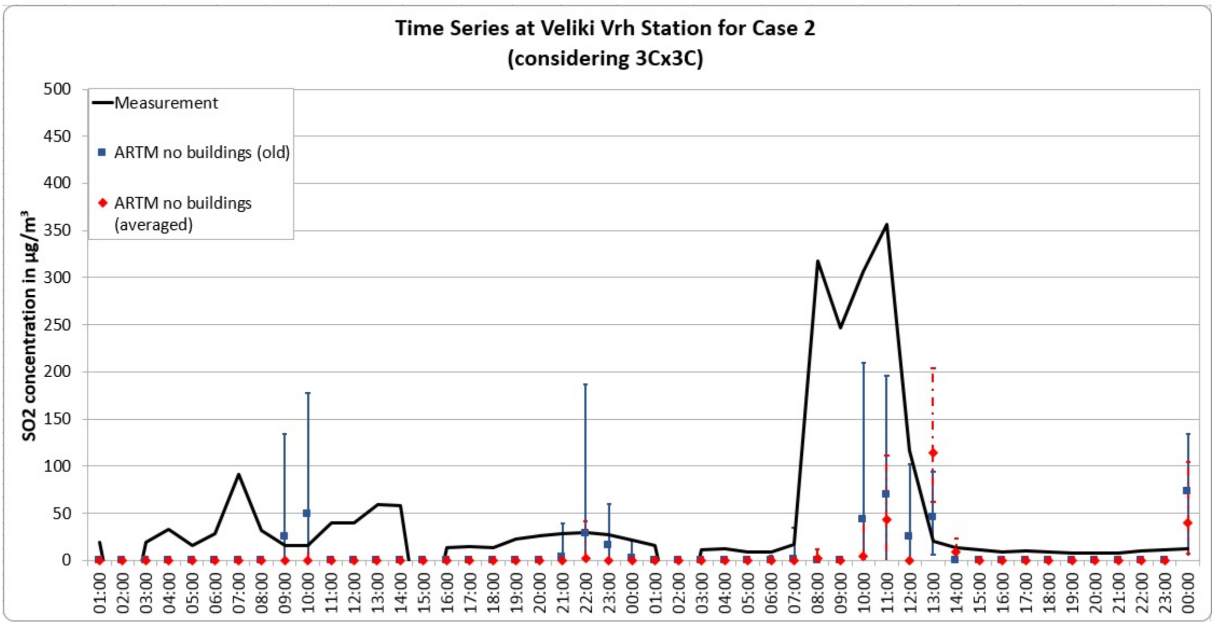

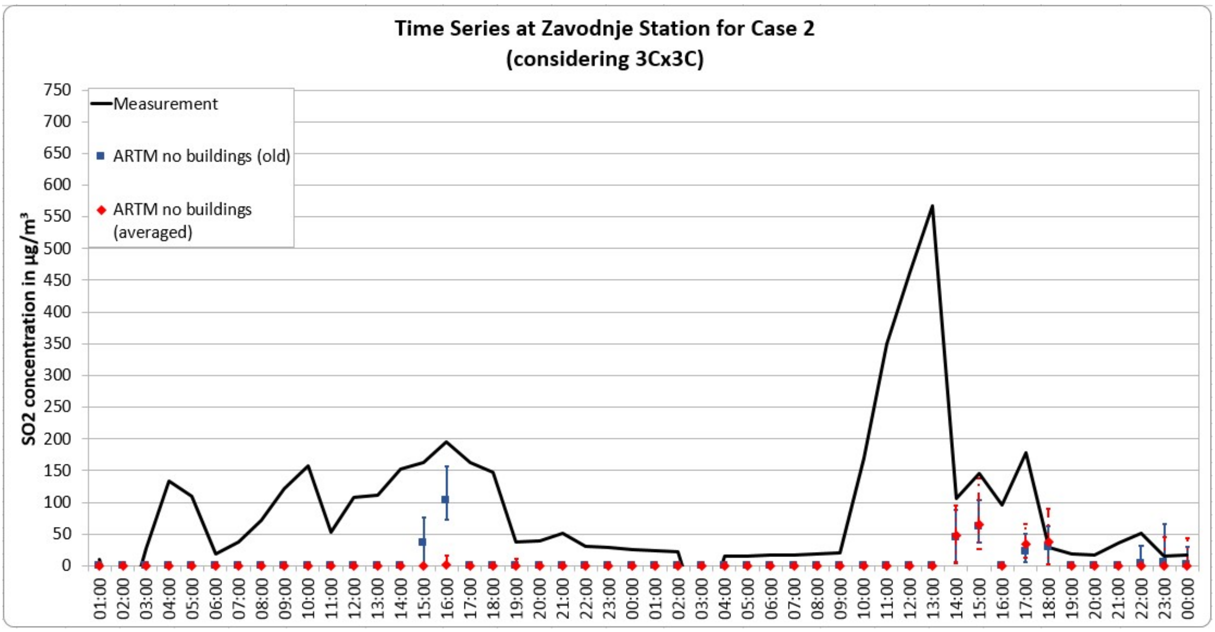

FIG. 51. ARTM results for the Veliki Vrh and Zavodnje stations.

The Veliki Vrh station is again better represented by the 'old' meteorology. Some values, for example on 1 April 1991 at 09:00 and 10:00 or on the evening at 21:00 to 22:00, nicely resemble the measurements. However, the larger peak in the morning does not appear, and also the second peak at noon has no match in the simulation. On 2 April 1991, again the first measured peak, which for Veliki Vrh is from around 07:00 to 09:00, cannot be reconstructed, and while the later large peak at 11:00 also appears in the simulation, the simulated values are at least one third smaller than the measurement.

The Zavodnje station is also not very well represented by the simulation data. While on the 1 April 1991 the 'old' meteorology shows 2 smaller peaks, the 'averaged' one does not show anything at all. Compared to the measurements that show, for almost all of the day, an SO_2 background with some smaller peaks, neither of the simulations represents the real situation here. For 2 April 1991, as for all other stations, the first high peak, which happens to be measured at this station around 13:00, cannot be found in the simulated results. Even though the simulations suggest that there are later peaks, the magnitudes of the simulation values are a maximum of half of the measurements.

4.6.5. LASAIR

In addition to ARTM, the decision support system LASAIR, which is specialized for nuclear hazards like dirty bombs and short term releases, was also applied to the Šoštanj release scenario by the same participant. LASAIR is a short term Lagrangian particle model which, due to its application for emergency situations, has an easy to handle graphical user interface and was trimmed towards short calculation intervals [18, 39]. More details on the model LASAIR can be found in Appendix III and Sections 2 and 3 of this publication and in [6].

In order to apply the model for the scenario, several adaptions and approximations had to be made due to the different main field of operations of the software:

- The number of emitting sources: LASAIR supports only one source per simulation run; therefore, Case 2 of the scenario had to be split and calculated separately for each of the stacks. These separately simulated values were added up for the results.
- Plume rise: LASAIR has no integrated function to automatically calculate the plume rise for hot sources; therefore the plume rise had to be calculated manually and added to the stack height.
- The maximum simulation time: Normally LASAIR is used for dispersions of a few minutes to a few hours. If calculations for a period longer than 8 hours need to be performed, it is possible to change the simulation time in the parameter file up to a maximum of exactly one day. For Case 2, the simulations had to be split into two single days; therefore, in the results file, the values in the hours following on the midnight date change can have large errors due to the 'clearing' from the simulation area of releases produced prior to the date change, which would still have been part of the actual dispersion situation.
- The number of simulation particles: In order to gain higher resolution results, the number of simulation particles was set from the standard of 60 000 to 1 008 000, being exactly 0.1% of the particle amount for ARTM simulations.
- Height of buildings: LASAIR allows for a maximum building height of only 200 m, so for Stack 5 with its 230 m in height, the height had to be cut to 200 m in the graphical

image (see Fig. 97 in Appendix III below). For the simulations, the stacks were not included as buildings to allow comparability with the ARTM results.

- The meteorological data: Since LASAIR does not allow for the input of wind speeds below 0.5 m/s for validation reasons, all meteorological values that are below this lower limit were set to 0.5 m/s, therefore producing another possible deviation in the final results of the simulation.

Details of these adaptations can be found in Appendix III.

As with ARTM, the two cases were modelled considering and not considering the buildings of the Šoštanj plant. Also, as described in Section 4.6.4 and Appendix III, four simulation modes (‘old’, ‘averaged’, ‘new categories’, and ‘averaged and new categories’) were applied for the LASAIR simulations.

Contrary to the results of the ARTM simulations, LASAIR did not face the issue of broken simulation runs due to the complex situation of the scenario. However, the ‘new categories’ and ‘averaged and new categories’ were not applied to Case 2. The different types of simulations performed are summarized in Table 12 above. Here only the most optimal simulation results from Table 13 were chosen to be described in detail in the following subsections.

4.6.5.1. LASAIR results, Case 1, 30 March 1991

The ‘new categories’ and ‘averaged and new categories’ produced a peak only around noon; therefore, these simulation results were discarded as too different from the real measurement data. The following diagrams were created considering a 5 by 5 measurement grid, where the different points are 150 × 150 m apart to be comparable to the other models. As before in Section 4.6.4, red or blue points in the diagrams show the simulated values as predicted directly at the measurement location. The error bars here account for the maximum and minimum value in the 5 by 5 grid. A statistical error, such as was done for ARTM, could not be determined for LASAIR simulations; therefore, it was not applied to the graphic. The black line in the graphics depicts the averaged measurement data in an hourly resolution.

Comparing the no building case with the building case (see Fig. 52) shows, just as before for the ARTM calculations (Section 4.6.4), that the influence of buildings in general leads to lower predicted values for the concentrations. Overall, the performance of LASAIR in this case is quite good, since almost all of the peaks are met, except the smaller ones at 16:00 and 18:00.

For the two different meteorological approaches, ‘old’ and ‘averaged’, it is more difficult with LASAIR than with ARTM to distinguish which predictions fit more accurately to the measurements. While for the case without buildings the values differ more between ‘old’ and ‘averaged’ than for the case with buildings, some of the ‘averaged’ results come closer to the measurements, for example at 08:00 or 12:00, and exactly hit the measurement line at 13:00 and 14:00. Furthermore, the ‘old’ values in the no building case have some members that fit better to the measurements or even hit them. Examples for this are at 07:00, 09:00, 10:00, 11:00 or at 23:00, where the ‘averaged’ ones are mostly far off.

Looking at the case with the buildings, the ‘averaged’ one here better represents the noon peak from 11:00 to 13:00, than the ‘old’ meteorology. Only at 14:00, the ‘old’ ones fit better to the measurements. The morning (from 07:00 to 10:00) and the evening (from 22:00 to 00:00) peaks are better met by the ‘old’ meteorology.

TABLE 13. LIST OF SIMULATIONS PERFORMED WITH LASAIR FOR THE ŠOŠTANJ SCENARIO[a]

Type of simulation	Case 1: 30 March 1991		Case 2: 1–2 April 1991	
Influence of Buildings	no	yes	no	yes
‘old’	X	X	X	X
‘new categories’	X	X	–	–
‘averaged’	X	X	X	X
‘averaged and new categories’	X	X	–	–

[a] X indicates simulations performed successfully; – indicates that a simulation was not performed.

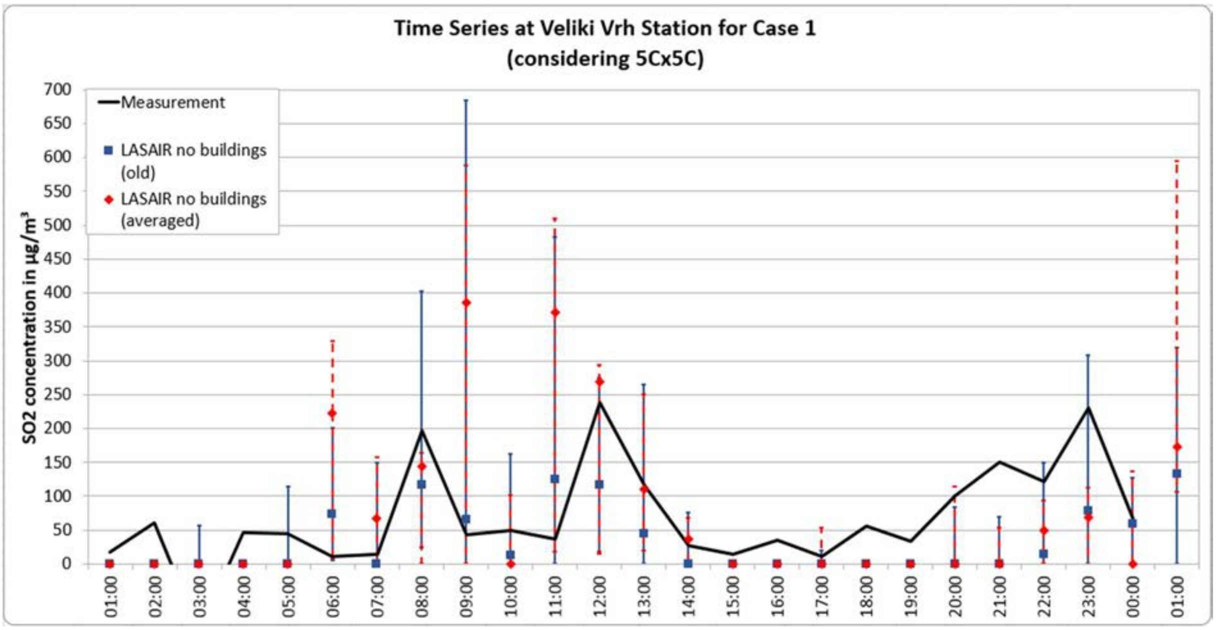

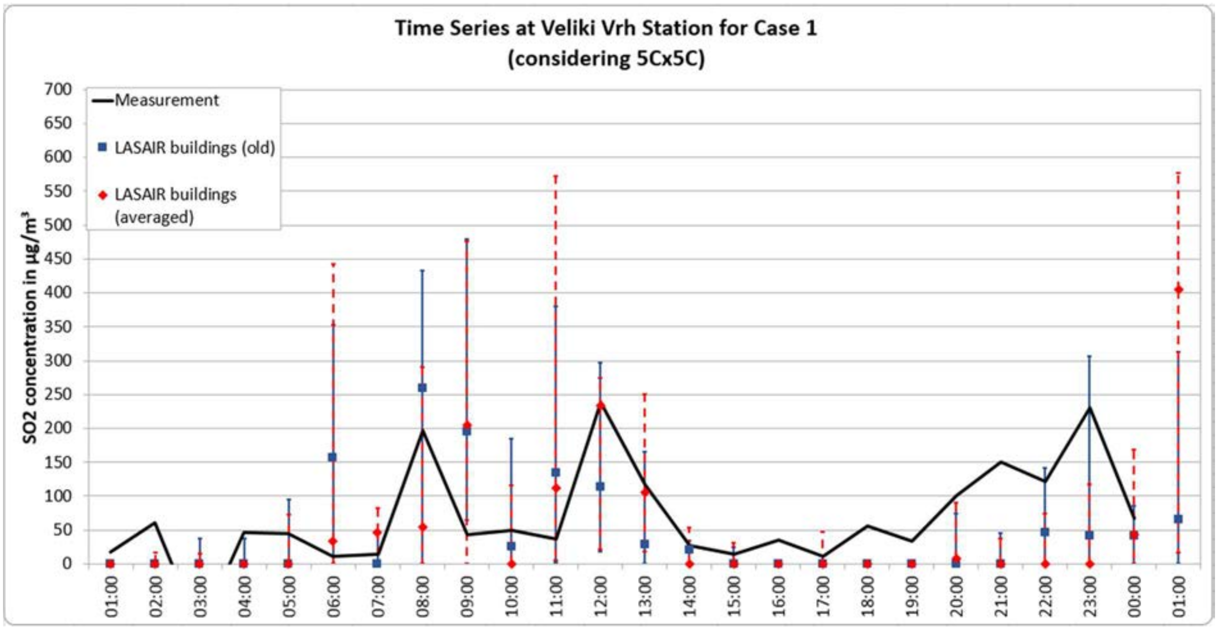

FIG. 52. LASAIR results without accounting for buildings (top) and with accounting for buildings (bottom).

4.6.5.2. LASAIR results, Case 2, 1–2 April 1991

For Case 2, the options 'new categories' and 'averaged and new categories' were not available (see Table 13). In order to be comparable to the simulations with ARTM, and due to lack of non-zero values in many cases for the Graška Gora and Velenje measurement stations, these two stations were neglected for the analysis of the LASAIR simulations. As with the results of the ARTM simulations from Section 4.6.4, also here the remaining stations are depicted in Figs 53–56. While here a 5×5 grid was available from the simulations, only a 3×3 one was chosen, to keep the comparability between the two models.

Similar to the ARTM results, the results for LASAIR at the Šoštanj station shown in Fig. 53 are quite far off from the measurements. Even though the first peak at 14:00 on 1 April 1991 is seen in both cases, with and without buildings, until 14:00 the predictions underestimate by a minimum of a factor of 2, and at 15:00 overestimated by one order of magnitude (2850 μg/m³ for the no buildings case and 2500 μg/m³ considering buildings, versus 161 μg/m³ resulting from the measurement). The highest peak, which appears in the measurements at 11:00 on 2 April 1991, is not seen in either of the two simulations. The following smaller peak shows up again, but is better represented in the building case with the 'averaged' mode; the last peak at 16:00 is overestimated in all cases.

For the Topolšica station (see Fig. 54), the no buildings case shows the more promising results that lie closer to the measurements, while distinguishing which approach, the 'old' or the 'averaged' one, is the more suitable one is not very distinct. The large peak on 2 April 1991 at 12:00 does not appear in the LASAIR simulations.

Figure 55 shows the results for the Veliki Vrh station. Interesting is that here in the LASAIR simulation a phantom peak appears for all cases at 10:00 on 1 April 1991 where there is no peak visible in the measurement data, and also the 11:00 value is still a factor 2 to 4 higher for the buildings and no buildings case, respectively. The flat plateau from 16:00 to 01:00 is first not seen in the models, and then appears at 22:00, while here the no building case with the 'old' meteorology shows the best congruency with the measured data. Only the second of the two peaks on 2 April 1991 can be reconstructed by LASAIR, starting with 10:00. Also here, the case without buildings comes closer to the measurement values for both modes, while the 'averaged' one here is preferable.

The results for the Zavodnje station (see Fig. 56) basically looks similar to the ARTM results shown in Section 4.6.4. Also, in LASAIR 1 April 1991 peaks are not well represented by the simulation data and show only 2 smaller peaks; the 'averaged' one does not show anything in the building case. The high peak on 2 April 1991 is not shown in the simulation data, and the smaller peaks also appear underestimated. The range of results is smaller for the buildings case, where the actual point reaches slightly closer to the measurement curve. In the no buildings case, the deviation bars almost reach the peaks, although the actual points lie deeper.

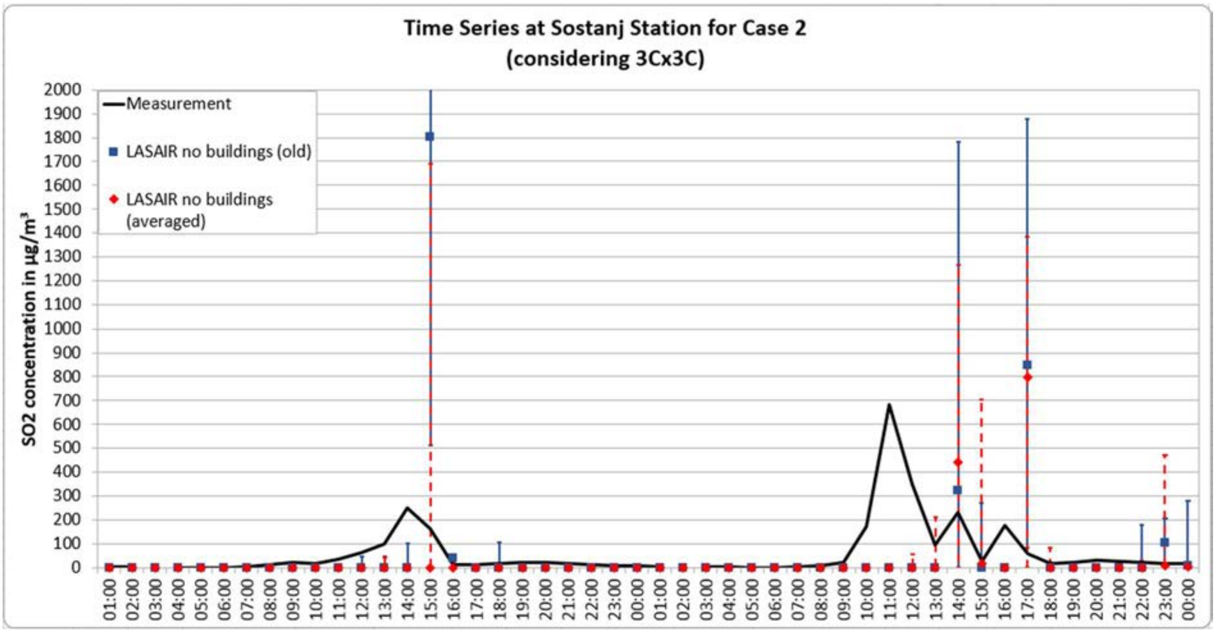

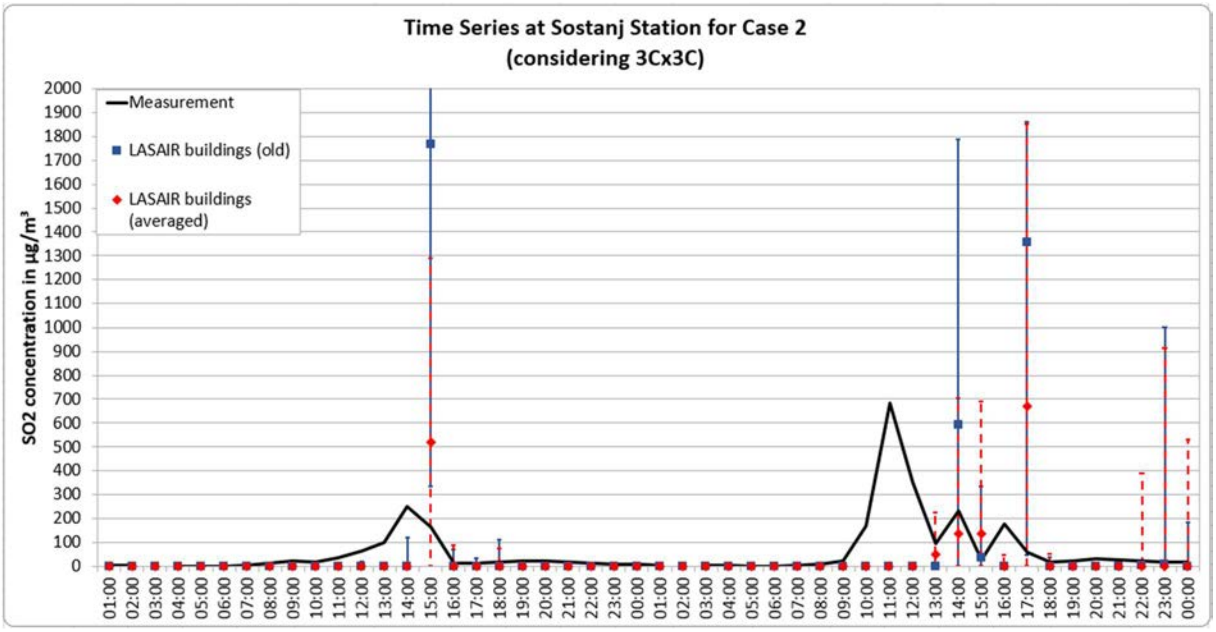

FIG. 53. LASAIR results for the Šoštanj station with and without building influence.

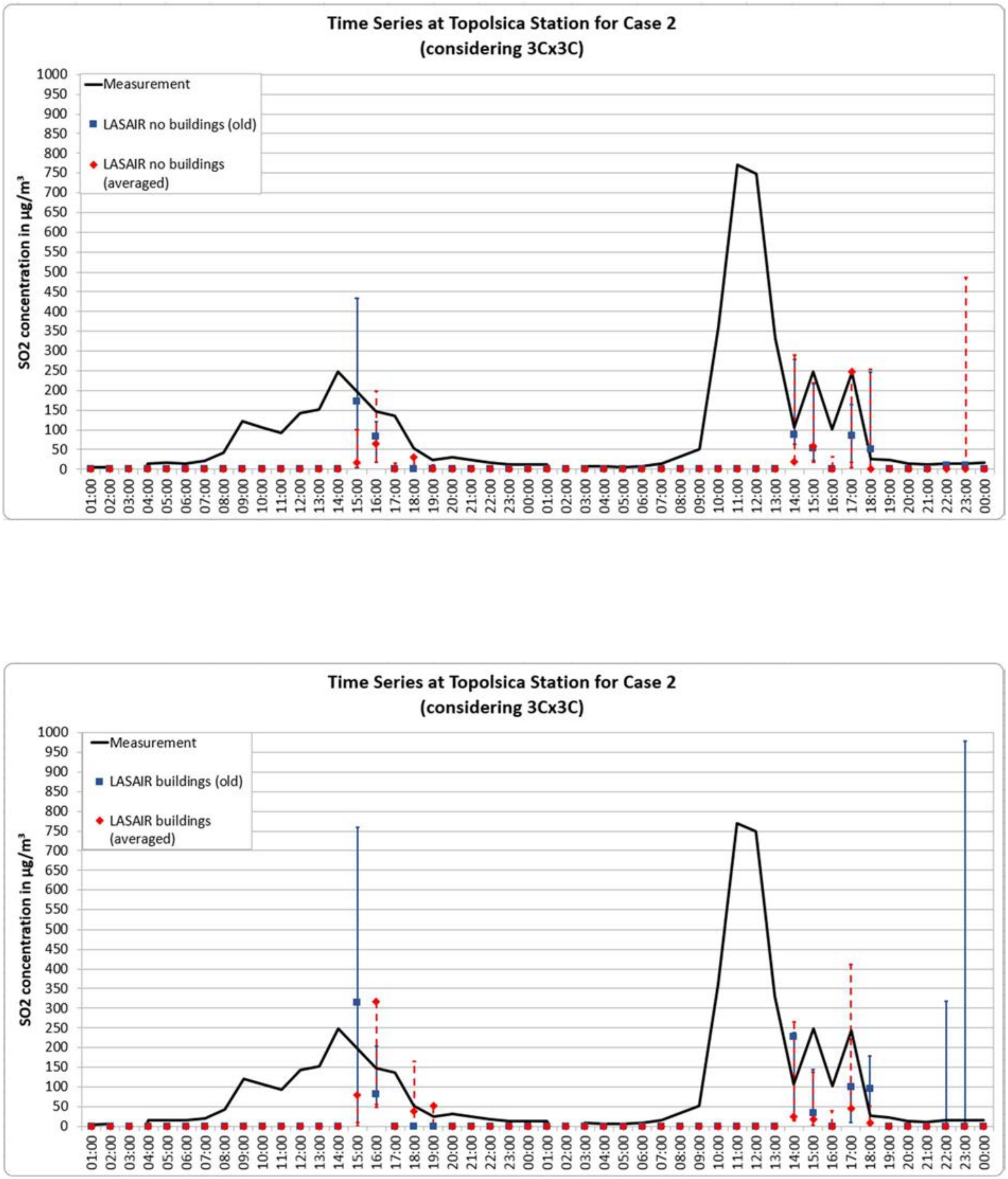

FIG. 54. LASAIR results for the Topolšica station with and without building influence.

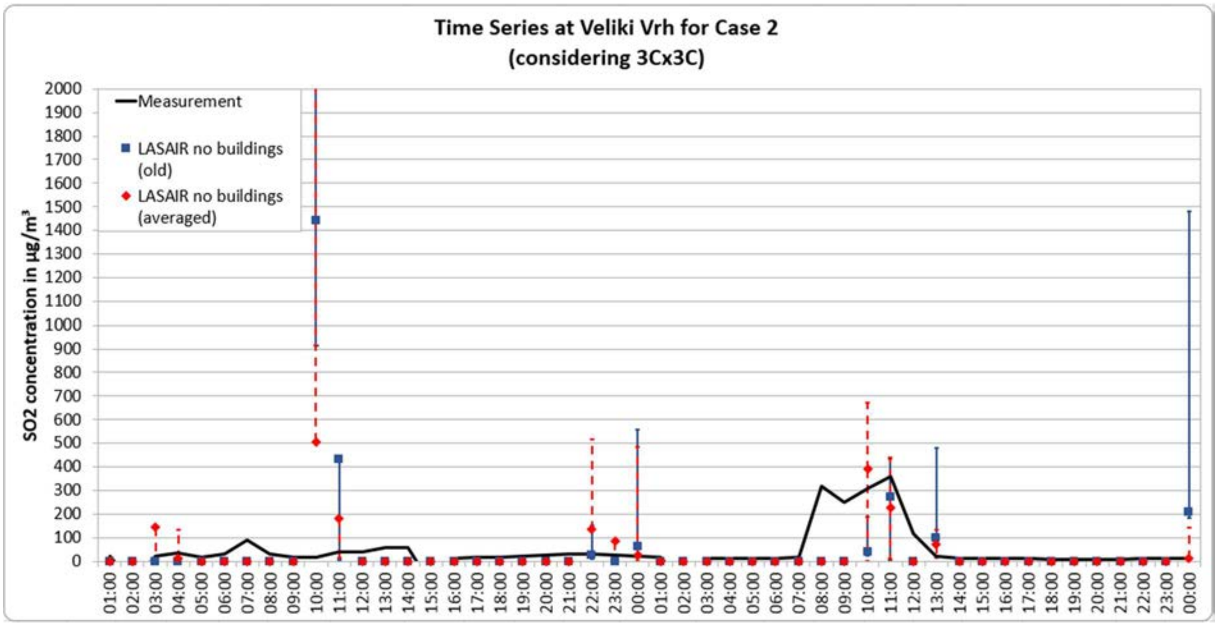

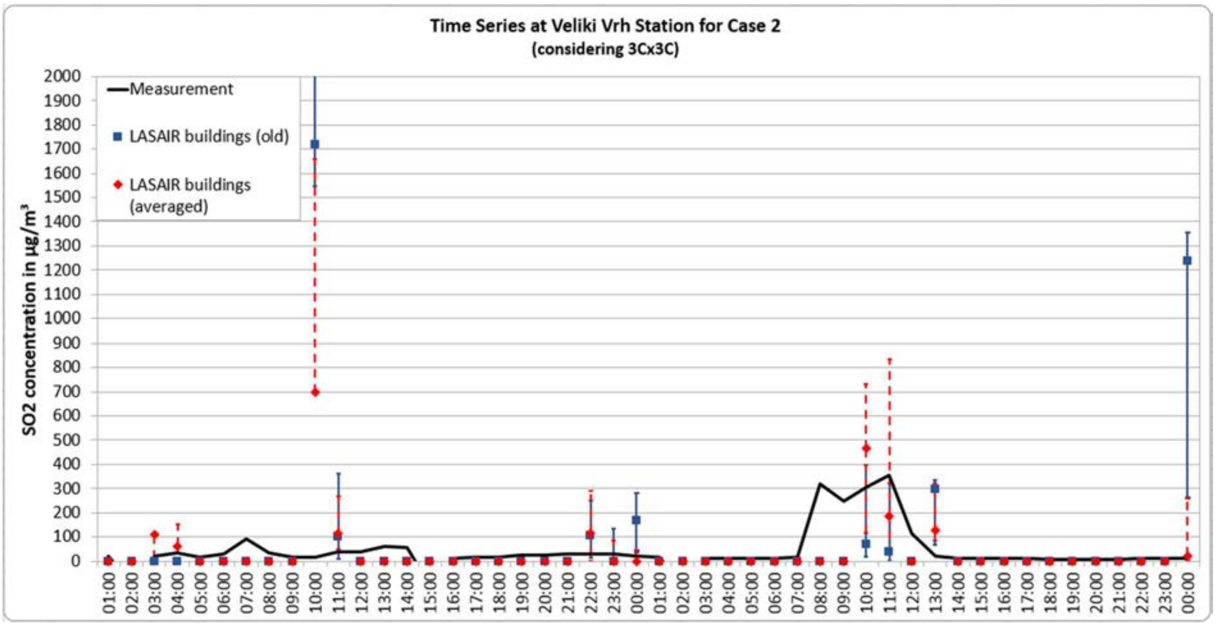

FIG. 55. LASAIR results for the Veliki Vrh station with and without building influence.

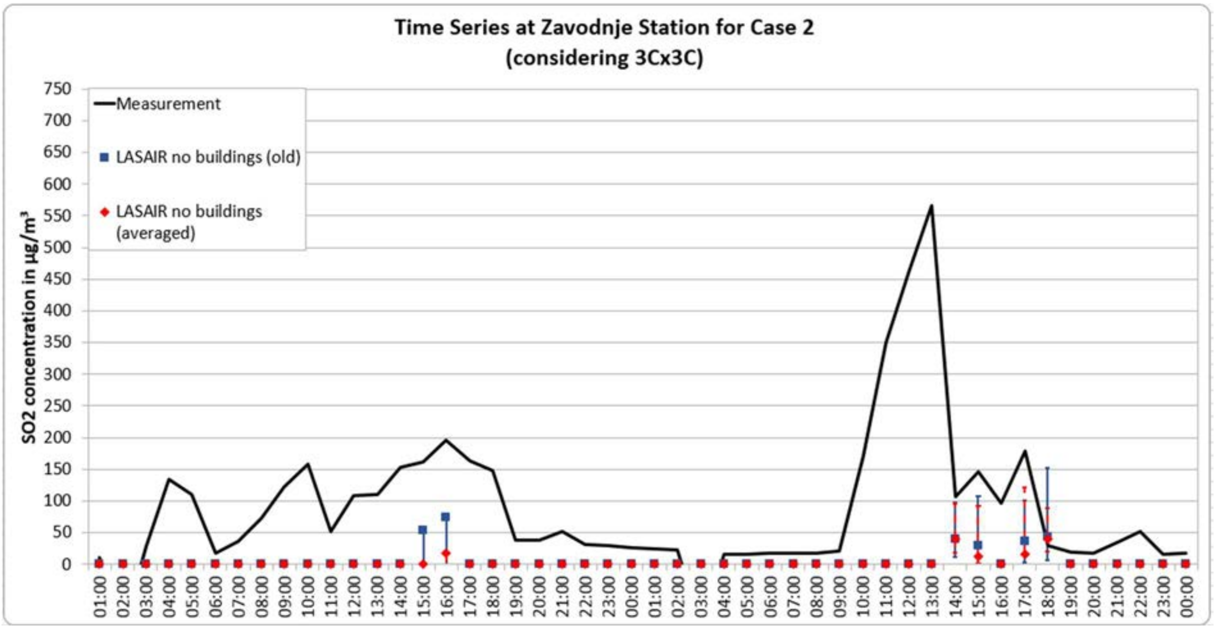

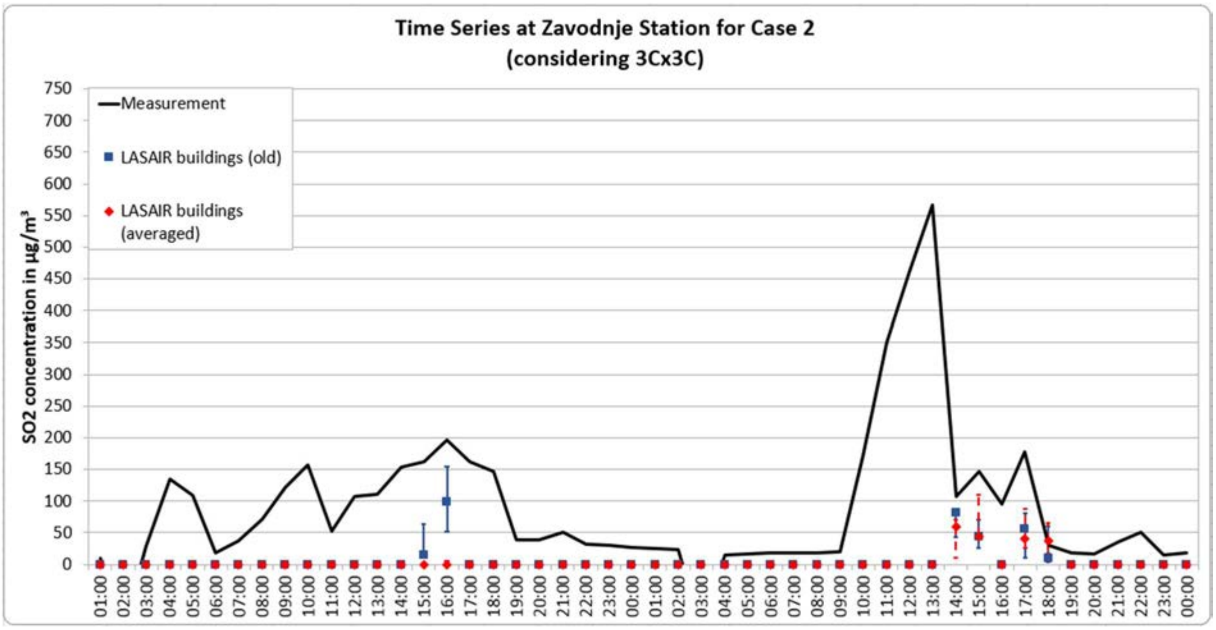

FIG. 56. LASAIR results for the Zavodnje station with and without building influence.

4.6.6. NFS_Vinca

4.6.6.1. Comparison of best results for Case 1, 30 March 1991, Veliki Vrh

One of the aims of the exercise was simulation of the maximum concentration of SO_2 that was measured at the control point Veliki Vrh on the 30 March 1991 at 12:00 local time. During that period only one source was active, namely TPPŠ, with a chimney height of 100 m. The measurements were accumulated concentrations over half hour periods. For the period 11:30–12:00, the accumulated concentration was 288 $\mu g/m^3$. The wind was for the whole period 11:30–12:00, from the source towards the Veliki Vrh station. The line from the source to the measurement point is uninterrupted by the topography, as shown in Fig. 57. Near the source, the vertical profile of the wind was measured using SODAR at heights 104 m, 158 m and 213 m as well as T2m (temperature at 2 m height) from the automatic meteorological station next to the SODAR station.

The Pasquill stability classes were obtained from the estimated vertical gradient. The estimation was made using T2m at two points and their respective height difference of 186 m (Sostanj 360 m a.s.l. and Veliki Vrh 546 m a.s.l.). The horizontal distance was about 2400 m. Estimates of C class stability were obtained from the measured T2m following the Pasquill-Gifford classification [40].

The same results for stability classes were obtained using σ_θ, a turbulence based method, which uses the standard deviation of the wind direction in combination with the scalar wind speed, adjusted in accordance with common practice, if the measurement height is other than 10 m [40]. Table 14 provides an example at 11:30.

From the half hour wind measurements, time interpolations to 10 min and 1 min intervals were made, which were used for the Gaussian plume and puff methods, respectively. To calculate the effective release heights the Egan hill concept was used and the Concawe method was applied for plume rise. The cross section between source and measurements points and the release height is shown in Fig. 58 (left panel). Using puff calculations for stability class C, 345 $\mu g/m^3$ was predicted at the control point. Figure 58 (right panel) shows the pollutant concentrations using a wind field calculated from the 104 m SODAR wind. This wind was used in the Gaussian plume model, as well as in the puff model.

In Fig. 59 (left panel), the wind field calculated is shown as a linear combination of SODAR wind and 10 meter wind at the control point at Veliki Vrh. The right panel shows the concentration field obtained with the puff model, with a new value for the concentration at the control point of 308 $\mu g/m^3$.

Figure 60 depicts the subdomain around the control point. Circled crosses are grid points with a grid distance of 150 m.

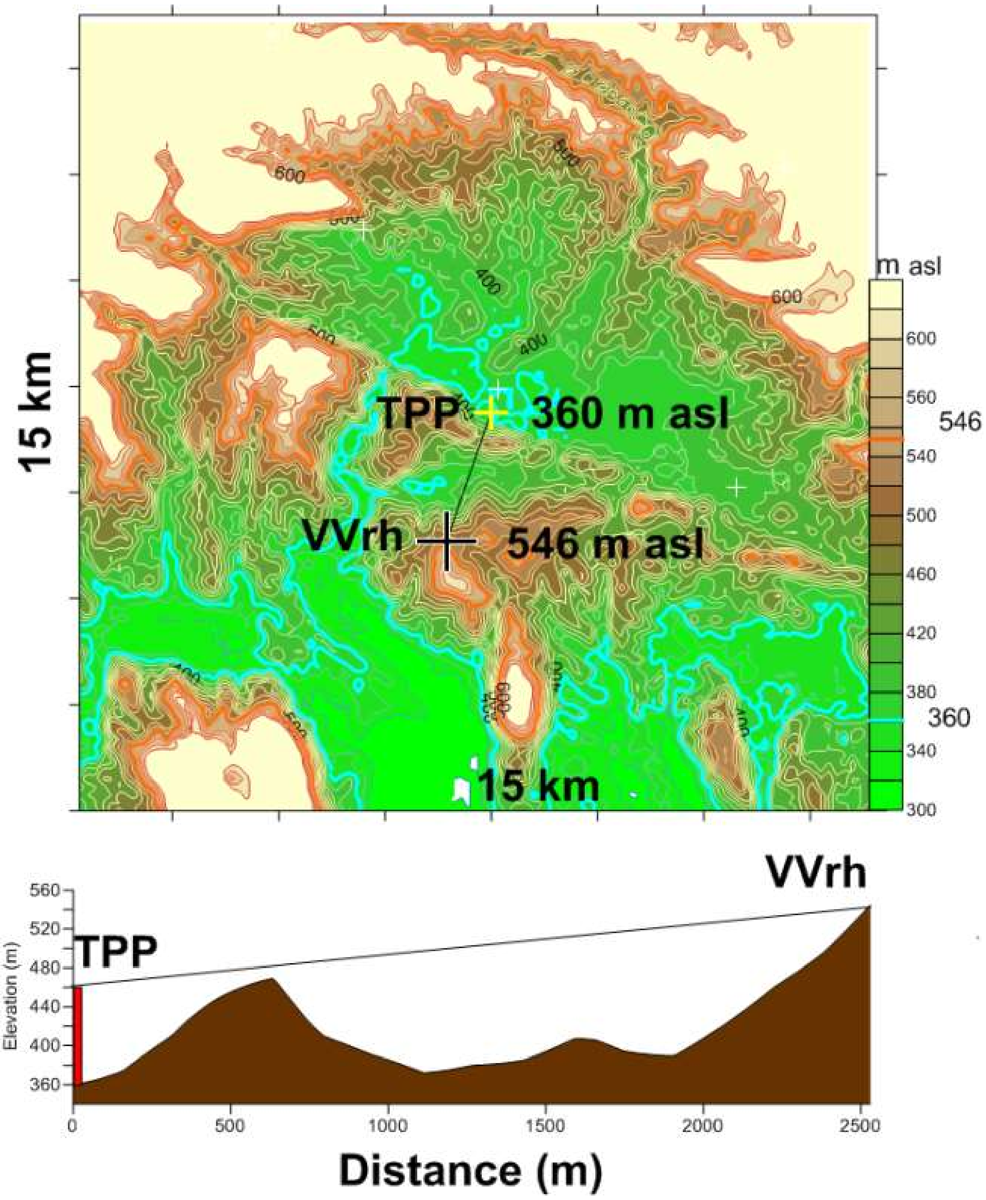

FIG. 57. Modelling domain (15 km × 15 km with the centre at TPPŠ).

TABLE 14. EXAMPLE OF STABILITY CLASSES OBTAINED USING THE σ_θ METHOD

Wind at height (m)	**σ_θ,**	**Estimated stability class**	**Corrected velocity (m/s)**	**The new stability class**
50	30	A	3.4	B
104	22	A	4.	C
158	21	A	5.1	C
213	16	A	5	D
267	15	A	5.9	C
322	14	A	6.1	D
367	11	A	6.1	D

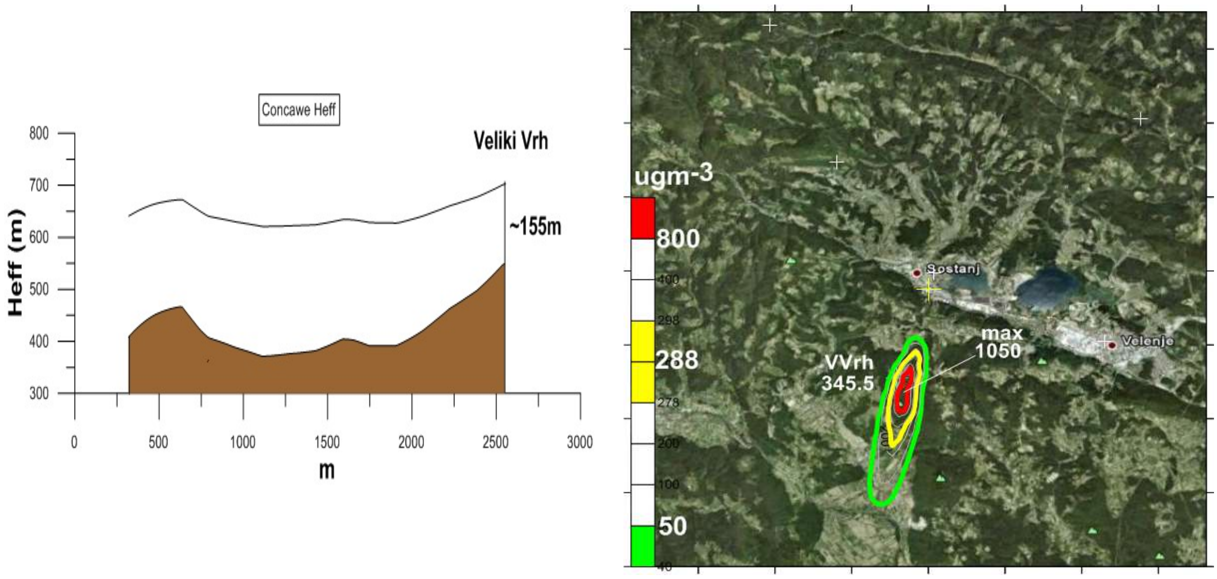

FIG. 58. The left panel has the effective release heights, using the Egan hill concept and Concawe method. The right panel shows pollutant concentrations using a wind field calculated from the 104 m SODAR wind.

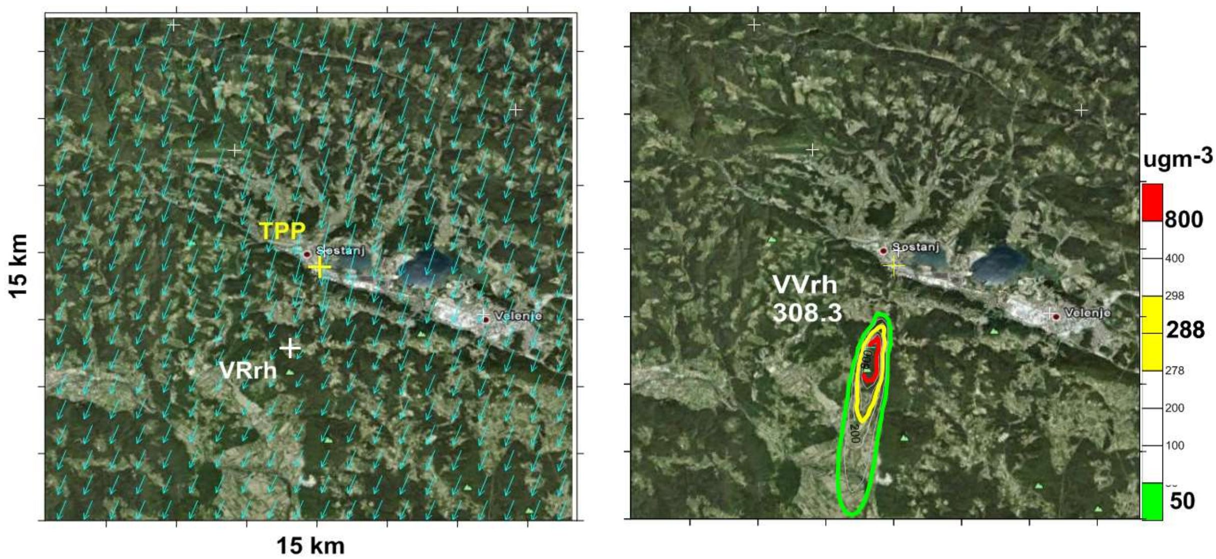

FIG. 59. The left panel shows the wind field calculated as a linear combination of SODAR wind at the source of the pollutant and the 10 m wind at the control point at Veliki Vrh. The right panel shows the concentration field obtained with the puff model using the calculated wind.

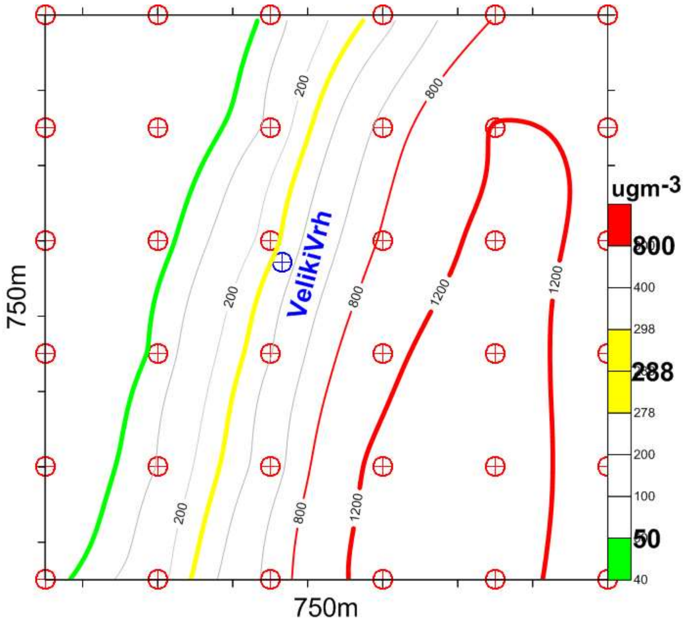

FIG. 60. Subdomain around the control point.

4.7. KEY CONCLUSIONS

The results of the model validation show that in order to obtain good modelling results, appropriate input measurement data need to be available. In this section, a summary is provided of the necessary measuring systems and models that are needed to generate realistic results that are relevant to the situation. In particular, focus is placed on complex conditions, where a nuclear facility is located on a more or less complex terrain.

The modelling system is thereby defined as the combination of the meteorological model for 3-D representation of the meteorological atmospheric conditions and the model for the representation of the dispersion of the cloud of contamination in the atmosphere.

4.7.1. Meteorological data

The collection and processing of meteorological data needs to be performed automatically in processing intervals ranging from 10 minutes to one hour. In this exercise, the meteorological data were available for intervals of 30 minutes. Using various methods, participants rearranged, revised, or interpolated the meteorological data to obtain model input information in time intervals ranging from 1 min or 10 min (NFS_Vinca) to 1 h (ARTM and LASAIR).

In the surroundings of the facility, some ground based weather stations, complying with WMO standards, need to be established at representative locations; it is suggested that 3–10 such stations be established, depending on the complexity of the terrain. Wind, temperature, relative humidity, global solar radiation, vertical temperature gradients and in particular, precipitation (for evaluation of deposition) need to be measured at each location. Further details are provided in Ref. [41].

In the direct vicinity of the facility or at a different location nearby, which is representative of the description of the vertical condition of the atmosphere, at least one SODAR needs to be placed to record the vertical wind profile at higher altitudes, where releases move and where the plume is expected to rise (at least a few hundred metres above ground). SODAR is the modern standard equipment, which operates automatically with perfected and tested technology. These data are of key importance to correctly represent the movement of the cloud of contamination. SODAR data can be complemented by measurements at a high meteorological tower, but due to constructional limitations, these generally record only the lower layer of the atmosphere, where releases emerge, and not the atmosphere at the altitude of the plume rise and dispersion of plumes in the atmosphere; this is the key deficiency which makes a high tower without SODAR insufficient. It is suggested that a radio acoustic sounding system (RASS), i.e. vertical temperature profiler, be used in combination with SODAR, since it is very reliable for measuring the vertical temperature profile, which is almost as important as wind, especially during a temperature inversion. All other findings and needs for RASS equal those for SODAR. The RASS technology was unfortunately not available in 1991 during the Šoštanj measurement campaign, although it is certainly accessible and affordable today.

Without appropriate data on the vertical meteorological profile in the atmosphere, the dispersion models cannot function as desired. For complex terrain, it is essential to know the entire atmosphere, including the measured profile.

In general, it can be assumed that all measurements together, ground based measurements and measurements of the atmosphere profile, will describe the atmosphere, which is inhomogeneous over complex terrain.

4.7.2. Meteorological models

The meteorological model, which is used as the basis for the dispersion model, need to be fitted to the purpose and complexity of the site of use. It has to ensure a 3-D numerical representation of the meteorological condition of the atmosphere for all key parameters, which are used in turn by the dispersion model (3-D wind field, turbulence, temperature etc.). The meteorological model is commonly a combination of the model for wind and turbulence and the pre-processor for all other meteorological values.

The model needs to be good enough to produce reconstructed meteorological parameters that are consistent with the measured data and no unnecessary errors are entered into the entire modelling system at this stage.

For use over complex terrain, such as that in the subject Šoštanj experiment, mass-consistent models for wind are most appropriate at this time. The numerical weather prediction (NWP) weather models are still very demanding in terms of calculations and are generally not yet successfully validated for use for fine resolution over complex terrain. For this assessment, cells that were 100–200 m in size over a terrain with the complexity of hlTc = (220 m, 1.5 km) (see Fig. 61 below) [42]. This corresponds to valleys with a width of 1.5 km and a difference in altitude of 220 m, which the model had to correctly 'see' to obtain appropriate final results. Similar challenges also occur during the use of computational fluid dynamics (CFD) models.

The NWP and CFD models can be used as soon as they are successfully validated for use over a terrain with the complexity such as that of the target use domain. What is needed for successful prior validation also apply to the previously mentioned mass-consistent models.

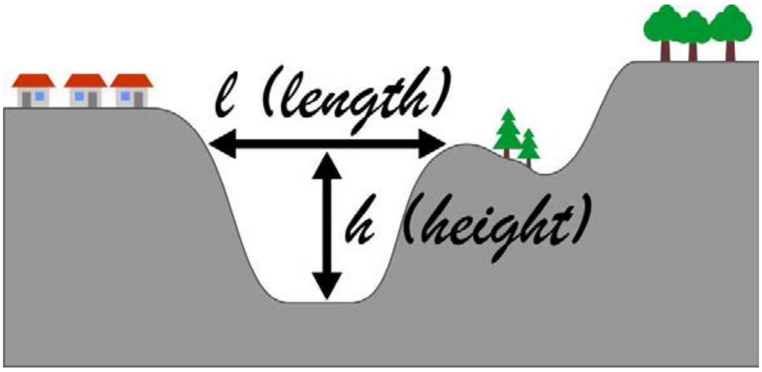

FIG. 61. Illustration of the hlTc (height and length of the topographic complexity) index. The figure presents the dimensions in the vertical cross-section [42].

When using all these models over the most complex terrain, it is important to be careful not to ‘smooth’ the terrain to an extent where the key characteristics of the meteorological processes are lost, as such processes are realistically complex and demanding precisely because of the complexity of the terrain in the subject domain.

4.7.3. Dispersion models

Just like the meteorological model, the capacity of the dispersion model has to be fitted to the complexity of the target use domain.

Based on the results of the validation using Šoštanj data, it can be concluded that simple Gaussian models are not appropriate for use over complex terrain. The Gaussian puff model (or Lagrangian puff model with Gaussian parameters of turbulence) is only conditionally useful for simple cases with strong wind, when representing direct contamination in the direction of the wind from the source to the location that is subject to analysis. It is not appropriate for more complex cases.

However, the numerical Lagrangian particle models are, according to their concept, appropriate for the most complex situations over complex terrain. The comparison of the validation results of several such models with the Šoštanj experiment clearly shows that the most complex cases still include scientific challenges, which have not yet been completely answered. The quality of the representation of the most complex cases depends on the main characteristics of the implementation of the models (compare the descriptions of the models used in this exercise) and the appropriate functioning of parameters to use over the domain in question. This especially includes the fact that the complexities of meteorological conditions can vary (e.g. the change between sea, lake, land; the complexity due to rough terrain; the transition between rural and urban environments).

The models used have to have the key capacity to correctly represent the effective plume rise of the cloud of contamination due to temperature buoyancy and/or due to the kinetic energy of the pollutants when entering the atmosphere. If this part of the representation does not function correctly, the model shows the movement of the cloud at a false altitude. The different wind and other meteorological conditions at the false altitude can cause the predicted cloud of pollutants to wander off into a completely wrong direction.

4.7.4. NEEDS for static data about the domain of use

For difficult cases, the two dimensional (2-D) digital elevation model and the land use classification needs to be used in a resolution that equals the natural horizontal resolution of the modelling system.

4.8. OVERALL SUMMARY

A modelling system (meteorological model + atmospheric dispersion model) may be used for real life purposes to ensure radiological safety or optimize routine discharges and to evaluate the possible effect of a nuclear facility on the air in the region. However, before a modelling system is used for such purposes, the system needs to be validated using tracer experiment data of a complexity that is similar to the complexity of the target domain. Besides the statistical evaluation, the check needs to also include a qualitative evaluation of meteorological conditions in which the model works well, as well as conditions in which it is expected, based on the validation, that the model has some deficiencies, which are being resolved.

It is, however, important that some of the most powerful modelling systems can already realistically represent even the most complex conditions of contaminant dispersion in the atmosphere. Based on the represented results, it can be concluded that the implementation, in practice, of appropriately powerful modelling systems that fit the complexity of the domain of use.

The key benefit of modelling systems compared to measurements of radiological contamination is that they represent a 3-D situation in the surroundings of the facility from which the releases emerge. Point measurements are not comprehensive enough. 3-D representations of the situation also enable correct action in case of accidents.

4.9. FUTURE CHALLENGES

This publication unfortunately does not deal with deposition (dry, wet, terrain touch factor), because these data were not available for the Šoštanj measurement campaign. Prediction of deposition remains a challenge to be solved in the future.

Another future challenge is the verification of the use of modelling systems for the timely forecast of contaminant dispersion, which is very important for planning and optimization of routine discharges and for planning of action in case of accidents.

4.10. ACKNOWLEDGEMENTS

The study was partially financed by the Slovenian Research Agency, Project No. L1-5475 and Project No. L2-6762. Acknowledgement goes also to Dragana Kokal for data elaboration and to Darko Popović for document formatting and preparation.

5. CONTAMINANT TRANSPORT AND COUNTERMEASURES EXERCISE

5.1. INTRODUCTION TO THE FUKUSHIMA EXERCISE

The Fukushima modelling exercise was intended to provide an opportunity to test model predictions for the effectiveness of remediation efforts in an urban situation. The exercise was based on measurements made in Japan following the accident at the Fukushima Daiichi Nuclear Power Plant in 2011 (1F accident) and on experiments carried out by Japan Atomic Energy Agency (JAEA). The exercise uses a realistic but hypothetical urban situation and is not intended to represent any actual city. The objective of the modelling exercise is to predict the doses that could be received by reference individuals both in the absence of any remediation actions and also with specified remediation actions. The exercise started with a generalized ‘current situation’ approximately three years after the accident. Thus, the contribution to dose of short lived radionuclides was not part of the exercise. Remediation efforts carried out prior to the ‘current situation’ were included as part of the history of the ‘current situation’, but the exercise did not specifically deal with ‘early’ remediation efforts.

Input information for the exercise includes information about the radionuclide composition and deposition densities, external dose rates, conditions of the initial deposition event, average meteorological conditions for the area, locations for modelling endpoints, and types of remediation efforts performed or being considered for use. Modelling endpoints for intercomparison among modellers include the deposition at specified outdoor locations, external dose rates at specified locations and times, contributions to external dose rate from relevant surfaces, external and internal doses to specified reference persons, effectiveness of various remediation efforts in reducing dose rates and doses, and estimates of the waste (volume and activity) generated by the remediation efforts. The first stage of the exercise was carried out during the MODARIA Programme and included two endpoints: (1) prediction of external dose rates at specified locations in the absence of remediation, and (2) prediction of the external dose to specified reference individuals in the absence of remediation. For both endpoints, predictions were requested for the starting point (‘current situation’) and 1 year increments to 10 years after the starting point.

5.2. DESCRIPTION OF THE TEST SITE

5.2.1. General description

The test site was a generalized urban situation in the area affected by the Fukushima accident. While the description of the area and the situation were based on real situations, the test site for this modelling exercise did not represent any actual town or city.

The test site was characterized by four ‘environments’: (1) indoors inside wooden houses, (2) indoors inside concrete constructions, (3) outdoor unpaved areas, and (4) outdoor paved areas. These ‘environments’ correspond to the main types of land use and to the main categories of remedial efforts. Land area of each ‘environment’ for the test site is provided in Fig. 62. Time spent by people outdoors in the residential and building area was classified as time spent in ‘outdoor paved areas’. Time spent by people outdoors in other areas (e.g. agricultural use areas, forest, etc.) was classified as time spent in ‘outdoor unpaved areas’. Table 15 shows dwelling types and construction materials in the test site. Approximately 80% of dwellings in the test site were of wooden construction. Concrete structures were used as work places and as public infrastructure (e.g. stores, community center, and recreation facilities).

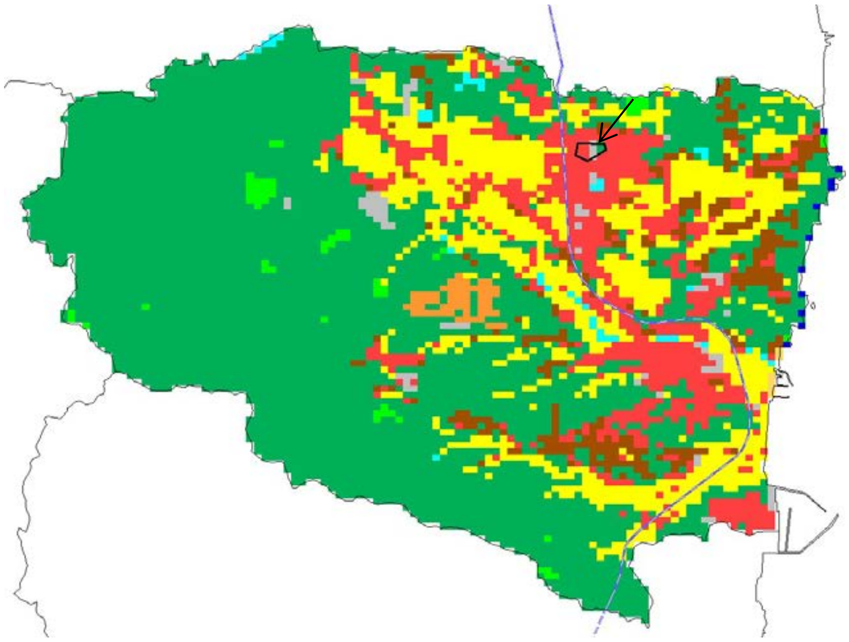

Land Type	Area (km^2)
rice field	11.5
land for other agricultural use	3.4
forest	42.5
waste land	0.7
Residential and building area	8.3
rivers and lakes	0.5
coastlines	0.1
ocean	0.1
golf course	0.6
other land use	0.8
Total	68.5

*:The size of rectangular dots is approximately 100 m × 100 m.

FIG. 62. Land use situation in the test site for the modelling exercise [43].

TABLE 15. DWELLING TYPES, CONSTRUCTION MATERIAL AND STORIES OF BUILDINGS IN THE TEST SITE [44]

Building type	Building size	Wooden construction	Fire safety wooden construction	Non-wooden construction	Total
Detached houses	1 Story	780	750	10	1540
	≥ 2 Stories	990	1720	60	2770
Tenement houses	1 Story	40	0	0	40
	≥ 2 Stories	0	100	0	100
Apartment house	1 Story	0	0	0	0
	2 Stories	0	290	540	830
	3–5 Stories	0	0	570	570
Others		0	30	10	40
Total		1810	2890	1190	5890

In this exercise, a specific 'location' was selected for assessment of doses, taking into account detailed conditions of the surrounding situation. This 'location' is characterized in terms of radiological situations and land use type. The geometry of this location is given in Fig. 63. Each mesh (grid cell) described in this figure is 10 m × 10 m in size. This location is comprised of residential area, ground and park, forest, a large building and paved surface (see Fig. 63).

5.2.2. Climatological characteristics

The test site is in Tohoku district in Japan and is located on the coastline of the Pacific Ocean. The type of climate is moderate coastal climate. Table 16 shows the average meteorological conditions: precipitation, temperature, wind speed and sunshine duration; averages were calculated from data measured in the period between 1981 and 2010 (Table 16).

5.2.3. Population characteristics

The population of the test site was 16 001. Tables 17 and 18 show the age structure and industrial structure of the site, respectively. About 20% of the population was below the age of 19 years, and about 60% were between 20 and 64 years old. The remainder of the population was aged 65 years or more. The number of workers in the primary sector of industry (e.g. agricultural work) accounted for 5.3% of the total, and those in the secondary sector of industry accounted for about 30%. Almost 65% of the inhabitants worked in the tertiary sector of industry.

5.3. RADIOLOGICAL CHARACTERIZATION OF THE SITE

5.3.1. Background levels of radioactivity

Before the 1F accident, the air absorbed dose measured in Fukushima prefecture was about 0.04 μGy/h [45].

5.3.2. Information about the deposition event

The relationship between ambient dose equivalent rate and precipitation is shown in Fig. 64. This figure shows time variations of ambient dose equivalent rates and precipitation during the first month after the accident. Time variation of the dose rate was measured at the test site. Several increases in the dose rate are visible in the figure. In particular, the main contamination event occurred on 15 March 2011, followed by sharp increases in dose rate on 16–17 March 2011. The figure also shows the time variation of precipitation, which was extracted from weather forecasting data provided by the Japan Meteorological Agency (JMA). These data are called 'GPV' (Grid Point Value) and include various weather parameters such as wind components, temperature and precipitation. These meteorological parameters are calculated by regularly spaced grids with a resolution of 5 km. One grid in the test site was selected, and the precipitation data of that grid were extracted. The figure shows the relationship between dose rate and precipitation, which often increased at the same time.

As shown in Fig. 64, radioactive fallout and contamination at the test site were estimated to have occurred during the period of 15–16 March 2011, often under wet conditions. The composition of the surface activity density of each radionuclide normalized to that of ^{137}Cs was taken from the reports of UNSCEAR [46] and WHO [47]. The relative isotopic composition of deposited radionuclides is shown in Table 19.

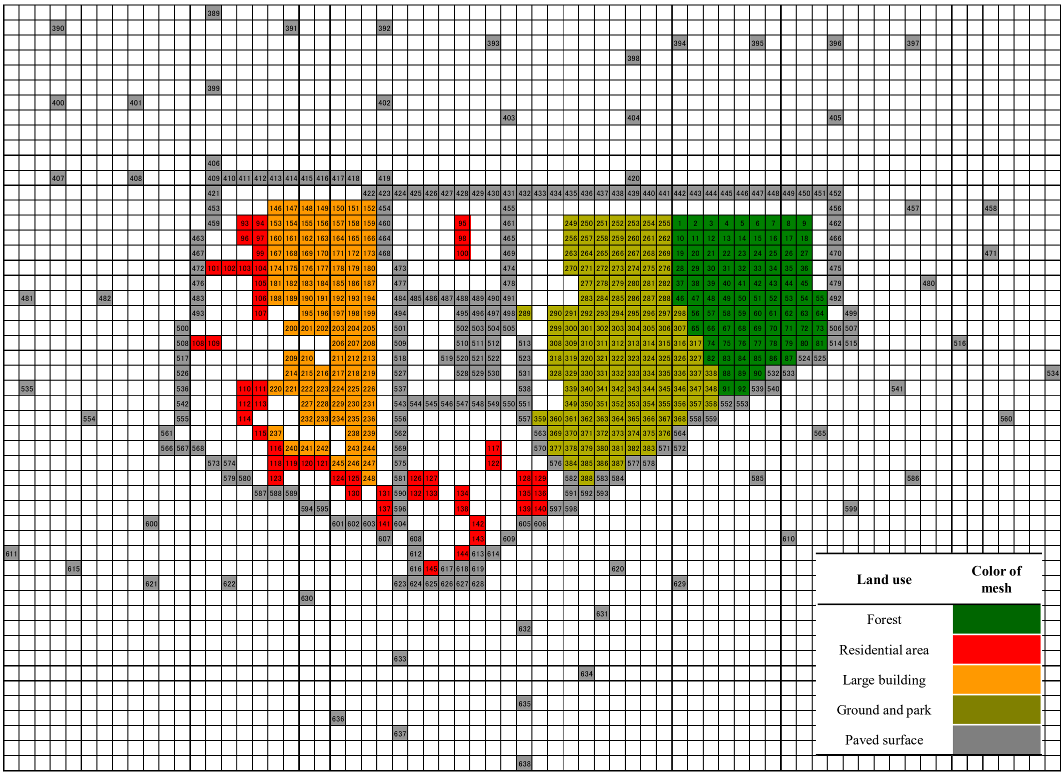

FIG. 63. Overhead view of the specified 'location'.

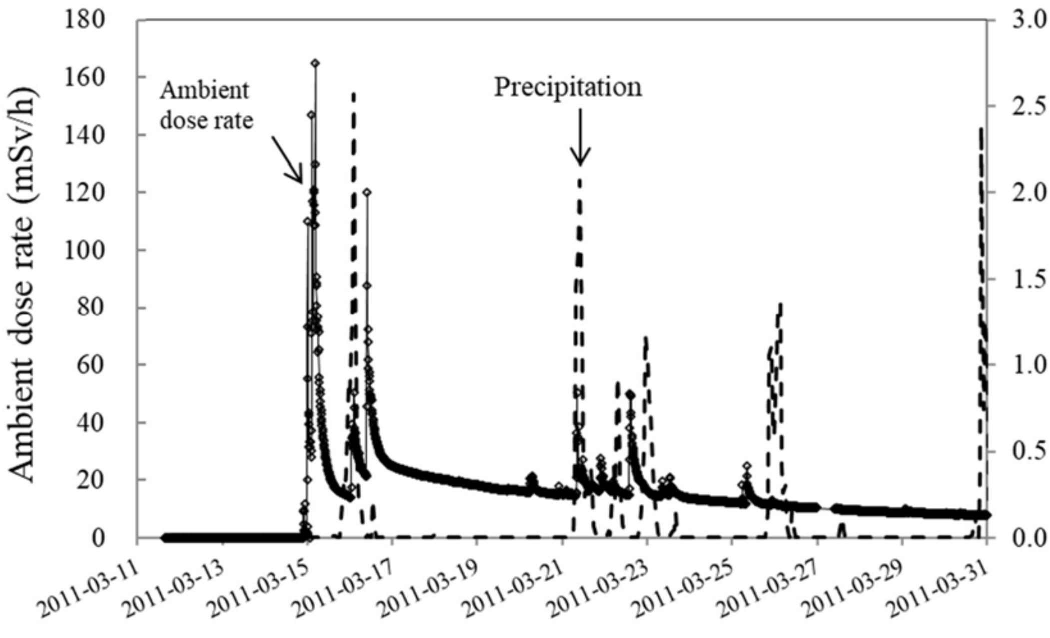

FIG. 64. Ambient dose equivalent rate and precipitation measured in the test site. The dose rate data are from [48].

TABLE 16. AVERAGE METEOROLOGICAL CONDITIONS OF THE TEST SITE [49]

Meteorological condition	**Monthly precipitation (mm)**	**Average temperature (ºC)**	**Daily maximum temperature (ºC)**	**Daily minimum temperature (ºC)**	**Average wind speed (m/s)**	**Hours of sunlight (h)**
Period of measurement	1981–2010	1981–2010	1981–2010	1981–2010	1981–2010	1986–2010
Number of years	30	30	30	30	30	25
January	48.9	2.1	7.1	-3	1.8	159.8
February	53.4	2.3	7.4	-2.9	1.8	157
March	91.8	5.1	10.3	-0.3	2	176.7
April	126.9	10.4	15.9	4.8	2	190.6
May	124	14.9	20.2	9.6	1.7	184.9
June	158.2	18.2	22.6	14.2	1.4	143.2
July	182.5	22	26.2	18.5	1.2	136.3
August	171.2	23.8	28.3	20.1	1.3	162.8
September	241.2	20.1	24.7	16.2	1.2	121.2
October	192.7	14.6	19.9	9.4	1.3	137.8
November	78.8	9.4	15.1	3.6	1.5	146.5
December	41.4	4.8	10.2	-0.5	1.7	152.5

TABLE 17. AGE DISTRIBUTION OF THE INHABITANTS OF THE TEST SITE [50]

Age group (years)	**Number of people**	**Percentage (%)**
0–9	1350	8.5
10–19	1790	11.3
20–64	9347	59.0
65+	3342	21.1
Sum of all generations	15 829	100.0

TABLE 18. CLASSIFICATION OF THE POPULATION BY TYPE OF INDUSTRY [50]

Large Category	**Small Classification**	**No. of people**	**Total**
Primary sector of industry	Agriculture, forestry	396	415 (5.3%)
	Fishery	19	
Secondary sector of industry	Mining, quarrying, gravel extraction	3	2331 (29.9%)
	Construction	1518	
	Manufacturing	810	
Tertiary sector of industry	Electricity, gas, heat supply, sewerage	642	5021 (64.5%)
	Information, communication	39	
	Traffic, postal service	158	
	Wholesale, retail trade	856	
	Finance, insurance business	108	
	Real estate, rental service	66	
	Academic research, expertise service	210	
	Lodging industry	478	
	Entertainment	254	
	Education and learning industry	310	
	Medical and welfare	654	
	Compositive service	52	
	Other service industry	918	
	Public service	276	
Non-classifiable		22	22 (0.3%)
Total			7789

TABLE 19. COMPOSITION OF DEPOSITED RADIONUCLIDES (AS OF 15 MARCH 2011) [47]

Radionuclides	**Deposited activity[a,b] normalized to ^{137}Cs**
I-131	11.5
Te-132+I-132	8
Cs-134	1.0
Cs-136	0.17
Cs-137	1.0
Ba-140	0.1
Ag-110m	0.0028
Te-129m	1.1

[a] The activities given in this table are decay corrected to 15 March 2011.
[b] The composition of radionuclides other than ^{140}Ba are taken from [46]. Deposited activity of ^{140}Ba normalized to ^{137}Cs was taken from [47].

5.3.3. Radioactivity levels at the test 'locations'

In the present study, the dose assessments were performed using the assumption that the contamination occurred at 00:00 on 15 March 2011. Results of environmental monitoring of deposition on ground surfaces, ambient dose equivalent rate, and activity concentration of ^{137}Cs in air are described below.

5.3.3.1. Deposition on ground surfaces

Measurement of ground deposition of ^{137}Cs was performed within about 80 km from the Fukushima Daiichi (1F) plant. The areas were divided into hypothetical 2 km meshes, and soil samples were collected from some of those meshes [51, 52]. Soil samples were taken from a depth of 5 cm from the ground surface during the period between 6 June 2011 and 8 July 2011. The results were given as decay corrected values as of 14 June 2011 (see Appendix II, Table 31 below). The data on contamination densities of the test site were given in terms of a 500 m grid.

5.3.3.2. Ambient dose equivalent rate

After the 1F accident, a vehicle borne monitoring survey was conducted in order to clarify the dose distribution along roads and to confirm the time dependence of the dose rates. The monitoring was performed along roads using vehicles. Figure 65 shows the dose rates measured by national authorities during 21 different time periods. The averages and standard deviations in Fig. 65 are given without classification of the contribution of dose rate from various land use situations. However, the numerical data for each land use situation are provided in Appendix II (see Table 32 below).

5.3.3.3. Activity concentration of ^{137}Cs in air

Figure 66 shows the time dependence of the activity concentration of ^{137}Cs in air, measured in Fukushima city during the period between March 2011 and February 2014. These values were measured at a height of 1 m above the ground. The sampling point is located near a parking space in an urban environment.

5.4. INFORMATION ABOUT REMEDIATION EFFORTS

Information on the effectiveness of individual remediation measures was obtained from experimental work performed by JAEA [53]. This information is summarized by 'environment' and specific remediation actions in each 'environment'. The following items are listed for each remediation action in Appendix II (see Table 33 below):

- Decontamination factor, derived from the change in measured surface count rate (including beta contributions);
- Reduction in surface dose rate;
- Amount of waste generated (per unit area remediated or per other relevant unit);
- Manpower (speed of implementation for a specified piece of equipment or team of workers);
- Cost (for the specific case of implementation within the Fukushima evacuated zone).

For the modelling exercise, it was assumed that the remediation happened 'now' (at the time of the 'current' situation).

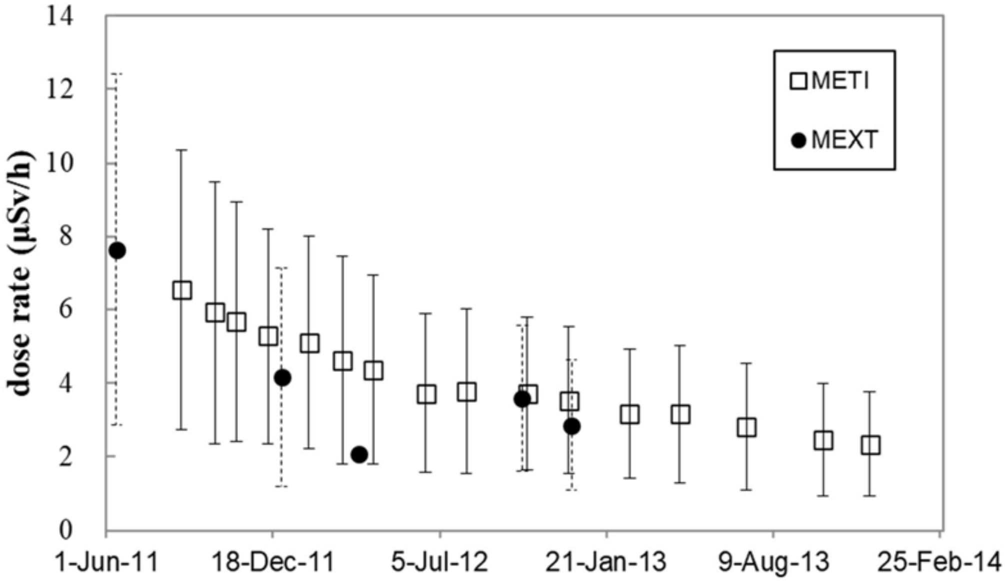

FIG. 65. Time dependence of ambient dose equivalent rate measured in the test site [52, 54, 55]. Symbols indicate means, and the vertical lines indicate 1 standard deviation.

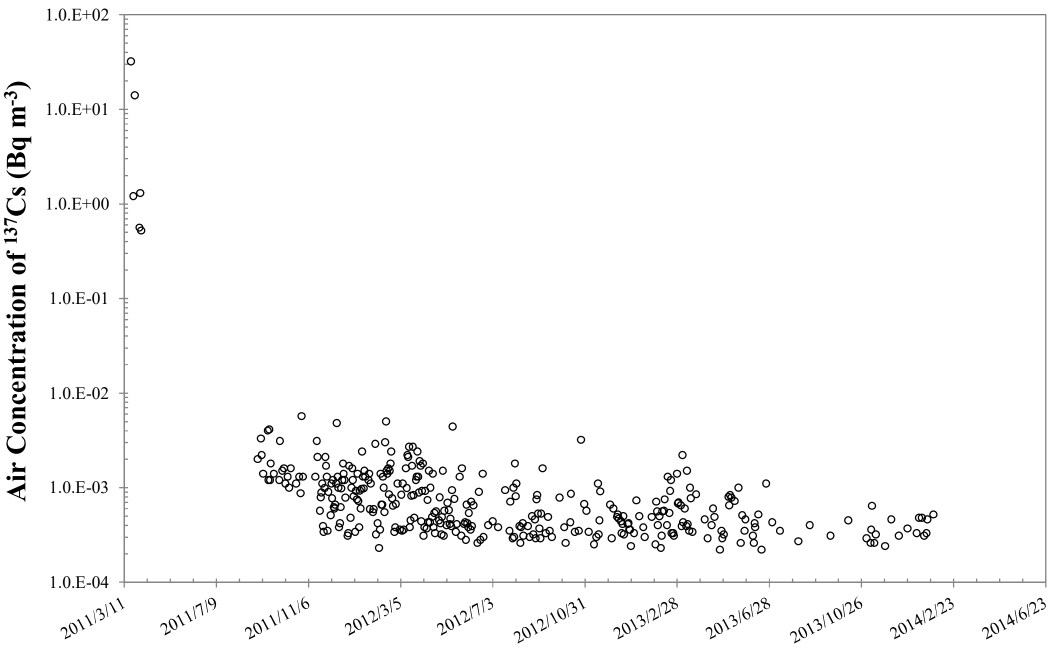

FIG. 66. Time dependence of the activity concentration of ^{137}Cs in air, measured in Fukushima city [56].

5.5. DESCRIPTION OF THE REFERENCE PERSONS

For the exercise, three reference persons were defined, based on differences in their daily habits: (1) Indoor workers, (2) Outdoor workers in an urban situation (not including agricultural workers), and (3) Agricultural workers. The reference persons are defined by occupancy factors for the four 'environments' in the test site. An occupancy factor is defined as the fraction of time spent by a specified population group in a specified type of environment. Table 20 provides occupancy factors for different population groups in various environments. These occupancy factors were based on data from actual surveys performed in Fukushima prefecture by JAEA [57].

5.6. MODELLING ENDPOINTS FOR THE EXERCISE

Two endpoints were modelled in the first stage of the exercise (during the MODARIA programme):

(1) For each 'environment' (the described 'location' for each 'environment'), predictions of the dose rates at the end of 1 year and for each subsequent year to 10 years, assuming no remediation.

(2) For each reference person, calculations of the external dose during the first year and for each subsequent year to 10 years, assuming no remediation.

Additional endpoints were described for modelling during later stages of the exercise:

(3) For each 'environment' (the described 'location' for each 'environment'), predictions of the contamination density and dose rates at the end of 1 year and by yearly increments to 10 years with the described remediation for each 'environment'.

(4) For each reference person, calculations of the external dose during 1 year and for each subsequent year to 10 years with the described remediation for each 'environment'.

(5) For each reference person, calculations of the internal dose from resuspension during 1 year and for each subsequent year to 10 years:
    (a) With no remediation, and
    (b) With the described remediation for each 'environment'.

(6) The most important 'surfaces' at each 'location' with respect to contribution to dose rate, before remediation and after remediation.

(7) Calculations of the short term (1 year) and long term (10 years) effectiveness of the remediation efforts:
    (a) For reducing dose rate at each 'location', and
    (b) For reducing overall dose to each reference person.

(8) Estimates of the total volume and activity of waste from the remediation for each 'environment'.

(9) The remediation efforts (by 'environment' or by individual remediation activity) that have the largest short term (1 year) and long term (10 years) effect in terms of dose reduction, for each reference person.

TABLE 20. OCCUPANCY FACTORS FOR INHABITANTS LIVING IN THE TEST SITE [57]

Type of environment	Occupancy factors			
	Indoor workers	Outdoor workers		Pensioner
		Urban worker	Agricultural worker	
Indoor	0.95	0.69	0.69	0.94
Wooden	0.67	0.57	0.66	0.90
Concrete	0.28	0.12	0.05	0.04
Outdoor	0.04	0.31	0.31	0.06
Paved	0.02	0.26	0.10	0.03
Unpaved	0.02	0.05	0.21	0.03

5.7. MODELS USED IN THE EXERCISE

Two organizations participated in the modelling exercise (see Table 21). Public Health England (PHE) used an existing European model called ERMIN, and JAEA developed a model specifically for Fukushima Daiichi. Modelling approaches of these participants are summarized below. The values that were used for key model parameters are summarized in Table 22.

5.7.1. ERMIN

The European Model for Inhabited Areas (ERMIN) has been developed collaboratively under a number of EC funded projects [58, 59]. It is both a model and a software tool. As a model it simulates the behavior of radionuclides in the inhabited environment and calculates the exposure of the resident population. As a tool it allows a user to explore different recovery options and refine a strategy with a map based interface. It has been designed to be implemented within the RODOS [60] and ARGOS Nuclear Emergency Decision Support Systems [61].

Input data needed by the model include a description of the environment, initial deposition on a reference surface and a description of countermeasures. Output information generated by the tool includes the average doses to members of the public from external exposure to deposited radionuclides and inhalation of resuspended radioactivity, the contamination on urban surfaces, the radionuclide concentrations in air, the doses to workers undertaking the recovery work, the quantity and activity of waste generated and the cost and work needed to implement the countermeasures.

The model uses ratios to distribute deposition on the reference surface onto all urban surfaces. Empirical functions represent the long term surface retention, and migration in soil is simulated using a convective-dispersive model. A library of dose rates for surfaces in idealized environments is applied to calculate dose rates indoors and outdoors. Countermeasures are represented by the modification of surface contamination and the dose rates. The ERMIN countermeasure database is based on the European inhabited area handbook [62].

5.7.2. JAEA

The JAEA model is being developed by Japan Atomic Energy Agency based on lessons learned from the Fukushima Daiichi Nuclear Power Plant accident. This analytical model does not consider transfer of material. Decreases in dose rate in various locations are determined based on the data measured in Japan after the accident (see Fig. 65 above). Dose reduction effects of buildings are also evaluated from the actual surveys in Fukushima prefecture. The results of these surveys have been published as a JAEA report [57].

TABLE 21. GENERAL DESCRIPTION OF MODELS USED IN THE FUKUSHIMA EXERCISE

Model	ERMIN	JAEA
Sponsoring organization	European Commission (EC), Public Health England (PHE), Karlesruhe Institute of Technology (KIT), Danish Emergency Management Agency (DEMA), Prolog Development Centre (PDC), Helmholtz Zentrum München (HMU), Bundesamt für Strahlenschutz (BfS), Technical University of Denmark (DTU)	Japan Atomic Energy Agency
Purpose of model	Generic model for estimating external and internal dose to public and workers from radioactivity deposited in urban environments. ERMIN also estimates surface contamination as a function of time, waste amount and activity, and costs of decontamination.	To calculate external and internal doses due to the Fukushima accident using probabilistic and deterministic approaches.
Type of model	Model combining empirical deposition, retention and decontamination parameters with a library of unit dose rates generated by Monte Carlo particle transport modelling in idealized urban environments. Some transfer between closely linked compartments (e.g. trees to soil, grass to soil below).	Analytical model; no transfer of material between compartments.
Approach of assessment	Deterministic	Probabilistic and deterministic
Compartment considered	Paved (road, pavement and other paved), grass, small plants, soil, trees, external walls, roofs and interior surfaces	Ground surface (paved and unpaved)

TABLE 22. COMPARISON OF PARAMETER VALUES USED IN THE FUKUSHIMA EXERCISE

			ERMIN[a]		JAEA	
Retention parameters			**Fraction**	**Half-life (d)**	**Fraction**	**Half-life (d)[b]**
Surface:	Paved surface[c]	Fast	0.7	0.40	0.54	0.95
		Slow	0.3	3.0	0.46	92
	Roofs	Fast	0.5	2.0	—	—
		Slow	0.5	35		
	Outer walls		1	7.0	—	—
	Grass	Fast	1	0.04	—	—
		Slow	0	0		
	Soil		Modelled convective-dispersive model, 9 layers are represented down to 25 cm		—	—
	Coniferous trees[d]		Assumed to lose leaves linearly for 5 years		—	—
Dose reduction parameters			**Reduction factor**		**Reduction factor**	
Building type:	Light building		0.42–0.37[e]		0.25–0.41	
	Concrete building		0.026–0.010		0.01–0.05	

[a] Retention parameters in ERMIN are provided by particle size groups, and radionuclides are represented as being deposited in different proportions in different particle size groups, depending on the element and the accident scenario (likely presence of fuel particles and degree of oxidation. Values given here are for the aerosol 0–2 µm particle size; all the caesium deposition is assumed to be in particles of this size.

[b] The values are derived from the time dependence of ambient dose equivalent rate measured in the test site (see Fig. 65 above). The contributions of ^{134}Cs and ^{137}Cs are not included in the values shown here.

[c] Parameters shown are only for roads; ERMIN has slightly different parameters for pavements and for other paved surfaces, representing the effects of less traffic.

[d] ERMIN also models deciduous trees, but for this exercise deciduous trees are assumed to be without leaves.

[e] ERMIN does not use dose reduction parameters explicitly. In developing ERMIN, Monte Carlo particle transport modelling was used to populate libraries of dose rate from 1 Bq/m^2 of each radionuclide on each surface to representative locations indoors and outdoors. The dose reduction parameters presented here are for comparison and were back calculated by dividing the total predicted indoor dose rate by the outdoor dose rate. Because different surfaces have different retention parameters, the dose reduction is time dependent.

5.8. RESULTS OF MODEL PREDICTIONS

As the first step of the exercise, modellers predicted the dose rate in each environment and the annual effective dose to various population groups due to external exposures. The values that were used for key model parameters are summarized in Table 22 above.

ERMIN was developed for a European situation. The important empirical parameters such as the initial deposition ratios that estimate the deposition on different urban surfaces from that measured or modelled on a reference surface, and the retention half lives that govern how long radioactivity is retained on the urban surfaces, are largely taken from observations following the Chernobyl accident, supplemented with experimental data where available. Similarly, the database of idealized urban environments represents the kinds of urban environments often found in Europe. It has not been calibrated to the Japan situation.

As mentioned above, JAEA model was developed based on empirical data from the Fukushima accident. The environmental half-life of the ambient dose equivalent rate was derived from data measured for various types of land use in the test site (see Section 5.3.3.2). In addition, the dose reduction factor due to sheltering in houses was determined by the measured values in Fukushima prefecture. Thus, the contributions from various surfaces, such as roofs and walls, are included in an implicit manner. However, for concrete buildings, since measurements in Fukushima prefecture were not available, the predictions were performed based on values reported in Ref. [63][7].

5.8.1. Ambient dose equivalent rates

Figure 67 shows the results of predictions of ambient dose equivalent rate in various locations. The projections by the ERMIN model were made using just two inputs of ^{137}Cs activity density, 1.71×10^5 Bq/m^2 and 1.61×10^6 Bq/m^2, which were given in the two 500 m mesh grids that encompass the test location. Deposition of the other radionuclides was estimated by applying the ratios in Table 19 above. The higher and lower values of predictions correspond to the higher and lower values of ^{137}Cs deposition, which differ by approximately 1 order of magnitude. The higher and lower predictions form a range; in Fig. 67, the midpoint of the range is given along with ‘error bars’ that encompass the range. Deposition was assumed to be wet, and there were assumed to be no leaves on deciduous trees. Two idealized environments from the ERMIN database were chosen to represent the wooden house and concrete constructions. These were, ‘a street of detached prefabricated houses’ and ‘a multistorey block of flats amongst other house blocks’. For these environments both indoor and outdoor dose rates can be calculated. In addition an ‘open area’ environment was modelled, representing an ‘ideal’ situation of a large expanse of lawn with no paved surfaces, trees or buildings.

The results of JAEA model were predicted by a probabilistic approach based on statistical analysis of surface activity density in the test site. JAEA modellers evaluated the geometric means (GMs) and geometric standard deviations (GSDs) for paved surfaces and unpaved surfaces, based on the radioactivity level data of MEXT [51] and NRA [52]. The GM and GSD of ^{137}Cs on paved surfaces were 5.7×10^5 Bq/m^2 and 2.5, respectively, and the values for unpaved surfaces were 5.9×10^5 Bq/m^2 and 2.6, respectively, as of 15 March 2011. The range of the results generated by JAEA represent the 5th to 95th percentiles of the prediction results.

---

[7] Before the Fukushima accident, dose reduction factors shown in this publication were used as a representative effectiveness of sheltering in Japan. The details are described in the emergency preparedness guidelines of the former Nuclear Safety Commission of Japan.

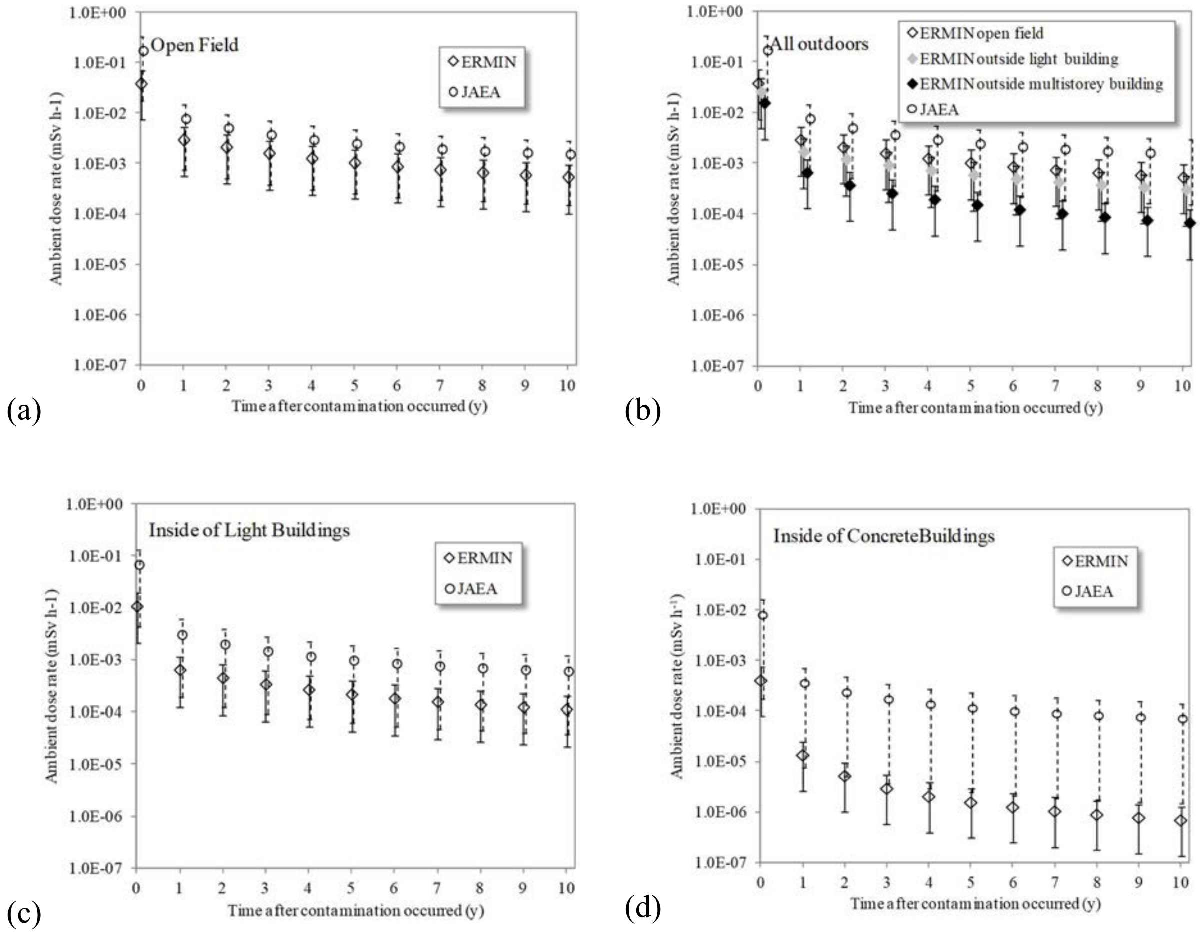

FIG. 67. Predicted external dose rates in various environments.

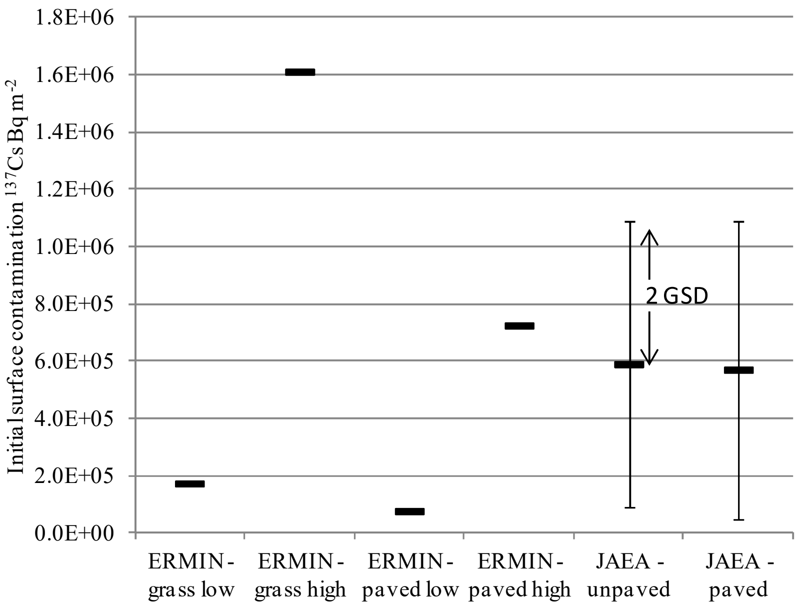

FIG. 68. Comparison of the values for initial deposition used by the models.

The gradients of the curves appear similar, so differences between the two sets of model predictions are largely due to the different initial depositions that were used. In particular, there is little difference between the ERMIN open field environment and the JAEA outdoor value, with ERMIN results only slightly smaller (Fig. 67(a)). However, the difference between the JAEA and the ERMIN outdoor dose rate increases as the environment becomes more heavily built up (Fig. 67(b)). The JAEA modelers used a deposition value for paved surfaces that was very similar to and only very slightly smaller than the value for the unpaved surface. However, ERMIN calculates a deposition to paved surfaces from the deposition on the grass and soil surface, using a library of empirical factors that are weather and particle size dependent. For the aerosol size particle during wet deposition, ERMIN uses a factor of 0.45, i.e. the deposition on paved surfaces is less than half of that on unpaved. Figure 68 above illustrates the various levels of initial deposition assumed. For ERMIN, Fig. 69 below shows the predicted contribution to dose rate from each individual type of surface.

Figures 67(c) and 67(d) show the indoor ambient dose rates. The differences outdoors are seen again indoors, magnified with respect to differences in shielding properties of the environments. It is not surprising that the biggest differences are seen in the concrete building environment (Fig. 67(d)).

In an open field in an urban area, while the difference in ambient dose equivalent dose predicted from the models was not significant, slight differences were observed, due to the difference in input contamination levels. However, the predictions for the first year show a significant difference between the models, which is attributable to the contributions of short lived radionuclides. In addition, differences in the predicted values for inside of concrete buildings are revealed. This can be explained by the difference of dose reduction effects of each model.

Figure 70 shows the results of predictions of annual effective doses to the various population groups. For indoor workers and pensioners, the differences in predicted values between the models were attributable to the same reason as the difference of ambient dose equivalent rates shown in Fig. 67, which means the difference in the contamination levels used as input to the models.

When the annual effective doses are compared between an urban outdoor worker and an indoor worker, the ratios of doses between the two groups for the ERMIN model are about 1.5 for both the higher values and the lower values of contamination levels. The ratios are the same for the higher and lower values because the ERMIN model used the same value of ^{137}Cs activity density for both houses and workplaces. On the other hand, these ratios were different for JAEA model. Values of 2.5 and 1.5 were found as the ratio for the 5th and 95th percentile of contamination level, respectively. This difference in doses to an indoor worker and an urban outdoor worker is because the JAEA probabilistic model used independent random numbers as the input for houses and workplaces.

The development of the dose assessment model based on the insights from the Fukushima accident is just getting started. The JAEA model will be improved with consideration of state of the art information gained from the Fukushima accident.

5.9. SUMMARY

Only the first stage of this exercise was carried out during the time frame of the MODARIA Programme. Differences in model predictions were related to differences in the two models used in the exercise: the JAEA model was based on empirical data for the relevant situation, while the ERMIN model was more generally based on contributions to external dose rate from individual types of surfaces. In addition, the ERMIN model was developed for Europe and was not calibrated for the Japanese situation. Later stages of the exercise will include assessment of the effects of various remediation efforts carried out in the test location.

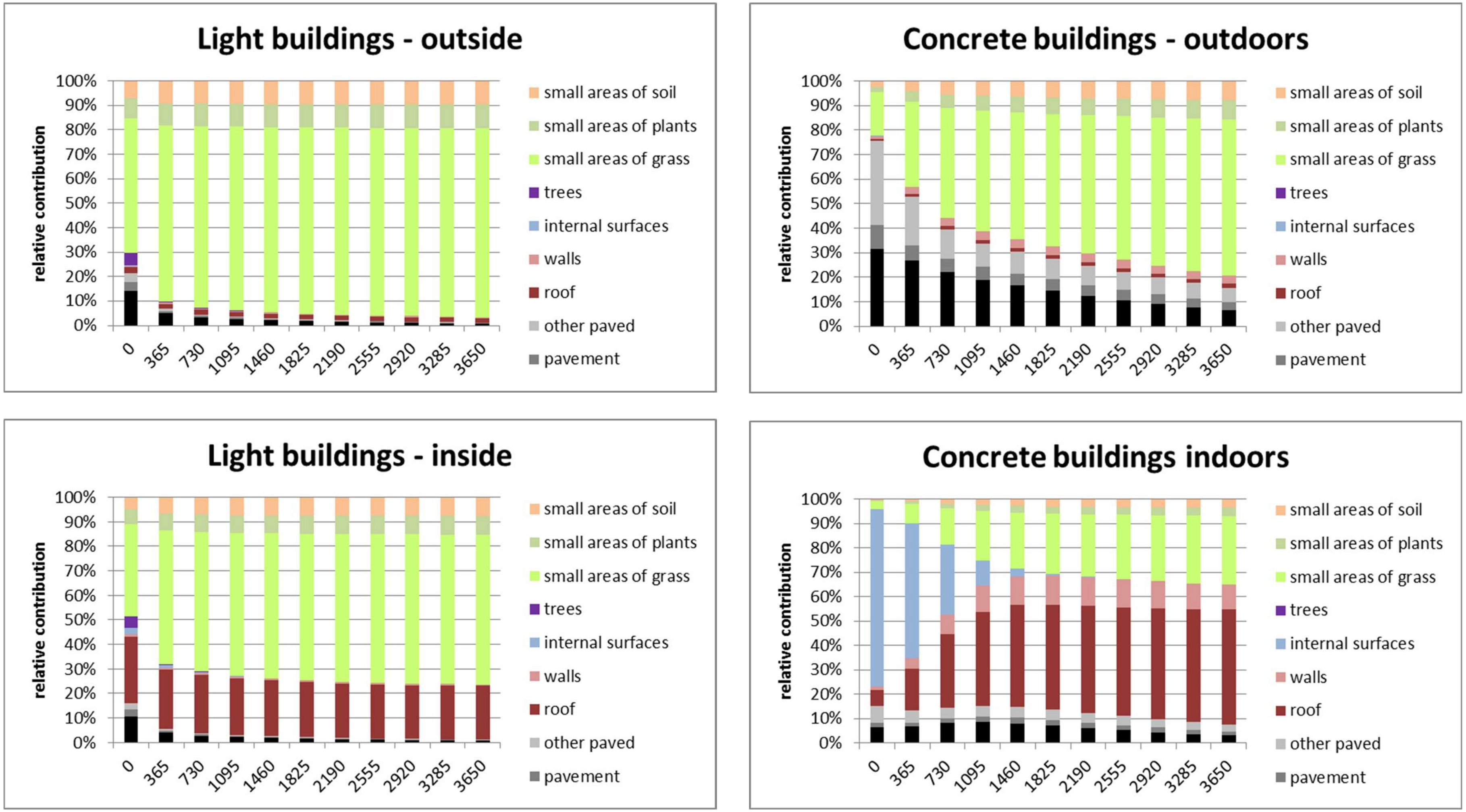

FIG. 69. Predicted contributions to dose rate of individual surfaces for various environments, obtained with ERMIN.

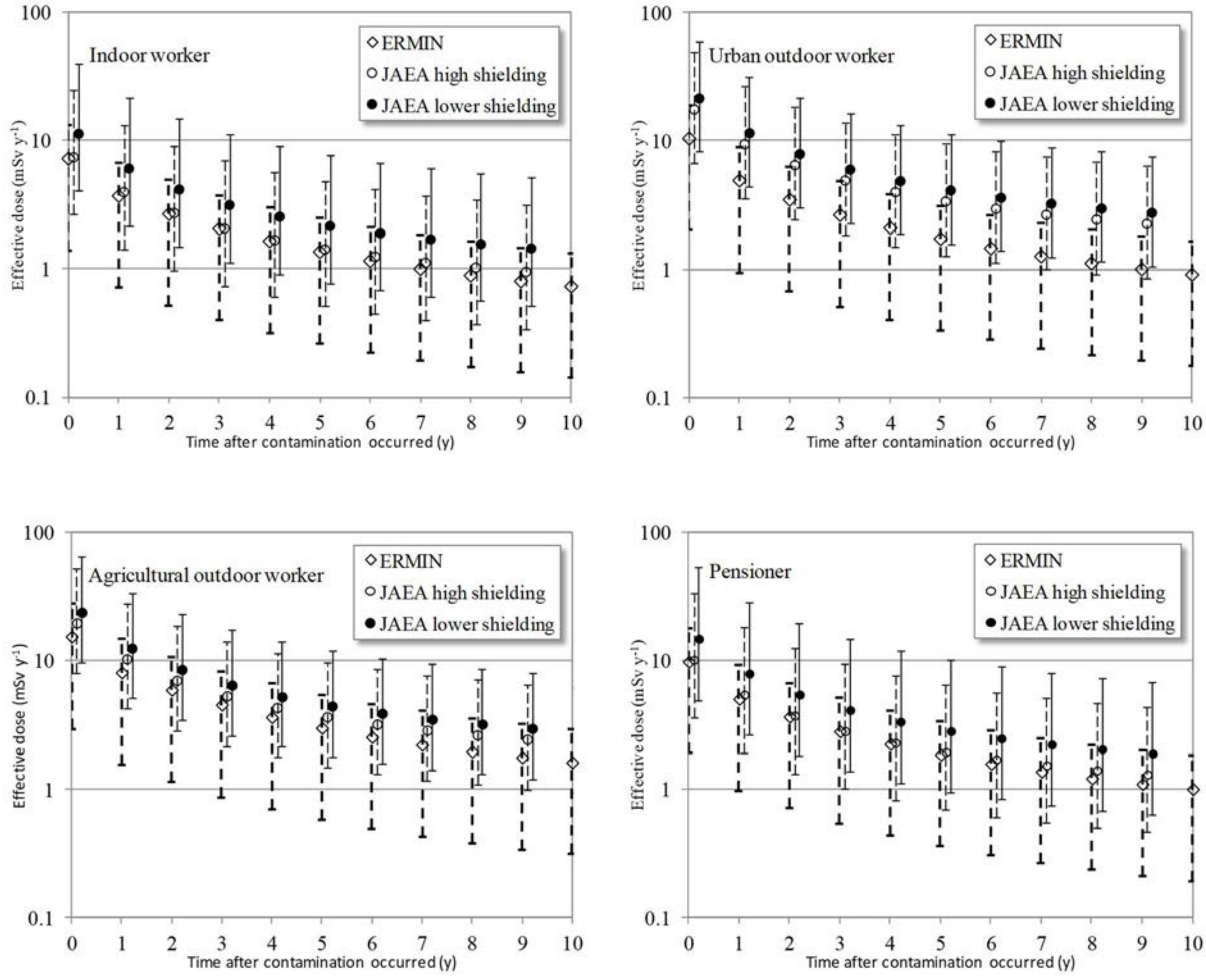

FIG. 70. Comparison of predicted annual effective doses to each population group, assuming no countermeasures.

6. SUMMARY OF MODEL REVIEW

An area of interest for WG2 was the development of a review of models for assessment of public exposures from acute releases. The main focus was on models (computer codes) for predicting transport of radioactive contaminants to urban environments, especially atmospheric dispersion, deposition, and environmental transport for situations such as an accident at a nuclear power plant. The objective of the review was to provide a comparison of key models in use or named in national regulations, their applicabilities and needs (computational and in terms of necessary data), intended uses, and other important features. The intent was not to provide an evaluation of which model is 'best', but to provide information that can help users to select the most appropriate model for their own needs.

Working Group participants developed the list of features and attributes to be considered in the review. A. Shroads of SC&A, Inc., prepared the initial version of the review. The format is an Excel® workbook with a separate page (worksheet) for each model, plus a table comparing major features or attributes of all of the included models, which is available as a complementary Electronic Appendix. Moreover, selected information is included in this Working Group 2 publication.

A number of participants have contributed summaries of models to this review, and the list of models included reflects the interests of those participants. It is recognized that this review does not include all models that might be of interest to readers of this publication, and that model information might not be up to date. Most of the information was collected during the time frame of the MODARIA Programme; however, several additional model summaries were contributed through 2017, prior to this publication being published. The final version of the review includes 31 models (see Table 23). Selected model characteristics are summarized in Table 24.

TABLE 23. LIST OF MODELS INCLUDED IN REVIEW

Model	Country	Website
ADDAM/CSA-ERM	Canada	–[a]
AgriCP	European Union	–
ARGOS	European Union	www.pdc-argos.com
ARTM	Germany	https://www.bfs.de/EN/topics/ion/environment/air-soil/emission-monitoring/artm.html
BDCC	United States	https://epa-bdcc.ornl.gov /
BRPG	United States	https://epa-bprg.ornl.gov/
CERES CBRN-E	France	–
CHERPAC	Canada	–
CHERURB	Canada	–
CROM6	Spain	–
CSA-DRL	Canada	–
ERMIN	European Union	–
ETMOD	Canada	–
GASPAR-II	United States	www.oecd-nea.org
HotSpot	United States	https://narac.llnl.gov/
JRodos	European Union	https://resy5.iket.kit.edu/JRODOS/
LASAIR	Germany	–
MACCS2	United States	https://energy.sandia.gov/energy/nuclear-energy/nuclear-energy-safety-technologies/melcor/
MSS	France, Italy	www.aria.fr
NFS_Vinca	Serbia	–
OSCAAR	Japan	–
PAVAN	United States	https://rsicc.ornl.gov/
PMSS	France, Italy	www.aria.fr
RASCAL	United States	https://rsicc.ornl.gov/
RATCHET	United States	www.pnl.gov
RESRAD-OFFSITE	United States	www.evs.anl.gov/resrad
RIMPUFF/URD	European Union	http://orbit.dtu.dk/
SDCC	United States	https://epa-sdcc.ornl.gov/
Spray3	Italy, Slovenia	www.aria-net.it
SPRG	United States	https://epa-sprg.ornl.gov/
XOQDOQ	United States	https://rsicc.ornl.gov/

[a] Not available.

TABLE 24. COMPARISON OF ATMOSPHERIC DISPERSION MODELS FOR NUCLEAR RELEASES

Model	Routine releases	Accidental releases	Emergency preparedness	Emergency response	Deterministic or probabilistic	Number of radionuclides	Progeny radionuclides	Format of results
ADDAM/CSA-ERM	No	Yes	N/A[a]	Yes	Probabilistic	N/A	N/A	N/A
AgriCP	Yes	Yes	Yes	Yes	Deterministic	66	No	Text/map
ARGOS	Yes	Yes	Yes	Yes	N/A	N/A	N/A	N/A
ARTM	Yes	No	No	No	Both	101	Yes	Table/map
BDCC	Yes	No	No	No	Deterministic	1252	Yes	Table
BRPG	Yes	No	No	No	Deterministic	1252	Yes	Table
CERES CBRN-E	Yes	Yes	Yes	Yes	Deterministic	~800	Yes	Table/map
CHERPAC	N/A	NA	N/A	N/A	Probabilistic	25	N/A	N/A
CHERURB	No	Yes	No	Yes	N/A	NA	N/A	N/A
CROM6	Yes	No	No	No	Deterministic	149	N/A	Table
CSA-DRL	Yes	N/A	N/A	N/A	N/A	N/A	N/A	N/A
ERMIN	Yes	Yes	Yes	Yes	Deterministic	66	Yes	N/A
ETMOD	N/A	Yes	N/A	N/A	N/A	2	N/A	Table
GASPAR-II	Yes	Yes	No	No	Deterministic	183	N/A	Table
HotSpot	No	Yes	No	Yes	Deterministic	800	No	Table/map
JRodos	Yes	Yes	Yes	Yes	Both	140	Yes	Shape file/table/map
LASAIR	Limited	Yes	Yes	Yes	Deterministic	860	N/A	Table/map
MACCS2	Yes	Yes	Yes	Yes	Both	825	Yes	Text
MSS	Yes	Yes	Yes	Yes	Probabilistic	N/A	N/A	Table
NFS_Vinca	Yes	Yes	Yes	Yes	Deterministic	N/A	N/A	Text/map
OSCAAR	No	Yes	Yes	Yes	Both	65	Yes	Text/table
PAVAN	No	Yes	No	No	Deterministic	N/A	N/A	Table
PMSS	Yes	Yes	Yes	Yes	N/A	N/A	N/A	Table
RASCAL	No	Yes	No	No	Deterministic	800	Yes	Text/map
RATCHET	Yes	Yes	No	No	Deterministic	N/A	N/A	Text
RESRAD-OFFSITE	Yes	No	No	No	Both	1252	Yes	Text/plot
RIMPUFF/URD	Yes	Yes	Yes	Yes	Deterministic	544	Yes	Image
SDCC	Yes	No	No	No	Deterministic	1252	Yes	Table
Spray3	Yes	Yes	Yes	Yes	Probabilistic	N/A	N/A	Table
SPRG	Yes	No	No	No	Deterministic	1252	Yes	Table
XOQDOQ	Yes	Yes	No	No	Probabilistic	2	N/A	Table
ADDAM/CSA-ERM	1	Polar	0.1–30	Yes	Yes	No	No	N/A

TABLE 24. COMPARISON OF ATMOSPHERIC DISPERSION MODELS FOR NUCLEAR RELEASES (cont.)

Model	Release points	Grid type	Grid range (km)	Cloudshine dose	Groundshine dose	Inhalation dose	Ingestion dose	Acute dose	Lifetime Dose
AgriCP	400	Discrete locations	N/A	Yes	Yes	Yes	Yes	N/A	Yes
ARGOS	NA	N/A	N/A	N/A	N/A	N/A	N/A	N/A	N/A
ARTM	50	Rectangular	0.1–100+	Yes	Yes	Yes	No	Yes	Yes
BDCC	N/A	Rectangular	N/A	N/A	N/A	N/A	N/A	N/A	Yes
BRPG	N/A	Rectangular	N/A	N/A	N/A	N/A	N/A	N/A	Risk[b]
CERES CBRN-E	Unlimited	Rectangular/polar	0.1–50	Yes	Yes	Yes	N/A	N/A	Yes
CHERPAC	N/A	N/A	N/A	Yes	Yes	Yes	Yes	N/A	Yes
CHERURB	N/A	N/A	N/A	Yes	Yes	Yes	Yes	N/A	Yes
CROM6	1	Linear	N/A	Yes	Yes	Yes	Yes	N/A	Yes
CSA-DRL	N/A	N/A	N/A	N/A	N/A	N/A	N/A	N/A	N/A
ERMIN	N/A	UTM	N/A	N/A	N/A	N/A	N/A	N/A	N/A
ETMOD	N/A	Rectangular	N/A	N/A	N/A	Yes	Yes	N/A	N/A
GASPAR-II	1	Polar	0–80	N/A	N/A	N/A	N/A	N/A	N/A
HotSpot	1	Linear/polar	0.01–200	Yes	Yes	Yes	No	Yes	Yes
JRodos	1	Rectangular	4.8–1536	Yes	Yes	Yes	Yes	Yes	Yes
LASAIR	1	Rectangular	1–40	Yes	Yes	Yes	No	Yes	Yes
MACCS2	1	Polar	0.05–9999	Yes	Yes	Yes	Yes	Yes	Yes
MSS	Unlimited	Rectangular	0.1–5	No	No	No	No	No	No
NFS_Vinca	Unlimited	Rectangular	10–30	Yes	Yes	Yes	No	N/A	N/A
OSCAAR	1	Polar	0.5–2000	Yes	Yes	Yes	Yes	Yes	Yes
PAVAN	1	Polar	0–10	N/A	N/A	N/A	N/A	N/A	N/A
PMSS	Unlimited	Rectangular	0.1–5	N/A	N/A	N/A	N/A	N/A	N/A
RASCAL	1	Polar/rectangular	3.2–80	Yes	Yes	Yes	N/A	Yes	Yes
RATCHET	1	Rectangular	82–106	N/A	N/A	N/A	N/A	N/A	N/A
RESRAD-OFFSITE	1+	Rectangular/polar	-80 to 80	Yes	Yes	Yes	Yes	Yes	Yes/risk[b]
RIMPUFF/URD	1+	UTM	N/A	N/A	N/A	N/A	N/A	N/A	N/A
SDCC	N/A	Rectangular	N/A	N/A	N/A	N/A	N/A	N/A	Yes
Spray3	Unlimited	Rectangular	2–100	No	No	No	No	No	No
SPRG	N/A	Rectangular	N/A	N/A	N/A	N/A	N/A	N/A	Risk[b]
XOQDOQ	5	Polar	0.4–80	N/A	N/A	N/A	N/A	N/A	N/A

[a] N/A: The information is not applicable for the model or was not available in the documentation reviewed.
[b] Model calculates lifetime risk of cancer morbidity.

7. CONCLUSIONS AND APPLICATIONS

The first three modelling exercises described in this publication involved two main types of atmospheric dispersion situations: (1) short range dispersion, relevant to a release in an urban situation (Sections 2 and 3), and (2) midrange dispersion, relevant to releases from a facility such as a nuclear power plant (Section 4). Several general conclusions can be drawn from these exercises and their application.

For modelling atmospheric dispersion from a fixed facility such as a nuclear power plant, the modelling system (meteorological model plus dispersion model) and meteorological measurement applicabilities can be planned to fit the actual site (especially a site with complex terrain) and modelling needs. Ideally, more than one ground based meteorological station needs to be used, together with equipment (SODAR, RASS) to measure the vertical profiles of wind and temperature. The vertical profiles are essential for modelling complex terrain and for 3-D modelling. Reconstructed meteorological parameters need to be consistent with actual point measurements. Domain and cell sizes need to be appropriate for the situation being modelled, such that complex terrain is not inappropriately ‘smoothed’. Generally, numerical Lagrangian particle models will be better suited than Gaussian models (including Gaussian puff models and Lagrangian puff models with Gaussian parameters of turbulence). Tracer experiments can be very important for validation of modelling systems for a given site and level of complexity.

For the short range dispersion exercises, model results agreed for some locations or time intervals and not for others. Differences in the models as implemented included different computational approaches, different domain sizes, and different values for some key parameters (e.g. wind speed and direction, atmospheric stability classes, roughness length, and dry deposition velocity). Some participants were able to use all available meteorological data (e.g. at several heights or locations), while others used only one set; similarly, some participants used time dependent meteorological data, while others used mean values. The measurements of deposition in one exercise (Section 2) demonstrated that the plume was more unstable than the models were able to simulate. Models also varied in their ability to handle building effects (obstacles), while overall the exercises demonstrated the importance of such effects on the dispersion. Comparison of model results was facilitated by use of contour plots of predicted and measured deposition.

Ideally, a model is selected or developed for a particular purpose, including specific sites. This is not always possible, and sometimes model implementation had to be customized for an exercise. Ideally, there will be consistency in terms of time intervals between the meteorological data available for model inputs and the preferred input applicabilities of the model; otherwise it may be necessary to rearrange, revise, interpolate, or otherwise manipulate the available measurements for use with a given model.

The fourth exercise described in this publication (Section 5) did not involve atmospheric dispersion modelling, but started with measurements of ground deposition and external dose rates, to predict time dependent changes in external dose rates and the external doses received over time by members of specified population groups. Only the first stage of the exercise was carried out during the MODARIA programme; later stages will include assessment of the effects of various remediation efforts. For this first stage, differences in model predictions were related to differences in the models themselves, one being based on empirical data for the relevant situation, and the other being more generally based on contributions to dose rate from specified surfaces.

The final section of this publication (Section 6) provides a brief summary of a number of models available for assessment of public exposures from acute releases. These models vary in their purposes and applicabilities. The summary is intended to provide information to help a user select an appropriate model (whether or not from this list) for a given purpose.

APPENDIX I. SCENARIO DESCRIPTION AND DOCUMENTATION OF DATA FOR THE SHORT RANGE ATMOSPHERIC DISPERSION EXERCISE

I.1. INTRODUCTION

The present model testing scenario is based on experimental data obtained from the dispersal of a short lived radionuclide with a small amount of explosive. The scenario is intended to provide an opportunity to test model predictions for a short range dispersion event, including the deposition resulting from the event. The present exercise during the MODARIA Programme built on an exercise conducted during the EMRAS II Programme [6]; the previous exercise considered four field tests (explosion events), and the present exercise involved two subsequent events.

Input information for the entire scenario includes information about each of the six explosion events, the amount of radioactivity involved, the arrangement of the various detectors in the vicinity of the explosion, meteorological information, and particle size information. Modelling endpoints for which comparisons with measurements could be made include surface contamination and dose rates as a function of distance, and air concentrations as a function of height and distance. Additional modelling endpoints for intercomparison among modellers include the surface contamination, dose rates, and air concentrations beyond the domain of the measurements, plus the zones in which 50%, 75% and 95% of the contamination was estimated to be deposited.

This appendix provides information about the situation to be modelled (input information) for the last two field tests (explosion events) and a list of the endpoints to be modelled. Information about the previous four field tests is available in the EMRAS II report [6]; this earlier information was available to MODARIA participants, e.g. for use in model calibration if desired. Participants in the exercise were also provided with additional detailed information in electronic formats.

I.2. DESCRIPTION OF THE EXPERIMENT

Several field tests were performed by the Czech National Radiation Protection Institute (SÚRO) on a test area belonging to the National Institute for Nuclear, Chemical and Biological Protection in Kamenna, located near Prague in the Czech Republic. The radioactive material was ^{99m}Tc (half-life 6 hours) in liquid form ($NaTcO_4$ in 0.9% NaCl solution), which was spread by detonation of a small amount of explosive in an open field (flat terrain) with a simulated structure for these two field tests. The measurements performed included monitoring of dose rate, surface contamination of ground and structures, activity concentrations in air, particle size distribution, time distribution of dust particles in air, thermo camera snapshots, and video recording using both standard and high speed cameras. The test area was selected for a stable wind direction under usual meteorological conditions. Additional details about the experiment were provided previously [6, 9].

I.3. DESCRIPTION OF THE TEST SITE

The test area belongs to the National Institute for Nuclear, Chemical and Biological Protection, located in Kamenna, located near Prague in the Czech Republic (see Fig. 71). The whole region is an area of former mining and processing of uranium and other metals in the vicinity of the town of Přibram (in Central Bohemia). There are several tailings piles left from uranium extraction; these tailings piles have higher dose rate values caused by uranium mineralization, and the whole area is very heterogeneous.

FIG. 71. Test site location with dispersion point coordinates (49.6268131N, 13.9946061E) marked: basic map, top; aerial map, bottom (map source: Mapy.cz, basic map © Seznam.cz, a.s., aerial map © Seznam.cz, a.s., © TopGis, Ltd.).

Two such piles are located near the test site (see Fig. 72), about 150 m to the north; the diameter of the bigger one is about 180 m. The lower pile (left one) is approximately 14 m high, while the higher one (right one) is about 17 m high. These estimates were obtained from Google Maps using the Daft Logic Google Maps Find Altitude[8] the accuracy of the Google data is unknown.

A digital model of relief (DMR) was not available, so one was created from the Google elevation data (see Fig. 73; same source as mentioned above). About 1800 input points and Multilevel B-Spline interpolation in SAGA GIS were used to calculate the elevation. The test polygon altitude (approximately 545 m) was taken as zero level.

The vegetation at the test site consists of mixed forest trees (mostly birch, but also hornbeam and some coniferous trees) and various bushes. Figures 74 (winter) and 75–76 (summer) show how the site looks and how high and dense the vegetation is. As seen in the winter photo (Fig. 74), most of the plants are broadleaved trees. The coniferous trees on the horizon (see Fig. 74) are more than 200 m from the dispersion point. Most of the field tests were performed in spring or summer. Figures 75 and 76 show the site with vegetation and Figs 77 and 78 show the test site in more detail.

All data generated by SÚRO use a custom Cartesian coordinate system in meters. The point (0,0) is always the dispersion point. It is also possible to use a standard geographic coordinate system (e.g. EPSG: 4326: WGS 84[9]). Most GPS receivers and also Google use this coordinate system. To achieve adequate accuracy, the coordinate system of SÚRO or a projected coordinate system, such as EPSG: 32634: WGS 84 / UTM zone 33N[10] or EPSG: 3395: WGS 84 / World Mercator[11], can be used. A conversion spreadsheet containing both Cartesian and geographic coordinates of the sampling points was available to participants.

I.4. INPUT INFORMATION

Information about the two field tests in the current exercise (Tests 5 and 6[12]) is summarized in Table 25. All available data for four previous tests [6, 9] were provided to the modellers, including measurements of surface contamination (Tests 1–4), dose rates (Test 2), and time integrated activity concentrations in air (Test 2). These data could be used for calibration of models as desired. For Tests 5 and 6, only the input information was provided to modellers during the exercise, and the exercise was conducted as a blind test.

Meteorological information for Tests 5 and 6 is summarized in Table 26. Detailed (time dependent) meteorological information from several stations was provided to participants in electronic form. Tables 27 and 28 provide the time dependent meteorological data at 10 m height.

The geometry of the test material is illustrated in Fig. 79 where the outer plastic case (shown in blue) is made from a standard 1 L PET plastic bottle, approximately 20 cm long. For Tests 5 and 6, the Tc solution was in a 6 mL spherical glass bottle inside the larger bottle. The dispersion site schema is shown in Fig. 80. A set of schematic drawings of the configuration used for the field tests was provided to the participants. For Tests 5 and 6 (dispersed liquid volume = 6 mL), most of the released inventory is thought to have been in an aerosol.

---

[8] See https://www.daftlogic.com/sandbox-google-maps-find-altitude.htm
[9] See http://spatialreference.org/ref/epsg/4326/
[10] See http://spatialreference.org/ref/epsg/32633/ (best solution)
[11] See http://spatialreference.org/ref/epsg/3395/
[12] Different numbering schemes have been used in some of the documentation of these field tests. This Appendix refers to Tests 5 and 6 in the text or to Tests 5/3P and 6/4P in Tables 25–30. Dates of the field tests are provided in these tables to facilitate identification of individual field tests.

FIG. 72. View of the tailings piles to the north of the test site.

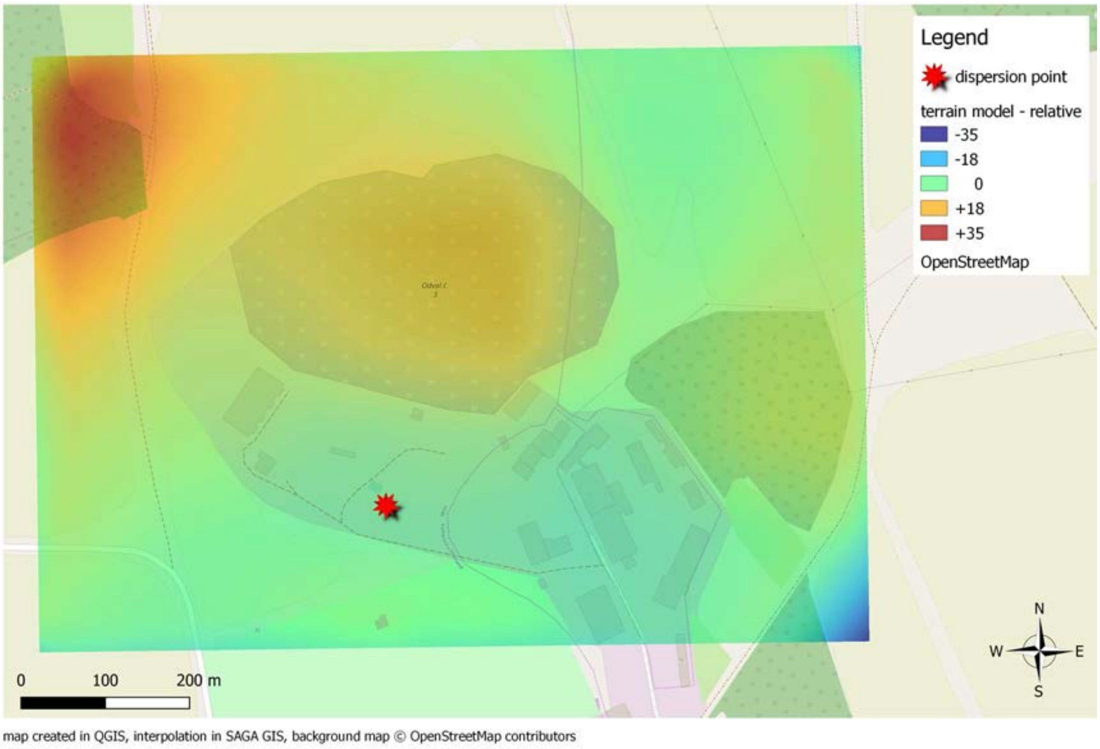

FIG. 73. DMR (digital model of relief) of the test site area on OpenStreetMap background in QGIS. Altitude data for the test site are in meters. The test polygon altitude (approximately 545 m) was taken as the zero level. Interpolated in SAGA GIS (www.saga-gis.org).

FIG. 74. Photo of the test site in winter (Test 1, 6 December 2007).

FIG. 75. Photo of the test polygon in summer (Test 4/2P, 14 July 2009). The dispersion point is on the right.

FIG. 76. Photo of the test polygon in summer (Test 4/2P, 14 July 2009). The photo was taken from the dispersion point.

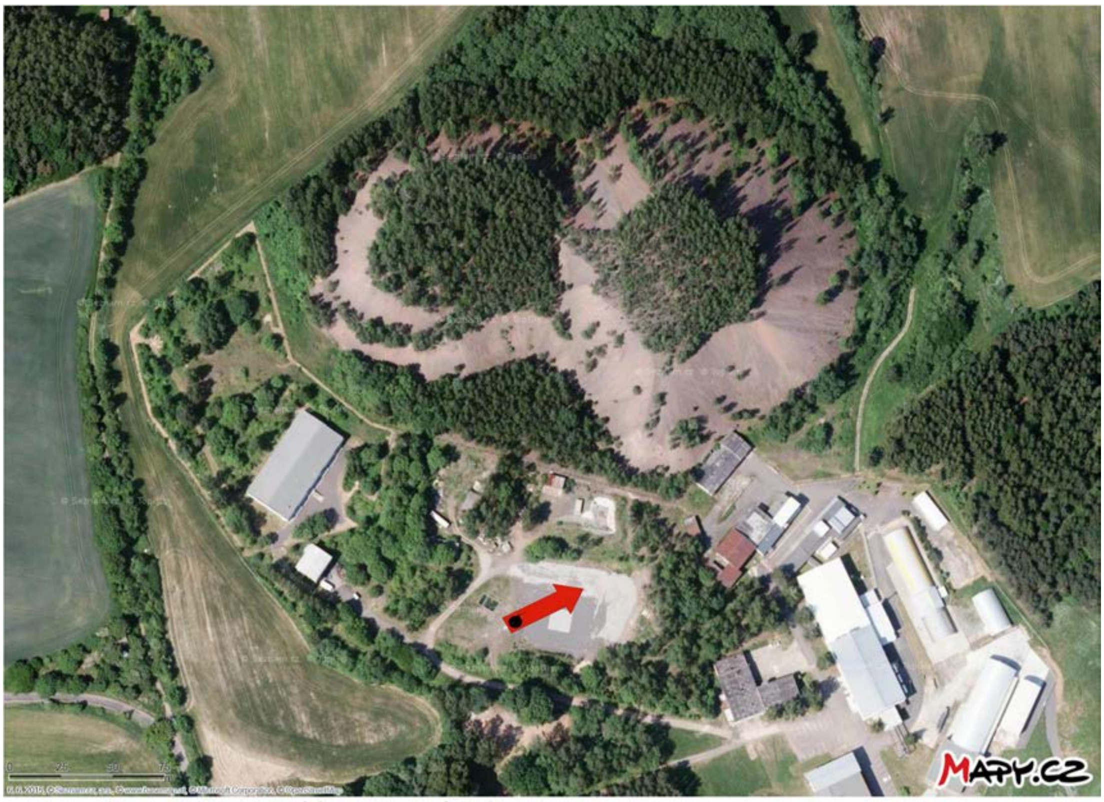

map source: Mapy.cz, 2015 aerial map © Seznam.cz, a.s., © TopGis, Ltd.

FIG. 77. Satellite image of the whole test area. The red arrow marks the planned direction of the dispersion. (background map source: Mapy.cz, 2015 aerial map © Seznam.cz, a.s., © TopGis, Ltd.).

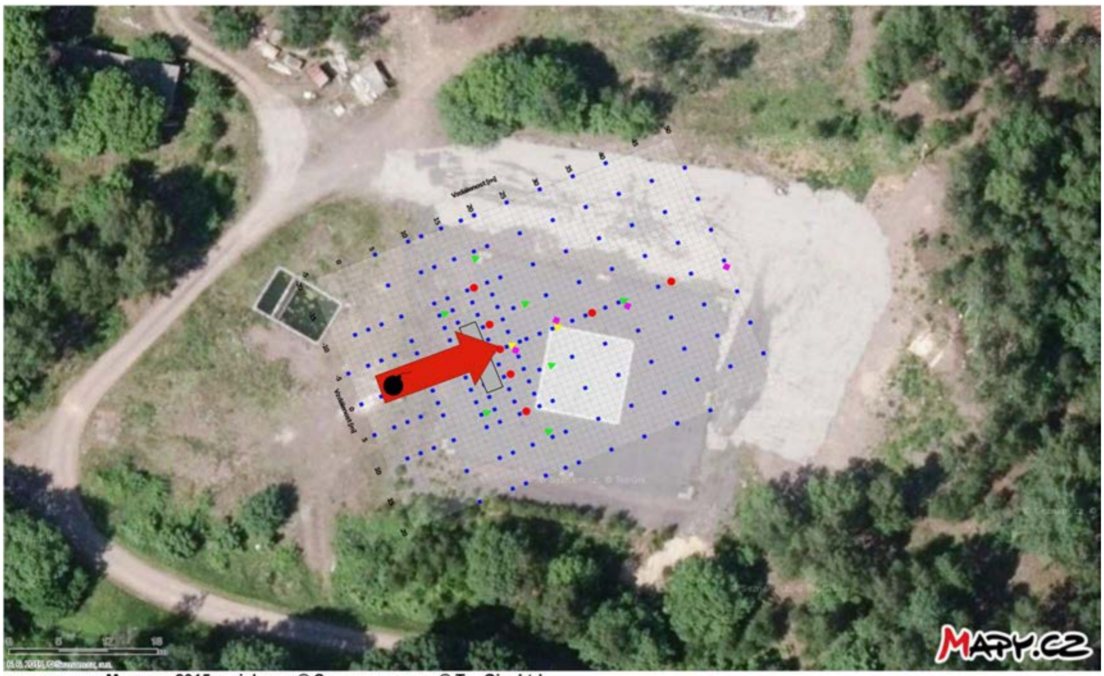

map source: Mapy.cz, 2015 aerial map © Seznam.cz, a.s., © TopGis, Ltd.

FIG. 78. Detailed view of the test polygon, with the experimental layout as used 4 May 2010 (background map source: Mapy.cz, 2015 aerial map © Seznam.cz, a.s., © TopGis, Ltd.).

FIG. 79. Configuration of the explosive and radioactive substance carrier. A standard 6 mL bottle (bottom) was used for Tests 5 and 6.

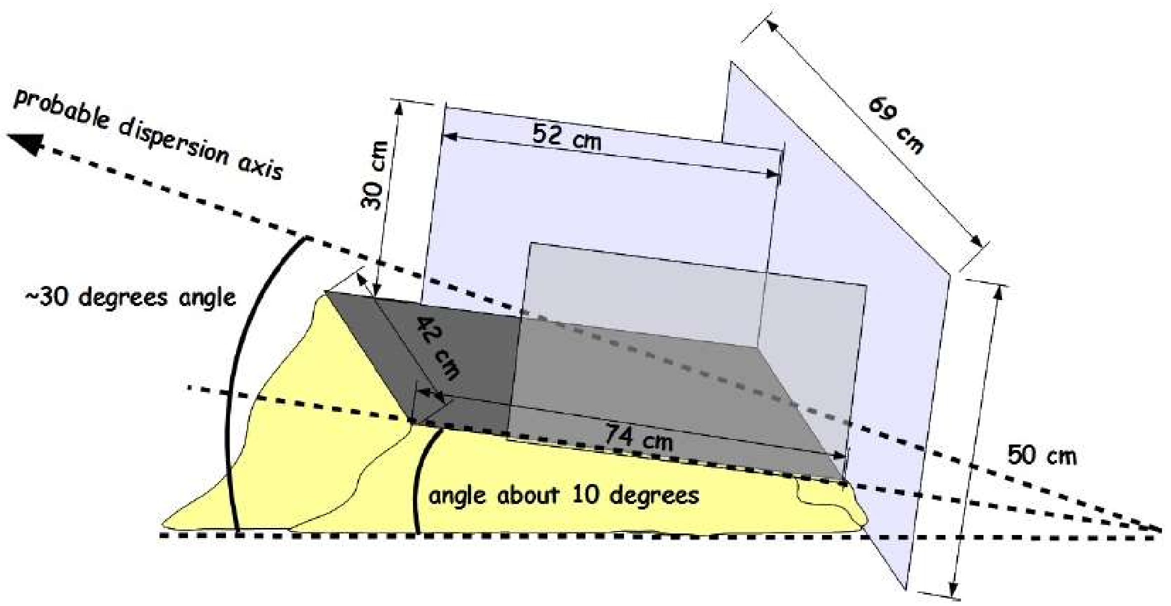

FIG. 80. Dispersion site schema.

TABLE 25. SUMMARY INFORMATION FOR TESTS 5 AND 6

Test No. **Date**	**Test 5/3P** **4 May 2010**	**Test 6/4P** **22 June 2010**
Explosion time[a]	14:15	12:06
Time of measurement of Tc-99m activity[a]	11:00	12:00
Activity of Tc-99m (MBq)	2119	2045
Amount of liquid containing the activity	6 mL	6 mL
Amount and type of explosive used[b]	Permon 10T 350 g	Permon 10T 350 g

[a] Twenty four hour system (12:00 = noon).
[b] Descriptions of the explosives were provided separately.

TABLE 26. SUMMARY OF WEATHER CONDITIONS DURING TESTS 5 AND 6[a]

Test No. **Date**	**Test 5/3P** **4 May 2010**	**Test 6/4P** **22 June 2010**
Temperature (°C)	10.1–10.2	18.5–18.9
Relative air humidity (%)	77–79	41–46
Condensation point (°C)	6.3–6.7	5.2–6.8
Wind speed (km/h)	3.2–13	4.7–11.2
Gust wind speed (km/h)	7.9–20.9	6.5–17.6
Wind direction (degrees)	90–270	0–270
Air pressure (hPa)	1013.6–1013.7	1013–1013.4

[a] More detailed meteorological data were provided in electronic form (see Appendix I). Measurements are at 10 m height. The indicated wind direction is the direction wind is blowing from.

TABLE 27. TIME DEPENDENT METEOROLOGICAL DATA FOR TEST 5/3P (4 MAY 2010)[a]

Time	Temperature (ºC)	Relative air humidity (%)	Condensation point (ºC)	Wind speed (m/s)	Maximum wind speed (m/s)	Wind direction (degrees)[b]	Air pressure (hPa)
14:00	10.5	78	6.8	0.9	1.8	0	1013.7
14:01	10.5	78	6.8	0.4	1.8	67.5	1013.6
14:02	10.5	79	7	1.3	2.7	202.5	1013.6
14:03	10.4	79	7	0.9	2.2	112.5	1013.6
14:04	10.4	79	7	2.7	4.9	67.5	1013.7
14:05	10.4	78	6.8	2.7	4	67.5	1013.6
14:06	10.4	78	6.8	1.8	2.7	67.5	1013.6
14:07	10.4	78	6.7	2.2	3.1	90	1013.7
14:08	10.4	78	6.7	3.1	4.5	90	1013.7
14:09	10.4	78	6.7	2.2	3.1	112.5	1013.6
14:10	10.3	78	6.7	2.2	3.6	67.5	1013.7
14:11	10.3	78	6.7	0.9	3.6	22.5	1013.7
14:12	10.3	78	6.7	2.2	3.1	90	1013.6
14:13	10.3	78	6.6	1.3	2.7	22.5	1013.6
14:14	10.3	78	6.6	1.8	4	90	1013.5
14:15	10.2	77	6.4	1.8	3.1	90	1013.7
14:16	10.2	78	6.6	1.8	3.6	112.5	1013.7
14:17	10.2	79	6.7	1.3	3.1	135	1013.6
14:18	10.2	79	6.7	0.9	2.2	112.5	1013.7
14:19	10.2	78	6.5	2.2	3.6	90	1013.7
14:20	10.2	78	6.5	2.2	2.7	112.5	1013.7
14:21	10.2	78	6.5	3.6	5.8	112.5	1013.7
14:22	10.1	78	6.4	2.7	4	90	1013.6
14:23	10.1	78	6.4	1.8	3.1	112.5	1013.7
14:24	10.1	77	6.3	2.2	3.6	112.5	1013.7
14:25	10.1	77	6.3	0.9	2.2	270	1013.7
14:26	10.1	78	6.4	1.3	2.7	112.5	1013.7
14:27	10.1	77	6.3	1.8	2.7	135	1013.6
14:28	10.1	77	6.3	2.2	4.9	67.5	1013.8
14:29	10.1	77	6.2	1.3	2.2	67.5	1013.7
14:30	10.1	77	6.2	0.9	1.8	0	1013.7

TABLE 27. TIME DEPENDENT METEOROLOGICAL DATA FOR TEST 5/3P (4 MAY 2010)[a] (cont.)

Time	Temperature (ºC)	Relative air humidity (%)	Condensation point (ºC)	Wind speed (m/s)	Maximum wind speed (m/s)	Wind direction (degrees)[b]	Air pressure (hPa)
14:31	10.1	77	6.2	1.8	3.1	112.5	1013.6
14:32	10.1	78	6.4	1.8	2.7	67.5	1013.7
14:33	10.1	78	6.4	2.2	3.1	90	1013.6
14:34	10.1	78	6.4	1.3	2.7	112.5	1013.7
14:35	10.1	78	6.4	1.8	3.1	135	1013.7
14:36	10.1	80	6.8	2.2	3.1	90	1013.7
14:37	10.1	80	6.8	1.8	3.6	90	1013.7
14:38	10	80	6.7	0.4	1.8	180	1013.6
14:39	10.1	81	6.9	2.2	3.6	112.5	1013.7
14:40	10.1	81	6.9	1.8	3.6	112.5	1013.6
14:41	10	80	6.7	2.2	3.6	112.5	1013.5
14:42	10	80	6.7	1.8	3.1	90	1013.5
14:43	10	80	6.7	2.2	4	112.5	1013.5
14:44	9.9	80	6.7	1.8	3.1	67.5	1013.5
14:45	9.9	80	6.7	1.3	2.2	135	1013.5

[a] Meteorological station at location (0,-20), height 10 m.
[b] Angle of 0º corresponds to North, 90º to East, etc.

TABLE 28. TIME DEPENDENT METEOROLOGICAL DATA FOR TEST 6/4P (22 JUNE 2010)[a]

Time	Temperature (ºC)	Relative air humidity (%)	Condensation point (ºC)	Wind speed (m/s)	Maximum wind speed (m/s)	Wind direction (degrees)[b]	Air pressure (hPa)
12:00	18.4	44	6.0	4.5	5.8	67.5	1013.4
12:01	18.4	44	6.0	4.0	6.7	90	1013.4
12:02	18.4	44	6.0	3.6	4.9	90	1013.4
12:03	18.4	45	6.3	3.6	4.9	67.5	1013.4
12:04	18.4	44	6.0	2.2	4.5	67.5	1013.4
12:05	18.5	46	6.7	2.7	4.0	90	1013.4
12:06	18.5	46	6.7	2.2	4.9	270	1013.4
12:07	18.6	43	5.8	1.8	4.5	0	1013.4
12:08	18.6	44	6.1	2.2	4.5	270	1013.4
12:09	18.6	43	5.8	1.3	4.0	202.5	1013.4
12:10	18.5	45	6.3	1.8	4.5	90	1013.4
12:11	18.6	46	6.8	2.2	4.0	112.5	1013.4
12:12	18.7	44	6.2	2.7	4.9	67.5	1013.4
12:13	18.8	42	5.6	3.1	4.9	90	1013.4
12:14	18.8	41	5.2	1.3	2.2	45	1013.4
12:15	18.8	41	5.2	1.3	2.7	22.5	1013.0
12:16	18.9	42	5.7	1.3	1.8	135	1013.0
12:17	18.9	43	6.1	0.4	1.3	135	1013.0
12:18	19.1	46	7.2	0.9	2.7	247.5	1013.0
12:19	19.1	44	6.6	2.2	3.6	270	1013.0
12:20	19.2	43	6.3	1.8	3.1	270	1013.0
12:21	19.4	45	7.1	1.8	2.7	112.5	1013.0
12:22	19.5	46	7.6	0.9	2.7	135	1013.0
12:23	19.7	45	7.4	0.9	2.2	22.5	1013.0
12:24	19.8	45	7.5	2.7	4.5	45	1013.0
12:25	19.8	39	5.4	2.2	4.5	247.5	1013.0
12:26	19.9	39	5.5	2.2	4.9	247.5	1013.0
12:27	19.9	40	5.9	4.0	6.7	292.5	1013.0
12:28	19.8	42	6.5	3.6	6.3	315	1013.0
12:29	19.8	42	6.5	2.2	4.5	292.5	1013.0
12:30	19.8	42	6.5	1.8	4.0	315	1012.8

[a] Meteorological station at location (0,-20), height 10 m.
[b] Angle of 0º corresponds to North, 90º to East, etc.

TABLE 29. MEASURED SURFACE CONTAMINATION (DEPOSITION) FOR TEST 5/3P, 4 MAY 2010 (Bq/m^2)

Coordinates (m)[a]		Deposition (Bq/m^2)
X	Y	
-37.58	79.78	16.67
-28.72	-91.77	4444.44
-25.12	102.91	22.22
-20.00	5.00	266.67
-20.00	10.00	95.56
-20.00	12.00	48.89
-20.00	15.00	22.22
-20.00	18.00	26.67
-20.00	20.00	80.00
-20.00	25.00	35.56
-20.00	30.00	18.89
-20.00	35.00	4.00
-20.00	40.00	8.56
-17.92	104.42	42.22
-15.00	5.00	511.11
-15.00	10.00	466.67
-15.00	12.00	184.44
-15.00	15.00	244.44
-15.00	18.00	153.33
-15.00	20.00	171.11
-15.00	25.00	8.44
-15.00	30.00	33.33
-15.00	35.00	4.44
-15.00	40.00	15.56
-15.00	45.00	4.22
-15.00	50.00	3.89
-10.00	-2.00	1946.67
-10.00	0.00	2222.22
-10.00	2.00	1577.78
-10.00	5.00	822.22
-10.00	10.00	577.78
-10.00	12.00	911.11
-10.00	15.00	466.67
-10.00	18.00	444.44
-10.00	20.00	400.00
-10.00	25.00	86.67
-10.00	30.00	131.11
-10.00	35.00	5.00
-10.00	40.00	3.89
-10.00	45.00	3.89
-10.00	50.00	5.78
-9.78	-94.85	7333.33
-8.00	10.00	955.56
-8.00	12.00	688.89
-8.00	15.00	644.44
-8.00	18.00	377.78

TABLE 29. MEASURED SURFACE CONTAMINATION (DEPOSITION) FOR TEST 5/3P, 4 MAY 2010 (Bq/m^2) (cont.)

Coordinates (m)[a] X	Y	Deposition (Bq/m^2)
-6.00	5.00	1511.11
-6.00	10.00	1177.78
-6.00	12.00	1200.00
-6.00	15.00	644.44
-6.00	18.00	644.44
-5.00	-5.00	2444.44
-5.00	-2.00	2888.89
-5.00	0.00	2444.44
-5.00	2.00	2888.89
-5.00	20.00	644.44
-5.00	25.00	311.11
-5.00	30.00	75.56
-5.00	35.00	84.44
-5.00	40.00	12.22
-5.00	45.00	9.89
-5.00	50.00	2.22
-4.00	5.00	2888.89
-4.00	10.00	2888.89
-4.00	12.00	4444.44
-4.00	15.00	622.22
-4.00	18.00	600.00
-2.00	5.00	10888.89
-2.00	10.00	33333.33
-2.00	12.00	64444.44
-2.00	15.00	1066.67
-2.00	18.00	488.89
0.00	-5.00	6888.89
0.00	-2.00	12000.00
0.00	3.00	2066666.67
0.00	4.00	800000.00
0.00	5.00	140000.00
0.00	6.00	115555.56
0.00	8.00	33333.33
0.00	9.00	37777.78
0.00	10.00	9777.78
0.00	12.00	64444.44
0.00	15.00	666.67
0.00	16.00	511.11
0.00	17.00	800.00
0.00	19.00	1000.00
0.00	20.00	1266.67
0.00	22.00	1911.11
0.00	24.00	2444.44
0.00	27.00	866.67
0.00	29.00	288.89
0.00	32.00	68.89
0.00	34.00	40.00
0.00	40.00	28.89
0.00	45.00	5.22

TABLE 29. MEASURED SURFACE CONTAMINATION (DEPOSITION) FOR TEST 5/3P, 4 MAY 2010 (Bq/m^2) (cont.)

Coordinates (m)[a] X	Y	Deposition (Bq/m^2)
0.00	50.00	10.44
2.00	5.00	1244444.44
2.00	10.00	14444.44
2.00	12.00	35555.56
2.00	15.00	1244.44
2.00	18.00	844.44
4.00	5.00	355555.56
4.00	10.00	28888.89
4.00	12.00	14222.22
4.00	15.00	1755.56
4.00	18.00	1688.89
4.16	-93.80	4000.00
4.29	105.94	3.56
5.00	-5.00	131111.11
5.00	-2.00	888888.89
5.00	0.00	1444444.44
5.00	2.00	977777.78
5.00	20.00	4000.00
5.00	25.00	2666.67
5.00	30.00	511.11
5.00	35.00	266.67
5.00	40.00	533.33
5.00	45.00	3.67
5.00	50.00	2.33
6.00	5.00	333333.33
6.00	10.00	197777.78
6.00	12.00	31111.11
6.00	15.00	6000.00
6.00	18.00	2888.89
8.00	10.00	106666.67
8.00	12.00	155555.56
8.00	15.00	68444.44
8.00	18.00	19555.56
10.00	-2.00	777777.78
10.00	0.00	824444.44
10.00	2.00	600000.00
10.00	5.00	422222.22
10.00	10.00	102222.22
10.00	12.00	77777.78
10.00	15.00	64444.44
10.00	18.00	42222.22
10.00	20.00	24444.44
10.00	25.00	8888.89
10.00	30.00	6222.22
10.00	35.00	88.89
10.00	40.00	400.00
10.00	45.00	8.78
10.00	50.00	10.11

TABLE 29. MEASURED SURFACE CONTAMINATION (DEPOSITION) FOR TEST 5/3P, 4 MAY 2010 (Bq/m^2) (cont.)

Coordinates (m)[a] X	Y	Deposition (Bq/m^2)
15.00	5.00	21777.78
15.00	10.00	26666.67
15.00	12.00	24444.44
15.00	15.00	24444.44
15.00	18.00	34666.67
15.00	20.00	26666.67
15.00	25.00	22222.22
15.00	30.00	12533.33
15.00	35.00	3333.33
15.00	40.00	33.33
15.00	45.00	5.11
15.00	50.00	3.67
20.00	5.00	13111.11
20.00	10.00	9777.78
20.00	12.00	27777.78
20.00	15.00	24444.44
20.00	18.00	17333.33
20.00	20.00	16222.22
20.00	25.00	2666.67
20.00	30.00	288.89
20.00	35.00	311.11
20.00	40.00	711.11
20.18	105.44	31.11
21.32	-91.98	2888.89
35.84	-89.09	1000.00

a Coordinates represent distances (m) from the dispersion point (0,0) in the grid area of the field test.

TABLE 30. MEASURED SURFACE CONTAMINATION (DEPOSITION) FOR TEST 6/4P, 22 JUNE 2010 (Bq/m^2)

Coordinates (m)[a] X	Y	Deposition (Bq/m^2)
-20.00	5.00	5866.67
-20.00	10.00	4911.11
-20.00	12.00	22444.44
-20.00	15.00	23888.89
-20.00	18.00	5177.78
-20.00	20.00	5055.56
-20.00	25.00	4300.00
-20.00	30.00	2944.44
-20.00	35.00	4700.00
-20.00	40.00	9766.67
-15.00	5.00	3488.89
-15.00	10.00	14066.67
-15.00	12.00	38888.89
-15.00	15.00	8577.78
-15.00	18.00	17888.89

TABLE 30. MEASURED SURFACE CONTAMINATION (DEPOSITION) FOR TEST 6/4P, 22 JUNE 2010 (Bq/m^2) (cont.)

Coordinates (m)[a] X	Y	Deposition (Bq/m^2)
-15.00	20.00	15444.44
-15.00	25.00	6600.00
-15.00	30.00	5788.89
-15.00	35.00	3822.22
-15.00	40.00	3855.56
-15.00	45.00	2966.67
-15.00	50.00	930.00
-10.00	-2.00	4244.44
-10.00	0.00	6977.78
-10.00	2.00	6311.11
-10.00	5.00	6688.89
-10.00	10.00	7511.11
-10.00	12.00	37777.78
-10.00	15.00	34888.89
-10.00	18.00	18888.89
-10.00	20.00	33222.22
-10.00	25.00	5333.33
-10.00	30.00	5777.78
-10.00	35.00	5211.11
-10.00	40.00	5400.00
-10.00	45.00	3855.56
-10.00	50.00	1422.22
-8.00	10.00	28888.89
-8.00	12.00	60888.89
-8.00	15.00	9766.67
-8.00	18.00	10533.33
-6.00	5.00	117555.56
-6.00	10.00	41333.33
-6.00	12.00	100666.67
-6.00	15.00	17222.22
-6.00	18.00	11444.44
-5.00	-5.00	4688.89
-5.00	-2.00	14222.22
-5.00	0.00	52666.67
-5.00	2.00	130222.22
-5.00	20.00	7455.56
-5.00	25.00	5077.78
-5.00	30.00	4300.00
-5.00	35.00	5633.33
-5.00	40.00	3788.89
-5.00	45.00	3666.67
-5.00	50.00	2211.11
-4.00	5.00	102000.00
-4.00	10.00	39111.11
-4.00	12.00	100444.44
-4.00	15.00	8133.33
-4.00	18.00	8366.67
-2.00	5.00	64888.89
-2.00	10.00	73777.78

TABLE 30. MEASURED SURFACE CONTAMINATION (DEPOSITION) FOR TEST 6/4P, 22 JUNE 2010 (Bq/m^2) (cont.)

Coordinates (m)[a] X	Y	Deposition (Bq/m^2)
-2.00	12.00	146666.67
-2.00	15.00	22111.11
-2.00	18.00	6722.22
0.00	-5.00	1680.00
0.00	-2.00	2933.33
0.00	2.00	179777.78
0.00	3.00	955555.56
0.00	4.00	180444.44
0.00	5.00	391111.11
0.00	6.00	340000.00
0.00	8.00	127111.11
0.00	9.00	124000.00
0.00	10.00	56888.89
0.00	12.00	93111.11
0.00	15.00	4566.67
0.00	16.00	3444.44
0.00	17.00	3988.89
0.00	19.00	4444.44
0.00	20.00	5877.78
0.00	22.00	2144.44
0.00	24.00	5933.33
0.00	27.00	3822.22
0.00	29.00	2366.67
0.00	32.00	2511.11
0.00	34.00	2411.11
0.00	40.00	4355.56
0.00	45.00	3622.22
0.00	50.00	1522.22
2.00	5.00	29333.33
2.00	10.00	147555.56
2.00	12.00	161111.11
2.00	15.00	9766.67
2.00	18.00	7666.67
4.00	5.00	15688.89
4.00	10.00	35333.33
4.00	12.00	150000.00
4.00	15.00	6266.67
4.00	18.00	17555.56
5.00	-5.00	2533.33
5.00	-2.00	5155.56
5.00	0.00	8000.00
5.00	2.00	11555.56
5.00	20.00	2855.56
5.00	25.00	3511.11
5.00	30.00	4322.22
5.00	35.00	4211.11
5.00	40.00	3655.56
5.00	45.00	2011.11
5.00	50.00	1611.11

TABLE 30. MEASURED SURFACE CONTAMINATION (DEPOSITION) FOR TEST 6/4P, 22 JUNE 2010 (Bq/m^2) (cont.)

Coordinates (m)[a]		**Deposition (Bq/m^2)**
X	**Y**	
6.00	5.00	14511.11
6.00	10.00	10466.67
6.00	12.00	7622.22
6.00	15.00	15666.67
6.00	18.00	6466.67
8.00	10.00	5822.22
8.00	12.00	10044.44
8.00	15.00	4600.00
8.00	18.00	6433.33
10.00	-2.00	13644.44
10.00	0.00	12888.89
10.00	2.00	12955.56
10.00	5.00	11622.22
10.00	10.00	4311.11
10.00	12.00	9644.44
10.00	15.00	7166.67
10.00	18.00	8311.11
10.00	20.00	5933.33
10.00	25.00	2411.11
10.00	30.00	2400.00
10.00	35.00	3866.67
10.00	40.00	2000.00
10.00	45.00	3133.33
10.00	50.00	1555.56
15.00	5.00	3800.00
15.00	10.00	19533.33
15.00	12.00	4644.44
15.00	15.00	8200.00
15.00	18.00	8477.78
15.00	20.00	4255.56
15.00	25.00	4366.67
15.00	30.00	2877.78
15.00	35.00	2888.89
15.00	40.00	3144.44
15.00	45.00	3233.33
15.00	50.00	2444.44
20.00	5.00	3933.33
20.00	10.00	3733.33
20.00	15.00	4366.67
20.00	18.00	4188.89
20.00	20.00	6188.89
20.00	25.00	2400.00
20.00	30.00	2244.44
20.00	35.00	3100.00
20.00	40.00	9766.67

[a] Coordinates represent distances (m) from the dispersion point (0,0) in the grid area of the field test.

The arrangement of detectors with respect to the dispersion point is shown for Tests 5 and 6 in Fig. 81. The arrangements of detectors and other detailed information for the tests are provided in Figs 82–86. Tests 5 and 6 included a large obstacle (a bus, 11 m × 3 m × 2.5 m; width, height, length). There were 7 vertical columns with filters: 5 at height 7 m, 1 at 12 m, and 1 at 35 m (boom lift). Additional sampling equipment included 5 DustTraks, 7 aerosol samplers, and an experimental aerosol sampler (diffusion grid or diffraction grating). Three dimensional (3-D) models of all experiments with appropriate viewing software were available to the modellers. Video footage of all field tests (in most cases from more than one location) was made available to participants in the exercise.

I.5. DATA FOR CALIBRATION

Measurement data for the first four field tests (6 December 2007, 15 May 2008, 5 May 2009 and 14 July 2009) [6] were available to the participants in this exercise. These data included surface contamination (Bq/m^2) for Tests 1–4, dose rates (nSv/h) for Test 2, and time integrated activity concentrations in air at selected locations (Test 2). Dose rates need to be used with caution, due to high background dose rates at the test site. The surface contamination and dose rates were made available to participants in electronic form.

I.6. MODELLING ENDPOINTS

Tests 5 and 6 (4 May 2010 and 22 June 2010) were used in the exercise for blind testing of models. Model predictions were compared with each other (model intercomparisons) and eventually with the available measurements, to the extent possible (Endpoints 1 and 2 below, within the range of measurements).

For purposes of model intercomparison, modellers were requested to use the following grid size, subject to model constraints:

— downwind distance 0–50 m: use a 5 × 5 m grid (Δx = 5 m);
— downwind distance 50–2000 m: use a 25 × 25 m grid (Δx = 25 m);
— upwind distance: to 100 m.

width: model dependent (measurements cover an area 50 m × 40 m, or 20 m each side of the centerline).

The activity of ^{99m}Tc at the time of the explosion was to be used.

Endpoints to be modelled for Tests 5 and 6:

(1) Surface contamination (Bq/m^2) as a function of distance, assuming the grid described above. Assume that the deposition has been completed.
(2) Time integrated activity concentrations in air (Bq·min·m^{-3}) as a function of height and distance along the centre line, out to 1000 m, for heights from 0–5 m.
(3) Estimated percentile contamination zones (50%, 75%, 95%) for each explosion event. The contamination zone is the area (for example, defined in terms of a radius from the explosion, or an angle and distance from the explosion, or some selected contour) which is expected to contain a given percentage of the contamination released by the explosion event. Specify whether the zones are defined as a percentage of total activity or a percentage of total deposition.

Where possible, uncertainties on the model predictions were requested.

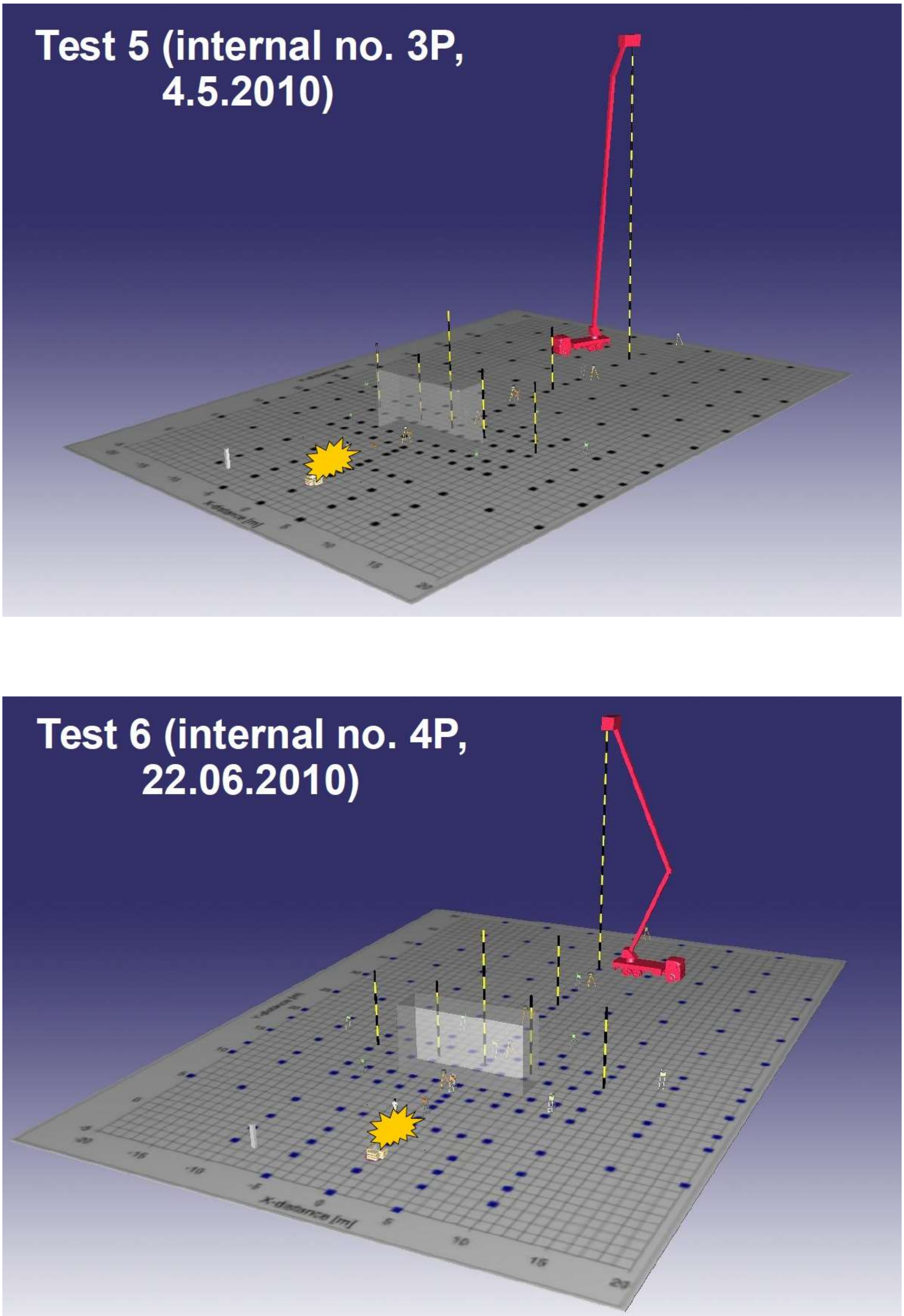

FIG. 81. Arrangement of filters, detectors and obstacles on the test polygon for Test 5/3P (4 May 2010; top) and Test 6/4P (22 June 2010; bottom).

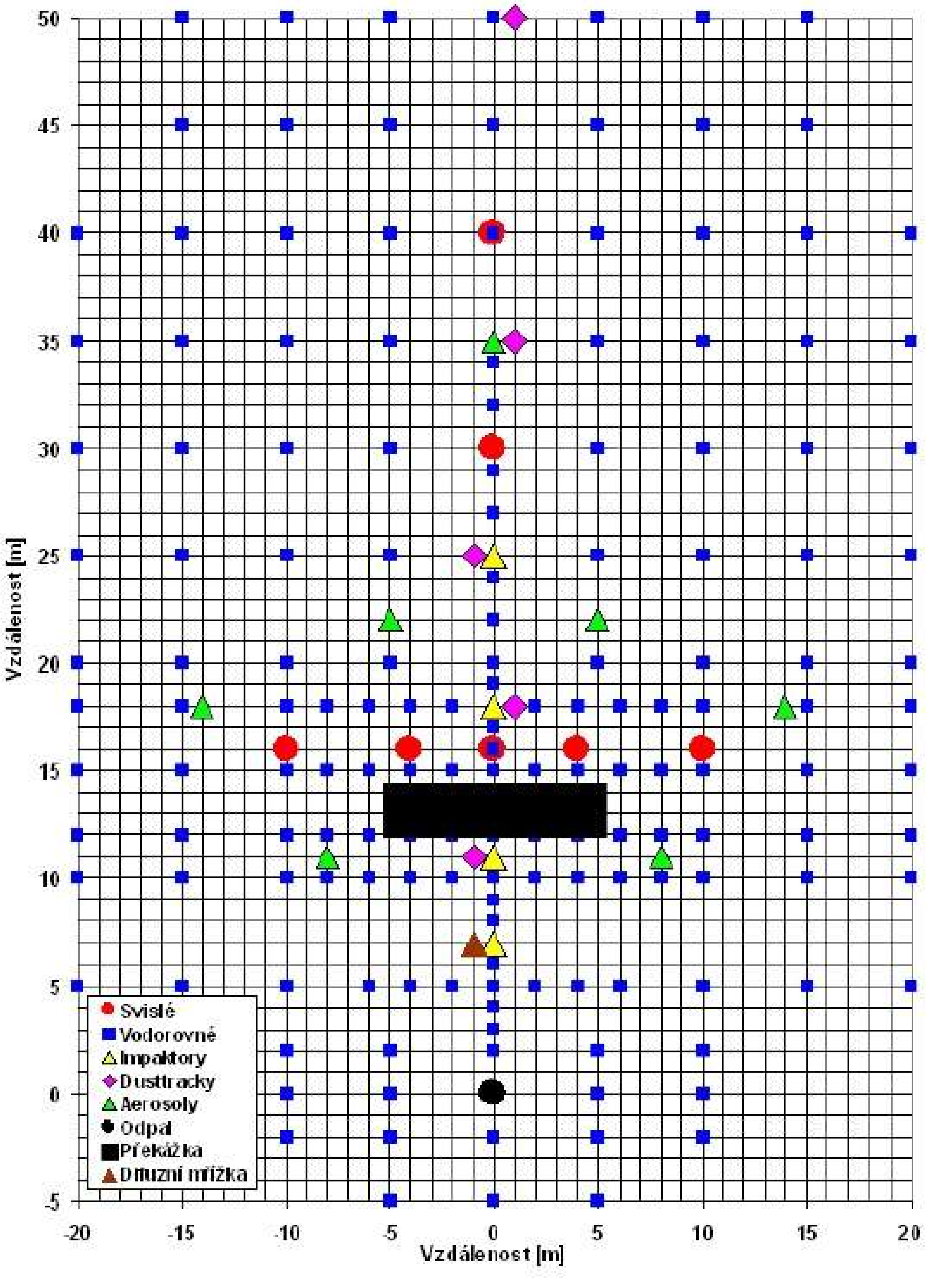

FIG. 82. Experimental layout for Test 5 (4 May 2010). Blue squares, ground filters; red circles, vertical columns; green triangles, aerosol samplers; yellow triangles, impactors; pink diamonds, DustTraks; black dot, dispersion point; black rectangle, obstacle. Axes are distance (m).

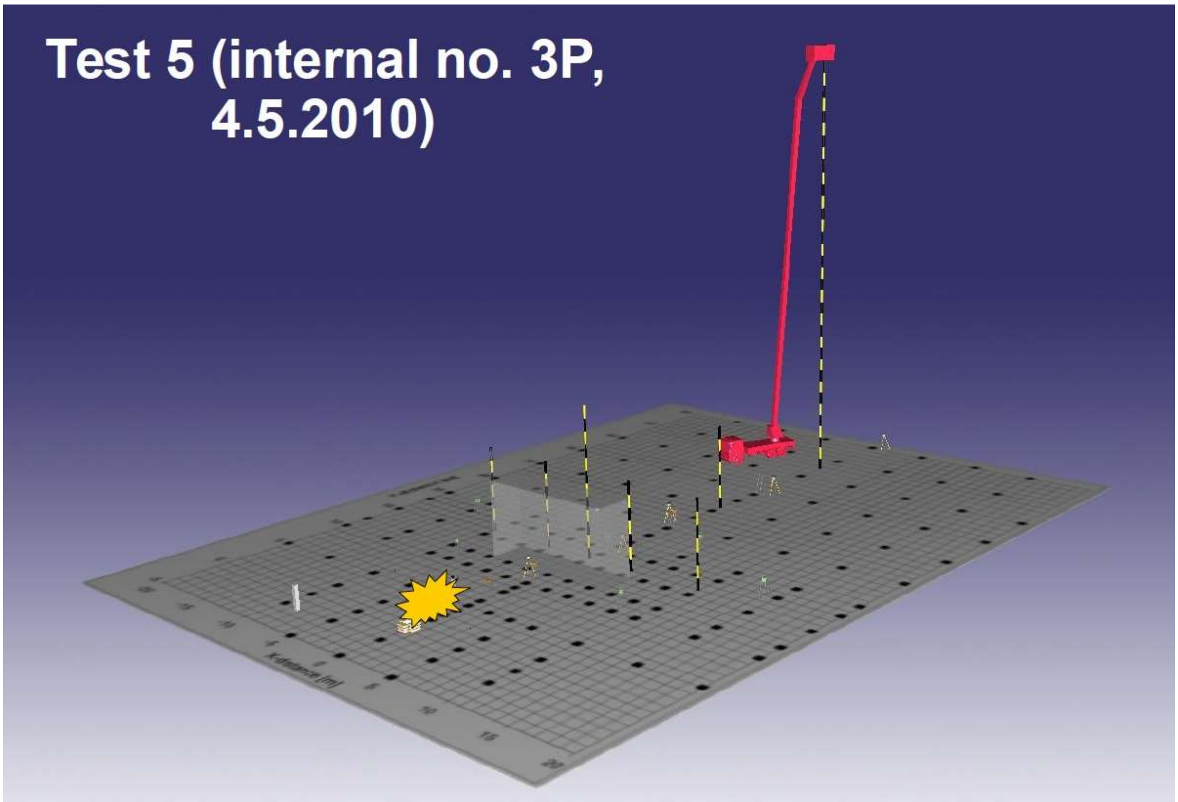

FIG. 83. Arrangement of filters, detectors and obstacles on the test polygon for Test 5/3P (4 May 2010).

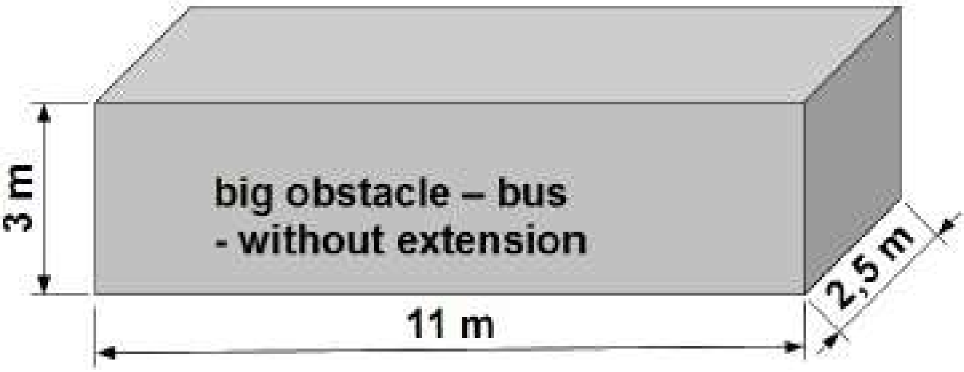

FIG. 84. Dimensions of obstacle used in Test 5/3P (4 May 2010) and Test 6/4P (22 June 2010).

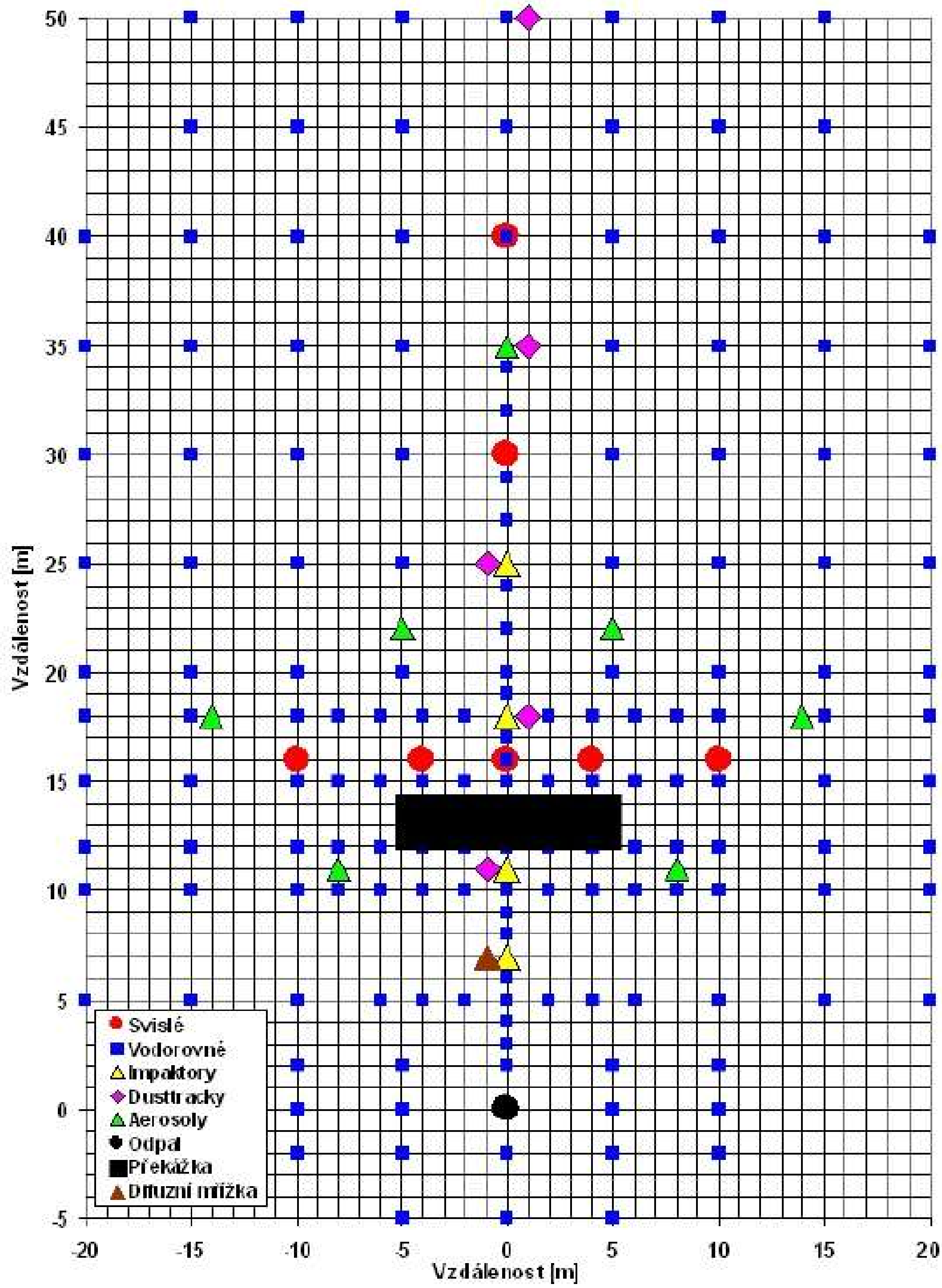

FIG. 85. Experimental layout for Test 6 (22 June 2010). Blue squares, ground filters; red circles, vertical columns; green triangles, aerosol samplers; yellow triangles, impactors; pink diamonds, DustTraks; black dot, dispersion point; black rectangle, obstacle. Axes are distance (m).

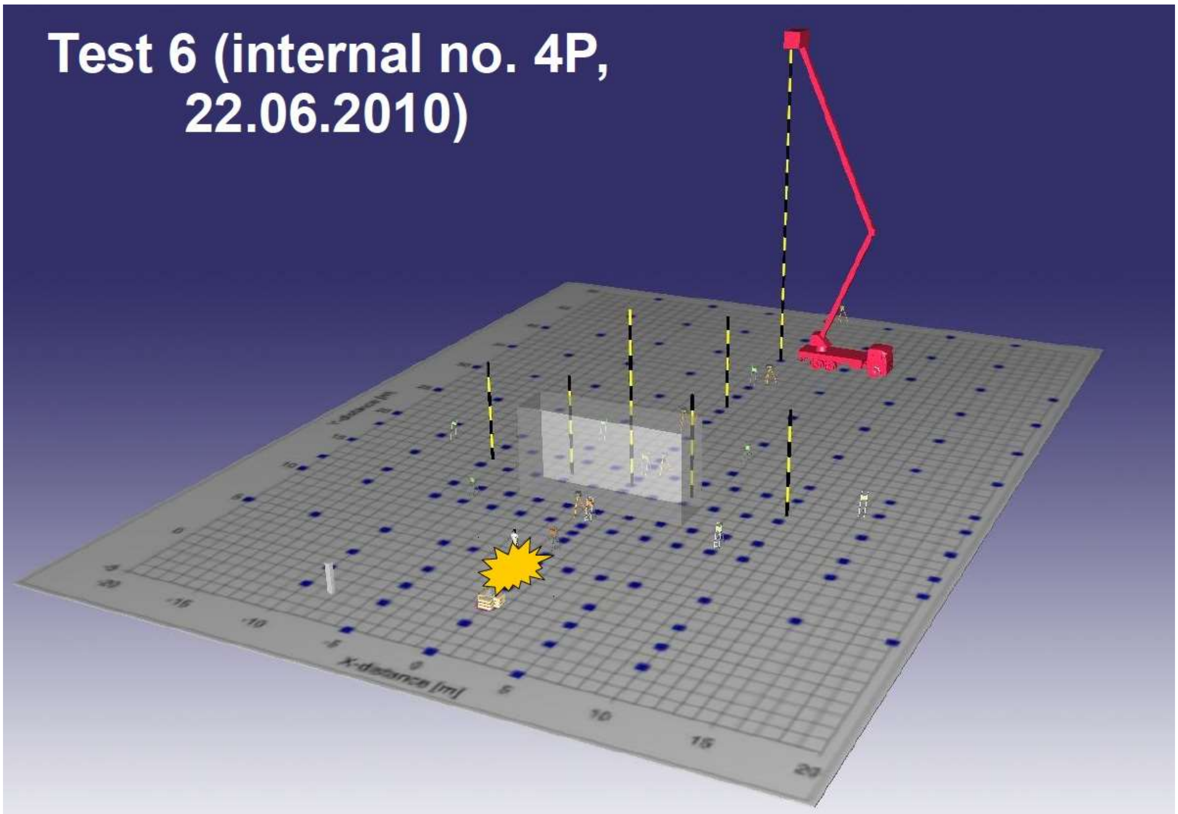

FIG. 86. Arrangement of filters, detectors and obstacles on the test polygon for Test 6/4P (22 June 2010).

I.7. DATA FOR COMPARISON WITH MODEL PREDICTIONS

The measured surface contamination for Tests 5 and 6 was not available to modellers during the exercise. These measurements are provided in Tables 29 and 30 above.

I.8. ADDITIONAL MODELLING ACTIVITIES

As described previously [6], additional modelling activities can be carried out for any of the field tests, using the measurements of dose rate or surface activity. Possible activities include estimation of the source term from available measurements, validation of location factors, and use of data assimilation to improve initial model predictions.

APPENDIX II. SUPPLEMENTARY INFORMATION FOR THE FUKUSHIMA EXERCISE

Tables 31–33 provide supplementary information that complements the information relating to the Fukushima exercise that have been included in Section 5 of this publication.

TABLE 31. DEPOSITION AND POPULATION DATA FOR THE TEST SITE (500 m MESH)

Data Number of cell	Mesh ID	Coordinates (x,y)	Deposition of ^{137}Cs as of 14 June 2011 (Bq/m^2)[a]	Population
1	5540_7769_3	(15,1)	3.2×10^5	33
2	5540_7769_4	(16,1)	3.2×10^5	17
7	5540_7778_3	(13,3)	2.4×10^5	5
8	5540_7778_4	(14,3)	2.4×10^5	0
4	5540_7779_1	(15,2)	2.4×10^5	0
5	5540_7779_2	(16,2)	3.2×10^5	0
9	5540_7779_3	(15,3)	4.9×10^5	0
10	5540_7779_4	(16,3)	4.9×10^5	0
27	5540_7785_4	(8,5)	4.4×10^4	0
15	5540_7786_2	(10,4)	4.4×10^4	0
28	5540_7786_3	(9,5)	4.4×10^4	0
29	5540_7786_4	(10,5)	4.4×10^4	0
16	5540_7787_1	(11,4)	4.4×10^4	0
17	5540_7787_2	(12,4)	4.4×10^4	0
30	5540_7787_3	(11,5)	4.4×10^4	0
31	5540_7787_4	(12,5)	4.4×10^4	0
18	5540_7788_1	(13,4)	2.4×10^5	0
19	5540_7788_2	(14,4)	4.9×10^5	0
32	5540_7788_3	(13,5)	4.4×10^4	7
33	5540_7788_4	(14,5)	4.9×10^5	0
20	5540_7789_1	(15,4)	4.9×10^5	0
21	5540_7789_2	(16,4)	4.9×10^5	0
34	5540_7789_3	(15,5)	4.9×10^5	0
35	5540_7789_4	(16,5)	4.9×10^5	52
41	5540_7795_1	(7,6)	2.8×10^4	0
42	5540_7795_2	(8,6)	4.4×10^4	0
56	5540_7795_3	(7,7)	2.8×10^4	0
57	5540_7795_4	(8,7)	7.4×10^5	0
43	5540_7796_1	(9,6)	4.4×10^4	0
44	5540_7796_2	(10,6)	4.4×10^4	0
58	5540_7796_3	(9,7)	7.4×10^5	0
59	5540_7796_4	(10,7)	7.4×10^5	0
45	5540_7797_1	(11,6)	4.4×10^4	0
46	5540_7797_2	(12,6)	4.4×10^4	25
60	5540_7797_3	(11,7)	7.4×10^5	0
61	5540_7797_4	(12,7)	7.4×10^5	32
47	5540_7798_1	(13,6)	4.9×10^5	11
48	5540_7798_2	(14,6)	4.9×10^5	68
62	5540_7798_3	(13,7)	5.3×10^5	37
63	5540_7798_4	(14,7)	4.9×10^5	4
49	5540_7799_1	(15,6)	4.9×10^5	55
50	5540_7799_2	(16,6)	4.9×10^5	125

TABLE 31. DEPOSITION AND POPULATION DATA FOR THE TEST SITE (500 m MESH) (cont.)

Data Number of cell	Mesh ID	Coordinates (x,y)	Deposition of ^{137}Cs as of 14 June 2011 (Bq/m^2)[a]	Population
64	5540_7799_3	(15,7)	4.9×10^5	10
65	5540_7799_4	(16,7)	4.9×10^5	135
3	5541_7060_3	(17,1)	3.2×10^5	0
6	5541_7070_1	(17,2)	1.4×10^5	0
11	5541_7070_3	(17,3)	1.4×10^5	5
12	5541_7070_4	(18,3)	1.4×10^5	21
13	5541_7071_3	(19,3)	1.3×10^5	0
14	5541_7071_4	(20,3)	1.3×10^5	0
22	5541_7080_1	(17,4)	1.4×10^5	23
23	5541_7080_2	(18,4)	1.4×10^5	95
36	5541_7080_3	(17,5)	1.4×10^5	47
37	5541_7080_4	(18,5)	1.4×10^5	77
24	5541_7081_1	(19,4)	1.4×10^5	0
25	5541_7081_2	(20,4)	1.4×10^5	0
38	5541_7081_3	(19,5)	1.4×10^5	2
39	5541_7081_4	(20,5)	1.4×10^5	41
26	5541_7082_1	(21,4)	1.3×10^5	0
40	5541_7082_3	(21,5)	1.4×10^5	0
51	5541_7090_1	(17,6)	1.4×10^5	138
52	5541_7090_2	(18,6)	1.4×10^5	138
66	5541_7090_3	(17,7)	5.9×10^5	551
67	5541_7090_4	(18,7)	5.9×10^5	301
53	5541_7091_1	(19,6)	1.4×10^5	42
54	5541_7091_2	(20,6)	1.4×10^5	83
68	5541_7091_3	(19,7)	5.9×10^5	622
69	5541_7091_4	(20,7)	9.8×10^5	114
55	5541_7092_1	(21,6)	9.8×10^5	2
70	5541_7092_3	(21,7)	9.8×10^5	12
71	5640_0703_2	(4,8)	1.7×10^4	0
89	5640_0703_3	(3,9)	1.1×10^6	0
90	5640_0703_4	(4,9)	5.6×10^5	0
72	5640_0704_1	(5,8)	2.8×10^4	0
73	5640_0704_2	(6,8)	2.8×10^4	0
91	5640_0704_3	(5,9)	5.6×10^5	0
92	5640_0704_4	(6,9)	7.5×10^5	0
74	5640_0705_1	(7,8)	2.8×10^4	0
75	5640_0705_2	(8,8)	7.4×10^5	0
93	5640_0705_3	(7,9)	7.4×10^5	0
94	5640_0705_4	(8,9)	7.4×10^5	0
76	5640_0706_1	(9,8)	7.4×10^5	0
77	5640_0706_2	(10,8)	7.4×10^5	12
95	5640_0706_3	(9,9)	7.4×10^5	0
96	5640_0706_4	(10,9)	7.4×10^5	34
78	5640_0707_1	(11,8)	7.4×10^5	31
79	5640_0707_2	(12,8)	7.4×10^5	0
97	5640_0707_3	(11,9)	7.4×10^5	36
98	5640_0707_4	(12,9)	5.3×10^5	0
80	5640_0708_1	(13,8)	5.3×10^5	0
81	5640_0708_2	(14,8)	5.3×10^5	0
99	5640_0708_3	(13,9)	5.3×10^5	0
100	5640_0708_4	(14,9)	5.3×10^5	47
82	5640_0709_1	(15,8)	4.9×10^5	0
83	5640_0709_2	(16,8)	5.9×10^5	16
101	5640_0709_3	(15,9)	5.3×10^5	28

TABLE 31. DEPOSITION AND POPULATION DATA FOR THE TEST SITE (500 m MESH) (cont.)

Data Number of cell	Mesh ID	Coordinates (x,y)	Deposition of ^{137}Cs as of 14 June 2011 (Bq/m^2)[a]	Population
102	5640_0709_4	(16,9)	5.9×10^5	165
108	5640_0712_2	(2,10)	1.1×10^6	0
129	5640_0712_4	(2,11)	5.6×10^5	0
109	5640_0713_1	(3,10)	5.6×10^5	0
110	5640_0713_2	(4,10)	5.6×10^5	0
130	5640_0713_3	(3,11)	5.6×10^5	0
131	5640_0713_4	(4,11)	5.6×10^5	0
111	5640_0714_1	(5,10)	5.6×10^5	0
112	5640_0714_2	(6,10)	7.5×10^5	0
132	5640_0714_3	(5,11)	7.5×10^5	0
133	5640_0714_4	(6,11)	7.5×10^5	0
113	5640_0715_1	(7,10)	7.5×10^5	0
114	5640_0715_2	(8,10)	7.4×10^5	0
134	5640_0715_3	(7,11)	7.5×10^5	0
135	5640_0715_4	(8,11)	7.5×10^5	0
115	5640_0716_1	(9,10)	7.4×10^5	0
116	5640_0716_2	(10,10)	7.4×10^5	1
136	5640_0716_3	(9,11)	7.4×10^5	0
137	5640_0716_4	(10,11)	7.4×10^5	0
117	5640_0717_1	(11,10)	7.4×10^5	0
118	5640_0717_2	(12,10)	5.3×10^5	0
138	5640_0717_3	(11,11)	7.4×10^5	0
139	5640_0717_4	(12,11)	5.3×10^5	0
119	5640_0718_1	(13,10)	5.3×10^5	0
120	5640_0718_2	(14,10)	5.3×10^5	0
140	5640_0718_3	(13,11)	5.3×10^5	0
141	5640_0718_4	(14,11)	5.3×10^5	10
121	5640_0719_1	(15,10)	5.3×10^5	45
122	5640_0719_2	(16,10)	5.3×10^5	21
142	5640_0719_3	(15,11)	5.3×10^5	13
143	5640_0719_4	(16,11)	1.7×10^5	247
150	5640_0722_1	(1,12)	5.6×10^5	0
151	5640_0722_2	(2,12)	5.6×10^5	0
172	5640_0722_3	(1,13)	5.6×10^5	0
173	5640_0722_4	(2,13)	5.6×10^5	0
152	5640_0723_1	(3,12)	5.6×10^5	0
153	5640_0723_2	(4,12)	5.6×10^5	0
174	5640_0723_3	(3,13)	5.6×10^5	0
175	5640_0723_4	(4,13)	5.6×10^5	0
154	5640_0724_1	(5,12)	7.5×10^5	0
155	5640_0724_2	(6,12)	7.5×10^5	0
176	5640_0724_3	(5,13)	7.5×10^5	0
177	5640_0724_4	(6,13)	7.5×10^5	0
156	5640_0725_1	(7,12)	7.5×10^5	0
157	5640_0725_2	(8,12)	7.5×10^5	0
178	5640_0725_3	(7,13)	7.5×10^5	0
179	5640_0725_4	(8,13)	7.5×10^5	0
158	5640_0726_1	(9,12)	7.5×10^5	0
159	5640_0726_2	(10,12)	7.4×10^5	0
180	5640_0726_3	(9,13)	7.5×10^5	0
181	5640_0726_4	(10,13)	7.9×10^5	0
160	5640_0727_1	(11,12)	7.9×10^5	0
161	5640_0727_2	(12,12)	7.9×10^5	0
182	5640_0727_3	(11,13)	7.9×10^5	0
183	5640_0727_4	(12,13)	7.9×10^5	31

TABLE 31. DEPOSITION AND POPULATION DATA FOR THE TEST SITE (500 m MESH) (cont.)

Data Number of cell	Mesh ID	Coordinates (x,y)	Deposition of ^{137}Cs as of 14 June 2011 (Bq/m^2)[a]	Population
162	5640_0728_1	(13,12)	5.3×10^5	22
163	5640_0728_2	(14,12)	1.7×10^5	26
184	5640_0728_3	(13,13)	7.9×10^5	26
185	5640_0728_4	(14,13)	1.7×10^5	41
164	5640_0729_1	(15,12)	1.7×10^5	24
165	5640_0729_2	(16,12)	1.7×10^5	161
186	5640_0729_3	(15,13)	1.7×10^5	310
187	5640_0729_4	(16,13)	1.7×10^5	617
194	5640_0732_1	(1,14)	5.6×10^5	0
195	5640_0732_2	(2,14)	5.6×10^5	0
216	5640_0732_3	(1,15)	5.6×10^5	2
217	5640_0732_4	(2,15)	5.6×10^5	0
196	5640_0733_1	(3,14)	5.6×10^5	0
197	5640_0733_2	(4,14)	7.5×10^5	0
218	5640_0733_3	(3,15)	5.6×10^5	0
219	5640_0733_4	(4,15)	7.5×10^5	0
198	5640_0734_1	(5,14)	7.5×10^5	0
199	5640_0734_2	(6,14)	7.5×10^5	0
220	5640_0734_3	(5,15)	7.5×10^5	0
221	5640_0734_4	(6,15)	7.5×10^5	0
200	5640_0735_1	(7,14)	7.5×10^5	0
201	5640_0735_2	(8,14)	7.5×10^5	0
222	5640_0735_3	(7,15)	7.5×10^5	0
223	5640_0735_4	(8,15)	7.5×10^5	2
202	5640_0736_1	(9,14)	7.5×10^5	0
203	5640_0736_2	(10,14)	8.9×10^5	5
224	5640_0736_3	(9,15)	9.1×10^5	13
225	5640_0736_4	(10,15)	8.9×10^5	30
204	5640_0737_1	(11,14)	7.9×10^5	1
205	5640_0737_2	(12,14)	7.9×10^5	28
226	5640_0737_3	(11,15)	8.9×10^5	77
227	5640_0737_4	(12,15)	7.9×10^5	66
206	5640_0738_1	(13,14)	7.9×10^5	30
207	5640_0738_2	(14,14)	1.7×10^5	213
228	5640_0738_3	(13,15)	7.9×10^5	56
229	5640_0738_4	(14,15)	7.9×10^5	21
208	5640_0739_1	(15,14)	1.7×10^5	383
209	5640_0739_2	(16,14)	1.7×10^5	720
230	5640_0739_3	(15,15)	1.7×10^5	286
231	5640_0739_4	(16,15)	1.7×10^5	923
239	5640_0742_2	(2,16)	5.6×10^5	0
260	5640_0742_4	(2,17)	5.6×10^5	0
240	5640_0743_1	(3,16)	5.6×10^5	0
241	5640_0743_2	(4,16)	7.5×10^5	0
261	5640_0743_3	(3,17)	5.6×10^5	0
262	5640_0743_4	(4,17)	7.5×10^5	0
242	5640_0744_1	(5,16)	7.5×10^5	0
243	5640_0744_2	(6,16)	7.5×10^5	0
263	5640_0744_3	(5,17)	7.5×10^5	0
264	5640_0744_4	(6,17)	7.5×10^5	0
244	5640_0745_1	(7,16)	7.5×10^5	0
245	5640_0745_2	(8,16)	7.5×10^5	0
265	5640_0745_3	(7,17)	7.5×10^5	0
266	5640_0745_4	(8,17)	7.5×10^5	0

TABLE 31. DEPOSITION AND POPULATION DATA FOR THE TEST SITE (500 m MESH) (cont.)

Data Number of cell	Mesh ID	Coordinates (x,y)	Deposition of ^{137}Cs as of 14 June 2011 (Bq/m^2)[a]	Population
246	5640_0746_1	(9,16)	9.1×10^5	53
247	5640_0746_2	(10,16)	9.1×10^5	80
267	5640_0746_3	(9,17)	9.1×10^5	0
268	5640_0746_4	(10,17)	9.1×10^5	62
248	5640_0747_1	(11,16)	9.1×10^5	122
249	5640_0747_2	(12,16)	9.1×10^5	87
269	5640_0747_3	(11,17)	9.1×10^5	16
270	5640_0747_4	(12,17)	9.1×10^5	1
250	5640_0748_1	(13,16)	7.9×10^5	127
251	5640_0748_2	(14,16)	1.6×10^6	22
271	5640_0748_3	(13,17)	9.1×10^5	9
272	5640_0748_4	(14,17)	1.6×10^6	22
252	5640_0749_1	(15,16)	1.6×10^6	158
253	5640_0749_2	(16,16)	1.6×10^6	494
273	5640_0749_3	(15,17)	1.6×10^6	78
274	5640_0749_4	(16,17)	1.6×10^6	20
281	5640_0753_2	(4,18)	7.5×10^5	0
282	5640_0754_1	(5,18)	7.5×10^5	0
283	5640_0754_2	(6,18)	7.5×10^5	0
297	5640_0754_4	(6,19)	3.4×10^5	0
284	5640_0755_1	(7,18)	3.4×10^5	0
285	5640_0755_2	(8,18)	3.4×10^5	0
298	5640_0755_3	(7,19)	3.4×10^5	0
299	5640_0755_4	(8,19)	3.4×10^5	0
286	5640_0756_1	(9,18)	3.4×10^5	0
287	5640_0756_2	(10,18)	9.1×10^5	36
300	5640_0756_3	(9,19)	3.4×10^5	0
301	5640_0756_4	(10,19)	3.4×10^5	28
288	5640_0757_1	(11,18)	9.1×10^5	12
289	5640_0757_2	(12,18)	9.1×10^5	0
302	5640_0757_3	(11,19)	3.4×10^5	0
303	5640_0757_4	(12,19)	9.1×10^5	15
290	5640_0758_1	(13,18)	9.1×10^5	19
291	5640_0758_2	(14,18)	1.6×10^6	144
304	5640_0758_3	(13,19)	9.1×10^5	69
292	5640_0759_1	(15,18)	1.6×10^6	0
293	5640_0759_2	(16,18)	1.6×10^6	0
84	5641_0000_1	(17,8)	5.9×10^5	110
85	5641_0000_2	(18,8)	5.9×10^5	378
103	5641_0000_3	(17,9)	5.9×10^5	306
104	5641_0000_4	(18,9)	5.9×10^5	734
86	5641_0001_1	(19,8)	9.8×10^5	526
87	5641_0001_2	(20,8)	9.8×10^5	249
105	5641_0001_3	(19,9)	9.8×10^5	209
106	5641_0001_4	(20,9)	9.8×10^5	93
88	5641_0002_1	(21,8)	9.8×10^5	23
107	5641_0002_3	(21,9)	9.8×10^5	21
123	5641_0010_1	(17,10)	5.9×10^5	172
124	5641_0010_2	(18,10)	9.8×10^5	156
144	5641_0010_3	(17,11)	1.1×10^6	194
145	5641_0010_4	(18,11)	1.1×10^6	6
125	5641_0011_1	(19,10)	9.8×10^5	160
126	5641_0011_2	(20,10)	9.8×10^5	16
146	5641_0011_3	(19,11)	9.8×10^5	290
147	5641_0011_4	(20,11)	9.8×10^5	11

TABLE 31. DEPOSITION AND POPULATION DATA FOR THE TEST SITE (500 m MESH) (cont.)

Data Number of cell	Mesh ID	Coordinates (x,y)	Deposition of ^{137}Cs as of 14 June 2011 (Bq/m^2)[a]	Population
127	5641_0012_1	(21,10)	9.8×10^5	1
128	5641_0012_2	(22,10)	9.8×10^5	0
148	5641_0012_3	(21,11)	9.8×10^5	43
149	5641_0012_4	(22,11)	9.8×10^5	0
166	5641_0020_1	(17,12)	1.1×10^6	38
167	5641_0020_2	(18,12)	1.1×10^6	78
188	5641_0020_3	(17,13)	1.1×10^6	114
189	5641_0020_4	(18,13)	1.1×10^6	135
168	5641_0021_1	(19,12)	1.1×10^6	169
169	5641_0021_2	(20,12)	1.1×10^6	76
190	5641_0021_3	(19,13)	1.1×10^6	101
191	5641_0021_4	(20,13)	1.1×10^6	50
170	5641_0022_1	(21,12)	1.1×10^6	46
171	5641_0022_2	(22,12)	1.1×10^6	0
192	5641_0022_3	(21,13)	1.1×10^6	36
193	5641_0022_4	(22,13)	1.1×10^6	0
210	5641_0030_1	(17,14)	1.1×10^6	335
211	5641_0030_2	(18,14)	1.1×10^6	52
232	5641_0030_3	(17,15)	1.1×10^6	555
233	5641_0030_4	(18,15)	1.1×10^6	67
212	5641_0031_1	(19,14)	1.1×10^6	45
213	5641_0031_2	(20,14)	1.1×10^6	79
234	5641_0031_3	(19,15)	1.1×10^6	28
235	5641_0031_4	(20,15)	1.1×10^6	71
214	5641_0032_1	(21,14)	1.1×10^6	14
215	5641_0032_2	(22,14)	1.1×10^6	0
236	5641_0032_3	(21,15)	1.1×10^6	99
237	5641_0032_4	(22,15)	1.1×10^6	28
238	5641_0033_3	(23,15)	5.1×10^6	0
254	5641_0040_1	(17,16)	5.0×10^6	362
255	5641_0040_2	(18,16)	5.0×10^6	137
275	5641_0040_3	(17,17)	5.0×10^6	4
276	5641_0040_4	(18,17)	5.0×10^6	8
256	5641_0041_1	(19,16)	5.0×10^6	3
257	5641_0041_2	(20,16)	5.0×10^6	21
277	5641_0041_3	(19,17)	5.0×10^6	0
278	5641_0041_4	(20,17)	5.0×10^6	2
258	5641_0042_1	(21,16)	5.1×10^6	53
259	5641_0042_2	(22,16)	5.1×10^6	22
279	5641_0042_3	(21,17)	5.1×10^6	1
280	5641_0042_4	(22,17)	5.1×10^6	41
294	5641_0050_2	(18,18)	5.0×10^6	1
295	5641_0051_1	(19,18)	5.0×10^6	0
296	5641_0051_2	(20,18)	5.1×10^6	8

[a] ^{137}Cs deposition was not measured within each 500 m mesh; the closest measurement point to the center of each 500 m mesh was identified, and that measurement was assigned for that mesh.

TABLE 32. MEASUREMENTS OF SURFACE CONTAMINATION DENSITY (kcpm) AND DOSE RATES (mSv/h) IN THE EXERCISE LOCATION, BEFORE AND AFTER DECONTAMINATION EFFORTS [a]

Data no.	Mesh ID	x coordinate	y coordinate	Land use	Remarks	Before decontamination					After decontamination				
						Measurement date	Contamination density (kcpm)	Dose rate (mSv/h)			Measurement date	Contamination density (kcpm)	Dose rate (mSv/h)		
							Surface	Surface (1 cm)	Ambient (50 cm)	Ambient (1 m)		Surface	Surface (1 cm)	Ambient (50 cm)	Ambient (1 m)
1	53@40	44	37	forest	asphalt	11/28/11	10.05	11.50	7.65	8.70	2/20/12	3.01	2.98	3.22	3.26
2	54@40	45	37	forest	forest (soil)	11/28/11	10.82	9.54	10.10	10.40	2/18/12	2.03	5.65	–	4.34
3	55@40	46	37	forest	forest (soil)	11/28/11	8.74	13.50	11.30	10.90	2/18/12	2.26	4.38	–	3.43
4	56@40	47	37	forest	forest (soil)	11/28/11	5.53	10.30	9.39	11.00	2/18/12	3.81	9.58	–	6.56
5	57@40	48	37	forest	forest (soil)	11/28/11	10.12	17.00	9.98	11.10	2/18/12	2.67	4.58	–	4.56
6	58@40	49	37	forest	forest (soil)	11/28/11	8.74	14.50	11.50	11.00	2/18/12	1.53	3.27	–	4.36
7	59@40	50	37	forest	forest (soil)	11/28/11	14.51	20.90	10.60	12.30	2/18/12	0.89	2.02	–	3.12
8	60@40	51	37	forest	forest (soil)	11/28/11	10.17	17.80	11.20	11.50	2/18/12	1.89	4.56	–	3.89
9	61@40	52	37	forest	forest (soil)	11/28/11	7.77	16.90	10.80	10.70	2/18/12	2.82	5.52	–	4.76
10	53@39	44	36	forest	asphalt	11/28/11	24.10	12.60	9.52	8.18	2/20/12	4.02	3.26	–	3.25
11	54@39	45	36	forest	forest (soil)	11/28/11	6.95	12.30	9.43	9.33	2/18/12	3.86	7.98	–	4.72
12	55@39	46	36	forest	forest (soil)	11/28/11	6.71	13.30	10.50	10.30	2/18/12	1.81	2.95	–	3.92
13	56@39	47	36	forest	forest (soil)	11/28/11	7.23	12.70	9.99	10.00	2/18/12	2.08	4.15	–	4.79
14	57@39	48	36	forest	forest (soil)	11/28/11	8.95	16.30	12.30	11.30	2/18/12	2.61	5.68	–	4.84
15	58@39	49	36	forest	forest (soil)	11/28/11	8.13	16.20	11.20	11.50	2/18/12	1.43	2.98	–	3.83
16	59@39	50	36	forest	forest (soil)	11/28/11	7.19	11.70	9.81	10.50	2/18/12	1.02	2.15	–	2.96
17	60@39	51	36	forest	forest (soil)	11/28/11	7.95	14.40	11.10	11.70	2/18/12	3.08	5.96	–	4.18
18	61@39	52	36	forest	forest (soil)	11/28/11	13.33	20.40	10.80	12.10	2/18/12	3.62	5.19	–	5.42
19	53@38	44	35	forest	asphalt	11/28/11	13.70	10.10	10.51	8.19	2/20/12	2.98	2.46	–	3.06
20	54@38	45	35	forest	forest (soil)	11/28/11	9.92	16.00	8.94	10.20	2/18/12	4.01	7.58	–	5.43
21	55@38	46	35	forest	forest (soil)	11/28/11	8.25	16.80	9.97	11.60	2/18/12	5.37	6.56	–	5.50
22	56@38	47	35	forest	forest (soil)	11/28/11	6.55	14.30	9.58	12.40	2/18/12	5.07	10.80	–	7.48
23	57@38	48	35	forest	forest (soil)	11/28/11	9.58	17.30	10.20	12.40	2/18/12	1.61	3.32	–	4.87
24	58@38	49	35	forest	forest (soil)	11/28/11	8.83	16.50	9.62	11.70	2/18/12	3.43	7.29	–	4.48
25	59@38	50	35	forest	forest (soil)	11/28/11	10.38	20.30	6.59	12.00	2/18/12	3.61	6.79	–	4.75
26	60@38	51	35	forest	forest (soil)	11/28/11	6.80	14.60	10.60	11.70	2/18/12	1.27	2.89	–	4.31
27	61@38	52	35	forest	forest (soil)	11/28/11	10.01	17.70	10.80	11.90	2/18/12	4.42	6.01	–	5.20
28	53@37	44	34	forest	asphalt	11/28/11	19.60	11.60	11.81	9.32	2/20/12	1.64	2.28	–	2.96
29	54@37	45	34	forest	forest (soil)	11/28/11	5.73	13.60	11.60	9.41	2/18/12	2.21	3.95	–	4.80
30	55@37	46	34	forest	forest (soil)	11/28/11	8.10	13.00	11.53	10.80	2/18/12	3.28	5.76	–	5.28
31	56@37	47	34	forest	forest (soil)	11/28/11	11.42	16.10	10.07	10.80	2/18/12	1.78	3.36	–	4.42
32	57@37	48	34	forest	forest (soil)	11/28/11	8.63	15.50	8.94	10.80	2/18/12	3.75	8.79	–	4.17
33	58@37	49	34	forest	forest (soil)	11/28/11	11.38	17.80	9.12	11.40	2/18/12	3.14	7.56	–	4.86
34	59@37	50	34	forest	forest (soil)	11/28/11	7.92	13.00	10.80	10.50	2/18/12	4.32	6.95	–	4.75
35	60@37	51	34	forest	forest (soil)	11/28/11	9.55	13.60	8.61	12.00	2/18/12	1.56	3.57	–	5.08
36	61@37	52	34	forest	forest (soil)	11/28/11	11.00	18.70	10.70	12.90	2/18/12	4.72	8.01	–	4.68
37	53@36	44	33	forest	asphalt	11/28/11	11.20	7.11	11.38	7.09	2/20/12	2.64	2.23	–	2.93
38	54@36	45	33	forest	forest (soil)	11/28/11	9.01	15.40	11.55	9.22	2/18/12	1.53	3.03	–	3.98
39	55@36	46	33	forest	forest (soil)	11/28/11	8.34	13.60	11.15	10.60	2/18/12	2.95	5.45	–	4.01
40	56@36	47	33	forest	forest (soil)	11/28/11	6.19	11.80	11.19	9.72	2/18/12	1.07	2.36	–	3.58
41	57@36	48	33	forest	forest (soil)	11/28/11	8.33	13.50	11.24	10.20	2/18/12	1.51	2.98	–	3.89
42	58@36	49	33	forest	forest (soil)	11/28/11	9.81	15.30	10.29	11.40	2/18/12	0.95	2.01	–	3.42

TABLE 32. MEASUREMENTS OF SURFACE CONTAMINATION DENSITY (kcpm) AND DOSE RATES (mSv/h) IN THE EXERCISE LOCATION, BEFORE AND AFTER DECONTAMINATION EFFORTS [a] (cont.)

Data no.	Mesh ID	x coordinate	y coordinate	Land use	Remarks	Before decontamination					After decontamination				
						Measurement date	Contamination density (kcpm)	Dose rate (mSv/h)			Measurement date	Contamination density (kcpm)	Dose rate (mSv/h)		
							Surface	Surface (1 cm)	Ambient (50 cm)	Ambient (1 m)		Surface	Surface (1 cm)	Ambient (50 cm)	Ambient (1 m)
43	59@36	50	33	forest	forest (soil)	11/28/11	9.62	14.40	11.37	10.70	2/18/12	1.45	2.67	–	3.95
44	60@36	51	33	forest	forest (soil)	11/28/11	8.33	14.90	9.25	10.60	2/18/12	4.40	8.45	–	5.32
45	61@36	52	33	forest	forest (soil)	11/28/11	8.95	14.80	9.40	10.60	2/18/12	2.25	4.95	–	4.52
46	53@35	44	32	forest	soil	11/28/11	10.50	12.20	11.01	8.25	2/20/12	2.95	2.67	–	3.01
47	54@35	45	32	forest	forest (soil)	11/28/11	7.13	12.40	11.51	9.21	2/18/12	2.01	4.45	–	4.17
48	55@35	46	32	forest	forest (soil)	11/28/11	8.72	15.50	10.52	10.00	2/18/12	3.07	5.03	–	4.25
49	56@35	47	32	forest	forest (soil)	11/28/11	6.35	11.80	10.64	9.73	2/18/12	1.75	3.58	–	3.47
50	57@35	48	32	forest	forest (soil)	11/28/11	10.00	16.60	10.84	11.20	2/18/12	1.11	2.57	–	3.17
51	58@35	49	32	forest	forest (soil)	11/28/11	8.19	15.90	10.89	10.90	2/18/12	4.83	8.76	–	5.56
52	59@35	50	32	forest	forest (soil)	11/28/11	7.66	11.00	10.60	10.60	2/18/12	1.01	2.40	–	4.69
53	60@35	51	32	forest	forest (soil)	11/28/11	8.18	12.50	8.73	11.00	2/18/12	2.53	5.46	–	4.62
54	61@35	52	32	forest	forest (soil)	11/28/11	7.34	13.20	8.92	10.50	2/18/12	2.12	4.48	–	4.57
55	62@35	53	32	forest	forest (soil)	12/1/11	8.79	14.50	10.30	10.58	2/18/12	2.08	4.53	–	3.86
56	54@34	45	31	forest	forest (soil)	11/28/11	8.73	14.20	11.20	10.30	2/18/12	3.51	5.48	–	3.78
57	55@34	46	31	forest	forest (soil)	11/28/11	5.41	9.73	11.90	9.96	2/18/12	1.80	3.36	–	3.71
58	56@34	47	31	forest	forest (soil)	11/28/11	6.39	12.70	9.58	10.00	2/18/12	1.75	3.49	–	3.20
59	57@34	48	31	forest	forest (soil)	11/28/11	8.54	12.10	10.30	9.99	2/18/12	1.43	3.15	–	3.05
60	58@34	49	31	forest	rest station	11/28/11	3.82	5.05	8.80	7.45	2/18/12	1.48	2.28	–	3.21
61	59@34	50	31	forest	forest (soil)	11/28/11	8.75	16.10	5.35	10.00	2/18/12	1.44	3.12	–	3.90
62	60@34	51	31	forest	forest (soil)	11/28/11	8.13	12.70	5.02	10.50	2/18/12	3.08	6.48	–	4.01
63	61@34	52	31	forest	forest (soil)	11/28/11	7.37	14.10	10.10	10.80	2/18/12	2.76	5.05	–	4.70
64	62@34	53	31	forest	forest (soil)	11/28/11	10.52	17.20	9.71	11.10	2/18/12	1.29	2.75	–	4.02
65	54@33	45	30	forest	ground (soil)	11/28/11	4.67	9.04	8.17	8.72	2/21/12	2.56	4.25	3.27	3.00
66	55@33	46	30	forest	forest (soil)	11/28/11	7.33	10.80	7.88	9.50	2/18/12	1.75	3.38	–	3.77
67	56@33	47	30	forest	forest (soil)	11/28/11	7.76	14.20	7.80	10.80	2/18/12	1.00	2.12	–	2.89
68	57@33	48	30	forest	forest (soil)	11/28/11	6.67	10.00	10.90	9.61	2/18/12	2.62	2.97	–	1.15
69	58@33	49	30	forest	forest (soil)	11/28/11	10.26	14.40	10.70	11.90	2/18/12	2.10	4.25	–	3.35
70	59@33	50	30	forest	forest (soil)	11/28/11	7.65	12.60	8.45	10.30	2/18/12	1.86	3.01	–	2.89
71	60@33	51	30	forest	forest (soil)	11/28/11	6.52	12.30	11.00	9.45	2/18/12	2.89	5.27	–	3.25
72	61@33	52	30	forest	forest (soil)	11/28/11	11.05	17.20	10.70	11.60	2/18/12	1.57	3.27	–	4.42
73	62@33	53	30	forest	forest (soil)	11/28/11	7.72	11.40	10.97	9.55	2/18/12	3.01	5.57	–	4.25
74	55@32	46	29	forest	forest (soil)	11/28/11	7.83	12.00	9.76	8.81	2/21/12	3.20	3.41	–	3.60
75	56@32	47	29	forest	forest (soil)	11/28/11	6.44	11.70	10.23	9.63	2/18/12	2.20	3.67	–	3.37
76	57@32	48	29	forest	forest (soil)	11/28/11	7.59	13.10	9.95	10.30	2/18/12	1.33	2.87	–	2.83
77	58@32	49	29	forest	forest (soil)	11/28/11	9.73	16.60	9.96	11.60	2/18/12	0.97	2.23	–	2.47
78	59@32	50	29	forest	forest (soil)	11/28/11	7.51	12.60	10.01	9.50	2/18/12	1.27	2.78	–	2.94
79	60@32	51	29	forest	forest (soil)	11/28/11	8.39	14.70	10.52	10.10	2/18/12	4.85	4.79	–	4.25
80	61@32	52	29	forest	forest (soil)	11/28/11	5.28	10.80	8.34	8.47	2/18/12	3.70	6.97	–	4.54
81	62@32	53	29	forest	forest (soil)	11/28/11	5.78	11.00	10.90	9.89	2/18/12	4.56	7.07	–	5.10
82	55@31	46	28	forest	forest (soil)	11/28/11	6.70	10.90	11.60	9.14	2/22/12	1.03	2.28	–	3.18
83	56@31	47	28	forest	forest (soil)	11/28/11	6.43	11.30	9.49	9.28	2/18/12	1.30	2.48	–	2.84
84	57@31	48	28	forest	forest (soil)	11/28/11	10.06	16.70	9.57	9.54	2/18/12	1.40	2.52	–	3.01

TABLE 32. MEASUREMENTS OF SURFACE CONTAMINATION DENSITY (kcpm) AND DOSE RATES (mSv/h) IN THE EXERCISE LOCATION, BEFORE AND AFTER DECONTAMINATION EFFORTS [a] (cont.)

Data no.	Mesh ID	x coordinate	y coordinate	Land use	Remarks	Before decontamination					After decontamination				
						Measurement date	Contamination density (kcpm)	Dose rate (mSv/h)			Measurement date	Contamination density (kcpm)	Dose rate (mSv/h)		
							Surface	Surface (1 cm)	Ambient (50 cm)	Ambient (1 m)		Surface	Surface (1 cm)	Ambient (50 cm)	Ambient (1 m)
85	58@31	49	28	forest	forest (soil)	11/28/11	7.70	11.80	7.06	9.41	2/18/12	1.61	3.02	–	3.03
86	59@31	50	28	forest	forest (soil)	11/28/11	10.93	15.30	10.10	9.57	2/18/12	1.39	2.98	–	2.84
87	60@31	51	28	forest	forest (soil)	12/1/11	10.90	15.25	9.77	9.52	2/18/12	2.16	3.40	–	3.54
88	56@30	47	27	forest	concrete	11/28/11	7.82	6.19	9.68	6.30	2/18/12	1.40	3.38	–	3.18
89	57@30	48	27	forest	soil	11/28/11	2.83	3.95	10.20	6.69	2/18/12	2.20	3.39	–	3.43
90	58@30	49	27	forest	soil	11/28/11	10.70	13.50	9.81	9.73	2/18/12	1.91	3.03	–	3.05
91	56@29	47	26	forest	forest (soil)	11/28/11	6.70	11.30	7.88	7.46	2/20/12	3.18	6.48	–	3.62
92	57@29	48	26	forest	forest (soil)	12/1/11	7.21	11.21	7.80	7.40	2/20/12	2.56	4.67	–	4.43
93	25@40	16	37	residential zone	soil	12/26/11	8.99	16.33	10.67	8.56	–	–	–	–	–
94	26@40	17	37	residential zone	soil	12/26/11	7.48	10.86	12.89	9.17	–	–	–	–	–
95	39@40	30	37	residential zone	soil	12/26/11	7.00	15.30	13.10	9.38	2/18/12	1.56	3.05	–	4.40
96	25@39	16	36	residential zone	soil	12/26/11	8.80	15.20	10.09	8.43	–	–	–	–	–
97	26@39	17	36	residential zone	soil	12/26/11	16.70	11.90	10.48	6.13	–	–	–	–	–
98	39@39	30	36	residential zone	soil	12/26/11	2.50	6.11	9.14	5.59	2/18/12	1.78	3.72	–	5.55
99	26@38	17	35	residential zone	concrete	12/26/11	18.90	9.49	8.80	4.18	–	–	–	–	–
100	39@38	30	35	residential zone	soil	12/26/11	9.00	11.90	11.26	8.55	2/18/12	1.27	2.18	–	3.36
101	23@37	14	34	residential zone	asphalt	12/26/11	29.20	15.70	10.80	8.88	–	–	–	–	–
102	24@37	15	34	residential zone	asphalt	12/26/11	12.70	7.66	11.20	5.67	–	–	–	–	–
103	25@37	16	34	residential zone	asphalt	12/26/11	9.13	5.91	11.40	4.81	–	–	–	–	–
104	26@37	17	34	residential zone	asphalt	12/26/11	14.40	10.60	11.20	5.14	–	–	–	–	–
105	26@36	17	33	residential zone	asphalt	12/26/11	30.20	14.80	11.70	7.67	–	–	–	–	–
106	26@35	17	32	residential zone	flowerbed (soil)	12/1/11	15.20	18.25	–	15.21	2/24/12	3.23	5.47	–	4.23
107	26@34	17	31	residential zone	flowerbed (soil)	12/1/11	12.30	10.25	–	12.30	2/24/12	5.34	9.21	–	4.43
108	22@32	13	29	residential zone	concrete	12/26/11	23.80	14.20	10.28	12.90	2/18/12	1.14	1.41	–	1.32
109	23@32	14	29	residential zone	concrete	12/26/11	20.20	13.20	10.95	11.60	2/18/12	0.92	1.22	–	0.92

TABLE 32. MEASUREMENTS OF SURFACE CONTAMINATION DENSITY (kcpm) AND DOSE RATES (mSv/h) IN THE EXERCISE LOCATION, BEFORE AND AFTER DECONTAMINATION EFFORTS [a] (cont.)

Data no.	Mesh ID	x coordinate	y coordinate	Land use	Remarks	Before decontamination					After decontamination				
						Measurement date	Contamination density (kcpm)	Dose rate (mSv/h)			Measurement date	Contamination density (kcpm)	Dose rate (mSv/h)		
							Surface	Surface (1 cm)	Ambient (50 cm)	Ambient (1 m)		Surface	Surface (1 cm)	Ambient (50 cm)	Ambient (1 m)
110	25@29	16	26	residential zone	grass	12/1/11	8.50	13.52	–	9.20	2/20/12	1.48	3.05	–	4.10
111	26@29	17	26	residential zone	grass	12/1/11	8.50	15.83	–	9.58	2/20/12	1.55	2.70	–	4.40
112	25@28	16	25	residential zone	grass	12/1/11	5.34	7.75	–	6.99	2/20/12	3.13	5.76	–	5.00
113	26@28	17	25	residential zone	grass	12/1/11	32.20	10.63	–	6.85	2/20/12	6.02	4.00	–	4.00
114	25@27	16	24	residential zone	grass	12/1/11	7.10	11.52	–	9.73	2/20/12	2.39	4.20	–	4.00
115	26@26	17	23	residential zone	grass	12/1/11	10.20	13.38	–	9.97	2/20/12	0.82	1.90	–	3.55
116	27@25	18	22	residential zone	grass	12/1/11	11.20	12.10	–	9.64	2/20/12	4.98	5.50	–	4.10
117	41@25	32	22	residential zone	soil	12/26/11	7.76	16.30	9.73	10.10	2/18/12	1.50	2.93	–	2.90
118	27@24	18	21	residential zone	gravel	12/26/11	14.80	10.30	10.46	6.72	2/18/12	1.41	1.92	–	1.82
119	28@24	19	21	residential zone	gravel	12/26/11	15.60	10.75	10.34	6.98	2/18/12	1.23	2.24	–	1.92
120	29@24	20	21	residential zone	grass	12/1/11	12.50	13.15	–	9.52	2/20/12	4.32	6.05	–	4.50
121	30@24	21	21	residential zone	grass	12/1/11	13.10	13.65	–	9.89	2/20/12	4.68	5.24	–	6.10
122	41@24	32	21	residential zone	soil	12/26/11	8.21	15.40	10.45	10.50	2/18/12	1.51	2.58	–	3.18
123	27@23	18	20	residential zone	gravel	12/26/11	15.20	10.11	11.90	7.02	2/18/12	1.22	1.89	–	2.11
124	31@23	22	20	residential zone	grass	12/1/11	17.10	12.70	–	9.08	2/20/12	4.68	8.30	–	3.60
125	32@23	23	20	residential zone	grass	12/1/11	8.10	14.10	–	9.66	2/20/12	1.62	3.50	–	4.50
126	36@23	27	20	residential zone	gravel	12/26/11	7.96	11.04	7.72	8.59	–	–	–	–	–
127	37@23	28	20	residential zone	gravel	12/26/11	7.73	11.00	10.60	8.50	–	–	–	–	–
128	43@23	34	20	residential zone	soil	12/26/11	6.37	10.90	11.19	7.64	2/18/12	0.61	1.39	–	2.44
129	44@23	35	20	residential zone	soil	12/26/11	7.96	11.90	11.29	6.52	2/18/12	0.79	1.50	–	2.22
130	32@22	23	19	residential zone	gravel	12/26/11	5.90	11.30	11.14	7.69	2/18/12	1.22	3.82	–	2.39

TABLE 32. MEASUREMENTS OF SURFACE CONTAMINATION DENSITY (kcpm) AND DOSE RATES (mSv/h) IN THE EXERCISE LOCATION, BEFORE AND AFTER DECONTAMINATION EFFORTS [a] (cont.)

Data no.	Mesh ID	x coordinate	y coordinate	Land use	Remarks	Before decontamination					After decontamination				
						Measurement date	Contamination density (kcpm)	Dose rate (mSv/h)			Measurement date	Contamination density (kcpm)	Dose rate (mSv/h)		
							Surface	Surface (1 cm)	Ambient (50 cm)	Ambient (1 m)		Surface	Surface (1 cm)	Ambient (50 cm)	Ambient (1 m)
131	34@22	25	19	residential zone	asphalt	12/26/11	17.20	12.85	13.20	7.98	2/18/12	17.20	12.22	–	7.97
132	36@22	27	19	residential zone	gravel	12/26/11	11.30	12.45	12.00	8.93	–	–	–	–	–
133	37@22	28	19	residential zone	gravel	12/26/11	4.98	13.32	12.80	8.27	–	–	–	–	–
134	39@22	30	19	residential zone	gravel	12/26/11	5.12	13.17	12.00	8.22	–	–	–	–	–
135	43@22	34	19	residential zone	soil	12/26/11	7.98	13.10	12.60	9.27	2/18/12	2.46	4.37	–	3.84
136	44@22	35	19	residential zone	soil	12/26/11	8.17	13.10	11.90	7.78	2/18/12	8.00	6.77	–	5.19
137	34@21	25	18	residential zone	asphalt	12/26/11	20.50	13.90	10.99	9.35	2/18/12	20.50	13.30	–	7.12
138	39@21	30	18	residential zone	soil	12/26/11	6.90	11.73	10.86	9.16	2/18/12	5.52	6.32	–	4.92
139	43@21	34	18	residential zone	soil	12/26/11	5.67	6.75	10.39	10.70	2/18/12	1.15	2.78	–	3.29
140	44@21	35	18	residential zone	soil	12/26/11	9.56	17.70	9.26	8.46	2/18/12	6.35	9.96	–	5.15
141	34@20	25	17	residential zone	asphalt	12/26/11	19.90	14.90	9.12	9.09	2/18/12	19.90	14.30	–	7.02
142	40@20	31	17	residential zone	concrete	12/26/11	21.50	9.20	9.68	6.82	2/18/12	17.70	9.10	–	4.34
143	40@19	31	16	residential zone	concrete	12/26/11	23.50	8.25	10.20	5.85	2/18/12	11.00	5.91	–	4.76
144	39@18	30	15	residential zone	tile	12/26/11	26.00	10.74	11.80	8.28	2/18/12	19.50	6.98	–	4.63
145	37@17	28	14	residential zone	gravel	12/26/11	14.30	16.58	12.50	8.51	–	–	–	–	–
146	27@41	18	38	large building	parking space (gravel)	11/28/11	11.30	14.10	–	10.30	2/18/12	9.24	2.02	–	3.20
147	28@41	19	38	large building	parking space (gravel)	11/28/11	7.95	11.60	–	9.17	2/18/12	0.72	1.64	–	2.50
148	29@41	20	38	large building	parking space (gravel)	11/28/11	7.00	11.30	–	10.00	2/18/12	1.45	2.45	–	2.90
149	30@41	21	38	large building	parking space (gravel)	11/28/11	3.83	9.15	–	6.70	2/18/12	2.32	4.16	–	3.45

TABLE 32. MEASUREMENTS OF SURFACE CONTAMINATION DENSITY (kcpm) AND DOSE RATES (mSv/h) IN THE EXERCISE LOCATION, BEFORE AND AFTER DECONTAMINATION EFFORTS [a] (cont.)

Data no.	Mesh ID	x coordinate	y coordinate	Land use	Remarks	Before decontamination					After decontamination				
						Measurement date	Contamination density (kcpm)	Dose rate (mSv/h)			Measurement date	Contamination density (kcpm)	Dose rate (mSv/h)		
							Surface	Surface (1 cm)	Ambient (50 cm)	Ambient (1 m)		Surface	Surface (1 cm)	Ambient (50 cm)	Ambient (1 m)
150	31@41	22	38	large building	parking space (gravel)	11/28/11	5.30	9.78	–	9.73	2/18/12	0.62	1.42	–	2.50
151	32@41	23	38	large building	bank	12/1/11	5.32	9.25	–	9.64	2/18/12	1.55	3.67	–	4.50
152	33@41	24	38	large building	bank	12/1/11	5.29	9.25	–	9.53	2/18/12	3.25	3.25	–	4.24
153	27@40	18	37	large building	parking space (gravel)	11/28/11	3.68	8.65	–	9.62	2/18/12	1.28	2.67	–	4.25
154	28@40	19	37	large building	parking space (gravel)	11/28/11	11.90	13.90	–	10.00	2/18/12	0.78	1.48	–	2.70
155	29@40	20	37	large building	parking space (gravel)	11/28/11	12.10	14.50	–	10.20	2/18/12	1.20	2.36	–	3.30
156	30@40	21	37	large building	parking space (gravel)	11/28/11	10.10	17.00	–	10.20	2/18/12	1.06	2.30	–	3.75
157	31@40	22	37	large building	parking space (gravel)	11/28/11	9.10	12.30	–	9.90	2/18/12	0.84	1.48	–	2.60
158	32@40	23	37	large building	soil	12/1/11	15.30	10.25	–	8.26	2/18/12	1.24	2.89	–	4.10
159	33@40	24	37	large building	asphalt	12/1/11	15.20	10.21	–	8.24	2/18/12	13.20	8.62	–	5.80
160	27@39	18	36	large building	asphalt	11/28/11	8.78	12.30	–	9.62	2/18/12	4.46	7.00	–	5.00
161	28@39	19	36	large building	asphalt	11/28/11	24.30	13.60	–	8.75	2/18/12	10.60	8.36	–	5.10
162	29@39	20	36	large building	asphalt	11/28/11	25.00	14.10	–	9.47	2/18/12	22.50	9.68	–	4.80
163	30@39	21	36	large building	asphalt	11/28/11	13.10	11.00	–	9.55	2/18/12	13.00	4.95	–	4.00
164	31@39	22	36	large building	asphalt	11/28/11	15.20	16.20	–	9.90	2/18/12	14.20	6.22	–	4.45
165	32@39	23	36	large building	asphalt	11/28/11	12.20	9.94	–	9.41	2/18/12	7.18	5.40	–	5.00
166	33@39	24	36	large building	asphalt	11/28/11	9.21	13.40	–	11.10	2/18/12	3.48	5.80	–	6.10
167	27@38	18	35	large building	asphalt	11/28/11	7.21	14.00	–	9.09	2/18/12	3.76	8.90	–	5.50

TABLE 32. MEASUREMENTS OF SURFACE CONTAMINATION DENSITY (kcpm) AND DOSE RATES (mSv/h) IN THE EXERCISE LOCATION, BEFORE AND AFTER DECONTAMINATION EFFORTS [a] (cont.)

Data no.	Mesh ID	x coordinate	y coordinate	Land use	Remarks	Before decontamination					After decontamination				
						Measurement date	Contamination density (kcpm)	Dose rate (mSv/h)			Measurement date	Contamination density (kcpm)	Dose rate (mSv/h)		
							Surface	Surface (1 cm)	Ambient (50 cm)	Ambient (1 m)		Surface	Surface (1 cm)	Ambient (50 cm)	Ambient (1 m)
168	28@38	19	35	large building	asphalt	11/28/11	18.10	14.50	–	8.20	2/18/12	10.50	8.43	–	4.65
169	29@38	20	35	large building	asphalt	11/28/11	24.10	14.80	–	8.19	2/18/12	7.34	8.48	–	5.10
170	30@38	21	35	large building	asphalt	11/28/11	21.20	13.30	–	6.49	2/18/12	7.00	7.08	–	3.85
171	31@38	22	35	large building	asphalt	11/28/11	21.20	13.30	–	6.49	2/18/12	7.88	3.26	–	4.50
172	32@38	23	35	large building	asphalt	11/28/11	6.69	6.01	–	7.77	2/18/12	5.54	5.55	–	6.90
173	33@38	24	35	large building	asphalt	11/28/11	23.60	13.00	–	10.00	2/18/12	22.50	10.10	–	5.15
174	27@37	18	34	large building	concrete	11/28/11	16.10	13.50	–	7.97	2/20/12	10.10	10.90	–	6.46
175	28@37	19	34	large building	staircase	11/28/11	13.60	12.30	–	8.01	2/20/12	1.55	1.48	–	1.08
176	29@37	20	34	large building	staircase	11/28/11	4.96	5.93	–	7.27	2/20/12	1.46	1.40	–	1.00
177	30@37	21	34	large building	staircase	11/28/11	15.20	4.88	–	2.77	2/20/12	2.29	1.27	–	1.04
178	31@37	22	34	large building	concrete	11/28/11	18.70	12.70	–	6.50	2/20/12	18.20	6.38	–	1.33
179	32@37	23	34	large building	flowerbed (soil)	12/1/11	14.20	11.25	–	9.65	2/18/12	5.16	8.23	–	5.80
180	33@37	24	34	large building	asphalt	11/28/11	14.50	11.00	–	9.99	2/18/12	13.80	8.10	–	6.50
181	27@36	18	33	large building	roof (gravel)	11/28/11	13.50	12.30	–	8.70	2/20/12	9.34	9.53	–	8.11
182	28@36	19	33	large building	roof (gravel)	11/28/11	12.50	10.80	–	9.00	2/20/12	10.40	8.25	–	7.81
183	29@36	20	33	large building	roof (gravel)	11/28/11	14.50	12.80	–	9.46	2/20/12	7.56	7.48	–	7.87
184	30@36	21	33	large building	roof (gravel)	11/28/11	16.50	12.80	–	9.30	2/20/12	9.56	7.56	–	8.88
185	31@36	22	33	large building	roof (gravel)	11/28/11	8.73	11.10	–	8.29	2/20/12	8.59	8.65	–	7.98
186	32@36	23	33	large building	flowerbed (soil)	12/1/11	14.32	14.52	–	9.11	2/18/12	5.10	6.87	–	4.75
187	33@36	24	33	large building	flowerbed (soil)	11/28/11	30.70	15.40	–	9.09	2/18/12	6.20	7.80	–	5.00
188	27@35	18	32	large building	roof (gravel)	11/28/11	16.70	19.30	–	15.40	2/20/12	11.80	6.72	–	6.25

TABLE 32. MEASUREMENTS OF SURFACE CONTAMINATION DENSITY (kcpm) AND DOSE RATES (mSv/h) IN THE EXERCISE LOCATION, BEFORE AND AFTER DECONTAMINATION EFFORTS [a] (cont.)

Data no.	Mesh ID	x coordinate	y coordinate	Land use	Remarks	Before decontamination					After decontamination				
						Measurement date	Contamination density (kcpm)	Dose rate (mSv/h)			Measurement date	Contamination density (kcpm)	Dose rate (mSv/h)		
							Surface	Surface (1 cm)	Ambient (50 cm)	Ambient (1 m)		Surface	Surface (1 cm)	Ambient (50 cm)	Ambient (1 m)
189	28@35	19	32	large building	roof (gravel)	11/28/11	14.40	12.40	–	11.00	2/20/12	7.36	6.18	–	5.09
190	29@35	20	32	large building	roof (gravel)	11/28/11	24.60	17.60	–	6.54	2/20/12	14.50	10.10	–	6.69
191	30@35	21	32	large building	roof (gravel)	11/28/11	7.67	8.02	–	6.43	2/20/12	8.00	7.77	–	6.50
192	31@35	22	32	large building	roof (gravel)	11/28/11	8.52	7.77	–	4.14	2/20/12	7.32	6.59	–	4.00
193	32@35	23	32	large building	flowerbed (soil)	11/28/11	5.82	10.40	–	7.69	2/20/12	3.28	8.27	–	5.66
194	33@35	24	32	large building	flowerbed (soil)	11/28/11	7.87	15.40	–	9.22	2/18/12	4.95	9.60	–	5.50
195	29@34	20	31	large building	roof (gravel)	11/28/11	7.98	10.00	–	7.39	2/20/12	8.26	10.00	–	6.37
196	30@34	21	31	large building	roof (gravel)	11/28/11	16.70	10.70	–	6.41	2/20/12	9.65	9.05	–	4.67
197	31@34	22	31	large building	roof (gravel)	11/28/11	16.50	13.10	–	7.97	2/20/12	11.10	10.90	–	6.52
198	32@34	23	31	large building	roof (gravel)	11/28/11	8.06	4.90	–	5.06	2/20/12	9.16	5.35	–	5.11
199	33@34	24	31	large building	flowerbed (soil)	11/28/11	4.92	10.20	–	8.83	2/18/12	3.37	7.17	–	6.00
200	28@33	19	30	large building	roof (gravel)	12/1/11	18.00	9.67	–	3.38	2/24/12	10.00	10.30	–	4.88
201	29@33	20	30	large building	roof (gravel)	11/28/11	18.00	12.60	–	7.59	2/20/12	16.20	8.70	–	7.22
202	30@33	21	30	large building	roof (gravel)	11/28/11	15.30	13.20	–	7.91	2/20/12	14.40	8.28	–	6.04
203	31@33	22	30	large building	roof (gravel)	11/28/11	8.95	10.80	–	7.18	2/20/12	11.30	7.34	–	7.11
204	32@33	23	30	large building	roof (gravel)	11/28/11	13.40	12.00	–	8.27	2/20/12	11.40	9.77	–	7.55
205	33@33	24	30	large building	flowerbed (soil)	11/28/11	10.46	10.80	–	8.47	2/18/12	5.36	9.27	–	6.10
206	31@32	22	29	large building	roof (gravel)	11/28/11	12.50	10.60	–	5.97	2/20/12	9.01	6.54	–	5.22
207	32@32	23	29	large building	roof (gravel)	11/28/11	6.91	13.40	–	8.37	2/20/12	7.20	8.72	–	8.11
208	33@32	24	29	large building	flowerbed (soil)	11/28/11	4.50	9.37	–	8.25	2/18/12	3.72	7.22	–	5.55
209	28@31	19	28	large building	grass	12/1/11	8.00	14.49	–	7.76	2/20/12	1.24	1.97	–	2.00

TABLE 32. MEASUREMENTS OF SURFACE CONTAMINATION DENSITY (kcpm) AND DOSE RATES (mSv/h) IN THE EXERCISE LOCATION, BEFORE AND AFTER DECONTAMINATION EFFORTS[a] (cont.)

Data no.	Mesh ID	x coordinate	y coordinate	Land use	Remarks	Before decontamination					After decontamination				
						Measurement date	Contamination density (kcpm)	Dose rate (mSv/h)			Measurement date	Contamination density (kcpm)	Dose rate (mSv/h)		
							Surface	Surface (1 cm)	Ambient (50 cm)	Ambient (1 m)		Surface	Surface (1 cm)	Ambient (50 cm)	Ambient (1 m)
210	29@31	20	28	large building	grass	12/1/11	10.60	15.93	–	9.79	2/20/12	1.64	2.80	–	2.60
211	31@31	22	28	large building	roof (gravel)	11/28/11	34.50	8.50	–	5.47	2/20/12	24.60	6.51	–	5.21
212	32@31	23	28	large building	roof (gravel)	11/28/11	11.20	17.10	–	9.10	2/20/12	7.21	8.29	–	8.24
213	33@31	24	28	large building	grass	12/1/11	19.10	13.51	–	8.28	2/18/12	4.56	9.48	–	4.70
214	28@30	19	27	large building	grass	12/1/11	8.40	14.83	–	9.10	2/20/12	1.28	2.18	–	2.35
215	29@30	20	27	large building	grass	12/1/11	8.63	15.52	–	10.46	2/20/12	2.60	3.15	–	2.70
216	30@30	21	27	large building	grass	12/1/11	12.60	14.63	–	9.19	2/20/12	1.90	3.12	–	3.50
217	31@30	22	27	large building	grass	12/1/11	7.20	10.57	–	6.32	2/20/12	4.21	5.74	–	3.70
218	32@30	23	27	large building	grass	12/1/11	7.10	10.83	–	6.20	2/20/12	3.24	2.98	–	3.05
219	33@30	24	27	large building	grass	12/1/11	7.60	13.32	–	10.58	2/20/12	2.24	3.78	–	4.55
220	27@29	18	26	large building	grass	12/1/11	10.70	15.01	–	10.32	2/20/12	1.00	2.73	–	3.15
221	28@29	19	26	large building	grass	12/1/11	8.20	14.12	–	10.26	2/20/12	3.14	5.52	–	4.50
222	29@29	20	26	large building	grass	12/1/11	7.36	14.13	–	11.03	2/20/12	1.75	3.83	–	4.30
223	30@29	21	26	large building	grass	12/1/11	8.16	15.72	–	10.53	2/20/12	1.90	3.50	–	2.70
224	31@29	22	26	large building	grass	12/1/11	17.20	9.26	–	6.48	2/20/12	3.14	4.79	–	3.35
225	32@29	23	26	large building	grass	12/1/11	7.10	10.82	–	6.20	2/20/12	1.76	3.36	–	2.60
226	33@29	24	26	large building	grass	12/1/11	7.60	15.96	–	10.20	2/20/12	1.38	2.25	–	2.75
227	29@28	20	25	large building	grass	12/1/11	6.23	14.26	–	9.63	2/20/12	2.87	4.46	–	3.40
228	30@28	21	25	large building	grass	12/1/11	9.36	15.06	–	11.42	2/20/12	1.22	2.20	–	2.15
229	31@28	22	25	large building	grass	12/1/11	19.70	13.94	–	9.18	2/20/12	4.12	4.52	–	3.20
230	32@28	23	25	large building	grass	12/1/11	4.90	7.98	–	6.81	2/20/12	0.82	2.00	–	2.90

TABLE 32. MEASUREMENTS OF SURFACE CONTAMINATION DENSITY (kcpm) AND DOSE RATES (mSv/h) IN THE EXERCISE LOCATION, BEFORE AND AFTER DECONTAMINATION EFFORTS [a] (cont.)

Data no.	Mesh ID	x coordinate	y coordinate	Land use	Remarks	Before decontamination					After decontamination				
						Measurement date	Contamination density (kcpm)	Dose rate (mSv/h)			Measurement date	Contamination density (kcpm)	Dose rate (mSv/h)		
							Surface	Surface (1 cm)	Ambient (50 cm)	Ambient (1 m)		Surface	Surface (1 cm)	Ambient (50 cm)	Ambient (1 m)
231	33@28	24	25	large building	grass	12/1/11	9.10	13.98	–	10.34	2/20/12	1.95	3.42	–	3.30
232	29@27	20	24	large building	grass	12/1/11	7.20	10.25	–	8.21	2/20/12	4.67	11.20	–	8.00
233	30@27	21	24	large building	grass	12/1/11	7.80	12.13	–	10.25	2/20/12	1.33	2.75	–	4.00
234	31@27	22	24	large building	grass	12/1/11	6.80	7.25	–	6.15	2/20/12	0.83	2.20	–	2.75
235	32@27	23	24	large building	grass	12/1/11	5.50	8.12	–	7.12	2/20/12	2.26	3.45	–	4.15
236	33@27	24	24	large building	grass	12/1/11	6.70	13.94	–	9.43	2/20/12	1.86	3.10	–	2.90
237	27@26	18	23	large building	grass	12/1/11	7.10	11.51	–	6.64	2/20/12	3.93	4.23	–	3.40
238	32@26	23	23	large building	grass	12/1/11	10.25	13.36	–	8.14	2/20/12	3.08	4.80	–	3.68
239	33@26	24	23	large building	grass	12/1/11	8.10	15.10	–	9.12	2/20/12	4.43	7.00	–	4.40
240	28@25	19	22	large building	grass	12/1/11	10.80	11.39	–	9.74	2/20/12	4.30	4.21	–	3.70
241	29@25	20	22	large building	grass	12/1/11	10.60	11.25	–	9.86	2/24/12	3.07	5.04	–	4.85
242	30@25	21	22	large building	grass	12/1/11	22.00	8.77	–	5.47	2/24/12	3.43	5.47	–	4.12
243	32@25	23	22	large building	grass	12/1/11	6.50	13.70	–	9.11	2/20/12	2.46	4.00	–	3.90
244	33@25	24	22	large building	grass	12/1/11	6.30	14.27	–	10.11	2/20/12	5.61	3.21	–	5.80
245	31@24	22	21	large building	grass	12/1/11	16.10	13.32	–	8.45	2/20/12	4.98	4.25	–	4.85
246	32@24	23	21	large building	grass	12/1/11	6.80	13.75	–	9.86	2/20/12	2.80	5.75	–	5.50
247	33@24	24	21	large building	grass	12/1/11	6.40	14.52	–	12.21	2/20/12	2.48	3.85	–	4.45
248	33@23	24	20	large building	grass	12/1/11	7.90	14.25	–	10.29	2/20/12	2.07	4.20	–	5.00
249	46@40	37	37	ground and park	playground (soil)	11/28/11	7.25	16.87	14.20	13.27	2/18/12	2.56	4.89	4.32	4.23
250	47@40	38	37	ground and park	playground (soil)	11/28/11	12.30	20.57	10.85	12.92	2/18/12	1.78	3.45	3.72	3.98
251	48@40	39	37	ground and park	playground (soil)	11/28/11	8.76	15.21	11.89	10.75	2/18/12	2.31	3.75	3.44	3.48

TABLE 32. MEASUREMENTS OF SURFACE CONTAMINATION DENSITY (kcpm) AND DOSE RATES (mSv/h) IN THE EXERCISE LOCATION, BEFORE AND AFTER DECONTAMINATION EFFORTS [a] (cont.)

Data no.	Mesh ID	x coordinate	y coordinate	Land use	Remarks	Before decontamination					After decontamination				
						Measurement date	Contamination density (kcpm)	Dose rate (mSv/h)			Measurement date	Contamination density (kcpm)	Dose rate (mSv/h)		
							Surface	Surface (1 cm)	Ambient (50 cm)	Ambient (1 m)		Surface	Surface (1 cm)	Ambient (50 cm)	Ambient (1 m)
252	49@40	40	37	ground and park	playground (soil)	11/28/11	10.40	19.83	10.31	9.44	2/18/12	1.73	2.29	3.95	3.98
253	50@40	41	37	ground and park	playground (soil)	11/28/11	11.41	14.66	10.31	10.98	2/18/12	3.56	6.58	4.12	4.15
254	51@40	42	37	ground and park	playground (soil)	11/28/11	6.52	11.43	10.35	11.70	2/18/12	1.57	2.92	3.63	3.68
255	52@40	43	37	ground and park	playground (soil)	11/28/11	10.20	16.41	9.56	11.82	2/18/12	4.03	7.68	4.92	4.95
256	46@39	37	36	ground and park	playground (soil)	11/28/11	6.97	14.43	11.10	12.54	2/18/12	3.78	5.89	3.88	3.89
257	47@39	38	36	ground and park	playground (soil)	11/28/11	6.61	9.22	8.90	9.74	2/18/12	1.28	2.45	3.18	3.28
258	48@39	39	36	ground and park	playground (soil)	11/28/11	10.08	16.56	11.40	11.25	2/18/12	2.28	3.95	3.78	3.82
259	49@39	40	36	ground and park	playground (soil)	11/28/11	10.10	15.26	10.65	11.24	2/18/12	3.01	5.59	5.82	5.48
260	50@39	41	36	ground and park	playground (soil)	11/28/11	8.43	13.83	10.51	10.52	2/18/12	3.25	7.89	6.15	5.45
261	51@39	42	36	ground and park	playground (soil)	11/28/11	5.23	9.52	8.10	10.34	2/18/12	1.01	2.48	3.64	4.32
262	52@39	43	36	ground and park	playground (soil)	11/28/11	10.60	11.48	9.31	9.32	2/18/12	3.95	9.86	7.67	6.98
263	46@38	37	35	ground and park	playground (soil)	11/28/11	8.63	13.72	11.42	10.69	2/20/12	4.02	6.62	4.44	4.48
264	47@38	38	35	ground and park	playground (soil)	11/28/11	5.75	12.36	11.08	10.72	2/20/12	0.65	1.80	2.68	2.71
265	48@38	39	35	ground and park	playground (soil)	11/28/11	12.70	12.44	11.75	11.70	2/20/12	3.91	5.47	3.00	3.06
266	49@38	40	35	ground and park	playground (soil)	11/28/11	7.31	15.00	11.37	10.97	2/20/12	2.35	6.20	4.75	4.28
267	50@38	41	35	ground and park	playground (soil)	11/28/11	7.46	13.73	11.46	10.87	2/20/12	3.74	7.32	6.75	6.27
268	51@38	42	35	ground and park	playground (soil)	11/28/11	8.31	14.58	11.89	12.11	2/20/12	4.24	8.86	7.08	6.32
269	52@38	43	35	ground and park	playground (soil)	11/28/11	8.51	14.11	11.52	11.86	2/20/12	2.71	5.67	4.82	4.69
270	46@37	37	34	ground and park	playground (soil)	11/28/11	11.50	16.06	11.50	11.36	2/20/12	1.83	2.67	3.44	3.45
271	47@37	38	34	ground and park	playground (soil)	11/28/11	5.86	11.57	11.69	10.14	2/20/12	1.55	2.86	3.35	3.38
272	48@37	39	34	ground and park	playground (soil)	11/28/11	7.15	14.33	11.60	11.03	2/20/12	1.44	2.62	3.00	3.01

TABLE 32. MEASUREMENTS OF SURFACE CONTAMINATION DENSITY (kcpm) AND DOSE RATES (mSv/h) IN THE EXERCISE LOCATION, BEFORE AND AFTER DECONTAMINATION EFFORTS [a] (cont.)

Data no.	Mesh ID	x coordinate	y coordinate	Land use	Remarks	Before decontamination					After decontamination				
						Measurement date	Contamination density (kcpm)	Dose rate (mSv/h)			Measurement date	Contamination density (kcpm)	Dose rate (mSv/h)		
							Surface	Surface (1 cm)	Ambient (50 cm)	Ambient (1 m)		Surface	Surface (1 cm)	Ambient (50 cm)	Ambient (1 m)
273	49@37	40	34	ground and park	playground (soil)	11/28/11	6.62	14.38	9.43	11.05	2/20/12	1.93	3.72	3.17	3.01
274	50@37	41	34	ground and park	playground (soil)	11/28/11	8.12	14.64	11.36	11.30	2/20/12	1.81	4.62	4.06	3.98
275	51@37	42	34	ground and park	playground (soil)	11/28/11	7.10	12.81	11.87	11.54	2/20/12	2.45	5.27	5.67	5.54
276	52@37	43	34	ground and park	playground (soil)	11/28/11	6.97	11.36	12.28	9.99	2/20/12	1.78	3.42	4.36	4.40
277	47@36	38	33	ground and park	playground (soil)	11/28/11	7.65	12.20	10.10	11.20	2/20/12	2.75	6.35	4.88	4.87
278	48@36	39	33	ground and park	playground (soil)	11/28/11	5.90	10.29	9.42	11.15	2/20/12	1.62	3.32	3.22	3.27
279	49@36	40	33	ground and park	playground (soil)	11/28/11	5.14	11.76	12.10	11.00	2/20/12	1.21	3.32	3.85	3.76
280	50@36	41	33	ground and park	playground (soil)	11/28/11	7.03	12.54	10.10	10.84	2/20/12	1.52	2.83	3.21	3.20
281	51@36	42	33	ground and park	playground (soil)	11/28/11	8.12	13.93	9.51	10.64	2/20/12	4.03	6.01	5.05	4.45
282	52@36	43	33	ground and park	playground (soil)	11/28/11	6.79	12.21	11.66	10.15	2/20/12	1.06	2.47	3.62	3.87
283	47@35	38	32	ground and park	asphalt	11/28/11	16.40	10.32	12.20	9.98	2/20/12	1.23	2.08	2.73	2.81
284	48@35	39	32	ground and park	playground (soil)	11/28/11	3.58	14.62	9.96	11.43	2/21/12	3.06	3.21	2.48	2.24
285	49@35	40	32	ground and park	playground (soil)	11/28/11	6.49	13.25	10.60	11.06	2/21/12	1.35	1.98	2.00	1.96
286	50@35	41	32	ground and park	playground (soil)	11/28/11	6.44	13.16	8.24	11.01	2/21/12	0.83	1.64	2.03	2.12
287	51@35	42	32	ground and park	asphalt	11/28/11	11.20	8.87	10.78	9.54	2/20/12	1.42	2.26	3.02	3.12
288	52@35	43	32	ground and park	playground (soil)	11/28/11	6.12	13.87	11.29	9.67	2/20/12	1.53	2.81	3.47	3.38
289	43@34	34	31	ground and park	concrete	12/26/11	28.50	12.10	12.30	7.72	–	–	–	–	–
290	45@34	36	31	ground and park	soil	12/26/11	4.30	5.91	11.50	5.97	–	–	–	–	–
291	46@34	37	31	ground and park	ground (soil)	11/28/11	9.91	14.90	9.84	10.87	2/21/12	1.12	2.36	1.92	1.96
292	47@34	38	31	ground and park	ground (soil)	11/28/11	9.13	15.02	9.74	11.13	2/21/12	1.09	1.84	1.69	1.67
293	48@34	39	31	ground and park	ground (soil)	11/28/11	7.75	15.10	9.70	11.48	2/21/12	1.17	1.65	1.63	1.68

TABLE 32. MEASUREMENTS OF SURFACE CONTAMINATION DENSITY (kcpm) AND DOSE RATES (mSv/h) IN THE EXERCISE LOCATION, BEFORE AND AFTER DECONTAMINATION EFFORTS [a] (cont.)

Data no.	Mesh ID	x coordinate	y coordinate	Land use	Remarks	Before decontamination					After decontamination				
						Measurement date	Contamination density (kcpm)	Dose rate (mSv/h)			Measurement date	Contamination density (kcpm)	Dose rate (mSv/h)		
							Surface	Surface (1 cm)	Ambient (50 cm)	Ambient (1 m)		Surface	Surface (1 cm)	Ambient (50 cm)	Ambient (1 m)
294	49@34	40	31	ground and park	ground (soil)	11/28/11	8.57	14.42	11.20	10.93	2/21/12	0.81	1.53	1.50	1.54
295	50@34	41	31	ground and park	ground (soil)	11/28/11	8.47	14.85	11.80	11.33	2/21/12	0.95	1.76	1.65	1.66
296	51@34	42	31	ground and park	ground (soil)	11/28/11	7.47	14.71	11.40	10.82	2/21/12	0.95	1.71	1.71	1.76
297	52@34	43	31	ground and park	ground (soil)	11/28/11	6.27	12.23	11.30	9.82	2/21/12	0.97	1.83	2.03	2.00
298	53@34	44	31	ground and park	ground (soil)	11/28/11	6.27	9.04	11.10	8.72	2/20/12	1.20	4.35	3.25	2.98
299	45@33	36	30	ground and park	soil	12/26/11	8.10	11.90	11.36	6.55	–	–	–	–	–
300	46@33	37	30	ground and park	ground (soil)	12/1/11	9.24	14.52	10.08	10.79	2/21/12	1.21	1.42	1.77	1.81
301	47@33	38	30	ground and park	ground (soil)	11/28/11	7.64	13.60	10.87	11.01	2/21/12	1.56	2.67	1.84	1.64
302	48@33	39	30	ground and park	ground (soil)	11/28/11	8.93	14.82	10.75	11.13	2/21/12	1.03	2.06	1.96	1.80
303	49@33	40	30	ground and park	ground (soil)	11/28/11	8.03	14.22	10.12	11.15	2/21/12	1.05	1.67	1.65	1.64
304	50@33	41	30	ground and park	ground (soil)	11/28/11	8.04	14.26	10.51	11.00	2/21/12	1.12	2.28	2.07	1.94
305	51@33	42	30	ground and park	ground (soil)	11/28/11	6.53	13.53	10.34	11.28	2/21/12	1.34	2.45	2.37	2.23
306	52@33	43	30	ground and park	ground (soil)	11/28/11	6.45	13.45	10.35	10.82	2/21/12	0.86	1.67	1.67	1.71
307	53@33	44	30	ground and park	ground (soil)	11/28/11	6.76	13.55	10.38	10.51	2/21/12	0.83	1.95	1.90	1.85
308	45@32	36	29	ground and park	soil	12/26/11	5.20	10.80	8.07	6.21	2/18/12	5.11	6.33	–	4.21
309	46@32	37	29	ground and park	ground (soil)	12/1/11	6.98	13.66	10.30	10.49	2/21/12	1.25	2.46	2.25	1.92
310	47@32	38	29	ground and park	ground (soil)	12/1/11	8.41	14.22	11.00	10.78	2/21/12	1.09	1.73	1.67	1.52
311	48@32	39	29	ground and park	ground (soil)	12/1/11	6.29	13.61	11.00	10.93	2/21/12	1.13	1.84	1.61	1.52
312	49@32	40	29	ground and park	ground (soil)	12/1/11	6.80	14.35	11.00	11.08	2/21/12	0.96	1.68	1.63	1.48
313	50@32	41	29	ground and park	ground (soil)	11/28/11	6.71	13.77	9.17	11.25	2/21/12	1.10	1.68	1.50	1.53
314	51@32	42	29	ground and park	ground (soil)	11/28/11	6.29	13.97	10.40	11.25	2/21/12	0.97	1.58	1.68	1.76

TABLE 32. MEASUREMENTS OF SURFACE CONTAMINATION DENSITY (kcpm) AND DOSE RATES (mSv/h) IN THE EXERCISE LOCATION, BEFORE AND AFTER DECONTAMINATION EFFORTS [a] (cont.)

Data no.	Mesh ID	x coordinate	y coordinate	Land use	Remarks	Before decontamination					After decontamination				
						Measurement date	Contamination density (kcpm)	Dose rate (mSv/h)			Measurement date	Contamination density (kcpm)	Dose rate (mSv/h)		
							Surface	Surface (1 cm)	Ambient (50 cm)	Ambient (1 m)		Surface	Surface (1 cm)	Ambient (50 cm)	Ambient (1 m)
315	52@32	43	29	ground and park	ground (soil)	11/28/11	6.48	12.99	10.20	11.03	2/21/12	0.86	1.59	1.60	1.64
316	53@32	44	29	ground and park	ground (soil)	11/28/11	6.98	13.26	10.50	10.49	2/21/12	1.28	2.47	2.10	1.97
317	54@32	45	29	ground and park	ground (soil)	11/28/11	6.85	12.28	10.20	10.01	2/21/12	1.08	2.25	2.39	2.53
318	45@31	36	28	ground and park	soil	12/26/11	17.12	10.30	9.50	6.53	2/18/12	6.30	6.52	–	4.10
319	46@31	37	28	ground and park	ground (soil)	11/28/11	6.41	13.71	7.88	10.76	2/21/12	3.68	6.81	3.32	6.62
320	47@31	38	28	ground and park	ground (soil)	11/28/11	6.97	13.47	9.01	10.81	2/21/12	1.02	2.02	1.68	1.70
321	48@31	39	28	ground and park	ground (soil)	11/28/11	8.90	14.79	10.70	10.81	2/21/12	0.48	1.04	1.28	1.37
322	49@31	40	28	ground and park	ground (soil)	11/28/11	7.61	13.75	10.40	11.04	2/22/12	0.96	1.75	1.42	1.48
323	50@31	41	28	ground and park	ground (soil)	11/28/11	7.92	13.96	10.70	11.13	2/22/12	0.42	0.98	1.03	1.06
324	51@31	42	28	ground and park	grass	11/28/11	7.63	13.58	11.20	10.71	–	–	–	–	–
325	52@31	43	28	ground and park	grass	11/28/11	6.50	13.60	11.19	10.83	–	–	–	–	–
326	53@31	44	28	ground and park	ground (soil)	11/28/11	5.91	12.60	11.15	10.87	2/22/12	0.75	1.28	1.51	1.66
327	54@31	45	28	ground and park	ground (soil)	11/28/11	6.21	12.25	9.08	11.32	2/24/12	1.75	4.34	2.47	2.28
328	45@30	36	27	ground and park	soil	12/26/11	7.23	6.04	8.76	7.42	2/18/12	2.05	4.21	–	3.70
329	46@30	37	27	ground and park	ground (soil)	11/28/11	7.09	14.70	8.16	11.30	2/21/12	0.89	1.45	1.54	1.68
330	47@30	38	27	ground and park	ground (soil)	11/28/11	7.15	15.50	11.30	11.80	2/21/12	1.01	1.62	1.53	1.46
331	48@30	39	27	ground and park	ground (soil)	11/28/11	7.52	15.50	8.53	11.40	2/21/12	0.78	1.19	1.09	1.24
332	49@30	40	27	ground and park	grass	11/28/11	6.87	14.20	5.14	11.30	–	–	–	–	–
333	50@30	41	27	ground and park	grass	11/28/11	6.32	14.50	10.50	11.30	–	–	–	–	–
334	51@30	42	27	ground and park	grass	11/28/11	6.85	14.40	7.15	11.20	–	–	–	–	–
335	52@30	43	27	ground and park	grass	11/28/11	6.51	14.50	7.94	11.00	–	–	–	–	–

TABLE 32. MEASUREMENTS OF SURFACE CONTAMINATION DENSITY (kcpm) AND DOSE RATES (mSv/h) IN THE EXERCISE LOCATION, BEFORE AND AFTER DECONTAMINATION EFFORTS [a] (cont.)

Data no.	Mesh ID	x coordinate	y coordinate	Land use	Remarks	Before decontamination					After decontamination				
						Measurement date	Contamination density (kcpm)	Dose rate (mSv/h)			Measurement date	Contamination density (kcpm)	Dose rate (mSv/h)		
							Surface	Surface (1 cm)	Ambient (50 cm)	Ambient (1 m)		Surface	Surface (1 cm)	Ambient (50 cm)	Ambient (1 m)
336	53@30	44	27	ground and park	ground (soil)	11/28/11	6.92	13.50	7.90	11.00	2/22/12	1.02	2.36	1.63	1.54
337	54@30	45	27	ground and park	ground (soil)	11/28/11	5.88	12.70	11.00	10.40	2/22/12	1.06	1.98	2.17	2.28
338	55@30	46	27	ground and park	asphalt	11/28/11	17.12	10.90	9.15	9.38	2/22/12	12.00	9.12	6.25	4.57
339	46@29	37	26	ground and park	ground (soil)	11/28/11	8.14	13.49	9.10	10.53	2/21/12	0.62	1.25	1.49	1.59
340	47@29	38	26	ground and park	ground (soil)	11/28/11	7.57	13.27	9.21	10.70	2/21/12	0.57	1.05	1.17	1.28
341	48@29	39	26	ground and park	grass	11/28/11	8.42	13.92	8.64	10.90	–	–	–	–	–
342	49@29	40	26	ground and park	grass	11/28/11	6.86	13.66	10.10	10.61	–	–	–	–	–
343	50@29	41	26	ground and park	grass	11/28/11	6.67	13.11	9.72	10.77	–	–	–	–	–
344	51@29	42	26	ground and park	grass	11/28/11	6.25	12.60	9.70	10.16	–	–	–	–	–
345	52@29	43	26	ground and park	grass	11/28/11	6.97	13.34	10.34	10.28	–	–	–	–	–
346	53@29	44	26	ground and park	ground (soil)	11/28/11	6.82	13.51	10.35	9.79	2/22/12	0.48	0.92	1.00	1.01
347	54@29	45	26	ground and park	ground (soil)	11/28/11	6.69	14.18	10.38	9.98	2/22/12	1.01	1.35	0.93	1.15
348	55@29	46	26	ground and park	asphalt	11/28/11	15.73	8.61	8.17	8.79	2/22/12	12.50	8.24	4.25	3.12
349	46@28	37	25	ground and park	ground (soil)	11/28/11	8.59	15.90	10.90	10.70	2/21/12	1.42	2.38	2.03	1.97
350	47@28	38	25	ground and park	ground (soil)	11/28/11	6.35	14.20	10.70	10.80	2/21/12	0.89	1.58	1.35	1.35
351	48@28	39	25	ground and park	grass, soil	11/28/11	2.29	5.25	8.45	10.00	–	–	–	–	–
352	49@28	40	25	ground and park	grass	11/28/11	7.17	14.70	11.00	10.80	–	–	–	–	–
353	50@28	41	25	ground and park	grass	11/28/11	6.35	13.40	10.70	10.80	–	–	–	–	–
354	51@28	42	25	ground and park	ground (soil)	11/28/11	6.31	14.30	10.30	10.80	2/24/12	0.64	1.27	1.40	1.10
355	52@28	43	25	ground and park	ground (soil)	11/28/11	6.76	14.80	10.90	10.80	2/22/12	0.82	1.37	0.98	1.03
356	53@28	44	25	ground and park	ground (soil)	11/28/11	8.46	15.00	11.00	10.80	2/22/12	0.93	1.42	1.32	1.35

TABLE 32. MEASUREMENTS OF SURFACE CONTAMINATION DENSITY (kcpm) AND DOSE RATES (mSv/h) IN THE EXERCISE LOCATION, BEFORE AND AFTER DECONTAMINATION EFFORTS [a] (cont.)

Data no.	Mesh ID	x coordinate	y coordinate	Land use	Remarks	Before decontamination					After decontamination				
						Measurement date	Contamination density (kcpm)	Dose rate (mSv/h)			Measurement date	Contamination density (kcpm)	Dose rate (mSv/h)		
							Surface	Surface (1 cm)	Ambient (50 cm)	Ambient (1 m)		Surface	Surface (1 cm)	Ambient (50 cm)	Ambient (1 m)
357	54@28	45	25	ground and park	ground (soil)	11/28/11	6.43	15.60	11.00	10.70	2/22/12	0.67	1.17	1.38	1.45
358	55@28	46	25	ground and park	ground (soil)	11/28/11	7.19	15.90	11.00	10.20	2/22/12	0.62	1.52	1.97	2.08
359	44@27	35	24	ground and park	parking space (soil)	11/29/11	6.44	13.00	9.17	9.54	2/20/12	0.74	1.68	–	2.56
360	45@27	36	24	ground and park	parking space (soil)	11/29/11	6.16	13.00	10.40	10.50	2/20/12	1.78	3.95	–	3.32
361	46@27	37	24	ground and park	parking space (soil)	11/28/11	8.13	15.20	10.20	10.40	2/20/12	0.95	2.27	–	3.35
362	47@27	38	24	ground and park	ground (soil)	11/28/11	9.46	14.10	10.50	10.40	2/21/12	0.69	1.49	1.37	1.63
363	48@27	39	24	ground and park	ground (soil)	11/28/11	7.31	14.20	10.20	10.70	2/24/12	0.98	1.64	1.55	1.47
364	49@27	40	24	ground and park	ground (soil)	11/28/11	6.27	12.64	9.76	9.64	2/21/12	0.96	1.41	1.28	1.22
365	50@27	41	24	ground and park	ground (soil)	11/28/11	6.04	12.78	10.23	10.00	2/21/12	0.90	1.53	1.39	1.40
366	51@27	42	24	ground and park	ground (soil)	11/28/11	6.23	12.77	9.95	9.96	2/24/12	0.67	1.12	1.07	1.03
367	52@27	43	24	ground and park	ground (soil)	11/28/11	6.70	13.08	9.96	10.26	2/22/12	0.62	1.06	1.21	1.44
368	53@27	44	24	ground and park	ground (soil)	11/28/11	6.02	11.97	10.01	10.00	2/22/12	0.64	1.57	1.60	1.73
369	45@26	36	23	ground and park	parking space (gravel)	11/29/11	12.20	14.30	7.88	8.15	2/20/12	1.89	5.32	–	3.53
370	46@26	37	23	ground and park	parking space (soil)	11/29/11	6.73	12.20	9.01	9.67	2/20/12	1.89	2.84	–	2.91
371	47@26	38	23	ground and park	ground (soil)	11/29/11	6.24	13.40	10.70	10.40	2/21/12	0.89	1.62	1.75	1.86
372	48@26	39	23	ground and park	ground (soil)	11/29/11	5.47	11.20	10.40	10.20	2/21/12	1.14	2.13	1.59	1.66
373	49@26	40	23	ground and park	ground (soil)	11/29/11	5.59	12.90	10.70	10.60	2/21/12	0.89	1.43	1.52	1.62
374	50@26	41	23	ground and park	ground (soil)	11/29/11	6.25	13.40	11.20	11.30	2/21/12	1.21	2.83	2.16	2.14
375	51@26	42	23	ground and park	ground (soil)	12/1/11	7.15	13.25	11.19	11.25	2/21/12	1.79	4.78	3.89	3.50
376	52@26	43	23	ground and park	ground (soil)	12/1/11	7.21	12.89	11.15	11.22	2/21/12	1.77	6.55	4.91	4.86

TABLE 32. MEASUREMENTS OF SURFACE CONTAMINATION DENSITY (kcpm) AND DOSE RATES (mSv/h) IN THE EXERCISE LOCATION, BEFORE AND AFTER DECONTAMINATION EFFORTS [a] (cont.)

Data no.	Mesh ID	x coordinate	y coordinate	Land use	Remarks	Before decontamination					After decontamination				
						Measurement date	Contamination density (kcpm)	Dose rate (mSv/h)			Measurement date	Contamination density (kcpm)	Dose rate (mSv/h)		
							Surface	Surface (1 cm)	Ambient (50 cm)	Ambient (1 m)		Surface	Surface (1 cm)	Ambient (50 cm)	Ambient (1 m)
377	45@25	36	22	ground and park	parking space (gravel)	11/29/11	9.20	11.20	9.08	9.00	2/20/12	0.71	1.67	–	2.10
378	46@25	37	22	ground and park	parking space (soil)	11/29/11	10.30	11.80	11.60	11.70	2/20/12	0.83	1.85	–	2.97
379	47@25	38	22	ground and park	ground (soil)	11/29/11	6.54	12.60	9.49	9.43	2/20/12	1.01	2.67	2.77	2.86
380	48@25	39	22	ground and park	ground (soil)	11/29/11	5.61	12.10	9.57	10.20	2/21/12	1.44	2.56	2.14	2.27
381	49@25	40	22	ground and park	ground (soil)	11/29/11	7.69	11.90	7.06	7.24	2/21/12	0.68	1.60	1.64	1.82
382	50@25	41	22	ground and park	ground (soil)	11/29/11	8.48	16.50	10.10	10.20	2/21/12	2.25	5.18	3.44	2.83
383	51@25	42	22	ground and park	ground (soil)	11/29/11	5.90	12.00	9.77	9.28	2/21/12	0.68	1.32	1.73	2.02
384	46@24	37	21	ground and park	parking space (gravel)	11/29/11	13.60	11.90	11.30	9.66	2/20/12	0.67	1.68	–	2.02
385	47@24	38	21	ground and park	parking space (gravel)	11/29/11	6.52	11.00	8.53	7.36	2/20/12	0.71	1.36	–	2.34
386	48@24	39	21	ground and park	soil	11/29/11	6.31	6.51	5.14	6.30	2/20/12	1.45	2.81	3.50	3.28
387	49@24	40	21	ground and park	ground (soil)	11/29/11	10.20	14.70	10.50	10.10	2/21/12	2.12	3.24	3.75	3.46
388	47@23	38	20	ground and park	parking space (gravel)	11/29/11	7.75	10.60	7.94	8.37	2/20/12	0.68	1.72	–	2.36
389	23@54	14	51	paved surface	asphalt	12/1/11	32.40	13.83	–	8.63	2/16/12	33.30	13.80	–	9.31
390	13@53	4	50	paved surface	asphalt	12/1/11	19.20	7.77	–	5.22	2/16/12	18.50	7.21	–	5.56
391	28@53	19	50	paved surface	asphalt	12/1/11	33.00	12.22	–	7.53	2/16/12	29.60	10.70	–	8.16
392	34@53	25	50	paved surface	asphalt	12/1/11	30.40	13.04	–	8.68	2/16/12	27.60	11.80	–	8.17
393	41@52	32	49	paved surface	asphalt	12/1/11	26.60	10.59	–	7.61	2/16/12	24.70	11.10	–	7.90
394	53@52	44	49	paved surface	asphalt	12/1/11	35.00	12.64	–	8.43	2/16/12	31.80	12.70	–	9.06
395	58@52	49	49	paved surface	asphalt	12/1/11	31.50	12.65	–	8.10	2/16/12	31.70	12.80	–	8.27

TABLE 32. MEASUREMENTS OF SURFACE CONTAMINATION DENSITY (kcpm) AND DOSE RATES (mSv/h) IN THE EXERCISE LOCATION, BEFORE AND AFTER DECONTAMINATION EFFORTS [a] (cont.)

Data no.	Mesh ID	x coordinate	y coordinate	Land use	Remarks	Before decontamination					After decontamination				
						Measurement date	Contamination density (kcpm)	Dose rate (mSv/h)			Measurement date	Contamination density (kcpm)	Dose rate (mSv/h)		
							Surface	Surface (1 cm)	Ambient (50 cm)	Ambient (1 m)		Surface	Surface (1 cm)	Ambient (50 cm)	Ambient (1 m)
396	63@52	54	49	paved surface	asphalt	12/1/11	36.20	12.02	–	7.69	2/16/12	31.10	11.90	–	7.56
397	68@52	59	49	paved surface	asphalt	12/1/11	32.20	11.71	–	7.64	2/16/12	31.90	11.50	–	8.14
398	50@51	41	48	paved surface	asphalt	12/1/11	26.80	12.88	–	8.40	2/16/12	28.80	11.40	–	7.83
399	23@49	14	46	paved surface	asphalt	12/1/11	36.00	13.89	–	8.41	2/16/12	35.70	13.60	–	8.56
400	13@48	4	45	paved surface	asphalt	12/1/11	39.20	15.34	–	9.62	2/16/12	38.30	14.20	–	11.80
401	18@48	9	45	paved surface	asphalt	12/1/11	39.40	15.47	–	8.96	2/16/12	39.10	14.50	–	9.63
402	34@48	25	45	paved surface	asphalt	12/1/11	25.70	15.14	–	8.80	2/16/12	33.10	13.80	–	8.76
403	42@47	33	44	paved surface	asphalt	12/1/11	24.40	9.68	–	7.31	2/16/12	26.30	10.30	–	6.89
404	50@47	41	44	paved surface	asphalt	12/1/11	27.10	11.22	–	7.79	2/16/12	22.90	9.58	–	6.44
405	63@47	54	44	paved surface	asphalt	12/1/11	33.70	12.53	–	7.65	2/16/12	31.70	11.60	–	7.84
406	23@44	14	41	paved surface	asphalt	12/13/11	19.07	10.97	–	7.79	2/19/12	18.67	10.23	–	6.41
407	13@43	4	40	paved surface	asphalt	12/1/11	9.14	7.22	–	6.95	2/16/12	4.32	7.16	–	7.27
408	18@43	9	40	paved surface	asphalt	12/1/11	4.27	6.32	–	6.00	2/16/12	3.35	5.98	–	1.00
409	23@43	14	40	paved surface	asphalt	12/13/11	29.27	22.94	–	8.39	2/20/12	18.97	8.92	–	5.90
410	24@43	15	40	paved surface	asphalt	12/13/11	21.30	12.01	–	8.26	2/19/12	17.36	8.04	–	5.86
411	25@43	16	40	paved surface	asphalt	12/13/11	23.97	12.46	–	8.12	2/19/12	15.80	8.40	–	6.25
412	26@43	17	40	paved surface	asphalt	12/13/11	30.83	17.23	–	8.19	2/19/12	14.78	8.04	–	6.17
413	27@43	18	40	paved surface	asphalt	12/13/11	25.03	13.51	–	8.58	2/19/12	20.10	10.50	–	6.54
414	28@43	19	40	paved surface	asphalt	12/13/11	25.27	12.50	–	7.70	2/19/12	21.87	7.80	–	5.54
415	29@43	20	40	paved surface	asphalt	12/13/11	28.43	11.51	–	7.75	2/19/12	25.80	10.17	–	5.40
416	30@43	21	40	paved surface	asphalt	12/13/11	19.37	10.27	–	7.67	2/19/12	16.37	7.63	–	5.10

TABLE 32. MEASUREMENTS OF SURFACE CONTAMINATION DENSITY (kcpm) AND DOSE RATES (mSv/h) IN THE EXERCISE LOCATION, BEFORE AND AFTER DECONTAMINATION EFFORTS [a] (cont.)

Data no.	Mesh ID	x coordinate	y coordinate	Land use	Remarks	Before decontamination					After decontamination				
						Measurement date	Contamination density (kcpm)	Dose rate (mSv/h)			Measurement date	Contamination density (kcpm)	Dose rate (mSv/h)		
							Surface	Surface (1 cm)	Ambient (50 cm)	Ambient (1 m)		Surface	Surface (1 cm)	Ambient (50 cm)	Ambient (1 m)
417	31@43	22	40	paved surface	asphalt	12/13/11	14.30	18.71	–	9.24	2/19/12	15.77	10.37	–	6.01
418	32@43	23	40	paved surface	asphalt	12/13/11	23.97	13.60	–	9.54	2/19/12	16.27	7.48	–	5.87
419	34@43	25	40	paved surface	asphalt	12/13/11	22.27	18.93	–	10.11	2/19/12	25.30	11.79	–	8.45
420	50@43	41	40	paved surface	asphalt	12/13/11	15.73	14.00	–	10.68	2/19/12	13.12	6.13	–	5.30
421	23@42	14	39	paved surface	asphalt	12/13/11	29.80	17.20	–	9.08	2/20/12	17.60	10.22	–	6.51
422	33@42	24	39	paved surface	asphalt	12/13/11	17.37	16.88	–	9.99	2/19/12	13.20	8.50	–	5.83
423	34@42	25	39	paved surface	asphalt	12/13/11	20.92	14.42	–	9.77	2/20/12	11.70	7.62	–	5.71
424	35@42	26	39	paved surface	asphalt	12/13/11	22.43	17.18	–	10.11	2/19/12	18.04	8.72	–	5.94
425	36@42	27	39	paved surface	asphalt	12/13/11	10.85	13.92	–	10.12	2/19/12	14.03	7.14	–	5.64
426	37@42	28	39	paved surface	asphalt	12/13/11	15.93	14.90	–	9.88	2/19/12	15.93	6.56	–	6.19
427	38@42	29	39	paved surface	asphalt	12/13/11	17.10	10.87	–	9.58	2/19/12	18.03	7.01	–	5.48
428	39@42	30	39	paved surface	asphalt	12/13/11	19.35	9.17	–	8.91	2/19/12	9.00	4.81	–	5.41
429	40@42	31	39	paved surface	asphalt	12/13/11	19.60	11.28	–	9.48	2/19/12	17.43	7.32	–	5.88
430	41@42	32	39	paved surface	asphalt	12/13/11	19.43	11.03	–	9.06	2/19/12	14.05	5.91	–	5.45
431	42@42	33	39	paved surface	asphalt	12/13/11	21.60	12.07	–	9.32	2/19/12	15.40	7.44	–	5.49
432	43@42	34	39	paved surface	asphalt	12/13/11	17.30	11.30	–	9.15	2/19/12	11.20	5.58	–	4.97
433	44@42	35	39	paved surface	asphalt	12/13/11	14.53	11.30	–	9.14	2/19/12	10.08	5.96	–	4.31
434	45@42	36	39	paved surface	asphalt	12/13/11	17.43	10.35	–	8.70	2/19/12	11.77	5.92	–	4.35
435	46@42	37	39	paved surface	asphalt	12/13/11	15.18	12.33	–	10.31	2/19/12	9.71	5.73	–	4.50
436	47@42	38	39	paved surface	asphalt	12/13/11	20.50	13.07	–	10.53	2/19/12	16.67	5.58	–	4.53
437	48@42	39	39	paved surface	asphalt	12/13/11	20.07	13.30	–	11.09	2/19/12	10.72	5.71	–	5.07

TABLE 32. MEASUREMENTS OF SURFACE CONTAMINATION DENSITY (kcpm) AND DOSE RATES (mSv/h) IN THE EXERCISE LOCATION, BEFORE AND AFTER DECONTAMINATION EFFORTS [a] (cont.)

Data no.	Mesh ID	x coordinate	y coordinate	Land use	Remarks	Before decontamination					After decontamination				
						Measurement date	Contamination density (kcpm)	Dose rate (mSv/h)			Measurement date	Contamination density (kcpm)	Dose rate (mSv/h)		
							Surface	Surface (1 cm)	Ambient (50 cm)	Ambient (1 m)		Surface	Surface (1 cm)	Ambient (50 cm)	Ambient (1 m)
438	49@42	40	39	paved surface	asphalt	12/13/11	21.97	13.30	–	10.57	2/19/12	15.13	5.93	–	4.28
439	50@42	41	39	paved surface	asphalt	12/13/11	17.47	12.70	–	10.50	2/19/12	12.17	6.42	–	4.96
440	51@42	42	39	paved surface	asphalt	12/13/11	12.30	14.79	–	10.80	2/19/12	8.42	9.24	–	5.36
441	52@42	43	39	paved surface	asphalt	12/13/11	12.46	11.13	–	8.91	2/19/12	11.01	4.49	–	4.98
442	53@42	44	39	paved surface	asphalt	12/13/11	21.40	12.30	–	8.81	2/19/12	9.04	5.77	–	4.28
443	54@42	45	39	paved surface	asphalt	12/13/11	15.73	13.90	–	10.51	2/19/12	10.54	6.96	–	5.09
444	55@42	46	39	paved surface	asphalt	12/13/11	20.67	12.73	–	9.91	2/19/12	13.07	6.92	–	5.85
445	56@42	47	39	paved surface	asphalt	12/13/11	20.80	12.37	–	9.80	2/19/12	15.57	5.87	–	4.86
446	57@42	48	39	paved surface	asphalt	12/13/11	17.50	13.77	–	9.82	2/19/12	8.42	5.34	–	4.74
447	58@42	49	39	paved surface	asphalt	12/13/11	17.97	11.18	–	9.18	2/19/12	14.70	6.38	–	4.72
448	59@42	50	39	paved surface	asphalt	12/13/11	15.03	11.67	–	9.60	2/19/12	10.03	5.90	–	5.15
449	60@42	51	39	paved surface	asphalt	12/13/11	18.20	12.03	–	10.36	2/19/12	11.57	6.14	–	4.70
450	61@42	52	39	paved surface	asphalt	12/13/11	20.83	12.57	–	9.42	2/19/12	14.37	6.64	–	4.36
451	62@42	53	39	paved surface	asphalt	12/13/11	18.47	12.10	–	9.64	2/19/12	9.66	6.09	–	5.18
452	63@42	54	39	paved surface	asphalt	12/13/11	23.21	14.02	–	8.88	2/19/12	14.04	7.92	–	6.18
453	23@41	14	38	paved surface	asphalt	12/13/11	33.93	16.20	–	9.18	2/20/12	21.60	9.18	–	6.23
454	34@41	25	38	paved surface	asphalt	12/13/11	20.80	11.73	–	9.34	2/20/12	15.20	6.32	–	5.07
455	42@41	33	38	paved surface	asphalt	12/13/11	26.70	14.60	–	8.76	2/20/12	12.09	5.52	–	3.73
456	63@41	54	38	paved surface	asphalt	12/13/11	15.63	11.88	–	9.10	2/19/12	11.46	5.84	–	4.83
457	68@41	59	38	paved surface	asphalt	12/1/11	19.00	9.44	–	7.69	2/16/12	21.10	9.98	–	7.17
458	73@41	64	38	paved surface	asphalt	12/1/11	18.90	7.67	–	7.13	2/16/12	18.90	8.09	–	7.46

TABLE 32. MEASUREMENTS OF SURFACE CONTAMINATION DENSITY (kcpm) AND DOSE RATES (mSv/h) IN THE EXERCISE LOCATION, BEFORE AND AFTER DECONTAMINATION EFFORTS [a] (cont.)

Data no.	Mesh ID	x coordinate	y coordinate	Land use	Remarks	Before decontamination					After decontamination				
						Measurement date	Contamination density (kcpm)	Dose rate (mSv/h)			Measurement date	Contamination density (kcpm)	Dose rate (mSv/h)		
							Surface	Surface (1 cm)	Ambient (50 cm)	Ambient (1 m)		Surface	Surface (1 cm)	Ambient (50 cm)	Ambient (1 m)
459	23@40	14	37	paved surface	asphalt	12/13/11	25.67	15.00	–	9.15	2/20/12	13.47	9.16	–	6.11
460	34@40	25	37	paved surface	asphalt	12/13/11	21.63	12.63	–	8.23	2/20/12	14.03	6.38	–	5.13
461	42@40	33	37	paved surface	asphalt	12/13/11	18.22	11.32	–	6.83	2/20/12	9.19	4.93	–	3.93
462	63@40	54	37	paved surface	asphalt	12/13/11	14.27	16.66	–	8.86	2/19/12	3.06	3.35	–	3.59
463	22@39	13	36	paved surface	asphalt	12/13/11	22.93	14.40	–	9.08	2/20/12	14.73	9.14	–	6.58
464	34@39	25	36	paved surface	asphalt	12/13/11	30.00	13.30	–	9.17	2/20/12	13.14	6.35	–	5.52
465	42@39	33	36	paved surface	asphalt	12/13/11	22.27	17.17	–	9.06	2/20/12	11.29	5.70	–	4.51
466	63@39	54	36	paved surface	asphalt	12/13/11	12.73	13.79	–	9.47	2/19/12	5.26	4.05	–	3.62
467	22@38	13	35	paved surface	asphalt	12/13/11	25.60	15.17	–	9.13	2/20/12	12.81	8.03	–	5.77
468	34@38	25	35	paved surface	asphalt	12/13/11	21.10	8.18	–	8.55	2/20/12	16.47	6.88	–	5.42
469	42@38	33	35	paved surface	asphalt	12/13/11	15.18	11.93	–	8.20	2/20/12	3.86	3.64	–	3.52
470	63@38	54	35	paved surface	asphalt	12/13/11	18.80	23.89	–	10.45	2/19/12	4.85	4.03	–	3.86
471	73@38	64	35	paved surface	asphalt	12/1/11	12.90	10.65	–	7.75	2/16/12	26.30	12.10	–	7.87
472	22@37	13	34	paved surface	asphalt	12/13/11	23.13	15.97	–	9.56	2/20/12	15.27	10.10	–	6.14
473	35@37	26	34	paved surface	asphalt	12/13/11	27.63	14.68	–	9.59	2/20/12	9.24	5.85	–	5.30
474	42@37	33	34	paved surface	asphalt	12/13/11	16.97	12.70	–	8.70	2/20/12	9.38	5.34	–	4.43
475	63@37	54	34	paved surface	asphalt	12/13/11	18.00	16.81	–	9.50	2/19/12	8.67	5.01	–	3.57
476	22@36	13	33	paved surface	asphalt	12/13/11	27.53	15.97	–	9.59	2/20/12	13.73	9.24	–	6.68
477	35@36	26	33	paved surface	asphalt	12/13/11	18.50	11.20	–	8.24	2/20/12	16.27	7.47	–	5.47
478	42@36	33	33	paved surface	asphalt	12/13/11	18.89	12.57	–	7.14	2/20/12	5.12	6.56	–	4.39
479	63@36	54	33	paved surface	asphalt	12/13/11	20.33	23.57	–	10.24	2/19/12	4.77	5.18	–	4.52

TABLE 32. MEASUREMENTS OF SURFACE CONTAMINATION DENSITY (kcpm) AND DOSE RATES (mSv/h) IN THE EXERCISE LOCATION, BEFORE AND AFTER DECONTAMINATION EFFORTS [a] (cont.)

Data no.	Mesh ID	x coordinate	y coordinate	Land use	Remarks	Before decontamination					After decontamination				
						Measurement date	Contamination density (kcpm)	Dose rate (mSv/h)			Measurement date	Contamination density (kcpm)	Dose rate (mSv/h)		
							Surface	Surface (1 cm)	Ambient (50 cm)	Ambient (1 m)		Surface	Surface (1 cm)	Ambient (50 cm)	Ambient (1 m)
480	69@36	60	33	paved surface	asphalt	12/1/11	26.60	10.59	–	6.74	2/16/12	23.50	10.40	–	6.92
481	11@35	2	32	paved surface	asphalt	12/1/11	37.70	14.20	–	9.99	2/16/12	38.20	14.20	–	9.63
482	16@35	7	32	paved surface	asphalt	12/1/11	33.50	13.34	–	9.63	2/16/12	36.20	14.30	–	8.86
483	22@35	13	32	paved surface	asphalt	12/13/11	26.53	14.23	–	9.28	2/20/12	12.97	8.43	–	5.64
484	35@35	26	32	paved surface	asphalt	12/13/11	27.57	12.77	–	8.55	2/20/12	12.53	6.22	–	5.23
485	36@35	27	32	paved surface	asphalt	12/13/11	32.17	16.70	–	7.61	2/20/12	24.63	9.14	–	5.44
486	37@35	28	32	paved surface	asphalt	12/13/11	21.83	11.80	–	6.10	2/20/12	20.10	8.83	–	4.47
487	38@35	29	32	paved surface	asphalt	12/13/11	12.53	10.67	–	6.80	2/20/12	16.77	9.43	–	5.15
488	39@35	30	32	paved surface	asphalt	12/13/11	38.03	17.43	–	9.94	2/20/12	35.77	18.80	–	8.25
489	40@35	31	32	paved surface	asphalt	12/13/11	30.03	13.13	–	8.36	2/20/12	27.23	10.80	–	4.56
490	41@35	32	32	paved surface	asphalt	12/26/11	14.98	11.25	13.80	8.28	2/20/12	13.98	7.26	–	3.98
491	42@35	33	32	paved surface	asphalt	12/13/11	19.37	12.73	–	8.34	2/20/12	12.22	5.82	–	4.76
492	63@35	54	32	paved surface	asphalt	12/13/11	19.00	16.19	–	9.31	2/19/12	7.89	4.74	–	4.21
493	22@34	13	31	paved surface	asphalt	12/13/11	21.80	12.87	–	8.60	2/20/12	12.33	7.53	–	5.77
494	35@34	26	31	paved surface	asphalt	12/13/11	21.63	11.72	–	8.22	2/20/12	13.72	7.18	–	5.41
495	39@34	30	31	paved surface	parking space (gravel)	12/1/11	10.20	12.23	9.68	9.27	2/20/12	0.98	1.92	–	2.85
496	40@34	31	31	paved surface	parking space (gravel)	12/1/11	8.20	12.41	9.15	9.10	2/20/12	4.72	5.71	–	3.28
497	41@34	32	31	paved surface	parking space (gravel)	12/1/11	9.00	12.71	11.00	10.30	2/20/12	2.83	4.36	–	3.27
498	42@34	33	31	paved surface	asphalt	12/13/11	18.21	12.00	–	8.68	2/20/12	10.18	5.43	–	4.04

TABLE 32. MEASUREMENTS OF SURFACE CONTAMINATION DENSITY (kcpm) AND DOSE RATES (mSv/h) IN THE EXERCISE LOCATION, BEFORE AND AFTER DECONTAMINATION EFFORTS [a] (cont.)

Data no.	Mesh ID	x coordinate	y coordinate	Land use	Remarks	Before decontamination					After decontamination				
						Measurement date	Contamination density (kcpm)	Dose rate (mSv/h)			Measurement date	Contamination density (kcpm)	Dose rate (mSv/h)		
							Surface	Surface (1 cm)	Ambient (50 cm)	Ambient (1 m)		Surface	Surface (1 cm)	Ambient (50 cm)	Ambient (1 m)
499	64@34	55	31	paved surface	asphalt	12/13/11	14.73	14.35	–	9.25	2/19/12	6.73	3.11	–	4.53
500	21@33	12	30	paved surface	asphalt	12/13/11	20.33	14.97	–	8.92	2/20/12	15.73	8.95	–	6.05
501	35@33	26	30	paved surface	asphalt	12/13/11	26.50	13.63	–	8.90	2/20/12	14.34	6.53	–	5.44
502	39@33	30	30	paved surface	parking space (gravel)	12/1/11	11.60	13.86	9.63	9.16	2/20/12	5.77	5.62	–	3.49
503	40@33	31	30	paved surface	parking space (gravel)	12/1/11	11.80	13.32	9.81	9.48	2/20/12	0.73	1.26	–	2.11
504	41@33	32	30	paved surface	parking space (gravel)	12/1/11	8.00	11.85	10.20	10.70	2/20/12	0.85	1.67	–	2.45
505	42@33	33	30	paved surface	asphalt	12/13/11	21.30	11.90	–	8.23	2/20/12	15.95	8.17	–	5.09
506	63@33	54	30	paved surface	forest (soil)	11/28/11	11.25	15.70	10.73	9.05	2/18/12	3.25	5.34	–	4.57
507	64@33	55	30	paved surface	asphalt	12/13/11	18.29	12.37	–	7.93	2/19/12	18.10	8.22	–	5.89
508	21@32	12	29	paved surface	asphalt	12/13/11	21.83	14.03	–	9.82	2/20/12	15.03	8.28	–	5.94
509	35@32	26	29	paved surface	asphalt	12/13/11	16.83	11.64	–	8.57	2/20/12	13.45	7.13	–	5.56
510	39@32	30	29	paved surface	parking space (gravel)	12/1/11	8.14	10.62	8.64	8.59	2/20/12	1.83	3.45	–	2.43
511	40@32	31	29	paved surface	parking space (gravel)	12/1/11	8.14	10.93	9.21	9.65	2/20/12	1.74	3.28	–	2.53
512	41@32	32	29	paved surface	parking space (gravel)	12/1/11	7.21	11.12	9.10	9.12	2/20/12	1.76	2.34	–	2.56
513	43@32	34	29	paved surface	asphalt	12/13/11	22.70	11.67	–	8.73	2/20/12	16.23	7.24	–	4.74
514	63@32	54	29	paved surface	asphalt	12/13/11	12.59	9.04	–	7.46	2/19/12	13.69	6.49	–	5.53
515	64@32	55	29	paved surface	asphalt	12/13/11	22.93	11.32	–	8.39	2/19/12	18.09	6.62	–	4.64
516	71@32	62	29	paved surface	asphalt	12/1/11	28.20	12.29	–	6.37	2/16/12	28.30	13.50	–	6.63

TABLE 32. MEASUREMENTS OF SURFACE CONTAMINATION DENSITY (kcpm) AND DOSE RATES (mSv/h) IN THE EXERCISE LOCATION, BEFORE AND AFTER DECONTAMINATION EFFORTS [a] (cont.)

Data no.	Mesh ID	x coordinate	y coordinate	Land use	Remarks	Before decontamination					After decontamination				
						Measurement date	Contamination density (kcpm)	Dose rate (mSv/h)			Measurement date	Contamination density (kcpm)	Dose rate (mSv/h)		
							Surface	Surface (1 cm)	Ambient (50 cm)	Ambient (1 m)		Surface	Surface (1 cm)	Ambient (50 cm)	Ambient (1 m)
517	21@31	12	28	paved surface	asphalt	12/13/11	20.97	13.87	–	9.23	2/20/12	14.87	9.07	–	6.10
518	35@31	26	28	paved surface	asphalt	12/13/11	19.53	12.46	–	8.93	2/20/12	11.32	5.67	–	5.22
519	38@31	29	28	paved surface	soil	12/26/11	8.20	15.00	9.01	8.20	2/18/12	6.10	7.23	–	7.73
520	39@31	30	28	paved surface	parking space (gravel)	12/1/11	9.78	12.35	9.70	8.95	2/20/12	0.87	1.93	–	2.01
521	40@31	31	28	paved surface	parking space (gravel)	12/1/11	7.15	10.93	9.72	9.59	2/20/12	1.35	2.67	–	2.23
522	41@31	32	28	paved surface	parking space (gravel)	12/1/11	10.90	13.52	10.10	9.79	2/20/12	2.01	3.32	–	2.59
523	43@31	34	28	paved surface	asphalt	12/13/11	21.07	10.51	–	7.99	2/20/12	15.50	7.23	–	4.35
524	61@31	52	28	paved surface	asphalt	12/13/11	16.93	10.69	–	8.42	2/19/12	12.84	7.22	–	5.61
525	62@31	53	28	paved surface	asphalt	12/13/11	19.48	10.90	–	8.21	2/19/12	14.49	6.46	–	5.40
526	21@30	12	27	paved surface	asphalt	12/13/11	14.43	13.03	–	9.04	2/20/12	10.99	7.43	–	6.19
527	35@30	26	27	paved surface	asphalt	12/13/11	27.07	12.29	–	9.35	2/20/12	15.63	6.46	–	5.21
528	39@30	30	27	paved surface	soil	12/26/11	13.30	12.30	10.50	4.93	2/18/12	3.88	4.77	–	4.92
529	40@30	31	27	paved surface	soil	12/26/11	15.60	11.80	9.02	5.11	2/18/12	3.92	4.68	–	3.51
530	41@30	32	27	paved surface	soil	12/26/11	15.30	13.10	9.22	5.24	2/18/12	6.88	9.57	–	5.22
531	43@30	34	27	paved surface	asphalt	12/13/11	13.58	12.20	–	7.93	2/20/12	8.25	5.74	–	4.02
532	59@30	50	27	paved surface	asphalt	12/13/11	15.22	11.93	9.63	8.80	2/19/12	9.49	8.34	–	5.54
533	60@30	51	27	paved surface	asphalt	12/13/11	16.13	12.05	–	8.56	2/19/12	15.29	6.32	–	5.01
534	77@30	68	27	paved surface	asphalt	12/1/11	28.20	10.95	–	7.11	2/16/12	25.50	11.30	–	7.23
535	11@29	2	26	paved surface	asphalt	12/1/11	35.50	12.92	–	9.64	2/16/12	35.30	13.60	–	9.88

TABLE 32. MEASUREMENTS OF SURFACE CONTAMINATION DENSITY (kcpm) AND DOSE RATES (mSv/h) IN THE EXERCISE LOCATION, BEFORE AND AFTER DECONTAMINATION EFFORTS [a] (cont.)

Data no.	Mesh ID	x coordinate	y coordinate	Land use	Remarks	Before decontamination					After decontamination				
						Measurement date	Contamination density (kcpm)	Dose rate (mSv/h)			Measurement date	Contamination density (kcpm)	Dose rate (mSv/h)		
							Surface	Surface (1 cm)	Ambient (50 cm)	Ambient (1 m)		Surface	Surface (1 cm)	Ambient (50 cm)	Ambient (1 m)
536	21@29	12	26	paved surface	asphalt	12/13/11	23.66	14.83	–	9.89	2/20/12	15.40	10.02	–	6.51
537	35@29	26	26	paved surface	asphalt	12/13/11	22.00	12.09	–	9.44	2/20/12	11.10	5.29	–	4.60
538	43@29	34	26	paved surface	asphalt	12/26/11	11.60	11.00	9.37	8.39	2/20/12	8.76	5.92	–	4.62
539	58@29	49	26	paved surface	asphalt	12/13/11	20.17	12.21	–	8.09	2/19/12	14.34	6.54	–	4.27
540	59@29	50	26	paved surface	asphalt	12/13/11	18.98	12.49	–	8.95	2/19/12	13.42	7.27	–	5.34
541	67@29	58	26	paved surface	asphalt	12/1/11	31.10	10.61	–	6.78	2/16/12	28.70	12.10	–	6.17
542	21@28	12	25	paved surface	asphalt	12/26/11	21.03	14.78	13.80	10.46	2/20/12	11.49	7.43	–	5.60
543	35@28	26	25	paved surface	asphalt	12/13/11	17.17	11.93	–	8.06	2/20/12	15.23	6.09	–	4.89
544	36@28	27	25	paved surface	asphalt	12/13/11	23.33	10.65	–	8.16	2/20/12	15.03	6.82	–	5.21
545	37@28	28	25	paved surface	asphalt	12/13/11	18.37	12.03	–	7.60	2/20/12	20.83	9.40	–	5.62
546	38@28	29	25	paved surface	asphalt	12/13/11	23.93	12.85	–	7.31	2/20/12	22.37	9.59	–	5.53
547	39@28	30	25	paved surface	asphalt	12/26/11	13.87	11.96	11.70	6.56	2/20/12	8.79	5.85	–	3.90
548	40@28	31	25	paved surface	asphalt	12/26/11	14.68	12.05	10.10	7.57	2/20/12	11.92	7.58	–	5.04
549	41@28	32	25	paved surface	asphalt	12/26/11	19.72	12.97	12.10	6.70	2/20/12	17.23	7.26	–	5.59
550	42@28	33	25	paved surface	asphalt	12/26/11	15.56	11.90	11.10	8.03	2/20/12	13.61	8.13	–	5.03
551	43@28	34	25	paved surface	asphalt	12/13/11	13.19	11.01	–	8.22	2/20/12	9.01	6.02	–	4.39
552	56@28	47	25	paved surface	asphalt	12/13/11	25.37	12.04	–	7.48	2/19/12	9.92	4.97	–	4.00
553	57@28	48	25	paved surface	asphalt	12/13/11	21.57	10.40	–	7.45	2/19/12	18.01	6.97	–	4.25
554	15@27	6	24	paved surface	asphalt	12/1/11	34.50	13.08	–	8.65	2/16/12	34.50	13.10	–	8.52
555	21@27	12	24	paved surface	asphalt	12/13/11	14.52	12.07	–	8.87	2/20/12	12.67	7.76	–	5.87
556	35@27	26	24	paved surface	asphalt	12/13/11	25.40	11.96	–	8.41	2/20/12	14.40	5.89	–	4.88

TABLE 32. MEASUREMENTS OF SURFACE CONTAMINATION DENSITY (kcpm) AND DOSE RATES (mSv/h) IN THE EXERCISE LOCATION, BEFORE AND AFTER DECONTAMINATION EFFORTS [a] (cont.)

Data no.	Mesh ID	x coordinate	y coordinate	Land use	Remarks	Before decontamination					After decontamination				
						Measurement date	Contamination density (kcpm)	Dose rate (mSv/h)			Measurement date	Contamination density (kcpm)	Dose rate (mSv/h)		
							Surface	Surface (1 cm)	Ambient (50 cm)	Ambient (1 m)		Surface	Surface (1 cm)	Ambient (50 cm)	Ambient (1 m)
557	43@27	34	24	paved surface	asphalt	12/13/11	10.09	11.30	–	8.14	2/20/12	8.91	5.74	–	4.61
558	54@27	45	24	paved surface	asphalt	12/13/11	11.99	11.35	10.52	8.95	2/22/12	7.95	5.25	4.79	4.16
559	55@27	46	24	paved surface	asphalt	12/13/11	19.13	10.17	–	8.16	2/19/12	13.28	5.84	–	4.28
560	74@27	65	24	paved surface	asphalt	12/1/11	29.80	13.95	–	6.56	2/16/12	29.80	11.90	–	6.17
561	20@26	11	23	paved surface	asphalt	12/13/11	24.17	12.77	–	9.06	2/20/12	14.13	7.88	–	5.89
562	35@26	26	23	paved surface	asphalt	12/13/11	19.73	10.92	–	8.16	2/20/12	10.13	5.52	–	4.96
563	44@26	35	23	paved surface	asphalt	12/13/11	12.32	10.88	8.34	8.71	2/20/12	6.80	3.90	–	3.13
564	53@26	44	23	paved surface	asphalt	12/13/11	22.53	11.87	–	7.83	2/19/12	12.36	4.92	–	4.56
565	62@26	53	23	paved surface	asphalt	12/1/11	25.90	10.59	–	6.85	2/16/12	25.60	10.30	–	6.53
566	20@25	11	22	paved surface	asphalt	12/13/11	23.51	13.90	–	9.26	2/20/12	21.12	9.99	–	6.73
567	21@25	12	22	paved surface	asphalt	12/26/11	14.69	15.18	9.90	8.62	2/19/12	11.25	5.83	–	3.12
568	22@25	13	22	paved surface	asphalt	12/13/11	31.83	15.37	–	7.39	2/19/12	21.70	7.18	–	4.65
569	35@25	26	22	paved surface	asphalt	12/13/11	22.00	12.24	–	7.12	2/20/12	9.04	7.30	–	5.47
570	44@25	35	22	paved surface	asphalt	12/13/11	16.33	11.30	–	8.30	2/20/12	14.12	6.86	–	4.19
571	52@25	43	22	paved surface	asphalt	12/13/11	19.43	10.61	–	8.51	2/19/12	10.58	5.63	–	4.90
572	53@25	44	22	paved surface	asphalt	12/13/11	18.97	15.27	–	8.59	2/19/12	14.16	6.51	–	5.44
573	23@24	14	21	paved surface	asphalt	12/13/11	29.60	13.07	–	7.23	2/19/12	20.27	6.26	–	4.25
574	24@24	15	21	paved surface	asphalt	12/13/11	23.30	12.83	–	7.05	2/19/12	25.07	8.61	–	5.89
575	35@24	26	21	paved surface	asphalt	12/13/11	24.10	11.65	–	8.57	2/20/12	13.78	6.54	–	5.45
576	45@24	36	21	paved surface	asphalt	12/13/11	15.70	10.65	8.16	8.45	2/20/12	12.03	5.94	–	3.65
577	50@24	41	21	paved surface	asphalt	12/13/11	13.33	9.44	–	7.41	2/19/12	10.85	5.91	–	4.21

TABLE 32. MEASUREMENTS OF SURFACE CONTAMINATION DENSITY (kcpm) AND DOSE RATES (mSv/h) IN THE EXERCISE LOCATION, BEFORE AND AFTER DECONTAMINATION EFFORTS [a] (cont.)

Data no.	Mesh ID	x coordinate	y coordinate	Land use	Remarks	Before decontamination					After decontamination				
						Measurement date	Contamination density (kcpm)	Dose rate (mSv/h)			Measurement date	Contamination density (kcpm)	Dose rate (mSv/h)		
							Surface	Surface (1 cm)	Ambient (50 cm)	Ambient (1 m)		Surface	Surface (1 cm)	Ambient (50 cm)	Ambient (1 m)
578	51@24	42	21	paved surface	asphalt	12/13/11	12.70	8.94	–	7.98	2/19/12	9.01	4.06	–	3.67
579	24@23	15	20	paved surface	asphalt	12/13/11	22.27	12.50	–	7.63	2/19/12	27.87	9.83	–	5.93
580	25@23	16	20	paved surface	asphalt	12/13/11	22.37	10.99	–	7.28	2/19/12	21.93	7.56	–	5.07
581	35@23	26	20	paved surface	asphalt	12/13/11	22.40	12.05	–	9.17	2/20/12	9.20	5.15	–	4.72
582	46@23	37	20	paved surface	asphalt	12/13/11	9.98	8.75	7.15	7.90	2/20/12	6.86	3.68	–	2.88
583	48@23	39	20	paved surface	asphalt	12/13/11	13.67	10.77	7.90	8.17	2/20/12	7.89	4.03	–	3.76
584	49@23	40	20	paved surface	asphalt	12/13/11	22.43	10.74	–	7.67	2/19/12	15.37	6.08	–	4.84
585	58@23	49	20	paved surface	asphalt	12/1/11	33.30	11.11	–	7.01	2/16/12	31.70	10.20	–	6.82
586	68@23	59	20	paved surface	asphalt	12/1/11	28.20	10.54	–	6.72	2/16/12	27.10	11.40	–	6.38
587	26@22	17	19	paved surface	asphalt	12/13/11	20.90	10.22	–	7.98	2/19/12	20.93	7.97	–	5.63
588	27@22	18	19	paved surface	asphalt	12/13/11	18.94	11.20	–	8.07	2/19/12	15.66	9.23	–	5.69
589	28@22	19	19	paved surface	asphalt	12/13/11	25.73	13.97	–	7.78	2/19/12	22.77	9.59	–	5.83
590	35@22	26	19	paved surface	asphalt	12/13/11	19.20	14.55	–	7.63	2/20/12	9.13	5.83	–	5.52
591	46@22	37	19	paved surface	asphalt	12/13/11	24.27	13.57	–	8.06	2/20/12	13.80	6.89	–	4.01
592	47@22	38	19	paved surface	asphalt	12/13/11	21.97	12.80	–	8.25	2/19/12	13.83	6.40	–	5.00
593	48@22	39	19	paved surface	asphalt	12/13/11	20.57	10.27	–	7.74	2/19/12	11.68	6.53	–	4.49
594	29@21	20	18	paved surface	asphalt	12/13/11	28.90	14.27	–	8.17	2/19/12	23.40	9.68	–	5.64
595	30@21	21	18	paved surface	asphalt	12/13/11	23.80	15.47	–	7.87	2/19/12	19.39	7.53	–	5.23
596	35@21	26	18	paved surface	asphalt	12/13/11	19.33	10.48	–	7.98	2/20/12	9.27	8.81	–	4.86
597	45@21	36	18	paved surface	asphalt	12/13/11	34.67	15.09	–	7.31	2/19/12	15.27	6.21	–	3.93
598	46@21	37	18	paved surface	asphalt	12/13/11	18.60	11.44	–	8.04	2/19/12	14.89	7.71	–	4.39

TABLE 32. MEASUREMENTS OF SURFACE CONTAMINATION DENSITY (kcpm) AND DOSE RATES (mSv/h) IN THE EXERCISE LOCATION, BEFORE AND AFTER DECONTAMINATION EFFORTS [a] (cont.)

Data no.	Mesh ID	x coordinate	y coordinate	Land use	Remarks	Before decontamination					After decontamination				
						Measurement date	Contamination density (kcpm)	Dose rate (mSv/h)			Measurement date	Contamination density (kcpm)	Dose rate (mSv/h)		
							Surface	Surface (1 cm)	Ambient (50 cm)	Ambient (1 m)		Surface	Surface (1 cm)	Ambient (50 cm)	Ambient (1 m)
599	64@21	55	18	paved surface	asphalt	12/1/11	25.30	11.59	–	6.99	2/16/12	25.10	12.30	–	7.14
600	19@20	10	17	paved surface	asphalt	12/1/11	8.11	7.08	–	6.12	2/16/12	8.17	8.38	–	5.43
601	31@20	22	17	paved surface	asphalt	12/13/11	20.00	14.00	–	7.76	2/19/12	18.50	7.20	–	4.74
602	32@20	23	17	paved surface	asphalt	12/13/11	27.43	17.20	–	7.13	2/19/12	16.75	7.63	–	5.93
603	33@20	24	17	paved surface	asphalt	12/26/11	12.68	10.12	9.57	8.17	2/19/12	11.53	7.97	–	7.10
604	35@20	26	17	paved surface	asphalt	12/13/11	14.20	9.50	–	7.27	2/20/12	11.67	5.40	–	4.95
605	43@20	34	17	paved surface	asphalt	12/13/11	25.43	11.13	–	6.31	2/19/12	17.03	7.32	–	4.39
606	44@20	35	17	paved surface	asphalt	12/13/11	25.47	11.42	–	6.27	2/19/12	16.37	6.30	–	4.18
607	34@19	25	16	paved surface	asphalt	12/26/11	19.97	13.66	11.30	8.34	2/19/12	20.53	10.57	–	6.84
608	36@19	27	16	paved surface	asphalt	12/13/11	19.43	14.00	–	8.06	2/20/12	12.63	7.08	–	5.47
609	42@19	33	16	paved surface	asphalt	12/13/11	27.67	11.64	–	6.23	2/19/12	15.95	6.97	–	4.83
610	60@19	51	16	paved surface	asphalt	12/1/11	28.20	9.60	–	6.63	2/16/12	26.50	9.48	–	6.58
611	10@18	1	15	paved surface	asphalt	12/1/11	21.10	11.56	–	9.29	2/16/12	21.20	11.41	–	8.57
612	36@18	27	15	paved surface	asphalt	12/13/11	12.43	10.43	–	7.76	2/19/12	15.60	9.16	–	6.97
613	40@18	31	15	paved surface	concrete	12/26/11	26.50	11.23	11.40	8.27	2/18/12	19.10	8.88	–	5.22
614	41@18	32	15	paved surface	asphalt	12/13/11	20.63	9.88	–	7.61	2/19/12	12.99	6.64	–	6.21
615	14@17	5	14	paved surface	asphalt	12/1/11	34.90	8.20	–	8.44	2/16/12	30.80	9.78	–	7.62
616	36@17	27	14	paved surface	asphalt	12/13/11	29.73	30.81	–	9.85	2/19/12	28.10	23.35	–	7.68
617	38@17	29	14	paved surface	soil	12/26/11	12.20	12.59	10.60	8.09	–	–	–	–	–
618	39@17	30	14	paved surface	soil	12/26/11	21.22	12.50	12.20	7.21	2/18/12	3.29	4.42	–	3.99
619	40@17	31	14	paved surface	asphalt	12/13/11	26.13	11.91	–	8.15	2/19/12	17.27	7.37	–	6.07

TABLE 32. MEASUREMENTS OF SURFACE CONTAMINATION DENSITY (kcpm) AND DOSE RATES (mSv/h) IN THE EXERCISE LOCATION, BEFORE AND AFTER DECONTAMINATION EFFORTS [a] (cont.)

Data no.	Mesh ID	x coordinate	y coordinate	Land use	Remarks	Before decontamination					After decontamination				
						Measurement date	Contamination density (kcpm)	Dose rate (mSv/h)			Measurement date	Contamination density (kcpm)	Dose rate (mSv/h)		
							Surface	Surface (1 cm)	Ambient (50 cm)	Ambient (1 m)		Surface	Surface (1 cm)	Ambient (50 cm)	Ambient (1 m)
620	49@17	40	14	paved surface	asphalt	12/1/11	27.70	13.46	–	6.73	2/16/12	28.10	12.50	–	6.62
621	19@16	10	13	paved surface	asphalt	12/1/11	14.70	12.44	–	7.68	2/16/12	13.50	11.70	–	6.50
622	24@16	15	13	paved surface	asphalt	12/1/11	33.80	13.15	–	6.97	2/16/12	29.50	13.60	–	6.53
623	35@16	26	13	paved surface	asphalt	12/13/11	24.70	22.88	–	8.94	2/19/12	23.33	8.50	–	6.73
624	36@16	27	13	paved surface	asphalt	12/13/11	21.13	12.07	–	8.70	2/19/12	25.77	10.58	–	7.07
625	37@16	28	13	paved surface	asphalt	12/13/11	19.40	14.48	–	9.09	2/19/12	22.57	10.58	–	7.41
626	38@16	29	13	paved surface	asphalt	12/13/11	21.87	16.04	–	8.42	2/19/12	21.70	9.87	–	8.06
627	39@16	30	13	paved surface	asphalt	12/13/11	18.30	17.05	–	9.11	2/19/12	16.53	7.79	–	7.84
628	40@16	31	13	paved surface	asphalt	12/13/11	27.47	19.70	–	9.42	2/19/12	25.13	9.26	–	6.44
629	53@16	44	13	paved surface	asphalt	12/1/11	25.30	11.50	–	6.66	2/16/12	24.60	9.48	–	6.13
630	29@15	20	12	paved surface	asphalt	12/1/11	26.30	8.93	–	7.20	2/16/12	25.70	9.01	–	6.47
631	48@14	39	11	paved surface	asphalt	12/1/11	23.60	11.10	–	6.24	2/16/12	23.40	9.08	–	6.37
632	43@13	34	10	paved surface	asphalt	12/1/11	18.60	8.90	–	6.41	2/16/12	18.90	9.20	–	6.33
633	35@11	26	8	paved surface	asphalt	12/1/11	21.10	7.62	–	7.29	2/16/12	19.70	6.53	–	6.18
634	47@10	38	7	paved surface	asphalt	12/1/11	23.40	9.74	–	6.54	2/16/12	23.20	8.70	–	6.18
635	43@8	34	5	paved surface	asphalt	12/1/11	27.40	13.66	–	6.28	2/16/12	25.70	10.60	–	6.20
636	31@7	22	4	paved surface	asphalt	12/1/11	31.80	12.71	–	8.37	2/16/12	31.40	12.50	–	8.21
637	35@6	26	3	paved surface	asphalt	12/1/11	13.80	6.42	–	6.43	2/16/12	13.70	5.71	–	6.12
638	43@4	34	1	paved surface	asphalt	12/1/11	25.20	12.77	–	6.20	2/16/12	23.90	10.80	–	6.10

[a] A dash (–) indicates that no measurement is available.

TABLE 33. SUMMARY OF DECONTAMINATION EFFORTS IN THE EXERCISE LOCATION[a]

Decontamination target	Method	Decontamination factor	Reduction of gamma dose rate	Amount of waste generated (per unit)	Manpower rate	Cost
Forest						
Ground surface:						
Flat lands	Manual removal of litter and humus soil layers	1.1–10	5–90%	20–90 L/m^2	50 m^2/(person day)	530 Yen/m^2
	Humus and thin layer topsoil removal	1.3–5	20–80%	100–200 L/m^2	45 m^2/(person day)	890 Yen/m^2
Slopes	Manual removal of litter and humus soil layers	1.1–10	5–90%	20–90 L/m^2	30 m^2/(person day)	760 Yen/m^2
Trees:						
Evergreen	Pruning	1.2–2.1	14–53%	~ 270 L/m^2	40 m^2/(person day)	580 Yen/m^2
Evergreen, broad leafed trees	Trunk washing and stripping	1.4–6.7	30–80%	~ 100–300 L/tree	8 trees/(person day)	3390 Yen/m^2
Ground surface:						
Flat lands	Strimming	–	–	~ 10 L/m^2	115 m^2/(person day)	160 Yen/m^2
Slopes	Strimming	–	–	5–10 L/m^2	80 m^2/(person day)	280 Yen/m^2
Agricultural land						
Paddy fields, vegetable fields	Reversal tillage	1.4–2.5	30–60%	–	1100 m^2/(person day)	33 Yen/m^2
	Interchanging topsoil with subsoil	~ 3	~ 65%	–	100 m^2/(person day)	310 Yen/m^2
	Stripping thin topsoil layer	~ 1.5	~ 35%	~ 30 L/m^2	70 m^2/(person day)	690 Yen/m^2
	Stripping thin soil layer	1.7–3.3	40–70%	30–80 L/m^2	50 m^2/(person day)	880 Yen/m^2
	Stripping thin soil layer	–	–	9–12 L/m^2	260 m^2/(person day)	100 Yen/m^2
	Mowing	–	–	9–12 L/m^2	500 m^2/(person day)	70 Yen/m^2
Residential areas						
Roof (tile, iron plate)	Surface brushing and washing	1.1–2	10–50%	5.6×10^{-3} L (Slug) 5.8×10^{-5} t/L (Solid per water treated)	20 m^2/(person day)	1090 Yen/m^2
Gutter	Removing and wiping	1.4–10	30–90%	1 m^3/house	25 m/(person day)	1100 Yen/m
	Removing and high pressure washing	~ 2.5	~ 60%	1 m^3/house	20 m/(person day)	1230 Yen/m
Wall	Brushing	1.2–1.3	20–30%	None	130 m^2/(person day)	100 Yen/m^2
Garden:						
Unpaved	Stripping thin topsoil layer	1.1–10	10–90%	–	70 m^2/(person day)	590 Yen/m^2
Gravel bedding	Gravel stripping	1.3–6.7	20–85%	–	30 m^2/(person day)	820 Yen/m^2
Pebbles	High pressure washing	2.5–20	60–95%	–	20 m^2/(person day)	930 Yen/m^2
Interlocking	High pressure washing	1.4–5.0	30–80%	0.2 L/m^2	15 m^2/(person day)	1320 Yen/m^2
Turf	Turf stripping	~ 5	~ 80%	20–50 L/m^2	15 m^2/(person day)	1500 Yen/m^2
Garden trees	Pruning and removal of soil below trees	1–1.3	0–20%	~ 30 L/m^2	30 m^2/(person day)	740 Yen/m^2

TABLE 33. SUMMARY OF DECONTAMINATION EFFORTS IN THE EXERCISE LOCATION[a] (cont.)

Decontamination target	Method	Decontamination factor	Reduction of gamma dose rate	Amount of waste generated (per unit)	Manpower rate	Cost
Residential land (large infrastructure)						
Large flat areas, scarcement, stairs, balcony (concrete surface)	Abrasion	2.5–5	60–80%	1 L/m^2	10 m^2/(person day)	1940 Yen/m^2
Hard floors, scarcement, roof, stairs, pavement (concrete surface, asphalt)	High pressure water jet based washing	~ 5	~ 80%	~ 3 L/m^2	80 m^2/(person day)	1150 Yen/m^2
Hard floors, scarcement, pavement (concrete surface, asphalt paved surface)	Abrasive blasting	~ 10	~ 90%	~ 3 L/m^2	270 m^2/(person day) (medium size) 170 m^2/(person day) (large size)	570 Yen/m^2
Concrete walls, scarcement (concrete surface)	Brushing surface and high pressure washing	1.3–3.3	20–70%	–	50 m^2/(person day)	960 Yen/m^2
Hard floors, scarcement, roof, stairs, balcony (concrete surface)	High pressure washing	1.3–3.3	20–70%	–	50 m^2/(person day)	960 Yen/m^2
Walls (concrete, mortar)	High pressure washing	1.3–3.3	20–70%	–	50 m^2/(person day)	960 Yen/m^2
Carriageways						
Pavement (asphalt pavement surface)	Decontamination with onboard road sweeper	1–2	0–45%	1–1.5 L/m^2	3500 m^2/(person day) Road surface cleaning vehicle 1750 m^2/(person day) Onboard road sweeper	10 Yen/m^2 Road surface cleaning vehicle 20 Yen/m^2 Onboard road sweeper
	High pressure washing	1–3	0–65%	–	50 m^2/(person day)	960 Yen/m^2
	Washing with draining type pavement washing vehicle	1–3	0–70%	–	1000 m^2/(person day)	150 Yen/m^2
	Dry ice blasting	2.5–10	60–90%	2 L/m^2	70 m^2/(person day)	1310 Yen/m^2
	Sand blasting	2.5–10	60–90%	20 L/m^2	5 m^2/(person day)	4190 Yen/m^2
	Shot blasting	3–23	60–95%	~ 3 L/m^2	170 m^2/(person day)	480 Yen/m^2
	Ultra-high pressure washing	2–15	40–95%	~ 3 L/m^2	80 m^2/(person day)	1150 Yen/m^2
	Stripping of road by TS asphalt stripping machine	22	~ 95%	~ 8 L/m^2	150 m^2/(person day)	390 Yen/m^2
	Stripping asphalt pavement by mechanical digger	3–10	70–90%	~ 150 L/m^2	26 m^2/(person day)	1620 Yen/m^2
Unpaved (gravel, soil surface)	Stripping gravel (soil surface) by mechanical digger	1–13	30–95%	20–50 L/m^2	90 m^2/(person day)	560 Yen/m^2
Gutters, collecting measures	Vacuum removal of debris	1–10	30–90%	100–200 L/m^2	28 m^2/(person day)	1080 Yen/m^2

TABLE 33. SUMMARY OF DECONTAMINATION EFFORTS IN THE EXERCISE LOCATION[a] (cont.)

Decontamination target	Method	Decontamination factor	Reduction of gamma dose rate	Amount of waste generated (per unit)	Manpower rate	Cost
Public infrastructure						
Roof and roof terrace (concrete, mortar)	Surface brushing and high pressure washing	1.4–3.3	30–70%	1 L/m^2	85 m^2/(person day)	340 Yen/m^2
Roof and roof terrace (waterproof sheets)	Surface brushing and high pressure washing	1.1–5	10–80%	1 L/m^2	140 m^2/(person day)	250 Yen/m^2
Vertical gutters	High pressure washing	~ 10	~ 90%	~ 20 L/m^2	65 m^2/(person day)	710 Yen/m^2
Ground	Stripping thin topsoil layer	5–10	80–90%	20–50 L/m^2	175 m^2/(person day)	360 Yen/m^2
Ground	Stripping thin topsoil layer	10	~ 90%	20–50 L/m^2	160 m^2/(person day)	290 Yen/m^2
Ground (flat ground) Unpaved	Stripping thin topsoil layer Interchanging topsoil	5–6.7	80–85%	–	150 m^2/(person day)	230 Yen/m^2
Ground (turf)	Turf stripping	1.8	~ 45%	20–50 L/m^2	180 m^2/(person day)	470 Yen/m^2
Ground (artificial turf)	Vacuum filling material	2.5–2.9	60–65%	10–20 L/m^2	2600 m^2/day (9 persons, 2 vacuum machines)	150 Yen/m^2
Pool	Water treatment and high pressure washing	2.5–10	60–90%	~ 1 L/m^2	45 m^2/(person day)	80000 Yen
Contaminated water	Coagulating sedimentation treatment	*	~ 100%	75 kg/m^3 (water)	11 m^3/(person day)	6000 Yen/m^3
Sloped surface	Strimming	–	–	5–10 L/m^2	~ 80 m^2/(person day)	200 Yen/m^2
Sloped surface	Vegetation removal within grating crib	~ 10	~ 90%	1500 L/m^2	–	–

[a] Data reproduced from Ref. [53].

APPENDIX III. DESCRIPTIONS OF MODELS

This Appendix includes descriptions for the following models used in the exercises described in this report: URD, SPRAY, CERES CBRN-E, RASCAL 3.0.5, ARTM, LASAIR (as applied for the Šoštanj exercise), and NFS_VINCA. Other models used in these exercises are described in the EMRAS II report [6] or in the text of the current report; these include ADDAM/CSA-ERM, LASAIR (as applied for other exercises), ERMIN, and JAEA. A complementary Electronic Appendix, which is in the format of an Excel® workbook with a separate page (worksheet) for each model, plus a table comparing major features or attributes of all of the included models, is also available.

III.1. DESCRIPTION OF URBAN RELEASE DISPERSION MODEL (URD)

III.1.1. Model description

III.1.1.1. Mathematical basis

The Urban Release Dispersion Model (URD), developed by Technical University of Denmark (DTU-RISØ), is a Gaussian Puff model which employs high resolution parameterizations as described in Ref. [64]. It empirically accounts for the effects of buildings on dispersion by reducing the extent of large scale horizontal dispersion, whilst increasing the effects of small scale dispersion and increasing the persistency of the plume within the stagnant zones [65].

This model is currently incorporated with the Danish Decision Support System: Accident Reporting and Guidance Operating System (ARGOS). It can be used either as a coupled urban dispersion model with another larger scale dispersion model, the RISØ Mesoscale Puff (RIMPUFF) model, or on its own.

III.1.1.2. Input parameters

Weather: The URD model is able to take in either time varying or constant weather information. It needs temperature at 2 m height and 0 m (ground level).

Source: The URD model characterizes the source resulting from an explosion (e.g. dirty bomb) via a vertical aerosol particle cloud. This vertical cloud consists of a number of smaller aerosol particle clouds at various heights. The concentration distribution of aerosol particles in each of these 'smaller aerosol particle clouds' is described by a Gaussian distribution. The aerosol particles may be monodispersed (single size) or poly-dispersed (various sizes of differing abundance for each size bin).

Building Geometry: The URD model is able to incorporate urban geometries in a shapefile format; this refers to a geospatial vector data format for geographic information system (GIS) characterization.

III.1.1.3. Output

The URD model is able to provide output in terms of Bq per unit area or volume and dose rate, with the dose arising from ground contamination and airborne contamination.

III.1.1.4. Mode and scope of use

The URD model is currently under evaluation by the Defence Science Organisation National Laboratories, Singapore. The model is not yet operational in Singapore (at the time of writing). The parameters used are not operational settings, but default ones set by the developers and adapted according to the needs of the specific scenarios.

III.1.2. Description and interpretation of Scenario(s): Tests 5 and 6 and modelling parameters adopted

III.1.2.1. Introduction

Tests 5 and 6 of the short range atmospheric dispersion scenario were modelled, as described in Section 2 of this publication. Ground contamination measurements (Bq/m^2) were taken within a 40 m (x-axis) by 55 m (y-axis) domain (see Fig. 87). The source (^{99m}Tc in 6 mL water, coupled with a ~1 kg explosive) was located at the origin of the domain (coordinates 0,5 in the modelling domain), with most of the measurements placed within 50 m of the 'projected' downwind distance (in the y direction). An obstacle (dimensions 11 m × 2.5 m × 3 m) was placed 12 m away (in the y direction) from the source. Weather measurements were taken at 2 m, 4 m and 10 m heights at 1 minute temporal resolution. No ground level (0 m) measurements were taken.

III.1.2.2. Scenario descriptions

In Test 5, following the dispersal of ~2 TBq of ^{99m}Tc via a ~1 kg explosive, prevailing winds (from the north, relative to the domain) advected the plume away from the 'projected' downwind distance (see Fig. 88, which shows the ground contamination zones, derived through the interpolation of measurements). A localized hotspot (~ 1×10^6 Bq/m^2) was also observed, shown as a red zone in Fig. 88.

In Test 6, following the dispersal of ~2 TBq of ^{99m}Tc via ~ 1 kg explosive, variable winds advected the plume in various directions. Thus, the plume did not advect in any general direction, as seen in the 1×10^4 Bq/m^2 light blue zone (see Fig. 89, which shows the ground contamination zones, derived through the interpolation of measurements). A localized hotspot (~1×10^5 Bq/m^2) was observed (red zone). In the Northeast direction, a slightly elevated zone of > 3×10^4 Bq/m^2 (coloured green) is observed, suggesting a more prolonged plume dispersal in that direction.

III.1.2.3. Scenario interpretation and parameters adopted

- Model Parameters:
  - No modifications were made to the URD model.
  - Two scales of simulations were performed: 2 km × 2 km scale at 10 m resolution to obtain the overall plume direction, and 40 m × 60 m scale at 1 m resolution for submission to Working Group for comparisons with measurements.
- Weather:
  - Winds measured at 10 m height at 1 minute temporal resolution were used to drive the model, as they were taken to be the most representative of the prevailing winds driving the plume, as they were least affected by the ground level turbulence, compared with the lower level measurements (2 m and 4 m).
  - As no ground temperature measurements were taken, the 2 m temperature was incorporated, with the ground temperature taken to be the same as that at 2 m.
- Source:
  - The aerosol particle size distribution at the source was derived from previous measurements taken near the source (Appendix I), where ^{99m}Tc was dispersed in a similar experiment.

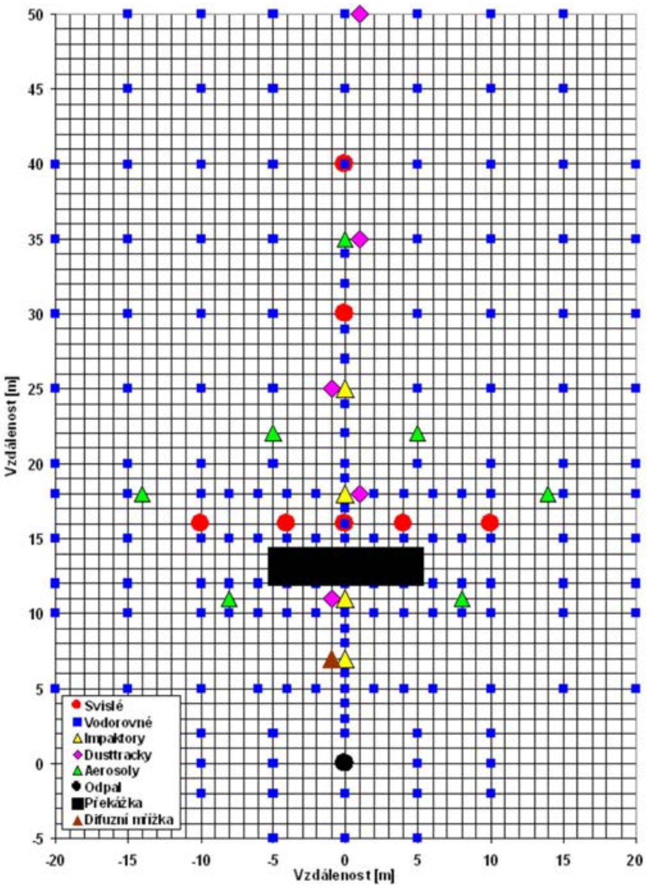

FIG. 87. Experimental domain of Tests 5 and 6(Appendix III). (Points of Interest: Back dot: source, Black rectangle: obstacle, Blue squares: Ground contamination measurements).

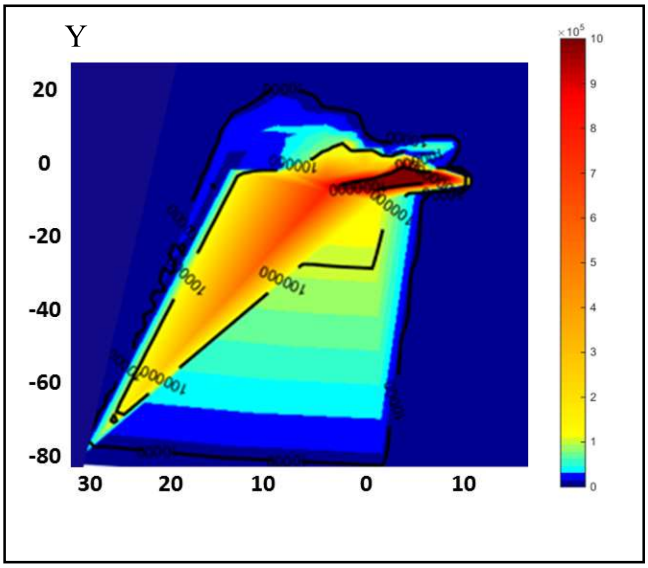

FIG. 88. Test 5 ground contamination (Bq/m^2) derived from measurements.

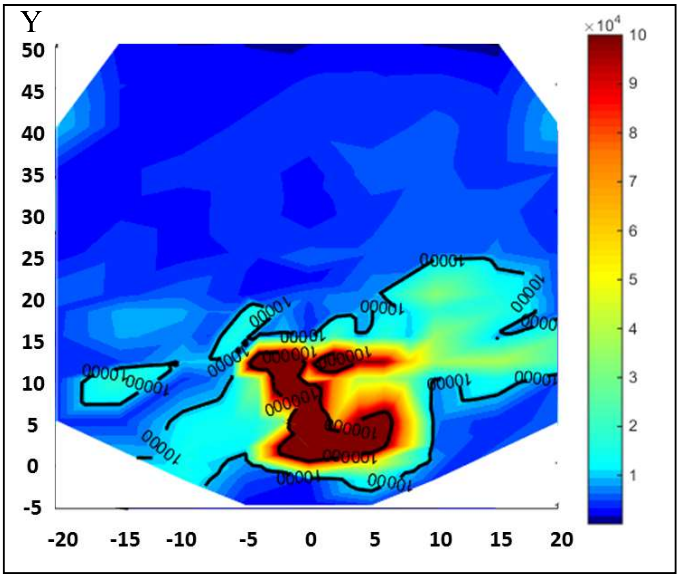

FIG. 89. Test 6 Ground Contamination (Bq/m^2) derived from measurements.

- The vertical cloud at the source was taken to be 11 m high. The aerosol particles were assumed to be equally distributed within the cloud. The cloud was assumed to be composed of 5 initial puffs of the same size, stacked on one another.
- The localized dynamics of the ballistic particles arising from the explosion were not modelled. All particles were assumed to be airborne within the vertical cloud at the source.

— Urban Geometry:
- To account for the effects of buildings, an urban geometry shapefile (*.shp) format was incorporated.

Note that only one attempt at simulation was done for each test case; these were submitted in June 2015 as a 'blind test', in exchange for measurement data for both test cases.

III.1.3. Results and discussion/evaluation

III.1.3.1. Test 5 results

The general direction of the modelled plume (see Fig. 90) is consistent with the prevailing 'north-easterly' wind direction, similar to the zoning derived from measurements (see Fig. 88 above). The extent of the 10 000 Bq/m^2 ground deposition zone is similar to what was obtained through measurements.

Observing the modelled plume within the 40 m × 60 m domain (see Fig. 91), a hotspot of 1 000 000 Bq/m^2 was present, similar in magnitude to that obtained from measurements (see Fig. 88 above). However, the regular 'Gaussian-like' shape of the modelled hotspot differs from the irregular hotspot zone obtained from the measurements.

III.1.3.2. Test 6 results

Owing to the variable wind direction during the period of dispersal, the modelled plume (see Fig. 92) was not dispersed along a prevailing direction (as also shown in Fig. 89, derived from measurements), although the modelled higher concentration zones (> 10 000 Bq/m^2) were dispersed towards the northeasterly direction.

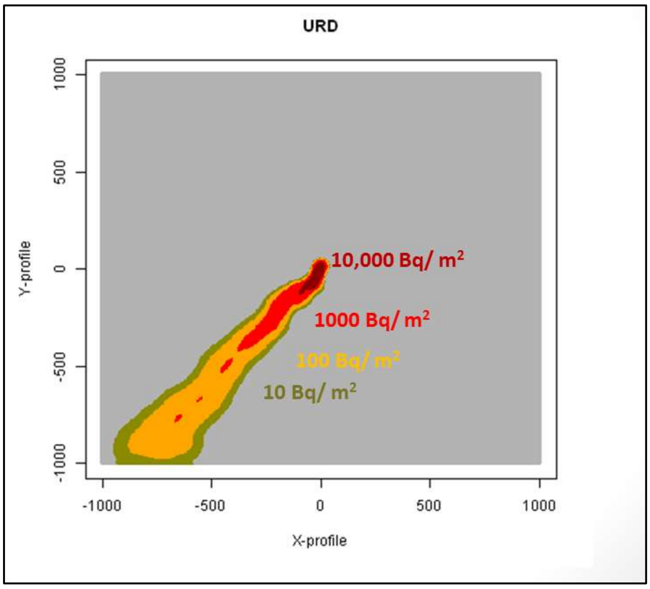

FIG. 90. Modelling results for Test 5 (2 km by 2 km).

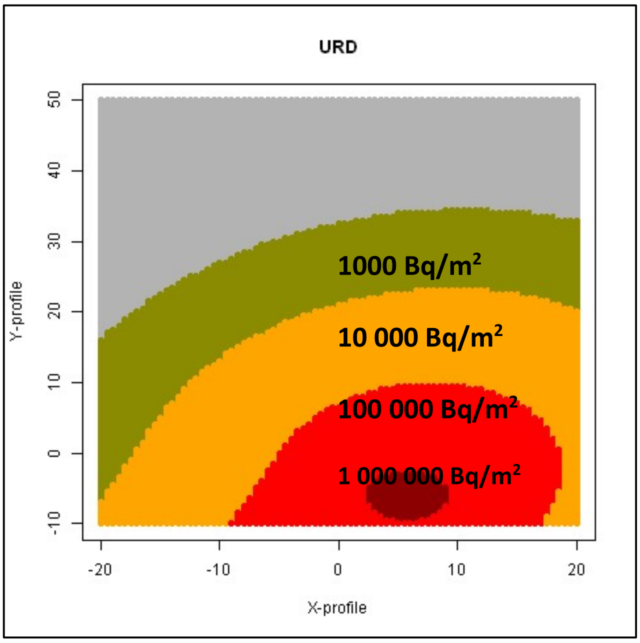

FIG. 91. Modelling results for Test 5 (40 m by 60 m).

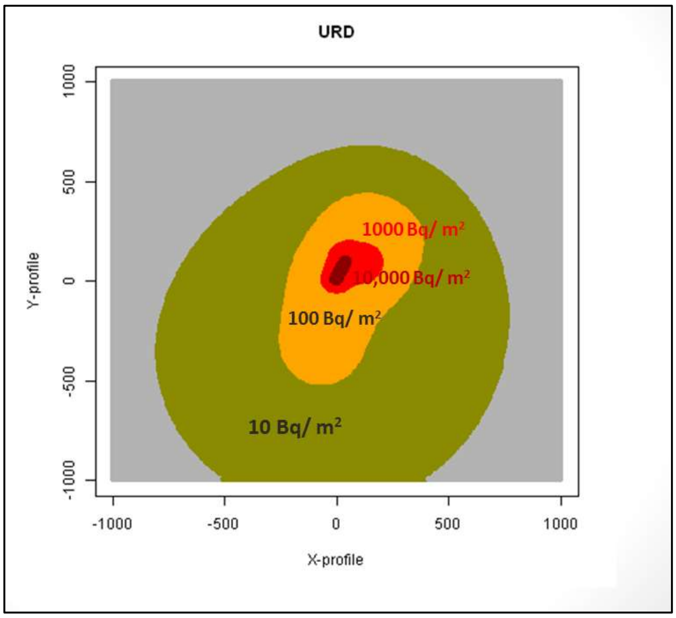

FIG. 92. Modelling results for Test 6 (2 km by 2 km).

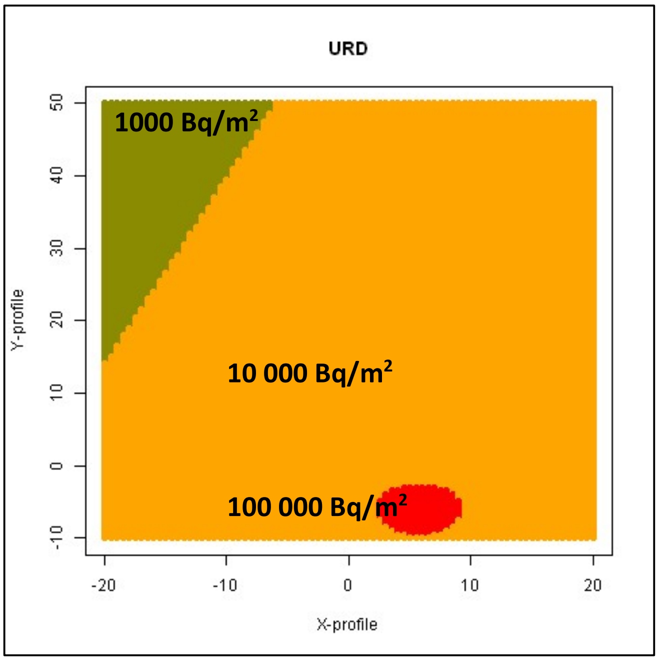

FIG. 93. Modelling results for Test 6 (40 m by 60 m).

Observing the modelled plume within the 40 m × 60 m domain (see Fig. 93), a hotspot of 100 000 Bq/m^2 was present, similar in magnitude to that obtained from measurements (see Fig 89). However, the regular 'Gaussian-like' shape of the modelled hotspot differs from the irregular hotspot zone obtained from the measurements.

III.1.3.3. Discussion and evaluation

The overall modelled plume direction was qualitatively similar to that obtained from measurements, suggesting that the 10 m wind measurements were representative of prevailing wind conditions and provided the necessary information for dispersion modelling. However, detailed dispersal patterns will necessitate detailed wind field characterization (which could be informed by lower level measurements) and will need to be pursued as further work.

Although the model was able to characterize the overall plume direction and hotspot contamination levels at the same order of magnitude as measurements, it was not able to characterize the irregular shape and size of the localized hotspot. These localized hotspots were likely to be due to the dispersal of the larger particles (> 10 microns) driven by the shorter range trajectory of the explosives. The model only assumed an airborne vertical cloud of aerosol particles and did not consider the shorter range dynamics of the larger particles. To adequately characterize such localized hotspots, detailed dynamics of larger particles need to be considered as further work.

III.1.4. Conclusions and applications

From this initial study, it was found that the overall plume direction could be modelled qualitatively similar to measurements, using wind measurements at 10 m height, suggesting the importance of measuring wind conditions at an appropriate height to obtain prevailing wind conditions. More detailed characterization of contamination zones due to dispersal of this nature would need detailed wind field characterization and detailed modelling of the transport of larger particles.

III.2. DESCRIPTION OF SPRAY

The name of the model is SPRAY, and its detailed description is given in papers by its authors [25, 66].

Atmospheric dispersion modelling was made using the AriaIndustry modelling package made by Arianet s.r.l. from Milan. The model consists of two main modules, Minerve and Spray. Minerve is a 3-D, diagnostic, mass consistent, wind field model. Spray is a numeric Lagrangian particle model for dispersion of atmospheric contamination. The models were coupled by MEIS modules for automatic input data preparation and modules for results realization and statistical elaboration.

The studies were made using measured release data. Modelling was made using consecutive half hour values as a time series, and results were saved as half hour average results in the database. The model takes into account a digital model of the terrain heights and CORINE land use data.

The models Spray and Minerve were verified in the past in research studies, all based on the 'Šoštanj measuring campaign' database from 1991, which is adopted in the scientific community as one of the suitable databases for complex terrain. Results of verification were published in air contamination papers and book [67–69] and demonstrated that these two models are suitable for modelling such complex terrain cases for all stability classes.

The Lagrangian numerical particle model Spray, coupled with the Minerve 3-D mass consistent wind field model and meteorological pre-processor, has the following characteristics (all referred to hereafter as the 'model'):

- The model takes into account the modelling domain, divided in the horizontal plane into 100 × 100 grid cells and in the vertical plane into 15 layers in the terrain following coordinates. The horizontal size of the grid cell is 150 m × 150 m. The ground level cell is 10 m in height, and higher levels have increasingly greater heights.
- The model is used to process a three-dimensional field in the coordinate system following the terrain.
- The model has appropriate expressions for description of meteorological parameters over topography which is less than 100% steep (less than 45 degrees).
- The model also works using release of 100 000 particles per hour when exploring very complex situations. The number of particles emitted per hour is adjusted to the complexity of the elaborated situations.
- The model has the applicability to accumulate particles in the explored domain. It can model the accumulation of pollutants below the inversion layer in cases of thermal inversion.
- The model uses a 2-D field of terrain heights taken from the digital model of the terrain heights. One value is taken for each horizontal grid cell.
- The model uses a 2-D field of land use data taken originally from the CORINE land cover database for Slovenia. One value is taken for each horizontal grid cell.
- The effective stack height calculation takes into account a dynamic formulation where the plume rise depends on both the atmospheric conditions at the location of the stack, and the atmospheric conditions along the path of the plume.
- Turbulences are calculated in the 3-D field of grid cells. Turbulences are calculated based on measured meteorological data and land use data, and are based on Monin Obukhov similarity theory [30].
- The model is capable of properly simulating intervals with zero wind (calm). For cases with a high percentage of calm, appropriate parameterizations that include the meandering effect are taken into account.
- The model recalculates a 2-D field of global solar radiation for a particular ground level cell (including terrain slope) based on at least one online measurement of global solar radiation in the domain.
- The model calculates a 2-D field of mixing heights. For unstable atmospheric conditions during the morning and afternoon it is computed based on global solar radiation; for stable conditions during the night it is computed based on a dynamic formulation using wind data and a temperature field.

Figure 94 shows the modelling domain (15 km × 15 km with the centre at TPPŠ). The red stars represent locations of meteorological measuring stations and locations of sources of release as seen by the model. The digital model of the terrain heights as seen by the model was slightly filtered using a convolution filter.

FIG. 94. Šoštanj area (15 km × 15 km with the centre at TPPŠ). Red stars represent locations of meteorological measuring stations and locations of sources of release, as seen by the model.

The model was chosen for validation for two main reasons:

- The first version of the model has already been validated on the 'Šoštanj91' field data set [25–27].
- The model has significantly evolved in recent years. It has moved from research usage to usage for operational regulatory purposes [66].

The Lagrangian particle dispersion model generates half hour average ground concentration fields at the same resolution (150 m) as the meteorological pre-processor. It uses Thomson's 1987 scheme with Gaussian random forcing [70]. The number of emitted virtual particles has been set to assure minimum resolution for ground level concentrations less than 1 μg m^{-3}. Anfossi's formulation [71] has been used for plume rise of hot stack plumes where horizontal and vertical variations of both mean wind and atmospheric stability have been taken into consideration.

Results from simulations are available in half hour intervals. Each half hour result represents the average atmospheric contamination over the complete domain for one half hour interval. This result is a 3-D concentration field describing concentrations for each cell of the domain.

III.3. DESCRIPTION OF CERES CBRN-E

CERES CBRN-E is an operational computational tool devoted to hazmat atmospheric dispersion modelling and impact assessment, gathering several source term models, various dispersion approaches (from Gaussian puff to advanced 4-D flow and dispersion computations) and health consequence modules adapted respectively to R-N, C or B (radiological-nuclear, chemical, or biological) noxious agents. CERES CBRN-E is able to compute atmospheric dispersion in complex environments including buildings (industrial sites or urban areas), assess the health consequences of the toxic releases on the population and first responders, and deliver operational results (e.g. danger zones, intervention zones, etc.) to rescue teams and decision makers in less than 15 minutes.

For the dispersion, CERES CBRN-E has a Lagrangian Particle Dispersion Model developed by the CEA and ARIA Technologies. This model is called PMSS, for Parallel Micro Swift Spray (PMSS).

III.3.1. The Lagrangian particle dispersion model PMSS in CERES CBRN-E

PMSS embedded in CERES is a 3-D Lagrangian particle dispersion model which reproduces the transport, dispersion, and dry and wet deposition of airborne chemically inert species released in complex meteorological conditions (low windspeed, flow over complex topography), often marked by spatial and temporal inhomogeneities of the meteo-diffusive variables (e.g. vertical wind shear, breeze due to the presence of terrain discontinuities). In addition, it is also possible to reproduce the dispersion of particulate releases, taking into account the gravitational vertical settling phenomenon. P-SPRAY can simulate releases from point, area or line, continuous and discontinuous sources, as well as exploit the available wind and turbulence measurements provided by advanced meteorological instruments. P-SPRAY can compute mean and instantaneous concentrations on a 3-D grid defined by the user, differentiating the calculation by 'chemical species' or by 'source'.

The velocity of the particles is mainly characterized by two components: a mean component, or 'transport component', which is defined by the mean velocity of the local wind, and a stochastic component, simulating the dispersion and reproducing the atmospheric turbulence. Mean values for wind speed are computed by P-SWIFT, which is external to the code, and which is able to build 3-D fields taking into account the presence of topography. P-SWIFT is a 3-D wind field model for complex terrain. It produces a mass-consistent wind field using data from a dispersed meteorological network. Temperature and humidity fields can also be interpolated.

P-SWIFT is designed to rapidly compute wind fields from on-site observations. These comply with the first Navier-Stokes equation [13], the mass conservation, to account for terrain effect on the flow structure. The influence of atmospheric stability on wind flow over terrain is modelled using a weighting factor alpha (ratio of the horizontal wind component to the vertical wind component). If obstacles such as buildings are included in a local scale simulation, their influence is modelled using a first guess prescription on the flow structure, and then mass consistency and impermeability are applied.

P-SWIFT and P-SPRAY principles and applications are described in Refs [11, 12].

III.3.2. Description of the diagnostic wind field model P-SWIFT

The wind field interpolation is based on two types of meteorological data that are derived from ground station observations (points) and from SODAR measurements (vertical profile).

The wind, temperature and humidity for the surface layer at above ground height are estimated from the ground measurements, corrected mainly by using the roughness length (derived from CORINE Land Cover database), the friction velocity and the Monin-Obukhov length [30]. Horizontal correction of interpolated data is then made according to the roughness length and the height of ground by using the 'influence–uninfluence' method.

The interpolation of surface wind data has been made with the 2-D Cressman method, which is based on a weighted interpolation of the measurements according to the distance of the selected grid point from the ground station.

The model uses the vertical wind profiles as source points in order to interpolate the wind on vertical grid levels. At upper air levels, the model uses the 2-D Cressman interpolation by level method. For grid points lying above the last measurement level, the profile is interpolated between the last measurement level and geostrophic wind that represents the flow in the upper atmospheric layers. This geostrophic wind is derived from the input data. Each grid level now has an interpolated measurement. A Cressman method is then applied to these measurements, using a horizontal range. The interpolated wind field is then adjusted by using an incompressible continuity equation.

By using the Moussiopoulos method [72], the model calculates a factor called 'alpha' which represents the stability of the atmosphere. In a stable situation, alpha tends to zero, the wind tends to bypass terrain obstacles, and vertical wind is very weak compared with horizontal wind. In unstable situations, the wind tends to cross the obstacle and vertical wind is stronger. Alpha tends to 1 in unstable situations.

The model interpolates the temperature field by using the data from the ground stations (points) and SODAR measurements (vertical profiles). The temperature gradient of the first level is applied to all grid points located below it. A dry adiabatic gradient is used for grid points above the last available measurement level.

The model also calculates the mixing layer height. In the surface layer the turbulence is sufficiently developed that molecular flow can be ignored in the presence of turbulent flows. The Monin-Obukhov length [30], the speed and the temperature are estimated. In the boundary layer, turbulent fluxes are also linked to vertical gradients of average magnitudes, but the vertical resolution is considered sufficient for computing the fluxes which are modelled.

The turbulent dispersion coefficients are estimated by using the Louis scheme [73], which is commonly used in operational models of Météo France and the European Center for Medium-Range Weather Forecasts (ECMWF). According to this scheme, the turbulent diffusivity coefficients are a function of the vertical shear of average horizontal wind and of static stability.

III.3.3. Description of the Lagrangian particle model P-SPRAY

P-SPRAY is a 3-D Lagrangian particle dispersion model. The model determines the random motion causing the dispersion thanks to turbulence variables calculated for 3-D fields. Time series of Surface Layer and atmospheric Planetary Boundary Layer scale variables (mixing layer height, friction velocity and Monin-Obukhov's length) [30] are provided by the 3-D meteorological model P-SWIFT as well as some of turbulence variables (e.g. vertical diffusion coefficient, turbulent kinetic energy, horizontal diffusion coefficient, wind speed component). P-SPRAY computes the other necessary turbulence variables as the Langrangian times and the standard deviation of velocity.

P-SPRAY takes into account some physical effects affecting the dynamics of the plume from buoyant sources. The plume rise is simulated by bulk equations.

III.3.4. Model characteristics for the Šoštanj Case

The following characteristics are used by PMSS to compute the dispersion for the two Sostanj cases:

- Southwest point coordinates of the domain in UTM (zone 33) are X = 496.249 m, Y = 5128.000.
- Northeast point coordinates of the domain in UTM (zone 33) are X = 511.250 m, Y = 5142.999 m.
- Horizontal resolution of grid cells is 100 m by 100 m.
- There are 25 vertical grid levels following the terrain. The ground level grid is 13 m in height, and the last level is 6000 m.
- Albedo, Bowen factor and roughness height are derived from the CORINE Land Cover database.
- Terrain elevation data come from the SRTM database.
- Effective height of release is computed with bulk equations which take into account dynamic and buoyant sources. Extra velocities of particles are then computed for hot sources from a stack.
- 60 particles are emitted per second per release, for a total of about 10^7 particles.
- The Lagrangian particle dispersion model computes the average concentration in half hour intervals for the 3-D grid.

III.4. DESCRIPTION OF RASCAL 3.0.5

The calculations were performed with RASCAL 3.0.5 (Radiological Assessment for Consequence Analysis for Windows) [74]. RASCAL was developed for use in consequence analysis by the U.S. Nuclear Regulatory Commission. One module in RASCAL 3.0.5 is 'Source Term to Dose', which estimates: (1) the source terms for a radiological release; (2) the atmospheric transport, diffusion, and deposition of radionuclides from the release; and (3) location dependent external and internal doses from exposure to the released materials.

III.4.1. Transport, diffusion

RASCAL 3.0.5 uses Gaussian models to describe the atmospheric dispersion of radioactive materials or chemicals released from nuclear facilities. The NRC has used earlier versions of these models in licensing and emergency response calculations, e.g. PAVAN [75], XOQDOQ [76], MESORAD [77, 78], and RASCAL Versions 2.0 [79] and 3.0 [80]. These models produce quick and reasonable estimates of radionuclide concentrations in the atmosphere, deposition, and doses, and do so even with limited information on topography and meteorology. RASCAL 3.0.5 uses a straight line Gaussian plume model, TADPLUME, for locations near the release point; at these distances, travel times are short, and there is little plume depletion associated with dry deposition. For longer distances, a Lagrangian-trajectory Gaussian puff model, TADPUFF, is used; at the longer distances, temporal or spatial variations in meteorological conditions can be significant, as can plume depletion due to dry deposition.

III.4.2. Model domains

TADPLUME and TADPUFF use different model domains. The TADPLUME domain is based on a polar grid; receptor nodes are placed at 10° intervals on circles at eight radial distances which can be adjusted to suit a given problem. The TADPUFF domain is based on a square Cartesian grid; receptor nodes are uniformly spaced throughout the domain. The plume model thus takes advantage of a higher node density near the release point on the polar grid, while the puff model takes advantage of the higher node density in the far field on the Cartesian grid.

III.4.3. Transport

III.4.3.1. TADPLUME transport

TADPLUME is a straight line Gaussian model, meaning that the model assumes straight line transport of released material, corresponding to the wind direction at the time and place of release. The wind direction is rounded to the closest 10°; thus, the axis of the plume is assumed to pass directly over the receptors. Released material is assumed to arrive instantaneously at the receptors, i.e. transit time is not considered in that part of the calculation. TADPLUME does not account for topography.

However, transit time (calculated using the wind speed at the release height) is used for estimation of the decay of radionuclides between the source and the receptors and also to calculate depletion of material in the plume due to dry or wet deposition. The model calculates decay at intervals of 5 min, while the entire transit time is used for estimation of depletion.

III.4.3.2. TADPUFF transport

Unlike TADPLUME, TADPUFF tracks the movement of each individual puff and calculates concentrations and doses based on the positions of the puffs. The model thereby explicitly accounts for the transit time in all calculations. The model calculates decay and ingrowth of radionuclides at intervals of 5 min; depletion of the puffs due to wet and dry deposition is also included in the calculations. TADPUFF may give more realistic patterns of concentrations and doses than TADPLUME, since the wind fields used by TADPUFF can be modified to account for topography.

Within TADPUFF, the movement of puffs is assumed to be determined by the wind at the center of each puff as it moves through the model domain. Two dimensional (2-D) fields of vectors are used to represent the spatial variation of winds; the vectors provide the directions and speeds of puff movements. The fields of vectors are updated at intervals of 15 minutes based on the available wind data.

Calculation of puff movement is a six step process [74]:

(1) Initial estimates of the direction and speed of the puff movement are based on the current position of the puff and the height of the puff above ground, using bilinear interpolation of the vectors at the nearest nodes of the vector field;
(2) Using the initial estimates of direction and speed (Step 1), estimates are made of the puff position at the end of the time interval;
(3) Using the estimated puff position at the end of the time interval (Step 2), new estimates are made of the direction and speed of puff movement;
(4) Using the new estimates of direction and speed of puff movement (Step 3), new estimates are made of the puff position at the end of the time interval;
(5) The end points estimated in Steps 2 and 4 are averaged;
(6) The final estimate of direction and speed of puff movement is estimated, using the initial position of the puff (Step 1) and the estimated average end point (Step 5).

The meteorological program produces vector fields for a height of 10 m above ground for use for ground level releases. For release heights greater than 12 m, wind speed profiles are used to adjust the transport speed from 10 m to the height of the puff transport, accounting for both surface friction and atmospheric stability.

III.4.4. Dispersion parameters

The horizontal dispersion parameters used in TADPLUME and TADPUFF are based on the results of a large number of dispersion experiments conducted in the 1950s and 1960s [74]. The experiments were conducted over relatively flat terrain; tracer releases ranged from about 10 min to 1 h in duration, and ground level concentration measurements were made at distances ranging from 100 m to several kilometers. Various summaries of dispersion parameters are available, including the Pasquill-Gifford curves [81].

NRC regulatory guidance includes graphic depiction of these curves, and numerical approximations to the curves are included in many NRC computer codes. In RASCAL 3.0.5, dispersion parameters are estimated using the same basic algorithms that were used in earlier NRC codes (e.g. PAVAN [75], XOQDOQ [76]) and in earlier versions of RASCAL [74]. Although these parameterizations are commonly attributed to Eimutis and Konicek [82], the σ_y parameterization is properly attributed to Tadmor and Gur [83], and the σ_z parameterization to Martin and Tikvart [84].

III.4.5. Simulation results for Šoštanj exercise

RASCAL 3.0.5 is intended for prediction of radionuclide concentrations. For the Šoštanj exercise, the calculations were made assuming the release of ^{131}I. Results from RASCAL 3.0.5, expressed in Bq s m^{-3}, were converted into μg/m^3 using the specific activity of ^{131}I (4.59×10^{15} Bq/g). The resulting values (expressed in μg/m^3) were assumed to be applicable for the SO_2 released from TTPŠ. The results were given as values of concentration in the six locations: Graskagora, Topolsica, Velenje, Velikivrh, Zavodnje and Sostanj.

III.5. DESCRIPTION OF ARTM

ARTM (Atmospheric Radionuclide Transport Model) was developed for the German Federal Office for Radiation Protection (BfS) by the Gesellschaft für Anlagen- und Reaktorsicherheit (GRS) based on the AUSTAL2000 program for ‘atmospheric dispersion of substances and odorants’ and is currently still under development [85, 86]. Both programs are mathematically based on the Lagrangian particle model following the guidelines of the Association of German Engineers (VDI) and the German Technical Instructions on Air Quality Control (TA Luft).

While AUSTAL2000 is focused on chemical particles and gases released by industrial facilities, ARTM was specifically designed for radioactive aerial releases [86]. As such, ARTM provides the opportunity to visualize dry and wet deposition of radioactive particles and cloud gamma submersion, as well as dose calculations with the dose module DARTM, developed by the BfS [86].

The GO-ARTM 2.0 version (graphical interface) based on ARTM 2.7.2 (released in December 2013) was used for this scenario. Since ARTM was developed as an operational tool to calculate atmospheric dispersion for regulatory purposes in Germany, the recent version is available only in German, and some internal parameters (e.g. the Coriolis parameter, the mixing layer height), are based on empirical values applicable for Germany. Therefore, the applicability of the model is limited.

III.5.1. Input parameters

In general, the input parameters for ARTM are structured into the following parameter types (see Fig. 95 below).

III.5.1.1. General parameters

Here the program asks for the name of the project to be inserted. The meteorological data file is one of the main components necessary to enable an ARTM run. This file includes wind speed, wind direction, the dispersion categories according to Klug/Manier [31], and information on the precipitation [86]. As an absolute minimum for ARTM simulations, the last one (precipitation) can be neglected, but the other three meteorological parameters are crucial. The formatting of such a file is demonstrated in Fig. 96 below.

An orography file can be read in as well, although this is optional. The model allows simulation with or without orographical information. If orographical information is provided, it has to be in equidistant form and lie within the Gauß-Krüger coordinate system (defined only for Germany and surrounding areas). In order to apply this model to the Šoštanj scenario, some adaptions had to be made (Section III.5.2).

The model also asks for the particle quality, i.e. the number of simulation particles released per hour. The standard value at particle quality level 0 is 63 million particles [86]. To decrease statistical errors, this number can be raised by increasing the particle quality; each step doubles the amount [86]. For the simulations of the Šoštanj scenario, particle quality level 4 with 1.008 billion particles was chosen.

The starting random number can also be chosen by the user. Depending on the starting random number, the results can have some statistical variation [86]; to keep this variation small, multiple starting random numbers were used (Section III.5.2).

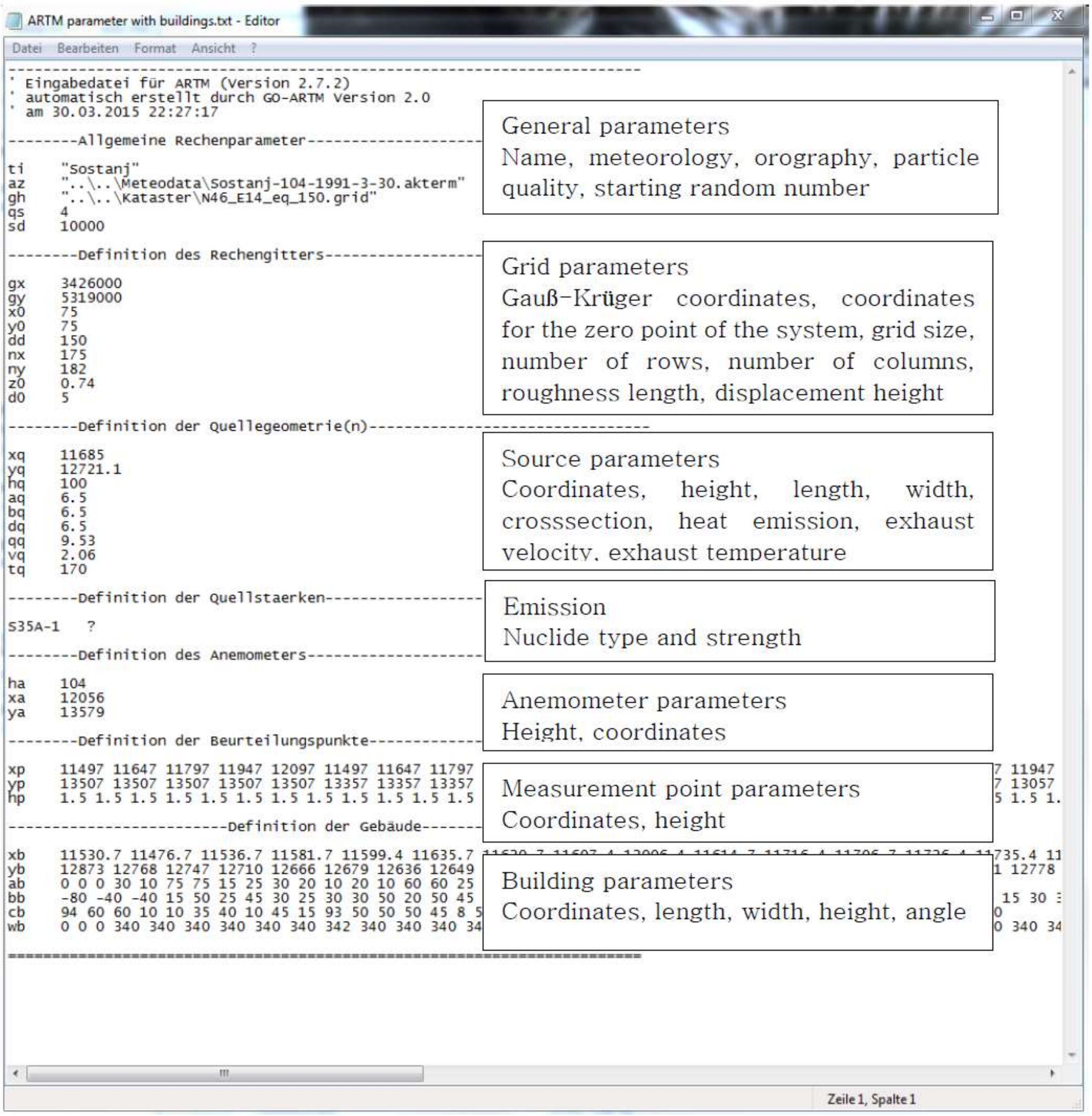

FIG. 95. ARTM input parameters.

Sostanj-104-1991-3-30.akterm - Editor

Datei Bearbeiten Format Ansicht ?

```
* AKTERM-Zeitreihe mit Niederschlag, Sostanj
* Zeitraum   3/1991  bis  3/1991
* anon. Daten, Stand  Tue Feb 25 13:32:37 2014
+ Anemometerhoehen (0.1 m):  32  41  57  74  98  144  200  244  283
AK 10000 1991 03 30 00 00 9 9 -99 -99 9 9 9 -999 9 990 9
AK 10000 1991 03 30 01 00 2 1 347  35 1 5 1 -999 9 990 1
AK 10000 1991 03 30 02 00 2 1 356  34 1 4 1 -999 9 990 1
AK 10000 1991 03 30 03 00 2 1 350  44 1 4 1 -999 9 990 1
AK 10000 1991 03 30 04 00 2 1   5  34 1 3 1 -999 9 990 1
AK 10000 1991 03 30 05 00 2 1  23  34 1 3 1 -999 9 990 1
AK 10000 1991 03 30 06 00 2 1  42  24 1 3 1 -999 9 990 1
AK 10000 1991 03 30 07 00 2 1  14  29 1 3 1 -999 9 990 1
AK 10000 1991 03 30 08 00 2 1 168   3 1 4 1 -999 9 990 1
AK 10000 1991 03 30 09 00 2 1 347  13 1 5 1 -999 9 990 1
AK 10000 1991 03 30 10 00 2 1  12  31 1 5 1 -999 9 990 1
AK 10000 1991 03 30 11 00 2 1  19  38 1 6 1 -999 9 990 1
AK 10000 1991 03 30 12 00 2 1   9  47 1 5 1 -999 9 990 1
AK 10000 1991 03 30 13 00 2 1 354  43 1 5 1 -999 9 990 1
AK 10000 1991 03 30 14 00 2 1 349  38 1 4 1 -999 9 990 1
AK 10000 1991 03 30 15 00 2 1 336  52 1 4 1 -999 9 990 1
AK 10000 1991 03 30 16 00 2 1 351  33 1 5 1 -999 9 990 1
AK 10000 1991 03 30 17 00 2 1 337  34 1 4 1 -999 9 990 1
AK 10000 1991 03 30 18 00 2 1 343  38 1 4 1 -999 9 990 1
AK 10000 1991 03 30 19 00 2 1   3  37 1 4 1 -999 9 990 1
AK 10000 1991 03 30 20 00 2 1 357  41 1 4 1 -999 9 990 1
AK 10000 1991 03 30 21 00 2 1   4  36 1 4 1 -999 9 990 1
AK 10000 1991 03 30 22 00 2 1   8  30 1 3 1 -999 9 990 1
AK 10000 1991 03 30 23 00 2 1  85  17 1 5 1 -999 9 990 1
AK 10000 1991 03 31 00 00 2 1   7  19 1 4 1 -999 9 990 1
```

Zeile 1, Spalte 1

FIG. 96. ARTM meteorological data file: Columns 1 and 2 define the station number (this can be neglected), Columns 3 to 7 define the date and time (all ARTM meteorological files need to start with 00:00 hour (midnight), Columns 8, 9, 12, 14, 16 and 18 are quality bits (these can be neglected), Column 10 is the wind direction in degrees from the north direction, Column 11 is the wind speed in 0.1 m/s, Column 13 is the dispersion category according to Klug/Manier [31] (1 = very stable to 6 = very unstable), Column 15 defines the mixing layer height (not yet used by ARTM version 2.7.2), and in Column 17 the precipitation is taken into account.

III.5.1.2. Grid parameters

The coordinates of the southwestern corner of the whole simulation region has to be inserted in the Gauß-Krüger coordinate system. For the adaptions made to enable the Šoštanj scenario, see Section III.5.2. The zero point, grid size (maximum, 500 m by 500 m; user defined below the maximum), displacement height, and the number of rows and columns of the grid need to be defined. ARTM provides the possibility to automatically read in the CORINE land use in order to determine the roughness length; however, this option is only implemented for Germany so far (Section III.5.2.).

III.5.1.3. Source parameters

Here all the coordinates and geometrical extensions of the source(s) can be inserted, as well as heat emission, exhaust velocity and temperature, and other source parameters.

III.5.1.4. Releases

Here follows a list of the chosen nuclides (101 different radionuclides, in different states or sizes) with their release strength in Bq/s per source.

III.5.1.5. Anemometer parameters

The coordinates and height of the anemometer have to be defined.

III.5.1.6. Measurement point parameters

Up to 50 measurement point can be defined by coordinate and height. Only for these points ARTM will create a time series as a result.

III.5.1.7. Building parameters

To account for buildings in the model area, ARTM can handle up to 100 buildings. These need to be defined by coordinates, length, width, height, and angle from the north direction.

III.5.1.8. Minimal model input needs

The minimal needs for the model input are the type of radionuclide and the release strength, along with hourly meteorological data including wind speed, wind direction and dispersion categories, and the position of the source and the anemometer. Orography, buildings and other input parameters are optional and are not needed for a successful run of ARTM, but the simulation results can significantly differ if these parameters are included.

III.5.2. Application of ARTM to the Šoštanj scenario

Due to the limitations and restrictions listed in Section III.5.1, in order to run the Šoštanj scenario with ARTM it was necessary to make several adaptations to the initial scenario data set prior to the simulations (described in Section 4.6.4). Adaptions were made with regards to the orography, the surface roughness length, and the meteorology:

III.5.2.1. Adaptations of the orographic data

The orographic data set provided within the framework of the Šoštanj scenario could not be used with the dispersion model in the first simulation trial, as it included inclines that were too steep, resulting in an abnormal abortion of the program.

Therefore, the orography was not taken from the original Šoštanj data set but was downloaded from geocomm.com and a customized adaptation was read in with ARTM. The data from geocomm.com has a rather poor resolution (minimum 0.0083°) for the grid size and has a non-equidistant grid; therefore, further adaptation and interpolation were needed before the data set could be used within ARTM. Due to the interpolation, the resulting adapted orographic map has smoother inclines than the originally provided one, but which are still well within the limitations for ARTM simulations.

In order to use the orography, since it was not within the Gauss-Krüger coordinate system defined area, a fake Gauss-Krüger coordinate had to be assigned just for the purpose of the map being accepted by ARTM.

III.5.2.2. Manual determination of the overall roughness length

As ARTM is designed to automatically read the surface roughness for the surroundings of nuclear facilities, and the graphical tool to assign surface roughness factors for the simulation area is not fully operational, the overall surface roughness was simply given by the value 0.74. ARTM rounds this down to 0.5 (unless a non-standard option is chosen), which is the mean value of the surface roughness map given in the Šoštanj data set.

III.5.2.3. Adaptations of the meteorological data

The data set for Šoštanj also provided meteorological data for the anemometer location as well as for each of the measurement locations; the data were provided in 30 minute intervals. In order to be of use for ARTM, some adaptations and assumptions had to be applied to these data, since ARTM only needs hourly meteorological data, including the dispersion classes according to Klug/Manier [31], as input.

Using the horizontal and vertical wind velocities from the SODAR measurements, the dispersion categories (Table 34) were assigned according to the guidelines of the German Nuclear Technological Committee (Kerntechnischer Ausschuss) [87].

In early simulations of the Šoštanj scenario, only the meteorological data of each full hour were taken into account for the simulations. As this method does not exactly represent the real case, in a second assessment the half hourly values for wind speed and wind direction were added via the method for vectorial addition to result in more accurate hourly values for the simulation with ARTM. For Case 1 (30 March 1991), additionally different dispersion categories were selected based on the Monin-Obukhov length [30], resulting in four different meteorological data sets (simulation mode; Section 4.6.4):

- ‘old’: the hourly values obtained by excluding the half hourly ones, using the dispersion categories according to [87];
- ‘averaged’: the half hourly values averaged to hourly values by the method of vectorial addition, using the dispersion categories according to [87];
- ‘new categories’: the hourly values obtained by excluding the half hourly ones, using new dispersion categories based on Monin-Obukhov length [30];
- ‘averaged and new categories’: the half hourly values averaged to hourly values by the method of vectorial addition, using new dispersion categories based on Monin-Obukhov length [30].

TABLE 34. DETERMINATION OF THE DISPERSION CATEGORIES BASED ON SODAR DATA (TRANSLATED FROM [87])

U_mean (m/s)	Sigma_vertical (m/s) Borders of the dispersion categories				
	A/B	B/C	C/D	D/E	E/F
0 to 0.9	0.51	0.42	0.32	0.2	0.14
1 to 1.9	0.55	0.43	0.33	0.2	0.14
2 to 2.9	0.63	0.47	0.35	0.21	0.15
3 to 3.9	0.72	0.53	0.38	0.22	0.15
4 to 4.9	0.83	0.58	0.42	0.22	0.15
5 to 5.9	0.94	0.66	0.45	0.23	0.16
6 to 6.9	1.07	0.73	0.49	0.25	0.16
7 to 7.9	1.2	0.81	0.54	0.26	0.17
8 to 8.9	1.33	0.89	0.58	0.27	0.18
9 to 9.9	1.46	0.98	0.63	0.29	0.18
10 to 10.9	1.59	1.06	0.68	0.31	0.19
11 to 11.9	1.74	1.15	0.73	0.32	0.2
12 to 12.9	1.88	1.24	0.79	0.34	0.21
13 to 13.9	2.03	1.33	0.84	0.36	0.21
14 to 14.9	2.15	1.42	0.89	0.38	0.22
15 to 15.9	2.29	1.5	0.94	0.4	0.23
16 to 16.9	2.44	1.59	1	0.42	0.24
17 to 17.9	2.58	1.68	1.06	0.44	0.25
18 to 18.9	2.73	1.77	1.11	0.46	0.26
19 to 19.9	2.87	1.87	1.17	0.48	0.27

III.6. DESCRIPTION OF LASAIR (MID-RANGE)

The LASAIR model as used in the short range exercises (see Sections 2 and 3 of this publication) was described in an earlier IAEA publication [6]. This section describes the application of the LASAIR model for use with the mid-range exercise described in Section 4 of the present publication.

LASAIR was developed mainly for the purpose of simulating short term dispersion from explosive events. Even though it provides the option to use a continuous release from a stack, the different purpose of LASAIR caused certain limitations for simulations such as the Šoštanj scenario. In order to run LASAIR successfully on this scenario, several adaptations and simplifications had to be made, especially with regards to the source of release, plume rise, the duration of release and corresponding duration of the simulation, number of simulation particles, height of buildings, and the meteorological data:

III.6.1. Limitations to the number of sources

LASAIR can handle only one source per simulation, which is sufficient for Case 1 of the Šoštanj scenario (30 March 1991) where only one stack was operating. But for Case 2 (1–2 April 1991), where two stacks are operating simultaneously, it is necessary to individually simulate the dispersion from each of the two operating stacks and then in the end to add the results from both simulations.

III.6.2. Manual plume rise calculations

As plume rise calculation, especially for hot sources such as the thermal power plant in Šoštanj, is not implemented in LASAIR, the plume rise has to be added manually to the stack height. This can be done only once per simulation, and therefore this is a source of uncertainty in the results of the simulations. The plume rise to be used was determined via the calculations given in the VDI 3782/3 guidelines based on the dispersion category (as determined already for ARTM simulations in Appendix III.5) and the heat emission (Eq. (6)) for each hour of the meteorological data set [88]:

$$Q = c_p \cdot R \cdot (T - T_A) \tag{6}$$

where T and T_A (in °C) are the exhaust temperature and the ambient temperature, respectively, and c_p is the specific heat capacity for pit coal firing [88], with:

$$c_p = 1.36 \cdot 10^{-3} MW \cdot s \cdot m^{-3} \cdot K^{-1} \tag{7}$$

and

$$R = \left(\frac{d_s}{2}\right)^2 \cdot \pi \cdot \frac{273.15K}{273.15K + T_s} \tag{8}$$

R, the release volume flux in Eq. (8), is calculated based on the source diameter d_s, using the given gas flow average value $\overline{\dot{V}}$ in m^3/h. R can be calculated as in Eq. (9):

$$R = \overline{\dot{V}} \cdot \frac{273.15K}{273.15K + T \cdot \frac{K}{°C}} \tag{9}$$

Depending on Q and on the dispersion class, the plume rise for each hour was calculated. For the average plume rise to be used within LASAIR, the average of the individual plume rises was taken after ignoring the highest and lowest value each (to decrease the weight of extreme values). The final average plume rises for the Šoštanj scenario are given in Table 35. Due to the limitation in LASAIR on source heights of a maximum of 300 m, only for Stack 123 on 30 March 1991 and 2 April 1991 was it possible to insert the actual stack height plus the plume rise, since the sum on each of those two days was still below 300 m. For the other cases, the maximum value of 300 m was used, which could have affected the accuracy of the model results.

TABLE 35. DETERMINED PLUME RISE FOR THE INDIVIDUAL STACKS DURING THE TWO CASES OF THE ŠOŠTANJ RELEASE SCENARIO AS USED FOR THE INPUT INTO LASAIR

Case	Stack 123 (100 m)	Stack 5 (230 m)
Case 1 (30 March)	154.39 m	–[a]
Case 2 (1 April)	426.77 m	1126.39 m
Case 2 (2 April)	129.34 m	1007.02 m

[a] A dash (–) indicates that no information is available.

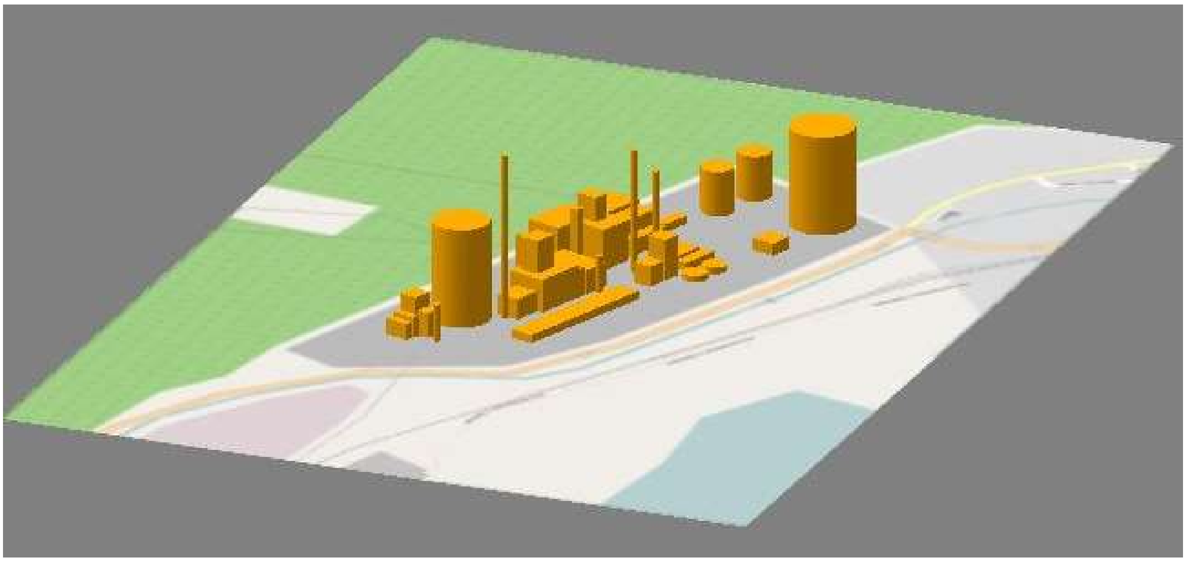

FIG. 97. LASAIR 3-D model of the Šoštanj power plant in its 1991 configuration.

III.6.3. Adaptation to the maximum simulation time

In its standard settings, LASAIR is set to a maximum of 8 h to be simulated. However, LASAIR was designed to calculate up to one day of dispersion simulation. In order to reach this, the parameter file had to be accessed manually, and the maximum simulation time set to 86 400 s. For each run of LASAIR it was necessary to load this alternative parameter file instead of the standard one.

III.6.4. Adaptation to the number of simulation particles

As a standard, LASAIR uses 60 000 simulation particles. In order to deliver comparative results to ARTM, which at the lowest level already uses 63 000 000 and at the highest 1 008 000 000 particles, the particle number in LASAIR was manually set to 1 008 000, equivalent to 0.1% of the ARTM value. Higher particle numbers in LASAIR proved to be inefficient, as the calculation time and memory needed were orders of magnitude higher. This setting also had to be implemented manually into the parameter file.

III.6.5. Limitations on the height of buildings

For the simulations where the buildings of the power plant were used, the maximum height of 200 m for buildings in LASAIR limited the correct implementation of stack 5 with its 230 m height (shown in Fig. 97).

III.6.6. Adaptation of meteorological data

Since the minimum wind speed LASAIR can accept is 0.5 m/s, every wind speed that was lower than that, had to be set at 0.5 m/s. This might introduce another uncertainty to the LASAIR results in the time resolution of the peaks.

Estimating the deviation for cases where 0.3 or 0.4 m/s had to be adjusted to 0.5 m/s for hourly time resolution shows that between 0.3 m/s and 0.5 m/s a difference in covered distance of at least 720 m exists, assuming one hour of travel time. At the resolution of the measurement locations, which are in a grid of 150 m × 150 m, means that for a 5 × 5 cell grid with 600 m width in total, the cloud can be just outside the range due to this adaptation. In time, this can shift the peak by around half an hour.

III.7. DESCRIPTION OF NFS_VINCA MODEL

The name of the model (computer code) for atmospheric diffusion, consists of the first letters of the name of the public company Nuclear Facilities of Serbia and of the geographical name of the location where the company is located near Neolithic settlement Vinca near Belgrade. The initial version of the model and code was made in the 'Laboratory for radiation and environmental protection' of Institute of Nuclear Sciences 'Vinca' and was based on USNRC regulatory guides 1.111 and 1.145 [89, 90]. In further development of the code, the structure of the Risø National Laboratory puff model was followed, as well as a number of IAEA publications [6, 91–93]. The improved version of the model was used for daily and periodic reports of safety of nuclear reactors, 'RA' in the Institute of Nuclear Sciences in Vinca.

The model has two basic modules, one for continuous releases, and one for the case of an instant release (explosion) or for a case relating to the time limited, continuous releases at the place of an accident.

Dispersion from continuous sources is modelled using a Gaussian straight line plume concept, as well as with the Gaussian puff concept, where continuous releases are viewed as a series of discrete volumes (puffs). For continuous, long term releases, using the straight line Gaussian concept, the x-axis is oriented downwind and is calculated using Eq. (10):

$$C(x,y,z) = \frac{Q}{2\pi\sigma_y\sigma_z u}\exp\left(-\frac{1}{2}\frac{y^2}{\sigma_y^2}\right)\left\{\exp\left[-\frac{1}{2}\frac{(z-H)^2}{\sigma_z^2}\right] + \exp\left[-\frac{1}{2}\frac{(z+H)^2}{\sigma_z^2}\right]\right\} \tag{10}$$

For short term releases, using the puff concept, the y-axis is oriented to the north (N), and Eq. (11) is used:

$$C(x,y,z,t) = \frac{q}{\sqrt{(2\pi)^3}\sigma_x\sigma_y\sigma_z}\exp\left\{-\left[\frac{(x-x_0)^2}{2\sigma_x^2}+\frac{(y-y_0)^2}{2\sigma_y^2}\right]\right\} \times \left\{\exp\left[-\frac{(z-z_0)^2}{2\sigma_z^2}\right] + \exp\left[\frac{(z+z_0)^2}{2\sigma_z^2}\right]\right\} \tag{11}$$

where:

x_0, y_0, z_0	are the coordinates of the center of each individual puff at time t (m);
x, y, z	are the coordinates of calculation points (m);
Q	is the source strength (mass or activity per unit time) of a continuous release, with units such as t/h or Bq/s);
q	is the mass or activity in the puff (e.g. t or Bq, corresponding to the units of Q);
σ_x, σ_y, σ_z	are the diffusion parameters in the x, y and z directions (m);
H	is the height above the calculation point of the plume axis or puff center (m);
u	is the wind speed at the effective height (m/s).

Parameters σ_x, σ_y, and σ_z in the model are calculated as Briggs sigma values for continuous release, as a function of downwind distance from the source and of atmospheric stability (Table 36, see Ref. [94]):

TABLE 36. BRIGGS DISPERSION PARAMETERS σ_y, σ_z FOR CONTINUOUS RELEASES (rural terrain, 10^2 m $\leq x \leq 10^4$ m) ([94])

Pasquill stability class	σ_y (m)	σ_z (m)
A	$0.22x(1 + 0.0001x)^{-0.5}$	$0.20x$
B	$0.16x(1 + 0.0001x)^{-0.5}$	$0.12x$
C	$0.11x(1 + 0.0001x)^{-0.5}$	$0.08x(1 + 0.0002x)^{-0.5}$
D	$0.08x(1 + 0.0001x)^{-0.5}$	$0.06x(1 + 0.0015x)^{-0.5}$
E	$0.06x(1 + 0.0001x)^{-0.5}$	$0.03x(1 + 0.0003x)^{-1}$
F	$0.04x(1 + 0.0001x)^{-0.5}$	$0.016x(1 + 0.0003x)^{-1}$

In the case of short term releases, the sigma parameters in the puff model use Taylor's theorem [95] and have the following form:

$$\sigma_{puff} = \left(\overline{v^2}\right)^{0.5} t, \text{ for } t \ll \tau_L \tag{12}$$

and

$$\sigma_{puff} \cong \left(\overline{v^2}\tau_L\right)^{0.5} t^{0.5}, \text{ for } t \gg \tau_L \tag{13}$$

where:

τ_L is the Lagrangian integral time scale;
$\overline{v^2}$ is the Eulerian velocity variance [96].

Each individual puff spreads around its own center in accordance with the change of values for the diffusion parameters σ_{puff}, which differ from the diffusion parameters σ_{plume} under which the plume extends laterally downwind, relative to its axis of propagation (Fig. 98).

For the case when a continuous release is seen as a series of puffs, it was assumed that $\sigma_{puff} = \sigma_{plume}$.

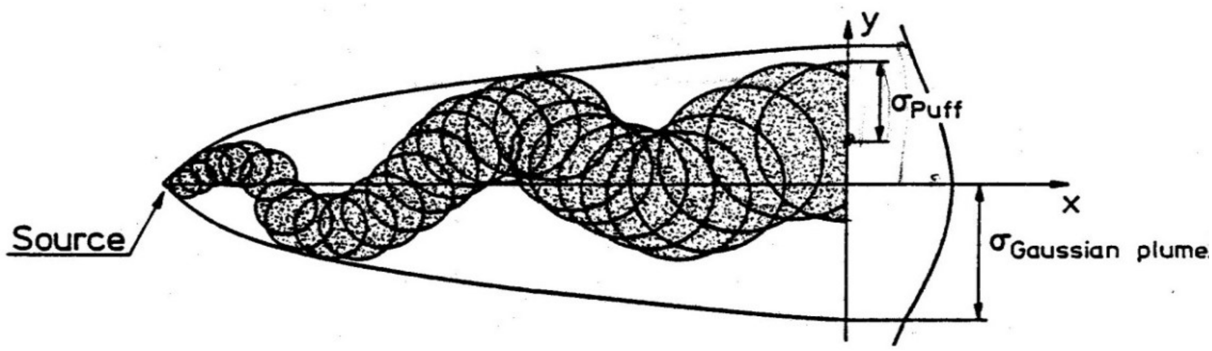

FIG. 98. Puff modelling principles relevant for dispersion calculations [97].

Both the plume and puff dispersion subroutines of the NFS_Vinca model use modules for:

- Stability category [98–100];
- Effective source height [101];
- Modification of height of plume axis or puff centre over calculation points, following terrain height [32, 102];
- Modification of height for heavy gases and particles [103];
- Wind speed at source height (wind power law) [104];
- Dry and wet deposition [105–107];
- Wind induced resuspension [108];
- Dose calculation from inhalation, cloud-shine (submersion) and ground-shine [109].

REFERENCES

[1] INTERNATIONAL ATOMIC ENERGY AGENCY. Environmental Modelling of Remediation of Urban Contaminated Areas. Report of the Urban Remediation Working Group of the EMRAS (Environmental Modelling for Radiation Safety) Programme (2012), In: INTERNATIONAL ATOMIC ENERGY AGENCY. Environmental Modelling for Radiation Safety (EMRAS), A Summary Report of the Results of the EMRAS Programme (2003–2007), IAEA-TECDOC-1678, IAEA, Vienna (2012).

[2] THIESSEN, K.M., BATANDJIEVA, B., ANDERSSON, K.G., ARKHIPOV, A., CHARNOCK, T.W., GALLAY, F., GASCHAK, S., GOLIKOV, V., HWANG, W.T., KAISER, J.C., KAMBOJ, S., STEINER, M., TOMÁS, J., TRIFUNOVIC, D., YU, C., ZELMER, R., ZLOBENKO, B., Improvement of modelling capabilities for assessing urban contamination: The EMRAS Urban Remediation Working Group, Appl. Radiat. Isot. **66** (2008) 1741–1744.

[3] THIESSEN, K.M., ARKHIPOV, A., BATANDJIEVA, B., CHARNOCK, T.W., GASCHAK, S., GOLIKOV, V., HWANG, W.T., TOMÁS, J., ZLOBENKO, B., Modelling of a large-scale urban contamination situation and remediation alternatives, J. Environ. Radioact. **100** (2009) 413–421.

[4] THIESSEN, K.M., ANDERSSON, K.G., BATANDJIEVA, B., CHENG, J.-J., HWANG, W.T., KAISER, J.C., KAMBOJ, S., STEINER, M., TOMÁS, J., TRIFUNOVIC, D., YU, C., Modelling the long-term consequences of a hypothetical dispersal of radioactivity in an urban area including remediation alternatives, J. Environ. Radioact. **100** (2009) 445–455.

[5] THIESSEN, K.M., ANDERSSON, K.G., CHARNOCK, T.W., GALLAY, F., Modelling remediation options for urban contamination situations, J. Environ. Radioact. **100** (2009) 564–573.

[6] INTERNATIONAL ATOMIC ENERGY AGENCY, Assessment of Radioactive Contamination in Urban Areas, Report of Working Group 9, Urban Areas of the EMRAS II Topical Heading Approaches to Assessing Emergency Situations, Environmental Modelling for Radiation Safety (EMRAS II) Programme, IAEA-TECDOC-1941, IAEA, Vienna (2021).

[7] THIESSEN, K.M., ANDERSSON, K.G., BERKOVSKYY, V., CHARNOCK, T.W., CHOUHAN, S.L., De WITH, G., ĎÚRAN, J., FUKA, V., HELEBRANT, J., HŮLKA, J., HWANG, W.T., KUČA, P., MANCINI, F., NAVARRO, E., PERIÁÑEZ, R., PROUZA, Z., SDOUZ, G., TOMÁS, J., TRIFUNOVIĆ, D., URSO, L., WALTER H., Assessing emergency situations and their aftermath in urban areas: The EMRAS II Urban Areas Working Group, Radioprotection **46** (2011) S601–S607.

[8] THIESSEN, K.M., CHARNOCK, T.W., CHOUHAN, S.L., HWANG, W.T., KAMBOJ, S., TOMÁS, J., YU, C., Modeling the effectiveness of remediation efforts in contaminated urban areas: An EMRAS II Urban Areas Working Group exercise, In: Proceedings of the WM2015 Conference, March 15–19, 2015, paper #15631 (2015).

[9] PROUZA, Z., BECKOVA, V., CESPIROVA, I., HELEBRANT, J., HULKA, J., KUCA, P., MICHALEK, V., RULIK, P., SKRKAL, J., HOVORKA, J., Field tests using radioactive matter, Radiat. Prot. Dosim. **139** (2010) 519–531.

[10] LEE, S., WOLBERG, G., SHIN, S.Y., Scattered data interpolation with multilevel B-splines, IEEE Transactions on Visualization and Computer Graphics **3** (1997) 228–244.

[11] TINARELLI, G., MORTARINI, L., TRINI-CASTELLI, S., CARLINO, G., MOUSSAFIR, J., OLRY, C., ARMAND, P., ANFOSSI, D., Review and validation of Micro-SPRAY, a Lagrangian particle model of turbulent dispersion, In Lagrangian Modeling of the Atmosphere, Geophysical Monograph, Volume 200, AGU (2013) 311–328.

[12] OLDRINI, O., NIBART, M., ARMAND, P., OLRY, C., MOUSSAFIR, J., ALBERGEL, A., Multi-scale build-up area integration in Parallel SWIFT, Proceedings of the Harmo' 15 Conference, May 6–9, 2013, Madrid, Spain (2013) 485–489.

[13] HIRSCH, C., Numerical Computation of Internal and External Flows: The Fundamentals of Computational Fluid Dynamics, Second Edition, Elsevier (2007).

[14] JANICKE, L., Particle Simulation of Inhomogeneous Turbulent Diffusion, Air Pollution Modelling and its Application (Weber (Ed.)), Plenum Press, NY (1983) 527–535.

[15] JANICKE, L., Particle simulation of Dust Transport and Deposition and Comparison with Conventional Models, Air Pollution Modelling and its Application, IV, C. de Wispelaere (Ed.), Plenum Press, NY (1985) 759–769.

[16] WALTER, H., Handling "Dirty Bomb" Scenarios with the Lagrangian Particle Model LASAIR, In: Proceedings of the 12th International Conference on Harmonisation within Atmospheric Dispersion Modelling for Regulatory Purposes, Cavtat, Croatia, 6–9 October 2008 (2008).

[17] WALTER, H., HEINRICH, G., Quick and clean: Dirty bomb scenarios evaluated with the decision support system LASAIR. International Conference on Radioecology and Environmental Radioactivity (ICRER 2011), Hamilton, Canada (2011).

[18] WALTER, H., HEINRICH, G., The decision support system LASAIR: New features for evaluating dirty bomb scenarios, Proceedings of the 16th International Conference on Harmonisation within Atmospheric Dispersion Modelling for Regulatory Purposes, 8–11 September 2014, Varna, Bulgaria (2014).

[19] VON ARX, C., GLAAB, H., GRIMM, C., PÄSLER-SAUER, R.J., SCHEUERMANN, W., SCHNADT, H., SCHUMACHER, P., TORCHIANI, S., WALTER, H., WILBOIS, T., Vergleich aktuell eingesetzter Modelle zur Beschreibung der atmosphärischen Ausbreitung radioaktiver Stoffe, Abschlussbericht zum Arbeitspaket AP 5500 im Projekt A 510 der Strahlenschutzkommission, Germany (2016) (in German).

[20] VEREIN DEUTSCHER INGENIEURE, Richtlinie 3783, Blatt 8, Umweltmeteorologie, Messwertgestützte Turbulenzparametrisierung für Ausbreitungsmodelle, Environmental meteorology – Turbulence parameters for dispersion models supported by measurement data, VDI 3783, 15 (2017) (in German and English).

[21] GRAŠIČ, B., MLAKAR, P., BOŽNAR, M.Z., Method for Validation of Lagrangian Particle Air Pollution Dispersion Model Based on Experimental Field Data Set from Complex Terrain, Advanced Air Pollution, Dr. Farhad Nejadkoorki (Ed.) (2011). Available from: http://www.intechopen.com/books/advanced-air-pollution/method-for-validation-of-lagrangian-particle-air-pollution-dispersion-model-based-on-experimental-fi

[22] GRAŠIČ, B., BOŽNAR, M.Z., MLAKAR, P., Re-evaluation of the Lagrangian particle modelling system on an experimental campaign in complex terrain, Il Nuovo Cimento C, Vol. 30, No. 6 (2007) 557–575.

[23] BLUMEN, W., BANTA, R.M., BERRI, G., CARRUTHERS, D.J., DALU, G.A., DURRAN, D.R., EGGER, J., GARRATT, J.R., HANNA, S.R., HUNT, J.C.R., MERONEY, R.N., MILLER, W., NEFF, W.D., NICOLINI, M., PAEGLE, J., PIELKE, R.A., SMITH, R.B., STRIMAITIS, D.G., VUKICEVIC, T., WHITEMAN, C.D., Atmospheric processes over complex terrain. Meteorological monographs, Vol. 23, No. 45, American Meteorological Society, Boston, MA (1990).

[24] ELISEI, G., BISTACCHI, S., BOCCHIOLA, G., BRUSASCA, G., MARCACCI, P., MARZORATI, A., MORSELLI, M.G., TINARELLI, G., CATENACCI, G., CORIO, V., DAINO, G., ERA, A., FINARDI, S., FOGGI, G., NEGRI, A., PIAZZA, G., VILLA, R., LESJAK, M., BOŽNAR, M., MLAKAR, P., SLAVIC, F., Experimental campaign for the environmental impact evaluation of Sostanj thermal power plant, Progress Report, ENEL S.p.A, CRAM-Servizio Ambiente, Milano, Italy, C.I.S.E. Tecnologie Innovative S.p.A, Milano, Italy, Institute Jozef Stefan, Ljubljana, Slovenia (1991).

[25] BRUSASCA, G., TINARELLI, G., ANFOSSI, D., Particle model simulation of diffusion in low windspeed stable conditions, Atmos. Environ. **26** (1992) 707–723.

[26] BOŽNAR, M., BRUASCA, G., CAVICCHIOLI, C., FAGGIAN, P., FINARDI, S., MINELLA, M., MLAKAR, P., MORSELLI, M.G., SOZZI, R., Model evaluation and application of advanced and traditional Gaussian models on the experimental Šoštanj (Slovenia, 1991) campaign, Cuvelier, C., (Ed.), Intercomparison of Advances Practical Short-Range Atmospheric Dispersion Models: Proceedings of the Workshop, August 30 – September 3, 1993, Manno-Switzerland (Joint Research Centre, EUR 15603 EN) Brussels, ECSC-EEC-EAEC (1993) 112–121.

[27] BOŽNAR, M., BRUSASCA, G., CAVICCHIOLI, C., FAGGIAN, P., FINARDI, S., MLAKAR, P., MORSELLI, M.G., SOZZI, R., TINARELLI, G., Application of advanced and traditional diffusion models to an experimental campaign in complex terrain, Baldasano, J.M. (Ed.), Second International Conference on Air Pollution, Barcelona, Spain, 1994, Air Pollution II, Volume 1, Computer simulation, Southampton; Boston: Computational Mechanics Publications (1994) 159–166.

[28] MLAKAR, P., BOŽNAR, M.Z., GRAŠIČ, B., BRUSASCA, G., TINARELLI, G., MORSELLI, M.G., FINARDI, S., Air pollution dispersion models validation dataset from complex terrain in Šoštanj, Int. J. Environ. Pollu. **57**(3/4) (2015) 227–237.

[29] MLAKAR, P., BOŽNAR, M.Z., Artificial Neural Networks – a Useful Tool in Air Pollution and Meteorological Modelling, Advanced Air Pollution, Dr. Farhad Nejadkoorki (Ed.) (2011).

[30] MONIN, A.S., OBUKHOV, A.M., Basic laws of turbulent mixing in the surface layer of the atmosphere, Tr. Akad. Nauk SSSR Geofiz. Inst. **24** (1954) 163–187.

[31] VEREIN DEUTSCHER INGENIEURE, Richtlinie 3782, Blatt 6, Unweltmeteorologie, Atmosphärische Ausbreitungsmodelle, Bestimmung der Ausbreitungsklassen nach Klug/Manier, Environmental meteorology – atmospheric dispersion models, Determination of Klug/Manier dispersion categories, VDI 3782, 6 (2017) (in German and English).
Available at:
https://www.vdi.de/fileadmin/pages/vdi_de/redakteure/richtlinien/inhaltsverzeichnisse/2601276.pdf

[32] EGAN, B.A., Turbulent Diffusion in Complex Terrain, In: Lectures on Air Pollution and Environmental Impact Analyses, D. Haugen (Ed.), American Meteorological Society, Boston, MA (1975) 112–135.

[33] GRŠIĆ, Z.J., PAVLOVIĆ, S., ARBUTINA, D., DRAMLIĆ, S.D., DRAMLIĆ, D.M., NIKEZIĆ, D., DIMOVIĆ, S., KALJEVIĆ, J., MILINCIC, M., Environmental Impact Assessment of the Nuclear Reactor in Vinca, Based on the Data on Emission of Radioactivity from the Literature – A Modeling Approach, Chemical Industry and Chemical Engineering Quarterly, CICEQ, 21(1) (2015) 189–199.

[34] GRSIC, Z., MILUTINOVIC, P., RAJKOVIC, B., DRAMLIC, D., VELIKIC, Z., DRAMLIC, S., Ash dust concentration in the vicinity of ash disposal site, depending on the size of pond (“Water mirror”), Chemical Industry and Chemical Engineering Quarterly, 16(3) (2010) 243–249.

[35] MILUTINOVIĆ, P., GRSIĆ, Z., ZIVKOVIC, N., DRAMLIC, D., VELIKIC, Z., DRAMLIC, S., System for automatically preventing the raising of ash from dedicated landfills, Chemical Industry and Chemical Engineering Quarterly, 18(4) (2012) 681–692.

[36] NIKEZIC, D.P., LONCAR, B.B., GRSIC, Z., DIMOVIC, S., Mathematical modeling of environmental impacts of a reactor through the air, Nuclear Technol. and Radiat. Protect. 29(4) (2014) 268–273.

[37] GRŠIĆ, Z., DRAMLIĆ, D., DRAMLIC, S., ABUTINA, D., NIKEZIĆ, D., DIMOVIĆ, S., JOKSIMOVIC, D., Verification mathematical models for atmospheric dispersion under IAEA programme MODARIA, XXVIII Simpozijum Društva za zaštitu od zračenja Srbije i Crne Gore, Vrsac, Serbia (2015).

[38] RICHTER, C., SOGALLA, M., THIELEN, H., MARTENS, R., Atmosphärisches Radionuklid-Transport-Modell mit Radon Postprozessor und SBG-Modul Modellbeschreibung zu Version 2.8.0[13]. Gesellschaft für Anlagen- und Reaktorsicherheit, Stand 2015-04-20 (2015) (in German).
Available at: https://docplayer.org/23244931-Artm-atmosphaerisches-radionuklid-transport-modell-mit-radon-posprozessor-und-sbg-modul-modellbeschreibung-zu-version.html

[13] At the time of the modelling work being carried out, Version 2.7.2 (2013) of this software was used, which has since been superseded by a newer version.

[39] JANICKE, U., JANICKE, L., Lagrangian Particle Modelling for Regulatory Purposes – A Survey of Recent Developments in Germany, Proceedings of the 11th International Conference on Harmonisation within Atmospheric Dispersion Modelling for Regulatory Purposes (2011).

[40] UNITED STATES ENVIRONMENTAL PROTECTION AGENCY, Meteorological Monitoring Guidance for Regulatory Modeling Applications, EPA-454/R- 99-005 (2000).

[41] UNITED STATES NUCLEAR REGULATORY COMMISSION, Regulatory Guide 1.23: Meteorological Monitoring Programs for Nuclear Power Plants, Rev. 1. Office of Nuclear Regulatory Research, Washington (2007).

[42] BOŽNAR, M., MLAKAR, P., GRAŠIČ, B., Short-term fine resolution WRF forecast data validation in complex terrain in Slovenia, In: Special issue on harmonization within the atmospheric dispersion modelling for regulatory purposes, 26 October 2011, Kos Island, Greece, Int. J. Environ. Pollu. **50**(1/4) (2012) 12–21.

[43] MINISTRY OF LAND, INFRASTRUCTURE, TRANSPORT AND TOURISM OF JAPAN, National Land Numerical Information Land utilization segmented mesh Data 2009, MLIT (2014) (in Japanese).
Available at: http://nlftp.mlit.go.jp/ksj/gml/datalist/KsjTmplt-L03-b.html

[44] MINISTRY OF INTERNAL AFFAIRS AND COMMUNICATIONS, Portal Site of Official Statistics of Japan, MIC (2014) (in Japanese).
Available at: http://www.e-stat.go.jp/SG1/estat/eStatTopPortal.do

[45] JAPAN CHEMICAL ANALYSIS CENTER, General Overview of Survey Results on Environmental Radioactivity Levels of Fiscal Year of 2009, JCAC (2011) (in Japanese).

[46] UNITED NATIONS SCIENTIFIC COMMITTEE ON THE EFFECTS OF ATOMIC RADIATION, Sources, Effects and Risks of Ionizing Radiation, UNSCEAR 2013 Report; Scientific Annex A: Levels and effects of radiation exposure due to the nuclear accident after the 2011 great east–Japan Earthquake and Tsunami, UNSCEAR (2013).

[47] WORLD HEALTH ORGANIZATION, Preliminary dose estimation from the nuclear accident after the 2011 Great East Japan Earthquake and Tsunami, WHO (2012).
Available at: http://apps.who.int/iris/bitstream/10665/44877/1/9789241503662_eng.pdf

[48] TOKYO ELECTRIC POWER COMPANY, Measurement data inside Fukushima Daini nuclear power plant, TEPCO (2011) (in Japanese).
Available at: http://www.tepco.co.jp/nu/fukushima-np/f2/indexold-j.html

[49] JAPAN METEOROLOGICAL AGENCY, Search of meteorological data of the past, JMA (2014) (in Japanese).
Available at: http://www.data.jma.go.jp/obd/stats/etrn/index.php

[50] MINISTRY OF INTERNAL AFFAIRS AND COMMUNICATIONS, Census of 2010, MIC (2010) (in Japanese).
Available at: http://www.stat.go.jp/data/kokusei/2010/index2.htm

[51] MINISTRY OF EDUCATION, CULTURE, SPORTS, SCIENCE AND TECHNOLOGY, The seventh conference for preparation of distribution map of radioactivity, MEXT (2011) (in Japanese).
Available at:
http://www.mext.go.jp/b_menu/shingi/chousa/gijyutu/017/shiryo/1310688.htm

[52] NUCLEAR REGULATORY AUTHORITY, Database of the Research of Radioactive Substances Distribution, NRA (2011).
Available at: radb.jaea.go.jp/mapdb_prev/en/

[53] JAPAN ATOMIC ENERGY AGENCY, Remediation of contaminated areas in the aftermath of the accident at the Fukushima Dai-ichi Nuclear Power Plant: Overview, analysis and lessons learned, Volume 1: A report on the 'Decontamination Pilot Project', JAEA, JAEA-Review 2014-051 (2014).

[54] NUCLEAR REGULATORY AUTHORITY, Survey on distributions of radioactive materials. Nuclear Regulatory Authority (2014) (in Japanese). Available at: http://radioactivity.nsr.go.jp/ja/list/338/list-1.html

[55] MINISTRY OF ECONOMY, TRADE AND INDUSTRY, Roadmap for the settlement of the nuclear power plant accident, METI (2014) (in Japanese).
Available at: http://www.meti.go.jp/earthquake/nuclear/release.html

[56] NUCLEAR REGULATORY AUTHORITY, Monitoring information of environmental radioactive level: Readings of dust sampling, NRA (2014).
Available at: http://radioactivity.nsr.go.jp/en/list/200/list-1.html

[57] TAKAHARA, S., IIJIMA, M., SHIMADA, K., KUSHIDA, T., SHIRATORI, Y., Development of Deterministic Approach to Assess Doses to the Public from External Exposures in the Areas Contaminated by the Fukushima Daiichi Nuclear Power Station Accident, Japan Atomic Energy Agency, JAEA-Research 2014-024 (2014).

[58] JONES, J.A., CHARNOCK, T.W., SINGER, L.N., ROED, J., ANDERSSON, K.G., THYKIER-NIELSEN, S., MIKKELSEN, T., ASTRUP, P., KAISER, J.C., MÜLLER, H., PRÖHL, G., RASKOB, W., HOE, S.C., JACOBSEN, L.H., SCHOU-JENSEN, F., GERING, F., Description of the Modelling of Transfer and Dose Calculations within ERMIN v1.0 and associated Data Libraries, Chilton, UK, EURANOS(CAT2)-TN(05)-04 (2007).

[59] CHARNOCK, T.W., JONES, J.A., SINGER, L.N., ANDERSSON, K.G., ROED, J., THYKIER-NIELSEN, S., MIKKELSEN, T., ASTRUP, P., KAISER, J.C., MÜLLER, H., PRÖHL, G., RASKOB, W., HOE, S.C., JACOBSEN, L.H., SCHOU-JESEN, L., GERING, F., Calculating the consequences of recovery, a European Model for Inhabited Areas, In: Proceedings of the International Conference of Radioecology and Environmental Radioactivity, Bergen, Norway, 15–20 June 2008, Radioprotection **44** (2009) 407–412.

[60] IEVDIN, I., TRYBUSHNY, D., ZHELEZNYAK, M., RASKOB, W., RODOS re-engineering: Aims and implementation details, Radioprotection **45** (2010) S181–S189.

[61] JACOBSEN, L.H., ANDERSSON, K.G., CHARNOCK, T.W., KAISER, J.C., GERING, F., HOE, S.C., LARSEN, L.J., Implementation in ARGOS of ERMIN and AGRICP, Radioprotection **45** (2010) S191–S198.

[62] BROWN, J., MORTIMER, K., ANDERSSON, K.G., DURANOVA, T., MRSKOVA, A., HÄNNINEN, R., IKÄHEIMONEN, T., KIRCHNER, G., BERTSCH, V., GALLAY, F., REALES, N., Generic handbook for assisting in the management of inhabited areas in Europe following a radiological emergency, Parts I–V, Chilton, UK, EURANOS(CAT1)-TN(07)-02 (2007).

[63] BURSON, Z.G., PROFIO, A.E., Structure shielding in reactor accidents. Health Physics **33** (1977) 287–299.

[64] FACKRELL, J.E., An examination of simple models for building influenced dispersion, Atmos. Environ. **18** (1984) 89–98.

[65] ANDERSSON, K.G., MIKKELSEN, T., ASTRUP, P., THYKIER-NIELSEN, S., JACOBSEN, L.H., SCHOU-JENSEN, L., HOE, S.C., NIELSEN, S.P., Estimation of health hazards resulting from a radiological terrorist attack in a city, Radiat. Prot. Dosim. **131** (2008) 297–307.

[66] TINARELLI, G., ANFOSSI, D., BIDER, M., FERRERO, E., TRINI CASTELI, S., A new high performance version of Lagrangian particle dispersion model SPRAY, some case studies, Air Pollution Modelling and Its Applications XIII, S.E. Gryning and E. Batchvarova (Eds.), Kluwer Academic/Plenum Press, New York (2000) 499–507.

[67] ANFOSSI, D., DESIATO, F., TINARELLI, G., BRUSASCA, G., FERRERO, E., SACCHETTI, D., TRANSALP 1989 experimental campaign—II. Simulation of a tracer experiment with Lagrangian particle models, Atmos. Environ. 32(7) (1998) 1157–1166.

[68] GRAŠIČ, B., BOŽNAR, M.Z., MLAKAR, P., TINARELLI, G., Re-evaluation of the Lagrangian particle modelling system on an experimental campaign in complex terrain, Nuovo Cimento- Societa Italiana Di Fisica Sezione C, 30(6) (2007) 557–575.

[69] GRAŠIČ, B., MLAKAR, P., BOŽNAR, M.Z., Method for validation of Lagrangian particle air pollution dispersion model based on experimental field data set from complex terrain, In Dr. F. Nejadkoorki (Ed.), Advanced air pollution (2011) 535–556.

[70] THOMSON, D.J., Criteria for the selection of stochastic models of particle trajectories in turbulent flows, J. Fluid Mech. **180** (1987) 529–556.

[71] ANFOSSI, D., FERRERO, E., BRUSASCA, G., MARZORATI, A., TINARELLI, G., A simple way of computing buoyant plume rise in Lagrangian stochastic dispersion models, Atmos. Environ. **27A** (1993) 1443–1451.

[72] MOUSSIOPOULOS, N., FLASSAK, T.H., KNITTEL, G.A., A refined diagnostic wind model, Environ. Soft. **3** 2 (1988) 85–94.

[73] LOUIS, J.F., A parametric model of vertical eddy fluxes in the atmosphere, Bound. Lay. Met. **17** (1979) 187–202.

[74] MCGUIRE, S.A., RAMSDELL, J.V., JR, ATHEY, G.F., RASCAL 3.0.5: Description of Models and Methods, U.S. Nuclear Regulatory Commission, NUREG-1887 (2007).

[75] BANDER, T.J., PAVAN, An Atmospheric Dispersion Program for Evaluating Design Basis Accidental Releases for Radioactive Materials from Nuclear Power Stations, U.S. Nuclear Regulatory Commission, NUREG/CR-2858 (1982).

[76] SAGENDORF, J.F., GOLL, J.T., SANDUSKY, W.F., XOQDOQ: Computer Program for the Meteorological Evaluation of Routine Effluent Releases at Nuclear Power Stations, U.S. Nuclear Regulatory Commission, NUREG/CR-4380 (1982).

[77] SCHERPELZ, R.I., et al., The Mesorad Dose Assessment Model, Vol. 1, U.S. Nuclear Regulatory Commission, NUREG/CR-4000 (1986).

[78] RAMSDELL, J.V., JR, et al., The MESORAD Dose Assessment Model, Vol. 2: Computer Code, U.S. Nuclear Regulatory Commission, NUREG/CR-4000, (1988).

[79] ATHEY, G.F., et al., RASCAL Version 2.0 User's Guide, Vol. 1, Rev. 1, U.S. Nuclear Regulatory Commission, NUREG/CR-5247 (1993).

[80] SJOREEN, A.L., RAMSDELL, J.V., JR, MCKENNA, T.J., MCGUIRE, S.A., FOSMIRE, C., ATHEY, G.F., RASCAL 3.0: Description of Models and Methods, U.S. Nuclear Regulatory Commission, NUREG-1741 (2001).

[81] GIFFORD, F.A., Turbulent diffusion-typing schemes: A review, Nucl. Saf. **17** (1976) 68–86.

[82] EIMUTIS, E.C., KONICEK, M.G., Derivations of continuous functions for the lateral and vertical atmospheric dispersion coefficients, Atmos. Environ. **6** (1972) 859–863.

[83] TADMORE, J., GUR, Y., Analytical expressions for vertical and lateral dispersion coefficients in atmospheric diffusion, Atmos. Environ. **3** (1969) 688–698.

[84] MARTIN, D.O., TIKVART, J.A., A general atmospheric diffusion model for estimating the effects on air quality of one or more source, In: 61st Annual Meeting of the Air Pollution Control Association for NAPCA, St. Paul, MN (1968).

[85] JANICKE CONSULTING, AUSTAL2000 Program Documentation of Version 2.5, ibj: austal2000/2.5/doc/austal2000 — 2011-08-01 (2011).

[86] RICHTER, C., SOGALLA, M., THIELEN, H., MARTENS, R., Atmosphärisches Radionuklid-Transport-Modell mit der graphischen Benutzeroberfläche GO-ARTM Programmbeschreibung zu Version 2.7.2 (GO-ARTM Version 2.0), Gesellschaft für Anlagen- und Reaktorsicherheit, 2013-12-16 (2013) (in German).

[87] KTA 1508 Fassung 11/06, Instrumentierung zur Ermittlung der Ausbreitung radioaktiver Stoffe in der Atmosphäre. Sicherheitstechnische Regel des KTA Fassung 11/06, BAnz-Nr. 37a (2006, earlier version: 22nd February 1989) (in German).

[88] VEREIN DEUTSCHER INGENIEURE, Richtlinie 3782, Blatt 3, Ausbreitung von Luftverunreinigungen in der Atmosphäre; Berechnung der Abgasfahnenüberhöhung, VDI 3782, 3 (1985) (in German and English).

[89] UNITED STATES NUCLEAR REGULATORY COMMISSION, Regulatory Guide 1.111: Methods for Estimating Atmospheric Transport and Dispersion of Gaseous Effluents in Routine Releases from Light-Water-Cooled Reactors, Office of Nuclear Regulatory Research, Washington (1976).

[90] UNITED STATES NUCLEAR REGULATORY COMMISSION, Regulatory Guide 1.145: Atmospheric Dispersion Models for Potential Accident Consequence Assessments at Nuclear Power Plants, Office of Nuclear Regulatory Research, Washington (1982).

[91] INTERNATIONAL ATOMIC ENERGY AGENCY, Testing of environmental transfer models using data from the atmospheric release of Iodine-131 from the Hanford site, USA, in 1963, Report of the Dose Reconstruction Working Group of the Biosphere Modelling and Assessment (BIOMASS) Programme, Theme 2 (IAEA-BIOMASS-2), IAEA, Vienna (2003).
Available from: https://www-pub.iaea.org/MTCD/Publications/PDF/Biomass2_web.pdf

[92] INTERNATIONAL ATOMIC ENERGY AGENCY, Environmental Modelling for Radiation Safety (EMRAS). A Summary Report of the Results of the EMRAS Programme (2003–2007), IAEA-TECDOC-1678, IAEA, Vienna (2012).

[93] INTERNATIONAL ATOMIC ENERGY AGENCY, Transfer of Tritium in the Environment after Accidental Releases from Nuclear Facilities, Report of Working Group 7 Tritium Accidents of EMRAS II Topical Heading Approaches for Assessing Emergency Situations, Environmental Modelling for Radiation Safety (EMRAS II) Programme, IAEA-TECDOC-1738, IAEA, Vienna (2014).

[94] BRIGGS, G.A., Diffusion Estimation for Small Emissions, in Environmental Research Laboratories, Air Resources Atmosphere Turbulence and Diffusion Laboratory, 1973 Annual Report, USAEC Report ATDL-106, National Oceanic and Atmospheric Administration, December 1974 (1974).

[95] TAYLOR, G.I., Diffusion by continuous movements, Proc. Royal Soc. London **20** (1921) 196–211.

[96] PELTIER, L.J., HAUPT, S.E., WYNGAARD, J.C., STAUFFER, D.R., DENG, A., LEE, J.A., LONG, K.J., ANNUNZIO, A.J., Parameterizing mesoscale wind uncertainty for dispersion modeling, J. Appl. Meteorol. Climat. **49** (2010) 1604–1614.

[97] MIKKELSEN, T., LARSEN, S.E., TROEN, I., Some Puff Modelling Principles Relevant for Dispersion Calculations in the Atmosphere, RISO-M-2258 (1980).

[98] INTERNATIONAL ATOMIC ENERGY AGENCY, Dispersion of Radioactive Material in Air and Water and Consideration of Population Distribution in Site Evaluation for Nuclear Power Plants, Specific Safety Guides, IAEA Safety Standards Series No. NS-G-3.2, IAEA, Vienna (2002).

[99] PASQUILL, F., SMITH, F.B., Atmospheric Diffusion, 3rd Edition, Wiley, New York (1983) 437 pp.

[100] INTERNATIONAL ATOMIC ENERGY AGENCY, UNITED NATIONS ENVIRONMENT PROGRAMME, Regulatory Control of Radioactive Discharges to the Environment, IAEA Safety Standards Series No. GSG-9, IAEA, Vienna (2018).

[101] KORSAKISSOK, I., MALLET, V., Comparative study of Gaussian dispersion formulas within the Polyphemus platform: Evaluation with prairie grass and Kincaid experiments, J. Appl. Meteorol. Climat. **48** (2009) 2459–2473.

[102] WITTEK, P., A survey of atmospheric dispersion models applicable to risk studies for nuclear facilities in complex terrain, KfK 3870 (1985).

[103] OVERCAMP, T.J., A general Gaussian diffusion-deposition model for elevated point sources, J. Appl. Meteorol. **15** (1976) 1167–1171.

[104] IRWIN, J.S., A theoretical variation of the wind profile power-law exponent as a function of surface roughness and stability, Atmos. Environ. **13** (1979) 191–194.

[105] SEINFELD, J.H., PANDIS, S.N., Atmospheric Chemistry and Physics, Wiley Interscience, New York (1998).

[106] CHAMBERLAIN, A.C., Aspects of travel and deposition of aerosol and vapor clouds, Atomic Energy Research Establishment HP/R 1261, Harwell, UK (1953) 33 pp.

[107] CHAMBERLAIN, A.C., Radioactive Aerosols, Cambridge University Press, Cambridge, UK (1991).

[108] MARTICORENA, B., BERGAMETTI, G., AUMONT, B., CALLOT, Y., N'DOUME, C., LEGRAND, M., Modeling the atmospheric dust cycle: 2, Simulations of Saharan dust sources, J. Geophys. Res. **102** (1997) 4387–4404.

[109] INTERNATIONAL ATOMIC ENERGY AGENCY, Safety Assessment for Decommissioning, Safety Reports Series No. 77, Annex I, Part B, IAEA, Vienna (2013).

LIST OF ABBREVIATIONS

2-D	Two dimensional
3-D	Three dimensional
ARGOS	Accident Reporting and Guidance Operating System
ARTM	Atmospheric Radionuclide Transport Model
BfS	German Federal Office for Radiation Protection
BMU	German Federal Ministry for Environment, Nature Conservation, and Nuclear Safety
CFD	Computational fluid dynamics
DIAL	Differential absorption lidar
DTU-RISØ	Technical University of Denmark
ECMWF	European Center for Medium-Range Weather Forecasts
EIS	Environmental Information System
EMRAS	IAEA programme Environmental Modelling for Radiation Safety, 2003–2007
EMRAS II	Follow-up to EMRAS, 2009–2011
ERMIN	European Model for Inhabited Areas
GIS	Geographic information system
GM	Geometric mean
GPV	Grid point value
GRS	Gesellschaft für Anlagen- und Reaktorsicherheit
GSD	Geometric standard deviation
IAEA-TECDOC	International Atomic energy Agency Technical Documents
JAEA	Japan Atomic Energy Agency
JMA	Japan Meteorological Agency
MFB	Mean fractional bias
MODARIA	IAEA programme on Modelling and Data for Radiological Impact Assessments, 2012–2015
MODARIA II	Follow-up to MODARIA, 2016–2019

MSE	Mean square error
NWP	Numerical weather prediction
PHE	Public Health England
PMSS	Parallel Micro Swift Spray
P-SPRAY	Particle spray model
RASCAL	Radiological Assessment for Consequence Analysis
RASS	Radio acoustic sounding system
RDD	Radiological dispersion device
RMSE	Root mean square error
SAGA GIS	System for Automated Geoscientific Analyses Geographic Information System
SODAR	Sonic detection and ranging
SRTM	Shuttle Radar Topography Mission
SÚRO	Czech National Radiation Protection Institute
TA Luft	German Technical Instructions on Air Quality Control
TPPŠ	Šoštanj Thermal power plant in Slovenia
URD	Urban release dispersion model
VDI	Verein Deutscher Ingenieure (Association of German Engineers)

CONTRIBUTORS TO DRAFTING AND REVIEW

Boznar, M.Z.	Modelling, Meteorology, Measurement, Environmental Information Systems Engineering, Republic of Slovenia
Charnock, T.W.	Health Protection Agency, United Kingdom
Chouhan, S.L.	Canadian Nuclear Laboratories, Canada
Grsic, Z.	Nuclear Facilities of Serbia, Serbia
Halsall, C.	International Atomic Energy Agency
Heinrich, G.	Bundesamt für Strahlenschutz, Germany
Helebrant, J.	National Radiation Protection Institute, Czech Republic
Hettrich, S.	Bundesamt für Strahlenschutz, Germany
Kuča, P.	National Radiation Protection Institute, Czech Republic
Mancini, F.	SOGIN S.p.A., Italy
Mlakar, P.	Modelling, Meteorology, Measurement, Environmental Information Systems Engineering, Republic of Slovenia
Patryl, L.	Commissariat à l'Energie Atomique, France
Sdouz, G.	Technical University of Vienna, Austria
Takahara, S.	Japan Atomic Energy Agency, Japan
Tay, B.K.	Defence Science Organisation National Laboratories, Singapore
Thiessen, K.M.	Oak Ridge Center for Risk Analysis, United States of America
Walter, H.	Bundesamt für Strahlenschutz, Germany
Yankovich, T.	International Atomic Energy Agency
Yu, C.	Argonne National Laboratory, United States of America

LIST OF PARTICIPANTS

Al Mahroos, L.A.S.	Public Commission for the Protection of Marine Resources, Environment and Wildlife, Bahrain
Alhbaib, A.A.	Atomic Energy Research Institute, Saudi Arabia
Alotaibi, K.	Presidency of Meteorology and Environment, Saudi Arabia
Bartusková, M.	National Radiation Protection Institute, Czech Republic
Benkrid, M.	Commissariat à l'Energie Atomique, Algeria
Boznar, M.Z.	Modelling, Meteorology, Measurement, Environmental Information Systems Engineering, Republic of Slovenia
Brown, J.	International Atomic Energy Agency
Bush-Goddard, S.	Nuclear Regulatory Commission, United States of America
Charnock, T.W.	Health Protection Agency, United Kingdom
Chouhan, S.L.	Canadian Nuclear Laboratories, Canada
D'Isidoro, M.	ENEA, Radiation Protection Institute, Italy
de With, G.	Nuclear Research and Consultancy Group, Netherlands
Ďúran, J.	VÚJE Inc., Slovakia
Fontaine-Lagrand, J.-É.	International Atomic Energy Agency
Fuka, V.	Charles University, Czech Republic
Grašič, B.	Modelling, Meteorology, Measurement, Environmental Information Systems Engineering, Republic of Slovenia
Grsic, Z.	Nuclear Facilities of Serbia, Serbia
Heinrich, G.	Bundesamt für Strahlenschutz, Germany
Helebrant, J.	National Radiation Protection Institute, Czech Republic
Hettrich, S.	Bundesamt für Strahlenschutz, Germany
Hůlka, J.	National Radiation Protection Institute, Czech Republic
Hwang, W.T.	Korea Atomic Energy Research Institute, Republic of Korea
Konoplev, A.	SPA “Typhoon”, Russian Federation
Kuča, P.	National Radiation Protection Institute, Czech Republic

Kudrin, I.	Burnasyan Federal Medical Biophysical Center, Russian Federation
Kwamena, N.-O.A.	Canadian Nuclear Safety Commission, Canada
Latouche, G.	Canadian Nuclear Safety Commission, Canada
Loo, H.K.	Defence Science Organisation National Laboratories, Singapore
Mancini, F.	SOGIN S.p.A., Italy
Melintescu, A.	"Horia Hulubei" National Institute of Physics and Nuclear Engineering, Romania
Messaci, M.	Commissariat à l'Energie Atomique, Algeria
Mlakar, P.	Modelling, Meteorology, Measurement, Environmental Information Systems Engineering, Republic of Slovenia
Mohapatra, D.	Atomic Energy Regulatory Board, India
Molnary, L.	Instituto de Pesquisas Energéticas e Nucleares, Brazil
Muikku, M.H.	Radiation and Nuclear Safety Authority, Finland
Patryl, L.	Commissariat à l'Energie Atomique, France
Qifan, W.	Tsinghua University, China
Quentric, E.	Institut de Radioprotection et de Sûreté Nucléaire, France
Rababa, A.B.	Jordanian Atomic Energy Commission, Jordan
Reisin, T.G.	Soreq Nuclear Research Center, Israel
Rozi, E.	South African Nuclear Energy Corporation Limited, South Africa
Santos, E.	University of Coimbra, Portugal
Sdouz, G.	Technical University of Vienna, Austria
Shroads, A.D.	SC&A, Inc., United States of America
Sim, E.	Defence Science OrganisationNational Laboratories, Singapore
Smejkalova, E.	Abmerit, Slovakia
Takahara, S.	Japan Atomic Energy Agency, Japan
Tay, B.K.	Defence Science Organisation National Laboratories, Singapore
Thiessen, K.M.	Oak Ridge Center for Risk Analysis, United States of America
Tschiersch, J.	Helmholtz-Zentrum München GmbH, Germany

Urso, L.	Helmholtz-Zentrum München GmbH, Germany
Walter, H.	Bundesamt für Strahlenschutz, Germany
Yankovich, T.	International Atomic Energy Agency
Yu, C.	Argonne National Laboratory, United States of America

MODARIA Technical Meetings, IAEA Headquarters, Vienna

19–22 November 2012, 11–15 November 2013, 10–14 November 2014,
9–13 November 2015

Interim Working Group Meetings, MODARIA Working Group 2

Vienna, Austria, 24–26 June 2013, 21–23 May 2014, 1–3 June 2015

IAEA
International Atomic Energy Agency

No. 26

ORDERING LOCALLY

IAEA priced publications may be purchased from the sources listed below or from major local booksellers.

Orders for unpriced publications should be made directly to the IAEA. The contact details are given at the end of this list.

NORTH AMERICA

Bernan / Rowman & Littlefield

15250 NBN Way, Blue Ridge Summit, PA 17214, USA
Telephone: +1 800 462 6420 • Fax: +1 800 338 4550
Email: orders@rowman.com • Web site: www.rowman.com/bernan

REST OF WORLD

Please contact your preferred local supplier, or our lead distributor:

Eurospan Group

Gray's Inn House
127 Clerkenwell Road
London EC1R 5DB
United Kingdom

Trade orders and enquiries:

Telephone: +44 (0)176 760 4972 • Fax: +44 (0)176 760 1640
Email: eurospan@turpin-distribution.com

Individual orders:

www.eurospanbookstore.com/iaea

For further information:

Telephone: +44 (0)207 240 0856 • Fax: +44 (0)207 379 0609
Email: info@eurospangroup.com • Web site: www.eurospangroup.com

Orders for both priced and unpriced publications may be addressed directly to:

Marketing and Sales Unit
International Atomic Energy Agency
Vienna International Centre, PO Box 100, 1400 Vienna, Austria
Telephone: +43 1 2600 22529 or 22530 • Fax: +43 1 26007 22529
Email: sales.publications@iaea.org • Web site: www.iaea.org/publications

22-02168E

International Atomic Energy Agency
Vienna